frontiers | Research Topics

Adaptation mechanisms of grass and forage plants to stressful environments, volume II

Edited by
Jin-Lin Zhang, Maofeng Chai, Jing Zhang, Sergey Shabala and Kehua Wang

Published in
Frontiers in Plant Science

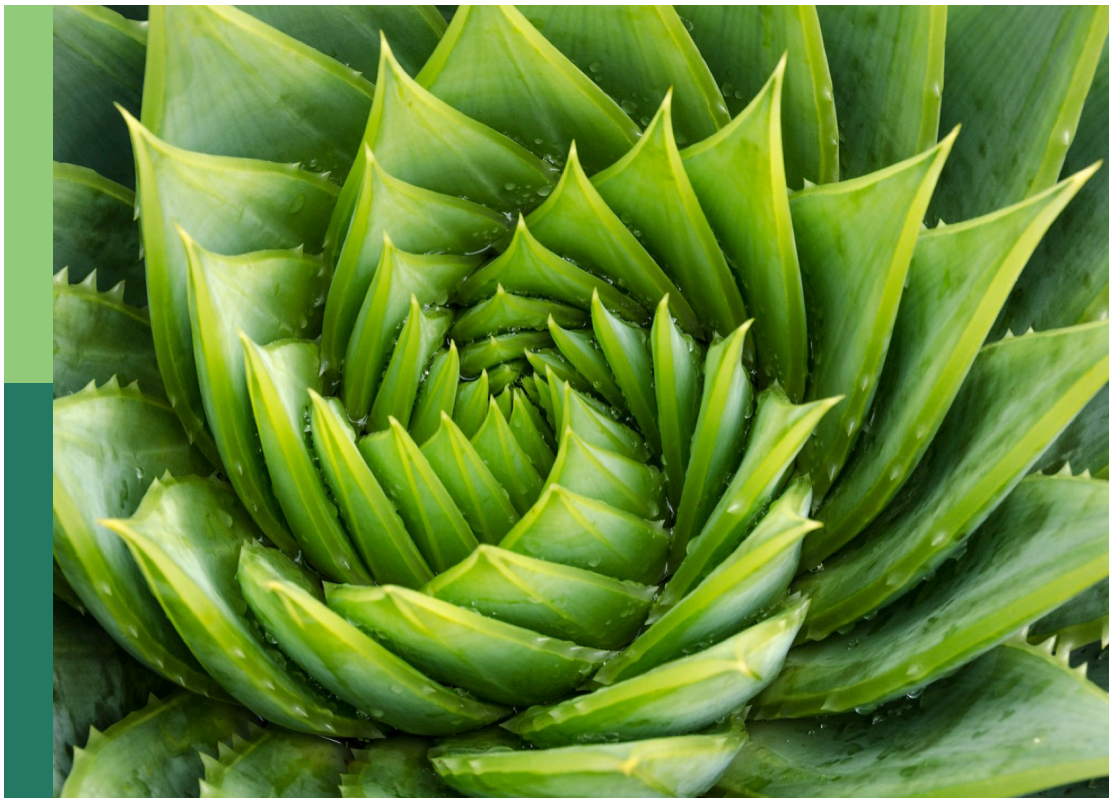

ISSN 1664-8714
ISBN 978-2-8325-3842-5
DOI 10.3389/978-2-8325-3842-5

About Frontiers

Frontiers is more than just an open access publisher of scholarly articles: it is a pioneering approach to the world of academia, radically improving the way scholarly research is managed. The grand vision of Frontiers is a world where all people have an equal opportunity to seek, share and generate knowledge. Frontiers provides immediate and permanent online open access to all its publications, but this alone is not enough to realize our grand goals.

Frontiers journal series

The Frontiers journal series is a multi-tier and interdisciplinary set of open-access, online journals, promising a paradigm shift from the current review, selection and dissemination processes in academic publishing. All Frontiers journals are driven by researchers for researchers; therefore, they constitute a service to the scholarly community. At the same time, the *Frontiers journal series* operates on a revolutionary invention, the tiered publishing system, initially addressing specific communities of scholars, and gradually climbing up to broader public understanding, thus serving the interests of the lay society, too.

Dedication to quality

Each Frontiers article is a landmark of the highest quality, thanks to genuinely collaborative interactions between authors and review editors, who include some of the world's best academicians. Research must be certified by peers before entering a stream of knowledge that may eventually reach the public - and shape society; therefore, Frontiers only applies the most rigorous and unbiased reviews. Frontiers revolutionizes research publishing by freely delivering the most outstanding research, evaluated with no bias from both the academic and social point of view. By applying the most advanced information technologies, Frontiers is catapulting scholarly publishing into a new generation.

What are Frontiers Research Topics?

Frontiers Research Topics are very popular trademarks of the *Frontiers journals series*: they are collections of at least ten articles, all centered on a particular subject. With their unique mix of varied contributions from Original Research to Review Articles, Frontiers Research Topics unify the most influential researchers, the latest key findings and historical advances in a hot research area.

Find out more on how to host your own Frontiers Research Topic or contribute to one as an author by contacting the Frontiers editorial office: frontiersin.org/about/contact

Adaptation mechanisms of grass and forage plants to stressful environments, volume II

Topic editors

Jin-Lin Zhang — Lanzhou University, China
Maofeng Chai — Qingdao Agricultural University, China
Jing Zhang — Nanjing Agricultural University, China
Sergey Shabala — University of Tasmania, Australia
Kehua Wang — China Agricultural University, China

Citation

Zhang, J.-L., Chai, M., Zhang, J., Shabala, S., Wang, K., eds. (2023). *Adaptation mechanisms of grass and forage plants to stressful environments, volume II*. Lausanne: Frontiers Media SA. doi: 10.3389/978-2-8325-3842-5

Table of contents

frontiers | Frontiers in Plant Science

TYPE Editorial
PUBLISHED 23 November 2023
DOI 10.3389/fpls.2023.1323841

OPEN ACCESS

EDITED AND REVIEWED BY
Luisa M. Sandalio,
Spanish National Research Council (CSIC), Spain

*CORRESPONDENCE
Jing Zhang
zhangjing12306@163.com
Jin-Lin Zhang
jlzhang@lzu.edu.cn

RECEIVED 18 October 2023
ACCEPTED 17 November 2023
PUBLISHED 23 November 2023

CITATION
Zhang J, Chen Y, Chai M-F, Shabala S, Wang K-H and Zhang J-L (2023) Editorial: Adaptation mechanisms of grass and forage plants to stressful environments, volume II.
Front. Plant Sci. 14:1323841.
doi: 10.3389/fpls.2023.1323841

Editorial: Adaptation mechanisms of grass and forage plants to stressful environments, volume II

Jing Zhang[1]*, Yu Chen[1], Mao-Feng Chai[2], Sergey Shabala[3], Ke-Hua Wang[4] and Jin-Lin Zhang[5]*

[1]College of Agro-grassland Science, Nanjing Agricultural University, Nanjing, China, [2]Key Laboratory of National Forestry and Grassland Administration on Grassland Resources and Ecology in the Yellow River Delta, College of Grassland Science, Qingdao Agricultural University, Qingdao, China, [3]Tasmanian Institute of Agriculture, University of Tasmania, Hobart, TAS, Australia, [4]Department of Turfgrass Science and Engineering, College of Grassland Science and Technology, China Agricultural University, Beijing, China, [5]State Key Laboratory of Herbage Improvement and Grassland Agro-ecosystems, Key Laboratory of Grassland Livestock Industry Innovation, Ministry of Agriculture and Rural Affairs; College of Pastoral Agriculture Science and Technology, Lanzhou University, Lanzhou, China

KEYWORDS

grass and forage plants, stress tolerance, gene functional characterization, organic acid, host-microbe interactions, nutrient uptake

Editorial on the Research Topic
Adaptation mechanisms of grass and forage plants to stressful environments, volume II

1 Introduction

In nature, plants encounter various challenges from stressful environments, including high and low temperatures, drought, salinity, heavy metals, and nutrient deficiency, which adversely affect plant growth and development (Zhang et al., 2022). It is well-established that global warming is occurring, leading to frequent and extreme climate fluctuations, resulting in frequent natural disasters and environmental problems. Additionally, the increasing global population presents greater challenges for food and ecological security (Gupta et al., 2020). Therefore, cultivating more stress-resistant crop varieties and increasing crop yield and quality are essential for addressing global food security and sustainable development issues.

Grass and forage plants with relatively more powerful stress resistance fulfill numerous functions, including beautifying landscapes, protecting the environment, enhancing recreational activities, and providing fodder for livestock and wildlife (Huang, 2021). In comparison to crops, grass and forage plants display a diverse range of breeding mechanisms, including cross-pollination, self-pollination, and hybridization between different species. This diversity contributes to a wide genetic variation within these plants and enables them to thrive in more stressful environments (Huang, 2021). Therefore, there is an imperative necessity to investigate the underlying stress-tolerant

mechanisms that might feedback grass, forage and crop plant breeding for stress tolerance improvement.

Despite significant advances in understanding the mechanisms of grass and forage plants to stressful environments, there remain knowledge gaps in these areas, and this Research Topic aims to address these gaps. In this Research Topic, 11 articles written by 75 researchers were published.

2 Functional characterization of genes relevant to stress tolerance

The Full-length cDNA overexpression (FOX) system is a molecular biology technique used for gene mining by overexpressing full-length complementary DNA (cDNA) in cells or organisms (Ichikawa et al., 2006). The FOX hunting system has been successfully applied for stress-tolerant genes screening in *Arabidopsis* and rice. For example, *TsHsfA1d* and *OsREX1-S* identified *via* FOX hunting system functioned as positive regulators of heat stress and cadmium stress, respectively (Higashi et al., 2013; Kunihiro et al., 2014). In this Research Topic, Zheng et al. identified eleven salt-tolerant genes using FOX hunting system in *Zoysia matrella*. They particularly focused on a novel salt-inducible candidate gene called *ZmGnTL*. Their findings revealed that *ZmGnTL* improves salt tolerance by regulating ion homeostasis, scavenging reactive oxygen species, and adjusting osmotic balance.

High-affinity K^+ transporters (HKTs) are transmembrane cation transporters that play a pivotal role in Na^+ or Na^+-K^+ co-transport, thereby regulating salt tolerance in plants (Horie et al., 2007). Therefore, *HKTs* represent valuable gene resources for enhancing plant salt tolerance. In this Research Topic, Haxim et al. characterized a novel *HKT* gene named *SeHKT1;2* from a halophyte *Salicornia europaea*. SeHKT1;2 selectively transports Na^+ rather than K^+ and is an important target for understanding the mechanisms of salt tolerance in plants.

Plant plasma membranes (PMs) serve important functions in maintaining intracellular stability and exchanging information with the external environment. Studying the dynamics of the PM proteome is crucial for elucidating cellular regulation in response to various stimuli. However, analyzing the PM proteome poses challenges due to the low abundance of PM proteins in the total cellular protein pool (Chen and Weckwerth, 2020). To enhance the separation and enrichment of PM proteins, Yang et al. developed a simplified method that combines differential centrifugation and Brij-58 treatment. This method increased the abundance of PM proteins in the enriched fraction while reducing contamination from other organellar proteins.

3 Regulations of natural metabolites or synthetic chemicals on stress tolerance

The remediation of saline-alkali and heavy metal-contaminated lands plays a crucial role in protecting the ecological environment, improving land availability, and promoting sustainable agriculture (Khan and Bhatt, 2023). Chemical substances, such as organic acids and biochar, have the potential to react with pollutants, neutralizing or transforming them into less harmful forms. In this Research Topic, Yang et al. discovered that the exogenous application of citric acid reduced soil salinity and increased soil nutrient content, root vigor, and photosynthesis in sweet sorghum. As a result, the stress tolerance of sweet sorghum was improved, leading to higher biomass yield. Additionally, Meng et al. found that the use of 5% corn straw biochar effectively alleviated the toxicity of Pb to red clover and the associated soil. Above findings contribute to sustainable development and foster the harmonious coexistence between humans and nature.

4 Omics-related studies

Recent significant progress in omics techniques, such as transcriptomics, genomics, proteomics, and metabolomics, has significantly contributed to the profound understanding of the molecular mechanisms underlying plant stress tolerance (Singhal et al., 2021). In this Research Topic, Wang et al. found that application of P fertilizer resulted in improved root structure and increased levels of soluble sugar and soluble protein. The integration of the transcriptome and metabolome revealed the impact of P on the biosynthesis of N-acetyl-L-phenylalanine, L-serine, lactose, and isocitrate during the cold acclimation period.

Strong ultraviolet radiation and low temperature environments can induce the synthesis of specific secondary metabolites in plants as a defense mechanism against severe environmental stresses. To understand the adaptive mechanism of *Draba oreades Schrenk* at high altitude, Lei et al. conducted a comprehensive evaluation of the metabolome in plants at 3800 m, 4000 m, and 4200 m, respectively. Based on the metabolome data, ten crucial metabolites were identified as potential biomarkers. The levels of L-phenylalanine, L-histidine, naringenin-7-O-Rutinoside-4'-O-glucoside, and apigenin, which are associated with flavonoid biosynthesis and plant disease resistance, increased with the increase of altitude.

5 Cross stress tolerance

In natural environments, plants frequently encounter various simultaneous stresses, leading to the occurrence of cross-tolerance phenomena (Zhang et al., 2023). Climate change exposes plants to multiple abiotic stresses simultaneously. While the responses of plants to individual stresses have been extensively studied, it is challenging to speculate and infer the effects of stress combinations based on solely these studies. In this Research Topic, Zhou et al. examined the responding mechanism of bermudagrass to combined low temperature and salt treatments. It was observed that low temperature treatment reduced the relative growth rate, chlorophyll fluorescence transient curve, biomass, and crude fat content. Conversely, mild salt addition alleviated cold stress-induced damage by enhancing photosynthesis and improving the

enzymatic activity of antioxidant. This study provides a comprehensive understanding of the probable interaction mechanism between low temperature and salt stress in grass plants, offering valuable insights for fodder growth in cold regions.

6 Future research

The articles presented in this Research Topic make a significant contribution to addressing gaps in our understanding of the role of complex signaling transduction pathways in grass and forage plants in response to various stressful environments. These articles also highlight the identification of stress-tolerant genes, beneficial natural metabolites, and root-associated microbes, which serve as valuable resources not only for grass and forage plants, but also for other crops. CRISPR/Cas is a valuable biotechnological approach for breeding crops with increased tolerance to stressful environments (Zhu et al., 2020), while no CRISPR/Cas-related research has been included in this Research Topic. We look forward to more articles to be published exploring the application of CRISPR/Cas and further advancements in creating stress-tolerant grass and forage germplasms without transgenic elements.

Author contributions

JZ: Funding acquisition, Supervision, Writing – original draft, Writing – review & editing. YC: Funding acquisition, Writing – review & editing. M-FC: Writing – review & editing. SS: Writing – review & editing. K-HW: Writing – review & editing. J-LZ: Writing – original draft, Writing – review & editing.

Funding

The author(s) declare financial support was received for the research, authorship, and/or publication of this article. This work was financially supported by the Fundamental Research Funds for the Central Universities (XUEKEN2022020 and YDZX2023001).

Acknowledgments

We greatly appreciate all authors and reviewers for their contribution to this Research Topic.

Conflict of interest

The authors declare that the research was conducted in the absence of any commercial or financial relationships that could be construed as a potential conflict of interest.

The author(s) declared that they were an editorial board member of Frontiers, at the time of submission. This had no impact on the peer review process and the final decision.

Publisher's note

References

Chen, Y., and Weckwerth, W. (2020). Mass spectrometry untangles plantmembrane protein signaling networks. *Trends Plant Sci.* 25, 930–944. doi: 10.1016/j.tplants.2020.03.013

Gupta, A., Rico-Medina, A., and Caño-Delgado, A. I. (2020). The physiology of plant responses to drought. *Science* 368 (6488), 266–269. doi: 10.1126/science.aaz7614

Higashi, Y., Ohama, A., Ishikawa, T., Katori, T., Shimura, A., Kusakabe, K., et al. (2013). HsfA1d, a protein identified via FOX hunting using Thellungiella salsuginea cDNAs, improves heat tolerance by regulating heat stress responsive gene expression. *Mol. Plant* 6, 411–422. doi: 10.1093/mp/sst024

Horie, T., Costa, A., Kim, T. H., Han, M. J., Horie, R., Leung, H. Y., et al. (2007). Rice OsHKT2;1 transporter mediates large Na^+ influx component into K^+-starved roots for growth. *EMBO J.* 26, 3003–3014. doi: 10.1038/sj.emboj.7601732

Huang, B. (2021). Grass research for a productive, healthy and sustainable society. *Grass Res.* 1, 1. doi: 10.48130/GR-2021-0001

Ichikawa, T., Nakazawa, M., Kawashima, M., Iizumi, H., Kuroda, H., Kondou, Y., et al. (2006). The FOX hunting system: an alternative gain-of-function gene hunting technique. *Plant J.* 48, 974–985. doi: 10.1111/j.1365-313X.2006.02924.x

Khan, M. M., and Bhatt, P. (2023). Editorial: Environmental pollutantsin agroecosystem: toxicity, mechanism, and remediation. *Front. Plant Sci.* 14, 1208405. doi: 10.3389/fpls.2023.1208405

Kunihiro, S., Kowata, H., Kondou, Y., Takahashi, S., Matsui, M., Berberich, T., et al. (2014). Overexpression of rice *OsREX1-s*, encoding a putative component of the core general transcription and DNA repair factor IIH, renders plant cells tolerant to cadmium- and UV-induced damage by enhancing DNA excision repair. *Planta.* 239, 1101–1111. doi: 10.1007/s00425-014-2042-1

Singhal, R. K., Saha, D., Skalicky, M., Mishra, U. N., Chauhan, J., Behera,, L. P., et al. (2021). Crucial cell signaling compounds crosstalk and integrative multi-omics techniques for salinity stress tolerance in plants. *Front. Plant Sci.* 12, 670369. doi: 10.3389/fpls.2021.670369

Zhang, H., Zhu, J., Gong, Z., and Zhu, J. K. (2022). Abiotic stress responses in plants. *Nat. Rev. Genet.* 23 (2), 104–119. doi: 10.1038/s41576-021-00413-0

Zhang, J., Chai, M.-F., Shabala, S., Wang, K.-H., and Zhang, J.-L. (2023). Editorial: Adaptation mechanisms of grass and forage plants to stressful environments. *Front. Plant Sci.* 14, 1132198.

Zhu, H., Li, C., and Gao, C. (2020). Applications of CRISPR-Cas in agriculture and plant biotechnology. *Nat. Rev. Mol. Cell Biol.* 21 (11), 661–677. doi: 10.1038/s41580-020-00288-9

frontiers | Frontiers in Plant Science

TYPE Original Research
PUBLISHED 27 September 2022
DOI 10.3389/fpls.2022.1020857

OPEN ACCESS

EDITED BY
Jin-Lin Zhang,
Lanzhou University, China

REVIEWED BY
Cinzia Margherita Bertea,
University of Turin, Italy
Thomas Vogt,
Leibniz-Institut für Pflanzenbiochemie (IPB), Germany
Huahua Wang,
Henan Normal University, China

*CORRESPONDENCE
Mengfei Li
lmf@gsau.edu.cn
Paul W. Paré
paul.pare@ttu.edu

SPECIALTY SECTION
This article was submitted to Plant Abiotic Stress, a section of the journal Frontiers in Plant Science

RECEIVED 16 August 2022
ACCEPTED 13 September 2022
PUBLISHED 27 September 2022

CITATION
Su H, Jin L, Li M and Paré PW (2022) Low temperature modifies seedling leaf anatomy and gene expression in *Hypericum perforatum*. *Front. Plant Sci.* 13:1020857. doi: 10.3389/fpls.2022.1020857

Low temperature modifies seedling leaf anatomy and gene expression in *Hypericum perforatum*

Hongyan Su[1], Ling Jin[2], Mengfei Li[1]* and Paul W. Paré[3]*

[1]State Key Laboratory of Arid Land Crop Science, Gansu Agricultural University, Lanzhou, China, [2]College of Pharmacy, Gansu University of Chinese Medicine, Lanzhou, China, [3]Department of Chemistry and Biochemistry, Texas Tech University, Lubbuck, TX, United States

Hypericum perforatum, commonly known as St John's wort, is a perennial herb that produces the anti-depression compounds hypericin (Hyp) and hyperforin. While cool temperatures increase plant growth, Hyp accumulation as well as changes transcript profiles, alterations in leaf structure and genes expression specifically related to Hyp biosynthesis are still unresolved. Here, leaf micro- and ultra-structure is examined, and candidate genes encoding for photosynthesis, energy metabolism and Hyp biosynthesis are reported based on transcriptomic data collected from *H. perforatum* seedlings grown at 15 and 22°C. Plants grown at a cooler temperature exhibited changes in macro- and micro-leaf anatomy including thicker leaves, an increased number of secretory cell, chloroplasts, mitochondria, starch grains, thylakoid grana, osmiophilic granules and hemispherical droplets. Moreover, genes encoding for photosynthesis (64-genes) and energy (35-genes) as well as Hyp biosynthesis (29-genes) were differentially regulated with an altered growing temperature. The anatomical changes and genes expression are consistent with the plant's ability to accumulate enhanced Hyp levels at low temperatures.

KEYWORDS

***hypericum perforatum*, temperature, green tissue, dark gland, secretory cell, hypericin**

1 Introduction

Hypericum perforatum L. (St John's wort) is a perennial herb widely distributed in Europe, Asia, Northern Africa and Northern America (Bagdonaitė et al., 2010). Aerial parts contain the metabolites hypericin (Hyp) and hyperforin that are used in traditional medicine as anti-depression, anti-viral, anti-microbial and anti-tumor agents, as well as other plant constituents such as flavonoids, tannins and volatile oils (Barnes et al., 2001; Napoli et al., 2018).

St John's wort has traditionally been used as an external anti-infammatory and healing remedy for the treatment of swellings, wounds and burns. It is of interest recently due to new and important therapeutic applications (Bombardelli and Morazzoni, 1995; Nahrstedt and Butterweck, 1997; Erdelmeier, 1998). The species is characterized by the presence of different types of secretory structure: translucent glands or cavities, black nodules and secretory canals (Ciccarelli et al., 2001). The frequency and diversity of these secretory structures is evidence of the intense secretory activity of the species. Previous studies have found that *H. perforatum* growth and Hyp accumulation are affected by the germplasm source (Couceiro et al., 2006; Soták et al., 2016; Zhang et al., 2021) as well as environmental factors such as light quality (Germ et al., 2010; Najafabadi et al., 2019; Tavakoli et al., 2020; Karimi et al., 2022), drought (Gray et al., 2003), and temperature (Zobayed et al., 2005; Couceiro et al., 2006; Yao et al., 2019; Tavakoli et al., 2020; Kaundal et al., 2021). Lower temperatures can enhance plant growth and Hyp accumulation; indeed cooler growth conditions can significantly increase plant biomass by inducing gene expression that favor growth (Brunáková et al., 2015; Yao et al., 2019; Tavakoli et al., 2020). Previous studies have found that *ca.* 750 genes are differentially expressed and 150 genes are involved in plant growth, Hyp biosynthesis and/or environmental responses in *H. perforatum* seedlings at different temperatures (Su et al., 2021). Based on this previous study, St John's wort expression levels for low-level gene candidates have been quantified by qRT-PCR (real time quantitative PCR), to further probe the mechanism of seedlings performance under a cool temperature. Secretory structures associated with leaf metabolite accumulation were also monitored under reduced temperature conditions.

2 Materials and methods

2.1 Plant materials

H. perforatum seedlings were grown from seed [collected Kangxian county (33°16′20″N, 105°31′50″E; 1050 m a.s.l.) located in Gansu province, China] and acclimated to defined temperatures according to previously published protocols (Yao et al., 2019; Su et al., 2021). Specifically, seeds were successively disinfected with 70% ethanol (v/v) and 0.1% $HgCl_2$ (w/v), and then the sterilized seeds were inoculated on Murashige and Skoog (MS) + 20.0 g/L sucrose + 4.0 g/L agar (pH 5.8) and germinated at 22°C (24 h/d photoperiod, white light, 500 $\mu mol{\cdot}m^{-2}{\cdot}s^{-1}$ Flux; 50 ± 5% relative humidity). After 25 days of germination at 22°C, seedlings (Figure S1) were transplanted to a new MS medium with 0.5 mg/L 1-Naphthylacetic acid (NAA) + 1.0 mg/L 6-Benzylaminopurine (6-BA). After 20 days of growth, half of the healthy seedlings were kept at 22°C and the other half was moved to 15°C (24 h/d photoperiod, white light, 500 $\mu mol{\cdot}m^{-2}{\cdot}s^{-1}$ Flux; 50 ± 5% relative humidity) in illuminated incubators (PDX-600A, KunCheng Scientific Instruments Co., Ltd., Shanghai, China). After 20 days growth at 15 and 22°C, the treated seedlings (Figure S2) were collected for seedlings dry weight (DW), Hyp quantification, anatomical observation and qRT-PCR validation. Herein, each treatment had 40 flasks with 3 seedlings per flask. Additionally, the criteria for choosing the temperatures is based on our previous findings that the aerial parts biomass and Hyp accumulation in *H. perforatum* are greater at 15°C compared with 22 and 30°C (Yao et al., 2019).

2.2 Measurement of chlorophyll and carotenoid contents

Chlorophyll and carotenoid contents were measured according to a previous protocol (Li et al., 2009; Yang et al., 2014). Briefly, fresh whole leaves (0.1 g) were finely ground in 80% acetone (v/v, 5 mL) and centrifuged at 5000 r/min and 4°C for 10 min. The supernatant was diluted to 25 mL with 80% acetone (v/v). Absorbance was taken at 662, 646 and 470 nm using a spectrophotometer (UV-6100, Shanghai, China). The specific calculations are as follows:

$$\text{Chlorophyll a concentration}: \ C_a(\text{mg/L}) = 12.2A_{662} - 2.81A_{646}$$

$$\text{Chlorophyll b concentration}: \ C_b(\text{mg/L}) = 20.13A_{646} - 5.03A_{662}$$

$$\text{Chlorophyll concentration}: \ C_T(\text{mg/L}) = C_a + C_b$$

$$\text{Carotenoid concentration}: \ C\,(\text{mg/L}) = 1000A_{470} - 3.27C_a - 104C_b)/229$$

$$\text{Pigment content}\,(\text{mg/g}) = (C \times V)/M$$

where "A_{662}", "A_{646}" and "A_{470}" represent the absorbance at 662, 646 and 470 nm, as well as "C", "V" and "M" represent the concentration of pigment (mg/L), volume of extract (L) and sample fresh weight (FW, g), respectively.

2.3 HPLC quantification of Hyp content

Hyp content was quantified according to previous protocols (Couceiro et al., 2006; Yao et al., 2019). Briefly, air-dried aerial parts of seedlings were finely powdered, samples (0.1 g) were soaked in 95% ethanol (v/v; 20 mL) and agitated in the dark at 22°C for 72 h, and centrifuged at 8000 r/min and 4°C for 10 min. The supernatant was evaporated and concentrated using a vacuum in a rotary evaporator at 60°C, and then the concentrated residue was re-dissolved in methanol (10 mL,

chromatography grade). After filtered with a durapore membrane (0.22 μm; Millipore, Sigma, USA), extracts (10 μL) were analyzed at 590 nm by HPLC (Eclipse Plus C18, 250 mm × 4.6 mm, 5 μm; Column temperature 30°C; Agilent 1100 series, Santa Clara, California, USA) and mobile phase with acetonitrile: 50 mmol/L triethylamine (70:30, v/v) at a flow rate of 1.0 mL/min. Hyp content was evaluated on peak area comparison with a reference standard (hypericin, 56690; Sigma Chemical Co., St. Louis, MO, USA). The specific calculations are as follows:

$$\text{Hyp content (mg/g DW)} = [Y/Y_0 \times \Omega \times V]/(M1 \times 1000)$$

where "Ω", "Y_0", "Y", "V", "$M1$" represent the standard concentration of Hyp (μg/mL), standard peak area of Hyp (mAU×s), sample peak area (mAU×s), volume of extract (L) and sample DW (g), respectively.

2.4 Leaf micro-structure observations

The middle adaxial leaf of 20 day-old plants was paraffin sectioned based on Li and Zhang, 2016. Briefly, fresh leaves were fixed with a formaldehyde-alcohol-acetic acid (FAA) solution at 4°C for 12 h; fixed samples were then washed with 70% ethanol (v/v) at 22°C for 10 min (thrice), and sequentially dehydrated in 30% ethanol (2 h), 50% (2 h), 70% (12 h), 85% (1 h), 95% (1 h), and 100% (0.5 h) (twice, v/v); dehydrated samples were then sequentially transparentized in the mixture of ethanol and dimethylbenzene (2:1, 1:1, 1:2 and 0:1, v/v) for 30 min. Samples were sequentially immersed in a mixture of dimethylbenzene-paraffin (1:1 and 2:1, v/v) at 56°C for 12 h, and immersed in paraffin at 58°C for 12 h (thrice), and then embedded in paraffin cubes (2 cm); finally, the samples were sliced (7 μm) (KD-2258, Cody, China) and stained (S8020 and F8130, Solarbio, China). Sample imaging was by fluorescence, brightfield and phase contrast microscopy (Revolve RVL-100-G, ECHO, USA).

2.5 Leaf ultra-structure analysis

Leaf ultra-structure was observed by transmission electron microscopy (Kornfeld et al., 2007), specific protocols and instrumentation followed previously published literature (Li et al., 2020). Briefly, small pieces (4 mm × 2 mm) of the middle adaxial leaf without mainly veins were firstly immersed into glutaraldehyde (2.5%, v/v) at 4°C for 12 h, then washed with 0.2 M sodium phosphate buffer (pH 7.4) at 22°C for 15 min (thrice), and then fixed with osmium tetroxide (1%, w/v) at 4°C for 5 h; secondly, the fixed samples were washed with the above buffer and then extracted sequentially in 50% ethanol (15 min), 70% (12 h), 80% (15 min), 90% (15 min), 100% (15 min), and acetone (100%) for 15 min (twice, v/v), the mixture agent of acetone and embedding (v/v, 1:1) for 7 h, and embedding medium (Epoxy resin, composed of MNA, EPon-812, DDSA and DMP-30) at 22°C for 12 h; thirdly, the treated leaves were transferred to a embedding plate and immersed in a embedding medium, and then dried sequentially at 35°C for 10 h, 45°C for 12 h and 68°C for 48 h; finally, the embedded samples were sliced (75 nm) with an ultra-microtome (EM UC6, Leica, Germany) and stained with uranyl acetate and lead citrate, and then ultra-structure was observed by a transmission electron microscope (JEM-1230, JEOL Ltd., Japan).

2.6 Gene excavation

RNA sequencing was by unigene expression analysis and basic annotation was conducted; 1584 high-level expressed genes with 749 characterized genes and 150 genes involved in plant growth, Hyp biosynthesis and environmental response have been identified with $|\log_2(\text{fold-change})| > 1$ in previously published article (Su et al., 2021). In this study, low-level genes were identified according to a criteria of $0.2 < |\log_2(\text{fold-change})| < 1.0$ (Robinson et al., 2009; Love et al., 2014), since low-level genes also play important roles in many biological processes (Maia et al., 2007; Gotor et al., 2010). Differentially Expressed Genes (DEGs) were annotated against the Swiss-Prot database (https://www.uniprot.org/), and 64 candidate genes (Table S1 and Table 1) involved in photosynthesis, energy and Hyp biosynthesis were dug out based on the biological functions.

2.7 qRT-PCR quantification

Primer sequences of the selected 32 candidate genes (Table S2) were designed using a Primer-BLAST tool in NCBI. The coding sequences (CDS) of the 32 genes are shown in Table S3. *Actin* (*ACT*) was selected as a reference gene. The extraction of total RNA, synthesis of first-strand cDNA and PCR amplification were performed using RNA kit, RT kit and SuperReal PreMix, respectively. The RNA quality was assessed using an Ultramicro spectrophotometer (Micro Drop, BIO-DL, Shanghai, China) (Table S4) and the integrity was evaluated by 1.0% (w/v) agarose gel electrophoresis (Figure S3), reverse transcription was performed to generate cDNA on the following protocol: 42°C for 15 min and then 95°C for 3 min, one cycle, PCR amplification was performed on the following protocol: one cycle at 95°C for 15 min, and 35 cycles at 95°C for 10 s, 60°C for 20 s and 72°C for 30 s, and melting curve analysis was performed after a 34 s incubation at 72°C (Yao et al., 2019). The concentrations of cDNA and primer were respectively diluted to 100 ng/μL (2 μL) and 10 μM (1.2 μL) for gene expression analysis. Gene expression was quantified using a

TABLE 1 Twenty nine genes involved in Hyp biosynthesis in green tissue and dark gland.

Gene name	Swissprot-ID	Protein name	log_2FC (15°C vs 22°C)
Green tissue (21)			
Glycolysis (10)			
PFK2	Q9FIK0	ATP-dependent 6-phosphofructokinase 2	0.22
PFK3	Q94AA4	ATP-dependent 6-phosphofructokinase 3	0.23
PFK4	Q9FKG3	ATP-dependent 6-phosphofructokinase 4, chloroplastic	0.28
PFK5	Q8VYN6	ATP-dependent 6-phosphofructokinase 5, chloroplastic	-0.20
LTA2	Q9SQI8	Dihydrolipoyllysine-residue acetyltransferase component 4 of pyruvate dehydrogenase complex, chloroplastic	-0.21
ENO1	P42896	Enolase	0.69
HXK1	Q9SEK2	Hexokinase-1	0.37
HXK2	P93834	Hexokinase-2	0.29
PFP-ALPHA	Q41140	Pyrophosphate–fructose 6-phosphate 1-phosphotransferase subunit alpha	0.26
PFP-BETA	Q41141	Pyrophosphate–fructose 6-phosphate 1-phosphotransferase subunit beta	0.33
Fatty acid metabolism (11)			
CUT1	Q9XF43	3-ketoacyl-CoA synthase 6	0.27
ACOT13	Q9NPJ3	Acyl-coenzyme A thioesterase 13	0.23
Acot9	Q9R0X4	Acyl-coenzyme A thioesterase 9, mitochondrial	0.26
LPD1	Q9M5K3	Dihydrolipoyl dehydrogenase 1, mitochondrial	0.40
At3g45770	Q8LCU7	Enoyl-[acyl-carrier-protein] reductase, mitochondrial	-0.49
MFP2	Q39659	Glyoxysomal fatty acid beta-oxidation multifunctional protein MFP-a	0.22
AIM1	Q9ZPI6	Peroxisomal fatty acid beta-oxidation multifunctional protein AIM1	0.28
PDH-E1	O24457	Pyruvate dehydrogenase E1 component subunit alpha-3, chloroplastic	0.27
ECR	Q9M2U2	Very-long-chain enoyl-CoA reductase	0.32
HACD2	Q2KIP8	Very-long-chain (3R)-3-hydroxyacyl-CoA dehydratase 2	0.28
KCR1	Q8L9C4	Very-long-chain 3-oxoacyl-CoA reductase 1	0.72
Dark gland (8)			
PKSA	O23674	Type III polyketide synthase A	0.43
PKSG5	F1LKH9	Polyketide synthase 5	-0.27
CHS	Q9LKP7	Chalcone synthase	0.99
CHS1	Q9XGX2	Chalcone synthase 1	-0.64
FGRAMPH1_01T20223	Q4I8Q4	Acyl-protein thioesterase 1	0.26
MALD1	O50001	Major allergen Pru ar 1	0.63
STH-2	P17642	Pathogenesis-related protein STH-2	0.27
At4g20800	Q9SVG7	Berberine bridge enzyme-like 17	0.94

LightCycler 96 (Roche, Switzerland). Relative expression level (REL) of gene at 15°C compared with 22°C (Control) was valuated based on a $2^{-\triangle\triangle Ct}$ method according to the following formula (Willems et al., 2008):

$$\triangle Ct_{Test\ gene} = Ct_{Test\ gene} - Ct_{Reference\ gene}$$

$$\triangle Ct_{Control\ gene} = Ct_{Control\ gene} - Ct_{Reference\ gene}$$

$$-\triangle\triangle Ct = -(\triangle Ct_{Test\ gene} - \triangle Ct_{Control\ gene})$$

$$\text{REL (Test gene/Control gene)} = 2^{-\triangle\triangle Ct}$$

2.8 Statistical analysis

Three biological replicates were performed; SPSS 22.0 software was used for a *t*-test analysis with $P<0.05$ for differences.

3 Results and discussion

3.1 Low temperature increases chlorophyll and carotenoid content

To probe physical and physiological changes in leaves with a change in median growth temperature, a series of growth

parameters were monitored. A 1.1- and 1.2-fold increase of chlorophyll (a + b) and carotenoid contents was observed at 15 compared with 22°C, respectively (Figure S4). These results were consistent with previous reports that low temperature can significantly increase chlorophyll content, plant growth and subsequently enhance biomass accumulation in comparison with high temperatures (22 and 30°C) (Yao et al., 2019; Su et al., 2021). Five photosynthetic encoded genes (*i.e. psbA*, *psbC*, *ycf4*, *ycf5* and *matK*) were up-regulated at 15°C compared with 22 and 30°C (Yao et al., 2019); and nine genes encoding chlorophyll a-b binding proteins (*i.e. CAB*, *CAB1*, *CAB1B*, *CAB3*, *CAB3C*, *CAB96*, *ELI_PEA*, *OHP2* and *RBCS-C*) were up-regulated at 15°C compared with 22 (Su et al., 2021). The up-regulation of these genes encoding chlorophyll a-b binding, light-induced and light-harvesting complexes proteins indirectly indicate that lower temperatures can improve the accumulation of chlorophyll pigments, which successively enhance photosynthesis and plant growth.

3.2 Low temperature increases biomass and Hyp content

As shown in Figure 1, there were greater biomass and Hyp content at lower temperature, with a 1.2-fold increase of the whole seedlings DW (Figure 1A) and 4.5-fold increase of Hyp content in aerial parts at 15 compared with 22°C (Figure 1B). The representative chromatograms of reference standard (50 μg/mL, injection volume 10 μL) as well as the extracts (10 mL, injection volume 10 μL) of aerial parts of seedlings at 15 and 22°C were shown in Figure 1C. Previous studies on *H. perforatum* have found that cooler temperatures can enhance Hyp accumulation. Specifically, there was a 1.4-fold increase of Hyp content on a DW basis at 15 compared with 22°C after the seedlings treated for 45 days (Yao et al., 2019); a maximum Hyp content on a DW basis at 4 and 8°C compared with 16 and 25°C, with about 10-fold increase at 4 compared with 25°C after the seedlings treated for 7 days (Tavakoli et al., 2020). These findings further demonstrate that Hyp accumulation in *H. perforatum* can be significantly enhanced by cooler temperatures. In fact, extensive experiments have demonstrated that bioactive compounds can be improved at cooler temperatures, such as podophyllotoxin content in *Sinopodophyllum hexandrum* at 15 compared with 22°C (Li et al., 2020), ferulic acid content in *Angelica sinensis* at 15 compared with 22°C (Dong et al., 2022), and total ginsenosides content in *Panax ginseng* at 10 compared with 25°C (Wang et al., 2019).

3.3 Low temperature changes leaf cell micro-structure

Leaf tissue structure alterations [*i.e.* lower epidermis (LE), upper epidermis (UE), palisade cell (PC), spongy tissue (ST) and leaf veins (LV)] as well as organelle density [*i.e.* chloroplast (Ch), dark gland (DG) and secretory cell (SC)] were observed based on growing temperatures (Figure 2). A 1.1-fold increase in leaf thickness was detected (Figure 3A). Previous studies have found that *H. perforatum* leaf morphology (*e.g.* leaf length/width, stem height and DG) are significantly affected by species, geographic,

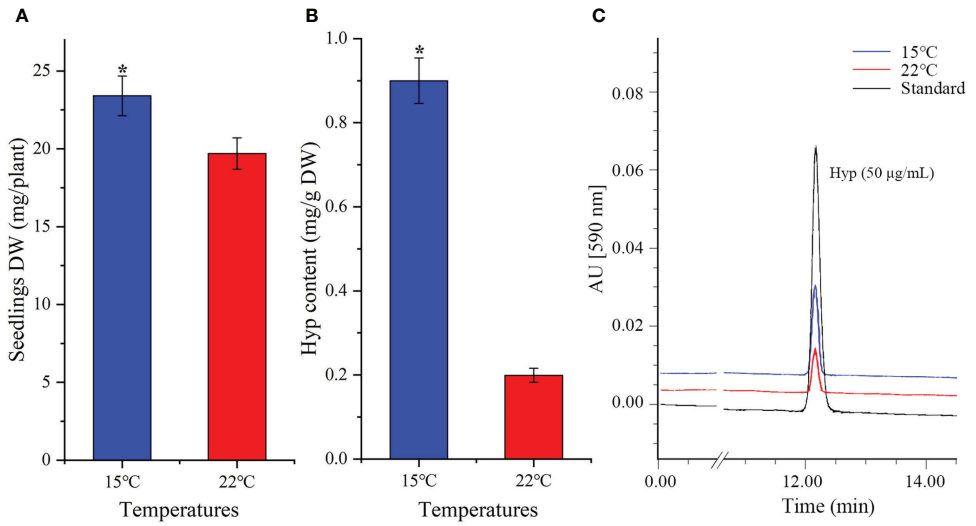

FIGURE 1
Seedlings DW **(A)**, Hyp content **(B)** and representative chromatograms of HPLC **(C)** in *H perforatum* grown at 15 and 22°C. Values of DW are average with their standard deviations (n = 25), and values of Hyp content are average with their standard deviations (n = 3). The "*" represents a significant difference ($P < 0.05$) between 15 and 22°C.

light and temperature conditions (Briskin and Gawienowski, 2001; Walker et al., 2001; Cirak et al., 2007; Stoyanova-Koleva et al., 2015; Su et al., 2021). Since Hyp biosynthesis occurs in dark glands (DG) and secretory cells (SC) is associated with Hyp accumulation (Lv and Hu, 2001; Zobayed et al., 2006; Kornfeld et al., 2007; Rizzo et al., 2019), these organelles were monitored. Increases in DG size and SC number of 1.2-fold and 1.9-fold, respectively for plants growing at the lower temperature was observed (Figures 3B, C). Studies with *Camellia oleifera* grown at 15 compared with 16°C exhibited an increased leaf thickness, of 1.2-fold (Hu et al., 2016). Previous studies on *H. perforatum* have found that the number of DG is more at 15°C compared with 22°C (Su et al., 2021). Thus, larger size of DG and more number of SC in this study further confirm previous studies that higher Hyp accumulates to a greater level at 15°C than 22°C (Su et al., 2021).

3.4 Low temperature changes leaf cell ultra-structure

Vacuole (V) occupied most of the space of whole cell, and chloroplasts (Ch) were near to the cell wall (CW) (Figure 4A, F); mitochondria (Mi) were near to the Ch (Figures 4B, G); starch grains (S) (Figures 4C, H), thylakoid grana (TG) and osmiophilic granules (OG) (Figures 4D, I) presented in the Ch; and hemispherical droplets (HD) (Figures 4E, J) appeared in the epidermal cell. Based on the observations (n=10), the number of Ch, Mi, S, TG and OG appeared to be greater and the size of HD was significantly larger at 15°C compared with 22°C (Figure 4). The number of Ch, Mi, S, TG and OG affected by abiotic stresses such as temperatures has been observed in other plants (Zhang et al., 2005; Li et al., 2020). Here, an increase in the number of Ch, Mi, S, TG and OG may be a low-temperature response for energy acquisition and utilization, since previously studying *H. perforatum* have reported that cooler temperature can enhance plant growth (Yao et al., 2019; Su et al., 2021). The HD, which seems to adhere to membranes or is somehow trapped in a hemispherical shape, may be associated with Hyp biosynthesis (Kornfeld et al., 2007). Here, an increase in the size of HD may play a certain role in enhancing Hyp biosynthesis at lower temperature.

3.5 Low temperature regulates gene expression related to photosynthesis and energy

Thirty-five genes related to photosynthesis and energy (Taiz and Zeiger, 2010) was observed to be differentially regulated with temperature (Table S1), and 16 genes were selected to validate the expression levels. Fifteen genes (*i.e. CAB13*, *CAB2R*, *LHCB1.2*, *CAP10A*, *PGRL1A*, *Os01g0913000*, *TRM1*, *CURT1B*, *THF1*, *At3g63540*, *TERC*, *NMAT1*, *NMAT2*, *SPS3* and *EMB2247*) presented a 1.4 to 9.3-fold up-regulation, while *PGR5* presented a 0.9-fold down-regulation at 15°C compared with 22°C (Figure 5). In previous studies, 12 high-level genes (*i.e.* six *CABs*, *ELI_PEA*, *ELIP2*, *OHP2*, *RBCS-C*, *RCA* and *RBCS-8B*) related to photosynthesis were differentially expressed at 15°C compared with 22°C (Su et al., 2021).

For the specific biological functions of the selected 8 genes related to chloroplast, *CAB13*, *CAB2R*, *LHCB1.2* and *CAP10A* encode light-harvesting chlorophyll a-b binding proteins (LHCs) that functions as a light receptor and play indispensable roles in capturing and delivering excitation energy to photo systems (Zou et al., 2020), *PGRL1A* and *PGR5*

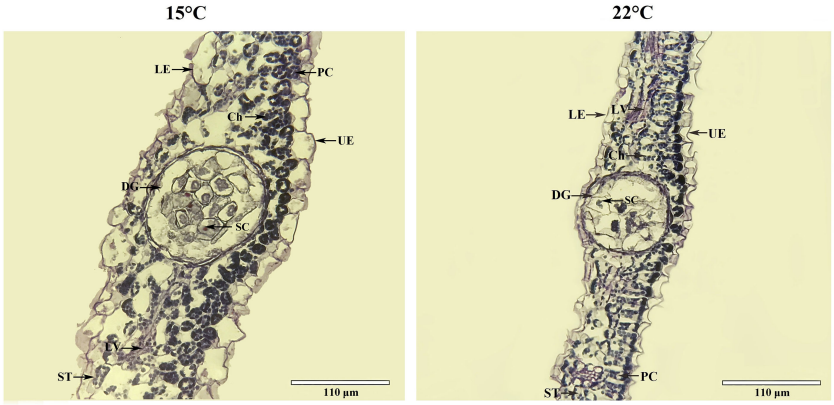

FIGURE 2
Cross-sectional micro-structure for leaves of seedlings grown at 15 and 22°C. Ch, chloroplast, DG, dark gland, LE, lower epidermis, LV, leaf veins, PC, palisade cell, SC, secretory cell, ST, spongy tissue, UE, upper epidermis.

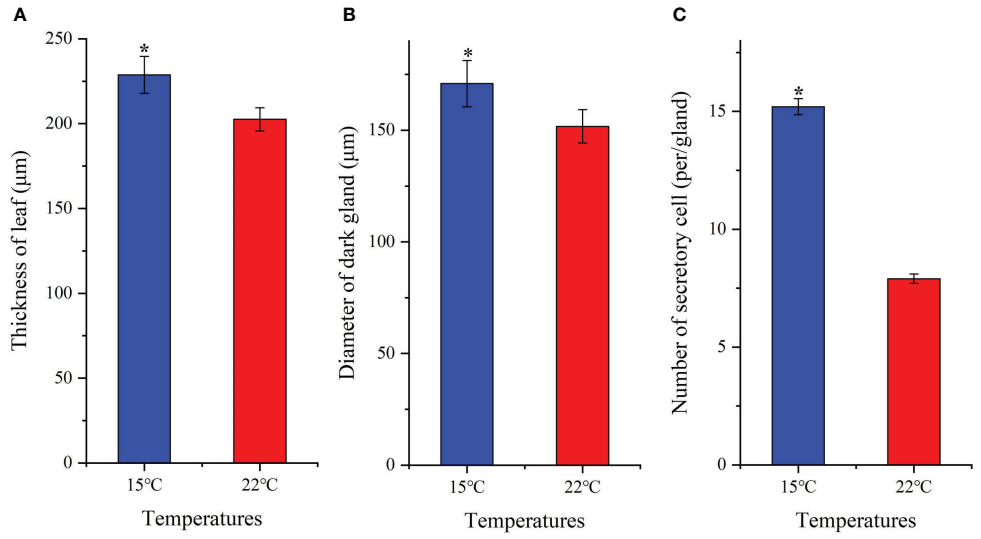

FIGURE 3
Changes of leaf thickness **(A)**, diameter of dark-gland **(B)** and number of secretory cell **(C)** for seedlings grown at 15 and 22°C. All the values are average with their standard deviations (n = 10). The "*" represents a significant difference ($P < 0.05$) between 15 and 22°C.

are involved in electron flow (Munekage et al., 2002; Hertle et al., 2013), *Os01g0913000* and *TRM1* are involved in various redox reactions (Capitani et al., 2000; Glauser et al., 2004). For selected genes associated with the thylakoid membrane, *CURT1B* determines thylakoid architecture by inducing membrane curvature (Armbruster et al., 2013), *THF1* is required for the formation of mature thylakoid stacks from the normal vesicles (Wang et al., 2004), *At3g63540* is involved in the folding and proteolysis of thylakoid proteins (Peltier et al., 2002), and *TERC* is involved in the thylakoid formation (Kwon and Cho, 2008; Schneider et al., 2014). For these four genes related to mitochondrion, *NMAT1* and *NMAT2* are required for mitochondrial biogenesis and the regulation of fundamental metabolic pathways during early developmental stages (Nakagawa and Sakurai, 2006), *SPS3* is involved in the ubiquinone-9 biosynthesis from solanesyl diphosphate (Ducluzeau et al., 2012), and *EMB2247* is involved in the formation of carbon-oxygen bonds in aminoacyl-tRNA (Berg et al., 2005). The up-regulation of these genes involved in photosynthesis and energy will confer *H. perforatum* seedlings to grow robust and adapt cooler temperatures compared with higher temperatures.

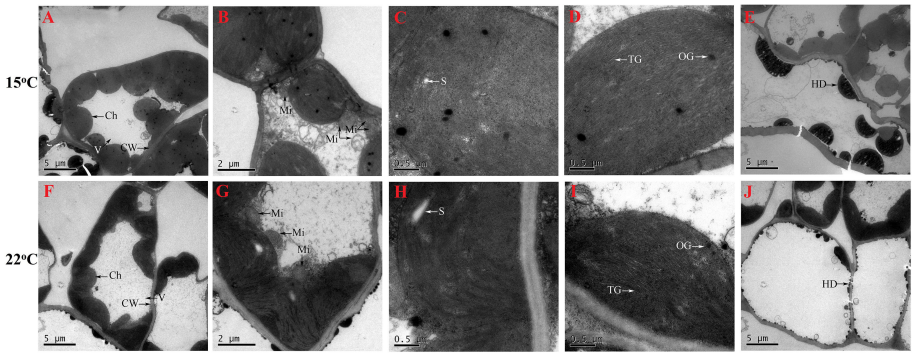

FIGURE 4
Cell ultra-structure for seedlings grown at 15 **(A–E)** and 22°C **(F–J)**. Ch, chloroplast, CW, cell wall; Mi, mitochondria; HD, hemispherical droplets; OG, osmiophilic granule; S, starch grain; TM, thylakoid grana; V, vacuole.

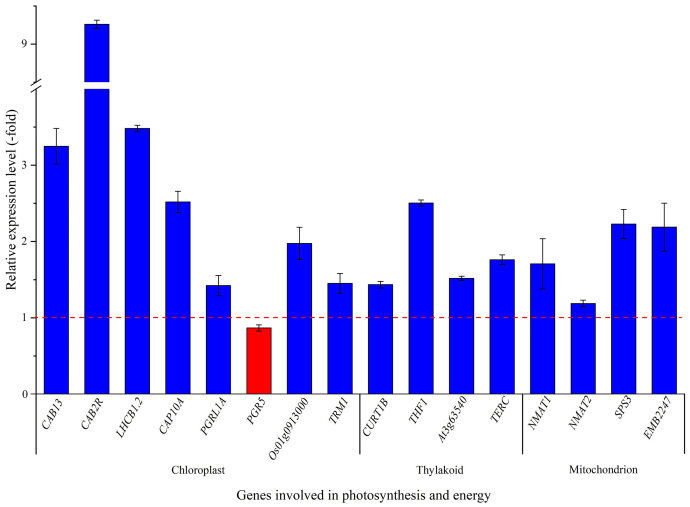

FIGURE 5
The expression level of genes involved in chloroplast, thylakoid and mitochondrion for seedlings grown at 15 versus 22°C, as determined by qRT-PCR (n=3). Column highlighted in blue represents gene up-regulation and red represents gene down-regulation. The red dotted line in the image differentiates up-regulation (>1) and down-regulation (<1) at 15°C compared with 22°C (Control), respectively.

3.6 Low temperature regulates gene expression related to Hyp biosynthesis

3.6.1 Mapping genes related to Hyp biosynthesis

While previous studies have revealed that Hyp is biosynthesized in two separated tissues including: (1) green tissue from glucose to acetyl- and malonyl-CoA, and (2) dark gland from octa-β-ketoacyl chain to Hyp (Zobayed et al., 2006; Rizzo et al., 2019; Yao et al., 2019; Rizzo et al., 2020; Su et al., 2021), Hyp biosynthetic has not been fully elucidated and some genes have still not been identified. In this study, twenty-nine genes participating in Hyp biosynthesis were identified, with 21 genes in green tissue including in glycolysis (10 genes, 8 up-regulated and 2 down-regulated) and fatty acid metabolism (11 genes, 10 up-regulated and 1 down-regulated), and 8 genes in dark gland (6 up-regulated and 2 down-regulated) (Table 1). In the green tissue, acetyl-CoA is formed through photosynthesis, glycolysis (*i.e. PFK2*, *PFK3*, *PFK4*, *PFK5*, *LTA2*, *ENO1*, *HXK1*, *HXK2*, *PFP-ALPHA* and *PFP-BETA*) and pyruvate dehydrogenase (*i.e. PDH-E1*), malonyl-CoA is formed from acetyl-CoA *via* acetyl-CoA carboxylase, meanwhile, fatty acid metabolism (*i.e. CUT1*, *ACOT13*, *Acot9*, *LPD1*, *At3g45770*, *MFP2*, *AIM1*, *ECR*, *HACD2* and *KCR1*) is involved in the biosynthesis of the acetyl-CoA and malonyl-CoA. For the biosynthetic pathway in the dark gland, an octa-β-ketoacyl chain is formed with one acetyl-CoA and seven malonyl-CoAs by the PKS (*i.e. PKSA* and *PKSG5*), emodin anthrone is formed through a series of aldolic condensation, thioesterase (TER) (*i.e. FGRAMPH1_01T20223*), decarboxylic and dehydration reactions, then emodin dianthrone is produced by the oxidation of emodin anthrone as well as the coupling of emodin with emodin anthrone by the phenoloxidative coupling protein (POCP) (*i.e. MALD1* and *STH-2*); finally, Hyp is generated by POCP or berberine bridge enzyme (BBE) (*i.e. At4g20800*) as well as light, oxidation and dehydration reactions (Figure 6). While there is a competitive relationship between the PKS and octaketide synthase (OKS) (*i.e. CHS* and *CHS1*) in this study, because the OKS can catalyze the 4-coumaroyl-CoA and malonyl-CoA precursors into flavonoids (*i.e.* 2',4,4',6'-tetrahydroxychalcone) (Ferrer et al., 1999).

3.6.2 Expression level of genes in green tissue

The relative expression of selected genes in the green tissue were observed to be differentially regulated, with up-regulation of 1.6-, 1.6-, 1.1-, 1.1-, 1.4- and 1.1-fold for the 6 genes *HXK1*, *PFP-ALPHA*, *CUT1*, *Acot9*, *AIM1* and *KCR1*, while down-regulation of 0.8- and 0.8-fold for the 2 genes *PFK2* and *ENO1*, respectively at 15°C compared with 22°C (Figure 7). For selected genes involved in glycolysis, *PFK2* is involved in the formation of fructose 1,6-bisphosphate by phosphorylating D-fructose 6-phosphate (Mustroph et al., 2007), *ENO1* is involved in catalyzing the formation of phosphoenolpyruvate from 2-phosphoglycerate (Allen and Whitman, 2021), *HXK1* and *PFP-ALPHA* are involved in the formation of D-glyceraldehyde 3-phosphate and glycerone phosphate (Todd et al., 1995; Giese et al., 2005). For genes involved in fatty-acid metabolism, *CUT1* participates in both decarbonylation and acyl-reduction wax synthesis pathways (Fiebig et al., 2000), *Acot9* is involved in the formation of free fatty acid and coenzyme A by hydrolyzing of acyl-CoAs (Poupon et al., 1999), *AIM1* is involved in the peroxisomal beta-oxidation pathway for the biosynthesis of benzoic acid (Bussell et al.,

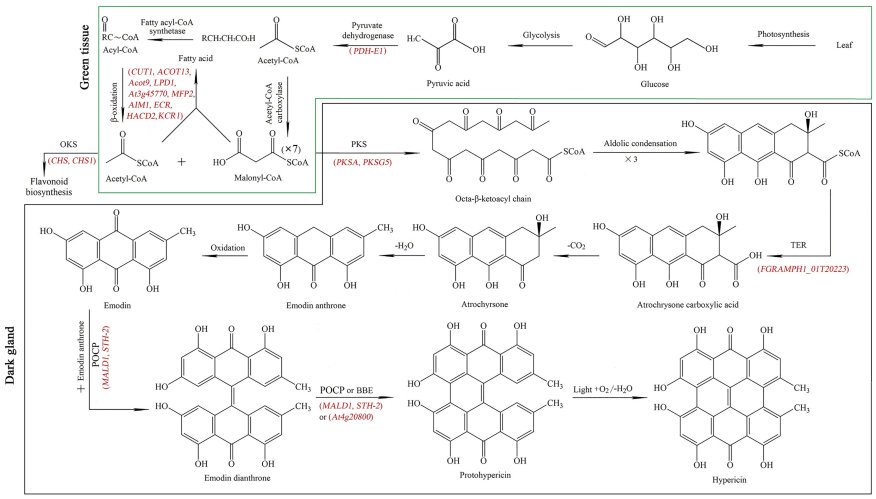

FIGURE 6
Key genes (red color) mapped in the Hyp biosynthetic pathway from glucose to acetyl- and malonyl-CoA in green tissue (green frame), and from acetyl- and malonyl-CoA to Hyp in dark gland (dark frame). PKS: polyketide synthase, OKS: octaketide synthase, TER: thioesterase, POCP: phenoloxidative coupling protein, BBE: berberine bridge enzyme. The Hyp biosynthetic pathway concludes from previous literatures (Zobayed et al., 2006; Rizzo et al., 2019; Rizzo et al., 2020; Su et al., 2021).

2014), and *KCR1* is responsible for the first reduction step in very long-chain fatty acids synthesis (Beaudoin et al., 2009). The up-regulation of these genes in green tissue at cooler temperature is likely to provide abundant acetyl-CoA and malonyl-CoA as precursors for downstream Hyp biosynthesis.

3.6.3 Expression level of genes in dark gland

The relative expression of selected genes in dark glands were also observed to be differentially regulated, with up-regulation of 1.5-, 1.5- and 1.2-fold for the 3 genes *PKSA*, *FGRAMPH1_01T20223* and *At4g20800*, while down-regulation of 0.9-, 0.9- and 0.5-fold for the

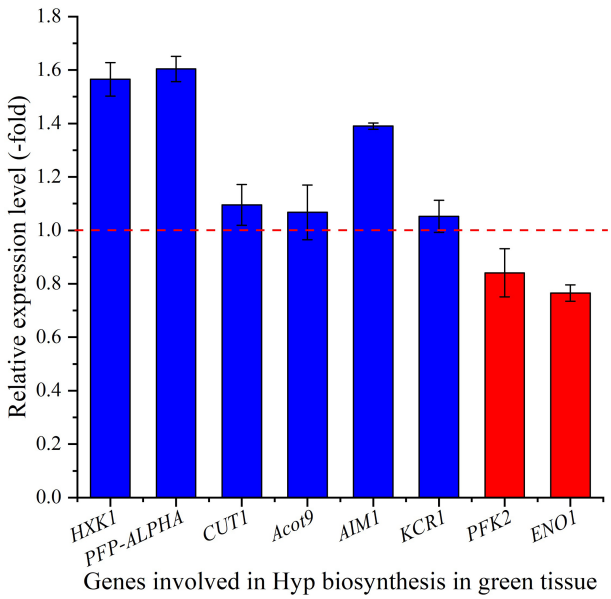

FIGURE 7
The expression level of genes involved in Hyp biosynthesis in green tissue for seedlings grown at 15 versus 22°C, as determined by qRT-PCR (n=3). Column highlighted in blue represents gene up-regulation and red represents gene down-regulation. The red dotted line in the image differentiates up-regulation (>1) and down-regulation (<1) at 15°C compared with 22°C (Control), respectively.

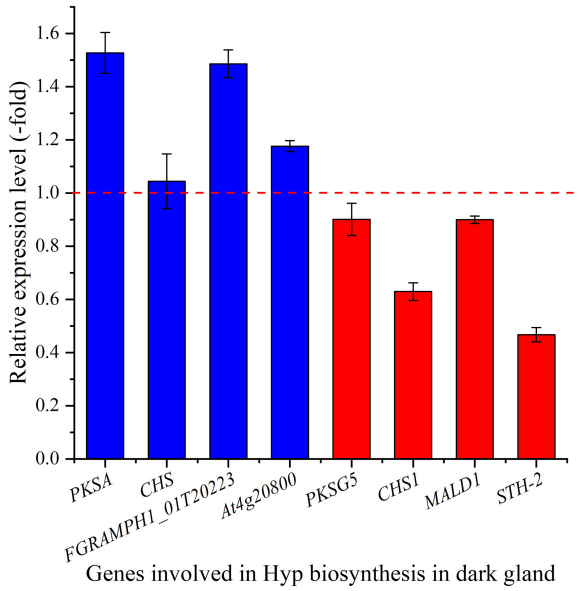

FIGURE 8
The expression level of genes involved in Hyp biosynthesis in dark gland for seedlings grown at 15 versus 22°C, as determined by qRT-PCR (n=3). Column highlighted in blue represents gene up-regulation and red represents gene down-regulation. The red dotted line in the image differentiates up-regulation (>1) and down-regulation (<1) at 15°C compared with 22°C (Control), respectively.

genes *PKSG5*, *MALD1* and *STH-2*, respectively at 15°C compared with 22°C (Figure 8). Both *PKSA* and *PKSG5* encode polyketide synthase that are involved in the condensation of malonyl-CoA units (Mizuuchi et al., 2008; Flores-Sanchez et al., 2010), *FGRAMPH1_01T20223* is predicted to encode TER1 that participates in the formation of emodin anthrone (Kong et al., 2013), *MALD1* and *STH-2* are predicted to encode POCP, and *At4g20800* encodes BBE-like 17 that catalyzes the oxidation of aromatic allylic alcohols (Daniel et al., 2015). The up-regulation of these genes (*PKSA*, *FGRAMPH1_01T20223* and *At4g20800*) in dark glands at a cooler temperature is predicted to play a role in inducing Hyp biosynthesis and accumulation. In this study, the two *CHS* and *CHS1* genes are not up-regulated, and the significant down-regulation (0.63-fold) of *CHS1* might indicate that the reduced temperatures negatively affect phenylpropanoid biosynthesis. If this effect is directly connected to the up-regulation of the Hyp biosynthetic pathway *via* redirecting the pool of 4-coumaroyl-CoA and malonyl-CoA precursors remains to be established. This will require quantitative phenolic profiling by LC-MS combined with flux analysis, but is beyond the scope of this manuscript.

4 Conclusions

In *Hypericum perforatum*, low temperature changes cell structure (*e.g.* dark gland, secretory cell and hemispherical droplet) associated with regulating plant growth and gene expression (*e.g. BBE*, *POCP* and *TER1*) associated with Hyp biosynthesis in leaf green tissue and dark gland. These findings not only further confirm that low temperature enhances plant growth and Hyp biosynthesis (Yao et al., 2019; Tavakoli et al., 2020), but also complement previous transcriptomic analysis (Su et al., 2021). Moreover, these findings will provide useful references for guiding *H. perforatum* cultivation in field or green house, cell and tissue culture, and revealing the mechanism of Hyp biosynthesis to increase Hyp accumulation.

Data availability statement

The datasets presented in this study can be found in online repositories. The names of the repository/repositories and accession number(s) can be found in the article/Supplementary Material.

Author contributions

HS: data curation and investigation. LJ: Resourses. ML: conceptualization, project administration and writing—original draft. PP: writing—review and editing. All authors contributed to the article and approved the submitted version.

Funding

This research was funded by State Key Laboratory of Aridland Crop Science/Gansu Agricultural University (GSCS-2021-Z03), Assurance Project of Ecological Planting and Quality of Daodi Herbs (202103003).

Conflict of interest

The authors declare that the research was conducted in the absence of any commercial or financial relationships that could be construed as a potential conflict of interest.

Publisher's note

Supplementary material

The Supplementary Material for this article can be found online at: https://www.frontiersin.org/articles/10.3389/fpls.2022.1020857/full#supplementary-material

References

Allen, K. N., and Whitman, C. P. (2021). The birth of genomic enzymology: discovery of the mechanistically diverse enolase superfamily. *Biochemistry* 60, 3515–3528. doi: 10.1021/acs.biochem.1c00494

Armbruster, U., Labs, M., Pribil, M., Viola, S., Xu, W., Scharfenberg, M., et al. (2013). *Arabidopsis* CURVATURE THYLAKOID1 proteins modify thylakoid architecture by inducing membrane curvature. *Plant Cell* 25, 2661–2678. doi: 10.1105/tpc.113.113118

Bagdonaitė, E., Mártonfi, P., Repčák, M., and Labokas, J. (2010). Variation in the contents of pseudohypericin and hypericin in *Hypericum perforatum* from Lithuania. *Biochem. Syst. Ecol.* 38, 634–640. doi: 10.1016/j.bse.2010.08.005

Barnes, J., Anderson, L. A., and Phillipson, J. D. (2001). St John's wort (*Hypericum perforatum* l.): a review of its chemistry, pharmacology and clinical properties. *J. Pharm. Pharmacol.* 53, 583–600. doi: 10.1211/0022357011775910

Beaudoin, F., Wu, X., Li, F., Haslam, R. P., Markham, J. E., Zheng, H., et al. (2009). Functional characterization of the *Arabidopsis* beta-ketoacyl-coenzyme a reductase candidates of the fatty acid elongase. *Plant Physiol.* 150, 1174–1191. doi: 10.1104/pp.109.137497

Berg, M., Rogers, R., Muralla, R., and Meinke, D. (2005). Requirement of aminoacyl-tRNA synthetases for gametogenesis and embryo development in *Arabidopsis*. *Plant J.* 44, 866–878. doi: 10.1111/j.1365-313X.2005.02580.x

Bombardelli, E., and Morazzoni, P. (1995). Hypericum perforatum. *Fitoterapia* 66, 43–68.

Briskin, D. P., and Gawienowski, M. C. (2001). Differential effects of light and nitrogen on production of hypericins and leaf glands in *Hypericum perforatum*. plant physiol. *Biochem* 39, 1075–1081. doi: 10.1016/S0981-9428(01)01326-2

Brunáková, K., Petijová, L., Zámecník, J., Turecková, V., and Cellárová, E. (2015). The role of ABA in the freezing injury avoidance in two *Hypericum* species differing in frost tolerance and potential to synthesize hypericins. *Plant Cell. Tiss. Org.* 122, 45–56. doi: 10.1007/s11240-015-0748-9

Bussell, J. D., Reichelt, M., Wiszniewski, A. A., Gershenzon, J., and Smith, S. M. (2014). Peroxisomal ATP-binding cassette transporter COMATOSE and the multifunctional protein abnormal INFLORESCENCE MERISTEM are required for the production of benzoylated metabolites in *Arabidopsis* seeds. *Plant Physiol.* 164, 48–54. doi: 10.1104/pp.113.229807

Capitani, G., Markovic-Housley, Z., DelVal, G., Morris, M., Jansonius, J. N., and ürmann, P. (2000). Crystal structures of two functionally different thioredoxins in spinach chloroplasts. *J. Mol. Biol.* 302, 135–154. doi: 10.1006/jmbi.2000.4006

Ciccarelli, D., Andreucci, A. C., and Pagni, A. M. (2001). Translucent glands and secretory canals in *Hypericum perforatum* L. (Hypericaceae): Morphological, anatomical and histochemical studies during the course of ontogenesis. *Ann. Bot.* 88, 637–644. doi: 10.1006/anbo.2001.1514

Cirak, C., Radušienė, J., Karabük, B., and Janulis, V. (2007). Variation of bioactive substances and morphological traits in *Hypericum perforatum* populations from northern Turkey. *Biochem. Syst. Eco.* 35, 403–409. doi: 10.1016/j.bse.2007.01.009

Couceiro, M. A., Afreen, F., Zobayed, S. M. A., and Kozai, T. (2006). Variation in concentrations of major bioactive compounds of st. john's wort: Effects of harvesting time, temperature and germplasm. *Plant Sci.* 170, 128–134. doi: 10.1016/j.plantsci.2005.08.011

Daniel, B., Pavkov-Keller, T., Steiner, B., Dordic, A., Gutmann, A., Nidetzky, B., et al. (2015). Oxidation of monolignols by members of the berberine bridge enzyme family suggests a role in plant cell wall metabolism. *J. Bio. Chem.* 290, 18770–18781. doi: 10.1074/jbc.M115.659631

Dong, H., Li, M. L., Jin, L., Xie, X. R., Li, M. F., and Wei, J. H. (2022). Cool temperature enhances growth, ferulic acid and flavonoid biosynthesis while inhibiting polysaccharide biosynthesis in *Angelica sinensis*. *Molecules* 27, 320. doi: 10.3390/molecules27010320

Ducluzeau, A. L., Wamboldt, Y., Elowsky, C. G., Mackenzie, S. A., Schuurink, R. C., and Basset, G. J. (2012). Gene network reconstruction identifies the authentic trans-prenyl diphosphate synthase that makes the solanesyl moiety of ubiquinone-9 in *Arabidopsis*. *Plant J.* 69, 366–375. doi: 10.1111/j.1365-313X.2011.04796.x

Erdelmeier, C. (1998). Hyperforin, possibly the major non-nitrogenous secondary metabolite of *Hypericum perforatum* L. *Pharmacopsychiatry* 31, 2–6. doi: 10.1055/s-2007-979339

Ferrer, J. L., Jez, J. M., Bowman, M. E., Dixon, R. A., and Noel, J. P. (1999). Structure of chalcone synthase and the molecular basis of plant polyketide biosynthesis. *Nat. Struct. Biol.* 6, 775. doi: 10.1038/11553

Fiebig, A., Mayfield, J. A., Miley, N. L., Chau, S., Fischer, R. L., and Preuss, D. (2000). Alterations in CER6, a gene identical to CUT1, differentially affect long-chain lipid content on the surface of pollen and stems. *Plant Cell* 12, 2001–2008. doi: 10.2307/3871209

Flores-Sanchez, I. J., Linthorst, H. J., and Verpoorte, R. (2010). In silicio expression analysis of *PKS* genes isolated from *cannabis sativa* L. *Genet. Mol. Biol.* 33, 703–713. doi: 10.1590/S1415-47572010005000088

Germ, M., Stibilj, V., Kreft, S., Gaberš˘cik, A., and Kreft, I. (2010). Flavonoid, tannin and hypericin concentrations in the leaves of st. john's wort (*Hypericum perforatum* L.) are affected by UV-b radiation levels. *Food Chem.* 122, 471–474. doi: 10.1016/j.foodchem.2010.03.008

Giese, J. O., Herbers, K., Hoffmann, M., Kloesgen, R. B., and Sonnewald, U. (2005). Isolation and functional characterization of a novel plastidic hexokinase from nicotiana tabacum. *FEBS Lett.* 579, 827–831. doi: 10.1016/j.febslet.2004.12.071

Glauser, D. A., Bourquin, F., Manieri, W., and Schurmann, P. (2004). Characterization of ferredoxin: Thioredoxin reductase modified by site-directed mutagenesis. *J. Biol. Chem.* 279, 16662–16669. doi: 10.1074/jbc.M313851200

Gotor, C., Alvarez, C., Bermúdez, M. A., Moreno, I., García, I., and Romero, L. C. (2010). Low abundance does not mean less importance in cysteine metabolism. *Plant Signal Behav.* 5, 1028–1030. doi: 10.4161/psb.5.8.12296

Gray, D. E., Pallardy, S. G., Garrett, H. E., and Rottinghaus, G. E. (2003). Effect of acute drought stress and time of harvest on phytochemistry and dry weight of st. john's wort leaves and flowers. *Planta Med.* 69, 1024–1030. doi: 10.1055/s-2003-45150

Hertle, A. P., Blunder, T., Wunder, T., Pesaresi, P., Pribil, M., Armbruster, U., et al. (2013). PGRL1 is the elusive ferredoxin-plastoquinone reductase in photosynthetic cyclic electron flow. *Mol. Cell* 49, 511–523. doi: 10.1016/j.molcel.2012.11.030

Hu, J. J., Wu, W., Cao, Z. H., Wen, J., Shu, Q. L., and Fu, S. L. (2016). Morphological, physiological and biochemical responses of camellia oleifera to low-temperature stress. *Pak. J. Bot.* 48, 899–905.

Karimi, M., Ahmadi, N., and Ebrahimi, M. (2022). Red LED light promotes biomass, flowering and secondary metabolites accumulation in hydroponically grown *Hypericum perforatum* L. (cv. topas). *Ind. Crop Prod.* 175, 114239. doi: 10.1016/j.indcrop.2021.114239

Kaundal, M., Sharma, R., and Kumar, R. (2021). Elevated CO_2 and temperature effect on growth, phenology, biomass and hypericin content of *Hypericum perforatum* L. in the western himalaya. *Plant Physiol. Rep.* 26, 116–127. doi: 10.1007/s40502-021-00571-7

Kong, E., Peng, S., Chandra, G., Sarkar, C., Zhang, Z., Bagh, M. B., et al. (2013). Dynamic palmitoylation links cytosol-membrane shuttling of acyl-protein thioesterase-1 and acyl-protein thioesterase-2 with that of proto-oncogene h-ras product and growth-associated protein-43. *J. Biol. Chem.* 288, 9112–9125. doi: 10.1074/jbc.M112.421073

Kornfeld, A., Kaufman, P. B., Lu, C. R., Gibson, D. M., Bolling, S. F., Warber, S. L., et al. (2007). The production of hypericins in two selected *Hypericum perforatu*m shoot cultures is related to differences in black gland structure. *Plant Physiol. Bioch.* 45, 24–32. doi: 10.1016/j.plaphy.2006.12.009

Kwon, K. C., and Cho, M. H. (2008). Deletion of the chloroplast-localized *AtTerC* gene product in *Arabidopsis* thaliana leads to loss of the thylakoid membrane and to seedling lethality. *Plant J.* 55, 428–442. doi: 10.1111/j.1365-313X.2008.03523.x

Li, L., Li, N. H., and Jiang, S. M. (2009). *Experimental guidance of plant physiology module* (Beijing: Science Press), 22–39.

Li, M. F., Lv, M., Yang, D. L., Wei, J. H., Xing, H., and Pare, P. W. (2020). Temperature-regulated anatomical and gene-expression changes in *sinopodophyllum hexandrum* seedlings. *Ind. Crop Prod.* 152, 112479. doi: 10.1016/j.indcrop.2020.112479

Li, X. F., and Zhang, Z. L. (2016). *Guidance for plant physiology experiments, 5th edition* (Beijing: Higher Education Press), 30–31.

Love, M. I., Huber, W., and Anders, S. (2014). Moderated estimation of fold change and dispersion for RNAseq data with DESeq2. *Genome Biol.* 15, 550. doi: 10.1186/s13059-014-0550-8

Lv, H. F., and Hu, Z. H. (2001). Studies on the development of secretory structures and their secretory products accumulation of *Hypericum perforatum*. *Acta Bota Boreal-Occident Sin.* 21, 287–292. doi: 10.3321/j.issn:1000-4025.2001.02.016

Maia, R. M., Valente, V., Cunha, M. A., Cunha, M. A. V., Sousa, J. F., Araujo, D. D., et al. (2007). Identification of unannotated exons of low abundance transcripts in drosophila melanogaster and cloning of a new serine protease gene upregulated upon injury. *BMC Genomics* 8, 249. doi: 10.1186/1471-2164-8-249

Mizuuchi, Y., Shimokawa, Y., Wanibuchi, K., Noguchi, H., and Abe, I. (2008). Structure function analysis of novel type III polyketide synthases from *Arabidopsis thaliana*. Biol. *Pharm. Bull.* 31, 2205–2210. doi: 10.1248/bpb.31.2205

Munekage, Y., Hojo, M., Meurer, J., Endo, T., Tasaka, M., and Shikanai, T. (2002). *PGR5* is involved in cyclic electron flow around photosystem I and is essential for photoprotection in *Arabidopsis*. *Cell* 110, 361–371. doi: 10.1016/S0092-8674(02)00867-X

Mustroph, A., Sonnewald, U., and Biemelt, S. (2007). Characterisation of the ATP-dependent phosphofructokinase gene family from *Arabidopsis thaliana*. *FEBS Lett.* 581, 2401–2410. doi: 10.1016/j.febslet.2007.04.060

Nahrstedt, A., and Butterweck, V. (1997). Biologically active and other chemical constituents of the herb of *Hypericum perforatum* L. *Pharmacopsychiatry* 30, 129–134. doi: 10.1055/s-2007-979533

Najafabadi, A. S., Khanahmadi, M., Ebrahimi, M., Moradi, K., Behroozi, P., and Noormohammadi, N. (2019). Effect of different quality of light on growth and production of secondary metabolites in adventitious root cultivation of *Hypericum perforatum.* Plant Signal. *Behav* 14, 1559–2324. doi: 10.1080/15592324.2019.1640561

Nakagawa, N., and Sakurai, N. (2006). A mutation in At-nMat1a, which encodes a nuclear gene having high similarity to group II intron maturase, causes impaired splicing of mitochondrial NAD4 transcript and altered carbon metabolism in *Arabidopsis thaliana*. *Plant Cell Physiol.* 47, 772–783. doi: 10.1093/pcp/pcj051

Napoli, E., Siracusa, L., Ruberto, G., Carrubba, A., Lazzara, S., Speciale, A., et al. (2018). Phytochemical profiles, phototoxic and antioxidant properties of eleven *Hypericum* species–a comparative study. *Phytochemistry* 152, 162–173. doi: 10.1016/j.phytochem.2018.05.003

Peltier, J. B., Emanuelsson, O., Kalume, D. E., Ytterberg, J., Friso, G., Rudella, A., et al. (2002). Central functions of the lumenal and peripheral thylakoid proteome of *Arabidopsis* determined by experimentation and genome-wide prediction. *Plant Cell* 14, 211–236. doi: 10.1105/tpc.010304

Poupon, V., Begue, B., Gagnon, J., Dautry-Varsat, A., Cerf-Bensussan, N., and Benmerah, A. (1999). Molecular cloning and characterization of MT-ACT48, a novel mitochondrial acyl-CoA thioesterase. *J. Biol. Chem.* 274, 19188–19194. doi: 10.1074/jbc.274.27.19188

Rizzo, P., Altschmied, L., Ravindran, B. M., Rutten, T., and D'Auria, J. C. (2020). The biochemical and genetic basis for the biosynthesis of bioactive compounds in *Hypericum perforatum* L., one of the largest medicinal crops in Europe. *Genes* 11, 1210. doi: 10.3390/genes11101210

Rizzo, P., Altschmied, L., Stark, P., Rutten, T., Guendel, A., Scharfenberg, S., et al. (2019). Discovery of key regulators of dark gland development and hypericin biosynthesis in st. john's wort (*Hypericum perforatum*). *Plant Biotechnol. J.* 17, 2299–2312. doi: 10.1111/pbi.13141

Robinson, M. D., McCarthy, D. J., and Smyth, G. K. (2009). EdgeR: A bioconductor package for differential expression analysis of digital gene expression data. *Brief Bioinform.* 26, 139–140. doi: 10.1093/bioinformatics/btp616

Schneider, A., Steinberger, I., Strissel, H., Kunz, H. H., Manavski, N., Meurer, J., et al. (2014). The *Arabidopsis* tellurite resistance c protein together with ALB3 is involved in photosystem II protein synthesis. *Plant J.* 78, 344–356. doi: 10.1111/tpj.12474

Soták, M., Czeranková, O., Klein, D., Jurčacková, Z., Li, L., and Čellárová, E. (2016). Comparative transcriptome reconstruction of four *Hypericum* species focused on hypericin biosynthesis. *Front. Plant Sci.* 7. doi: 10.3389/fpls.2016.01039

Stoyanova-Koleva, D., Stefanova, M., Ganeva, T. S., and Cellárová, E. (2015). Structural modifications in the mesophyll associated with cryopreservation of seven *Hypericum* species. *Biol. Plantarum.* 59, 214–520. doi: 10.1007/s10535-015-0528-8

Su, H. Y., Li, J., Chen, S. J., Sun, P., Xing, H., Yang, D. L., et al. (2021). Physiological and transcriptomic analysis provide insight into low temperature enhancing hypericin biosynthesis in *Hypericum perforatum*. *Molecules* 26, 2294. doi: 10.3390/molecules26082294

Taiz, L., and Zeiger, E. (2010). "The control of flowering," in *Plant physiology, 5th Edition*. Eds. D. E. Fosket and R. Amasino (Sunderland, MA, USA: Sinauer Associates, Inc), 559–590.

Tavakoli, F., Rafieiolhossaini, M., Ravash, R., and Ebrahimi, M. (2020). UV-B radiation and low temperature promoted hypericin biosynthesis in adventitious root culture of *Hypericum perforatum.* Plant Signal. *Behav* 15, 1764184. doi: 10.1080/15592324.2020.1764184

Todd, J. F., Blakeley, S. D., and Dennis, D. T. (1995). Structure of the genes encoding the alpha- and beta-subunits of castor pyrophosphate-dependent phosphofructokinase. *Gene* 152, 181–186. doi: 10.1016/0378-1119(94)00646-A

Walker, L., Sirvent, T., Gibson, D., and Vance, N. (2001). Regional differences in hypericin and pseudohypericin concentrations and five morphological traits among *Hypericum perforatum* plants in the northwestern united states. *Can. J. Bot.* 79, 1248–1255. doi: 10.1139/cjb-79-10-1248

Wang, S. H., Liang, W. X., Yao, L., Wang, J., and Gao, W. Y. (2019). Effect of temperature on morphology, ginsenosides biosynthesis, functional genes, and transcriptional factors expression in *Panax ginseng* adventitious roots. *J. Food Biochem.* 43, e12794. doi: 10.1111/jfbc.12794

Wang, Q., Sullivan, R. W., Kight, A., Henry, R. L., Huang, J., Jones, A. M., et al. (2004). Deletion of the chloroplast-localized thylakoid formation1 gene product in *Arabidopsis* leads to deficient thylakoid formation and variegated leaves. *Plant Physiol.* 136, 3594–3604. doi: 10.1104/pp.104.049841

Willems, E., Leyns, L., and Vandesompele, J. (2008). Standardization of real-time PCR gene expression data from independent biological replicates. *Anal. Biochem.* 379, 127–129. doi: 10.1016/j.ab.2008.04.036

Yang, J. J., Qu, Y., and Cui, X. M. (2014). Determination of chloropyll and carotenoid in the aerial part of Panax Notoginseng. *Special Wild Econ. Animal Plant Res.* 2, 63–66. doi: 10.3969/j.issn.1001-4721.2014.02.016

Yao, Y. Y., Kang, T. L., Jin, L., Liu, Z. H., Zhang, Z., Xing, H., et al. (2019). Temperature-dependent growth and hypericin biosynthesis in *Hypericum perforatum*. Plant Physiol. *Biochem* 139, 613–619. doi: 10.1016/j.plaphy.2019.04.012

Zhang, J. H., Huang, W. D., Liu, Y. P., and Pan, Q. H. (2005). Effects of temperature acclimation pretreatment on the ultrastructure of mesophyll cells in young grape plants (*Vitis vinifera* l. cv. jingxiu) under cross-temperature stresses. *J. Integr. Plant Biol.* 47, 959–970. doi: 10.1111/j.1744-7909.2005.00109.x

Zhang, R. F., Ji, Y. Y., Morcol, T., Lin, F. K., Gu, R. H., Kennelly, E. J., et al. (2021). UPLC-QTof-MS chemical profiling and characterization of antiproliferative and anti-inflammatory compounds from seven *Hypericum* species in China. *Ind. Crop Prod.* 173, 114156. doi: 10.1016/j.indcrop.2021.114156

Zobayed, S. M. A., Afreen, F., Goto, E., and Kozai, T. (2006). Plant–environment interactions: Accumulation of hypericin in dark glands of *Hypericum perforatum*. *Ann. Bot.* 98, 793–804. doi: 10.1093/aob/mcl169

Zobayed, S. M. A., Afreen, F., and Kozai, T. (2005). Temperature stress can alter the photosynthetic efficiency and secondary metabolite concentrations in st. john's wort. *Plant Physiol. Biochem.* 43, 977–984. doi: 10.1016/j.plaphy.2005.07.013

Zou, Z., Li, M. Y., Jia, R. Z., Zhao, H., He, P. P., Zhang, Y. L., et al. (2020). Genes encoding light-harvesting chlorophyll a/b-binding proteins in papaya (*Carica papaya* l.) and insight into lineage-specific evolution in *Brassicaceae*. *Gene* 748, 144685. doi: 10.1016/j.gene.2020.144685

frontiers | Frontiers in Plant Science

TYPE Original Research
PUBLISHED 28 October 2022
DOI 10.3389/fpls.2022.1042855

OPEN ACCESS

EDITED BY
Jin-Lin Zhang,
Lanzhou University, China

REVIEWED BY
Peng Zhou,
Shanghai Jiao Tong University, China
Faisal Zulfiqar,
The Islamia University of Bahawalpur, Pakistan

*CORRESPONDENCE
Jinmin Fu
turfcn@qq.com

†These authors have contributed equally to this work

SPECIALTY SECTION
This article was submitted to Plant Abiotic Stress, a section of the journal Frontiers in Plant Science

RECEIVED 13 September 2022
ACCEPTED 11 October 2022
PUBLISHED 28 October 2022

CITATION
Zhou X, Yin Y, Wang G, Amombo E, Li X, Xue Y and Fu J (2022) Mitigation of salt stress on low temperature in bermudagrass: resistance and forage quality.
Front. Plant Sci. 13:1042855.
doi: 10.3389/fpls.2022.1042855

Mitigation of salt stress on low temperature in bermudagrass: resistance and forage quality

Xiuwen Zhou†, Yanling Yin†, Guangyang Wang, Erick Amombo, Xiaoning Li, Ying Xue and Jinmin Fu*

Coastal Salinity Tolerant Grass Engineering and Technology Research Center, Ludong University, Yantai, China

Climate change causes plants encountering several abiotic stresses simultaneously. Responses of plants to a single stress has been comprehensively studied, but it is hard to speculated infer the effects of stress combination based on these researches. Here, the response mechanism of bermudagrass to low temperature and salt treatment was investigated in this study. The results showed that low temperature (LT) treatment decreased the relative growth rate, chlorophyll fluorescence transient curve, biomass, and crude fat content of bermudagrass, whereas low temperature + salt (LT+S) treatment greatly undermined these declines. Furthermore, at 6 h and 17 d, the expression levels of *glyoxalase I* (*GLYI*), *Cu-Zn/superoxide dismutase* (*Cu-Zn/SOD*), *peroxidase 2* (*POD2*), and *oxidative enzyme 1*(*CAT1*) in roots were considerably higher in the low temperature + salt treatment than in the low temperature treatment. Low temperature stress is more detrimental to bermudagrass, but mild salt addition can mitigate the damage by enhancing photosynthesis and improving the expression of antioxidant system genes (*Cu-Zn/SOD*, *POD2* and *CAT1*) and glyoxalase system *GLYI* gene in roots. This study summarized the probable interaction mechanism of low temperature and salt stress on bermudagrass, which can provide beneficial reference for the growth of fodder in cold regions.

KEYWORDS

bermudagrass, low temperature, salt, photosynthesis, antioxidant, glyoxalase

Abbreviations: CK, control treatment; S, salt treatment; LT, low temperature treatment; LT+S, low temperature + salt treatment; GLY, glyoxalase; SOD, superoxide dismutase; POD, peroxidase; CAT, oxidative enzyme; MG, methylglyoxal; GSH, glutathione; ASA, ascorbic acid; SOS, salt overly sensitive; HKT, high affinity transporter.

1 Introduction

Bermudagrass, as a popular forage and warm season turfgrass, shows limited growth and begins to wilt when the daily mean temperature goes below 12°C, and then it enters the dormancy period when the temperature reaches 7-10°C (Munshaw et al., 2004; Huang et al., 2019). Low temperature restricts the establishment of bermudagrass in cold region. In addition, bermudagrass has advantages in the restoration of saline-alkali land due to resistance against salt stress (Xie et al., 2017). Therefore, bermudagrass often suffers from combination both of low temperature and salt stress.

Low temperature and salt stress lead to shared or specific physiological, metabolic and genes expression responses. It is well known that low temperature and salt stress restrain plant growth and reduce photosynthesis (Allen and Ort, 2001; Hasdai et al., 2006; Li et al., 2019; Zulfiqar and Ashraf, 2021b; Zulfiqar et al., 2022b). Plants experienced chloroplast structural damage, chlorophyll degradation, stomatal closure and enzyme activity decrease during both low temperature and salt stress (Meloni et al., 2003; Nowicka et al., 2018). Oxidative stress resulted from over accumulation of reactive oxygen species (ROS) and osmotic stress appear in plant response to both low temperature and salt stress (Hasanuzzaman et al., 2020a; Zulfiqar and Ashraf, 2021a; Zulfiqar and Ashraf, 2022a). Both oxidative and osmotic stress have negative effects on plant metabolism, molecular biosynthesis and cell viability (Mahajan and Tuteja, 2005; Liang et al., 2018; Zulfiqar et al., 2019; Munns et al., 2020; Zhao et al., 2021). Furthermore, both low temperature and salt stress cause alteration in ion homeostasis, which destroy the biological activity of membrane and some enzymes (Fürtauer et al., 2019; Shao et al., 2020). Differently, salt stress results in a toxic concentration of Na^+ and inhibits absorption of K^+ (Kim et al., 2007; Yang and Guo, 2018). Many specific ions transported genes are responsible for transportation of Na^+ and K^+, such as *SOS* (salt overly sensitive) family genes and *HKT* (high affinity transporter) (Li et al., 2019). Low temperature disturbs transmembrane H^+ gradient by changing the activity of a H^+ pumping protein, H^+-ATPase (Ponce-Pineda et al., 2021).

Plants are equipped with fine tune resistant mechanisms to counter low temperature and salt stress (Banerjee et al., 2018). Osmoprotectants such as proline and soluble sugar are biosynthesized to remit molecular denaturation (Fürtauer et al., 2019; Zulfiqar et al., 2019; Munns et al., 2020). Plants have a complex antioxidant system, which includes enzymatic system as well as the glutathione-ascorbic acid (GSH-ASA) cycle (Bela et al., 2015). Antioxidant systems are activated to scavenge ROS. For example, antioxidant enzymes such as SOD (superoxide dismutase), POD (enzymes peroxidase) and CAT (oxidative enzyme) and their encoding genes are upregulated in the early stress response (Hasanuzzaman et al., 2020a; Hasanuzzaman et al., 2020b; Shao et al., 2020; Zulfiqar et al., 2020a; Zulfiqar and Ashraf, 2021a; Jabeen et al., 2022; Zulfiqar and Ashraf, 2022a). SOD has the ability to catalyze the conversion of superoxide anions to H_2O_2 and O_2, which is the primary substance for scavenging free radicals in living things. H_2O_2 is scavenged by enzymes CAT and POD through synergistic action to maintain a stable level of free radicals in plants (Yan et al., 2010). In addition, glyoxalase (GLY) system, closely related to GSH metabolism, was reported to participate in stress responses in the past, such as salt and heavy metal stress (Yadav et al., 2005; Singla-Pareek et al., 2006; Roy et al., 2008; Singla-Pareek et al., 2008). GLY is a type of intracellular enzyme found in both prokaryotes and eukaryotes which is mostly sublocalized in the cytoplasm and organelles. GLY system has long been known in animals and is assumed to be engaged in a variety of tasks, including cell division, proliferation, and protection against oxoaldehyde toxicity (Thornalley, 1990). In plants, salt stress increased GlLYI activity, which is accompanied by MG detoxification and decrease in GSH concentration(Parvin et al., 2019).

At the moment, the global climate and environment are rapidly changing, and plants are being subjected to an increasing number of abiotic stresses (Zulfiqar and Hancock, 2020b; Zulfiqar et al., 2021c). However, plants are endowed with unique physiological responses under combined stress which are completely different from those under single stress (Bai et al., 2018; Henriet et al., 2019). Many studies have reported that the negative effects of stress interactions on crop productivity are much higher than when different stress components are applied alone (Mittler and Blumwald, 2010; Suzuki et al., 2014). The relative water content of tomato (Rong et al., 2017) and the biomass of Phragmites Karka (Abideen et al., 2022) were significantly decreased under compound stress. Drought and heat stress can lead to a significant reduction in Arabidopsis growth, but their combined stress has a more deleterious effect (Vile et al., 2012). However, other studies have reported the beneficial effects of the interaction of two different stresses applied simultaneously (Suzuki et al., 2014). For example, drought stress may offer protection against O_3 damage in plants (Biswas and Jiang, 2011; Zhang et al., 2019) and resulted in reduced susceptibility to powdery mildew and Botrytis cinerea (Achuo et al., 2006). Combined stress of drought and salt can reduce boron toxicity in plants (Liu et al., 2018)

Previous research has typically focused on either low temperature or salt stress, with only a few studies have been done related to the combined effect of low temperature and salt stress on plants. Bermudagrass is a valuable forage grass and warm season turfgrass with a high salt tolerance. It is critical to investigate the physiological and molecular mechanisms of bermudagrass under the combined stress of low temperature and salt, in order to improve tolerance and lengthen the growth cycle. In this study, we used physiological and molecular methods to assess the effects of low temperature and salt stress on growth traits, photosynthesis, forage quality, and stress-

related gene expression in this study. As a result, the goals of this study were to: (1) investigate the interaction of low temperature and salt on bermudagrass; and (2) elucidate the synergistic mechanism of low temperature and salt.

2 Materials and methods

2.1 Plant materials and growth condition

In this investigation, bermudagrass (*Cynodon dactylon*(L.) Pers.) "A12359" was used. On 6 July 2019, the bermudagrasses with uniformly cut roots were transplanted from the fields into plastic containers (4 cm in diameter and 21 cm deep) which filled with commercially available plant media, 36 pots in total were transplanted. The plants were kept in a controlled greenhouse with natural light (240 $\mu molm^{-2}s^{-1}$), a 30/24°C average day/night temperature, and 50% relative humidity. The grasses were fertilized with 1/2 Hoagland nutrient solution ($NH_4H_2PO_4$ (0.5 mM), KNO_3 (2.5 mM), Ca $(NO_3)_2.4H_2O$ (2.5 mM), $MgSO_4.7H_2O$ (1 mM), H_3BO_3 (1.43 mg), $ZnSO_4.7H_2O$ (0.11 mg), $CuSO_4{\cdot}5H_2O$ (0.04 mg), $MnCl_2.4H_2O$ (0.91 mg), H_2MoO_4 (0.05 mg), Fe-EDTA (0.04 mM)) twice a week. After three weeks, 24 potted plants were selected and clipped consistently to 14 cm, then placed to a plant incubator on 27 July 2019.

2.2 Treatments and experimental design

Control (CK), salt (S), low temperature (LT), low temperature +salt (LT+S) were the four experimental treatments. There were six pots for each treatment and a random block design was used to minimize the impact of environmental conditions. The LT and LT +S treatments were 15/10°C (day/night), while the others were 35/30°C (day/night). S and LT+S treatments were grown for 3 d with 1.0 percent salt solution, then 1.5 percent for 3 d, and finally 2.0 percent salt solution, until the material exhibited a substantial phenotype difference (17 d). Dilution of sea water yielded the saline solution. In the plant incubator, the plants were kept at $240\mu molm^{-2}s^{-1}$ photosynthetically active radiation, a 16-hour photoperiod, and 50% relative humidity. At 17 d following treatment (August 13, 2019), leaves and roots were harvested for physiological investigation, and gene expression levels in the leaves and roots were measured at 6 h and 17 d. These plants' chlorophyll fluorescence and chlorophyll content were also measured at 3, 6 and 17 d of age.

2.3 Methods

2.3.1 Phenotypic determination

Root length: All treated plants was measured with a ruler after roots had been washed and drained on absorbent paper.

Plant height: On d 3 (July 30, 2019), 6 (August 2, 2019) and 17 (August 13, 2019), the plant height was measured with a ruler.

Plant samples were heated in an oven at 105°C for 30 minutes before being dried to constant weight at 80°C and weighed on a 1/10000 precision balance.

2.3.2 Chlorophyll content

We took 0.1 g of fresh leaves and cut them short (about 0.5 cm long), then placed them in a 15 ml centrifuge tube with 10 ml dimethyl sulfoxide and shaded them for 2-3 d. In a centrifuge tube, 1ml chlorophyll extract and 2 ml dimethyl sulfoxide were mixed and poured into a colorimetric dish. The absorbance is measured at 663 nm and 645 nm wavelengths using dimethyl sulfoxide as the blank. Three potted plants were collected per treatment.

2.3.3 Chlorophyll a fluorescence transient and the JIP-Test

A pulse-amplitude modulation fluorometer was used to create a fluorescence transient of chlorophyll a. (PAM2500, Heinz Walz GmbH). After 30 minutes of dark adaptation, the shoots (same position of plants in each treatment) were exposed to a red light of 3,000µmol photons $m^{-2}s^{-1}$. There were three replicates from different potted plants of each treatment. JIP-test was used as Table 1 to better analyze the OJIP curve.

2.3.4 Measurement of nutritive value

Na^+ and K^+: We weighed 0.1 g of the material into the desiccating tube, added 10 ml H2SO4, and placed it in the graphite digesting device. The amount of Na^+ and K^+ was determined using a flame spectrophotometer after the desiccated sample was diluted 100 times. For each treatment, three biological replicates collected from different potted plants.

2.3.5 Quantitative RT -PCR analysis

For each treatment, three biological replicates were taken from different potted plants. Trizol reagent (Invitrogen, America) was used to isolated total RNA from about 0.1 g samples of leaves and roots. DNaseI was used to remove contaminating genomic DNA from RNA. A UV spectrophotometry NanoDrop was used to examine the RNA concentration and purity (Thermo Fisher Scientific, Lenexa, Ks, USA). Using a Hifair III 1st Strand cDNA Synthesis SuperMix for qPCR with genome-DNA-removing enzyme, 2.5 ug RNA was reverse transcribed to cDNA (Yesen, Nanjing, China). The qPCR was carried out on a Quant Studio 6 detection system (ABI, Forster City, CA, USA) with a SYBR green PCR mix (Takara, RR420A, Shika, Japan). The following was the real-time PCR program: 95°C for 5 minutes; 40 cycles of 95°C for 10 seconds and 60°C for 30 seconds. Table 2 contains a list of primers. For gene expression level analysis, the bermudagrass

TABLE 1 Photosynthetic parameters deduced by the JIP-test analysis of fluorescence transients.

	1.0% Salt				1.5% Salt				2.0% Salt				Definitions
	CK	S	LT	LT +S	CK	S	LT	LT +S	CK	S	LT	LT+S	
DATA EXTRACTED FROM THE RECORDED OJIP FLUORESCENCE TRANSIENT CURVES													
F_0=F20$_{\mu s}$	0.54b	0.55b	0.65a	0.63ab	0.53ab	0.47b	0.61a	0.58a	0.64a	0.57a	0.56a	0.58a	Fluorescence at time t after onset of actinic illumination
F_K	1.09a	1.12a	1.08a	0.99a	1.18a	1.00b	0.87b	0.88a	1.48a	1.26b	0.68d	0.81c	Fluorescence value at 300μs
F_J	1.32ab	1.39a	1.23ab	1.13b	1.38a	1.27a	0.97b	0.99b	1.60a	1.42b	0.87c	0.71d	Fluorescence value at the J-step of OJIP
F_I	1.78a	1.78a	1.59b	1.38c	1.75a	1.69a	1.16b	1.11b	1.85a	1.68b	0.74d	0.96c	Fluorescence value at the I-step of OJIP
F_P=F_M	1.91a	1.89a	1.68b	1.47c	1.87a	1.81a	1.18b	1.25b	1.94a	1.76b	0.79c	1.03d	Fluorescence value at the peak of OJIP test
M_0	1.61a	1.72a	1.66a	1.71a	1.93a	1.57b	1.82b	1.82ab	0.93a	0.93a	0.79b	0.83b	Approximate value of the initial slope of fluorescence transient curves
V_J	0.57a	0.63a	0.56a	0.60a	0.64a	0.60a	0.64a	0.61a	0.74a	0.71a	0.67ab	0.62b	Relative variable fluorescence at J-step
Area	24.57a	22.58a	21.56a	18.83a	21.4b	24.79a	14.82c	15.98b	18.64a	18.31a	10.53c	14.7b	the area above the chlorophyll fluorescence curve between Fo and Fm
N	49.90b	46.06b	61.70a	61.27a	48.26b	48.43b	75.47a	71.02a	49.95b	50.01a	150.60a	112.94ab	number of Q_A redox turnovers until Fm is reached
SPECIFIC ENERGY FLUXES (PER ACTIVE PSII REACTION CENTER)													
ABS/RC	3.91b	3.86b	4.81a	5.05a	4.25b	3.55c	5.99a	5.55a	5.21b	4.82b	11.35a	7.82ab	Absorbed photon flux per RC
TR_0/RC	2.82a	2.75a	2.95a	2.89a	3.04a	2.63b	2.87ab	2.99ab	3.51a	3.23a	3.36a	3.33a	Trapped excitation flux (leading to QA reduction) per RC
ET_0/RC	1.20a	1.03a	1.30a	1.17a	1.11a	1.06a	1.05a	1.16a	0.93a	0.95a	1.12a	1.16a	Electron transport flux (further than QA-) per RC
QUANTUM YIELDS AND EFFICIENCIES/PROBABILITIES													
φP_0= TR_0/ ABS	0.72a	0.71a	0.62b	0.57b	0.71a	0.74a	0.48b	0.54b	0.68a	0.67a	0.30c	0.43b	Maximum quantum yield for primary photochemistry
ΨE_0= ET_0/TR_0	0.43a	0.37a	0.44a	0.41a	0.36a	0.40a	0.36a	0.39a	0.17b	0.30b	0.33ab	0.38a	Efficiency/probability with which a PSII trapped electron is transferred from Q_A to Q_B
φE_0= ET_0/ABS	0.31a	0.27a	0.27a	0.24a	0.26a	0.30a	0.18b	0.21b	0.18a	0.20a	0.10b	0.16a	Quantum yield of the electron transport flux from Q_A to Q_B
σR_0= RE_0/ET_0	0.23b	0.22b	0.20b	0.27a	0.25ab	0.23b	0.35a	0.35a	0.27b	0.26b	0.64a	0.46ab	Efficiency/probability with which an electron from Q_B is transferred until PSI acceptors
φR_0= RE_0/ABS	0.65a	0.57a	0.55a	0.65a	0.67a	0.70a	0.63a	0.77a	0.05b	0.05b	0.06ab	0.08a	Quantum yield for reduction of end electron acceptors at the PSI acceptor side
γRC	0.21a	0.21a	0.17b	0.17b	0.19b	0.22a	0.14c	0.15c	0.16a	0.18a	0.08b	0.12b	Probability that a PSII Chl molecule functions as RC
RC/ABS	0.26a	0.26a	0.21b	0.21b	0.24b	0.28a	0.17c	0.18c	0.19a	0.21a	0.13b	0.09b	Number of QA reducing RCs per PSII antenna Chl
PERFORMANCE INDEXES (PI, COMBINATION OF PARAMETERS)													
PI_{ABS}	0.40a	0.32ab	0.22ab	0.15b	0.29b	0.43a	0.08c	0.12c	0.12a	0.15a	0.02b	0.06b	PI (potential) for energy conservation from exciton to the reduction of intersystem electron
PI_{total}	0.12a	0.09a	0.06a	0.06a	0.09b	0.13a	0.04d	0.06c	0.05a	0.05a	0.04a	0.05a	PI (potential) for energy conservation from exciton to the reduction of PSI end acceptors

Each parameter is calculated according to pervious method (Yusuf et al., 2010). Subscript "0" denotes that the parameter refers to the onset of illumination. Values are given as the average of 3 replicates, and different letters denote statistic significant difference at $P < 0.05$ among the treatments by Tukey's multiple range tests.

Actin gene was used as an inner control, and the comparative Ct method was used.

2.4 Data analysis

All treatments were repeated three times. All the data was subjected to analysis of variance (AVOVA) with the Duncan's multiple range tests means at a significant level of $P<0.05$ using the statistical package SPSS 16.0, Origin Pro 9.0 and Excel 2019 for Windows.

3 Results

3.1 Effects of low temperature and salt stress on the growth and physiological characteristics of bermudagrass

Bermudagrass growth was hindered under the three stress regimes. However, the development of bermudagrass under the LT+S treatment was superior to that under the LT treatment

(Figure 1A). LT treatment and LT+S treatment drastically decreased the relative growth rate of shoot compared to control (Figure 1B). In comparison to the relative growth rate of shoots under 1.0 percent salt concentration, the relative growth rate of shoots under 1.5 percent and 2.0 percent salt concentration was further reduced with the continuous increase of salt concentration. However, there was no statistically significant difference in relative growth rate between combined stress and LT treatment (Figure 1B). When plants were subjected to salt and low temperature stress, the length of their roots exhibited an obvious elongation character (Figure 1C). Plant shoots dry weight decreased in all three stress treatments when compared to the control, and there was no difference between the LT and LT+S treatments (Figure 1D). The root dry weight increased significantly after salt treatment alone, and combined stress alleviates single low temperature damage (Figure 1E).

3.2 Effects of low temperature and salt stress on the photosynthetic efficiency of bermudagrass

The OJIP fluorescence transient curves were plotted in Figure 2 to show the effects of low temperature and salt on the photosynthetic efficiency of bermudagrass. The chlorophyll fluorescence transient response curve did not change significantly when treated with 1.0 percent salt compared to the control, but it was significantly reduced when treated with low temperature (Figure 2A). Furthermore, in the 2.0 percent range, the LT+S treatment curve rose with increasing salt concentration and was significantly higher than the LT treatment alone (Figure 2C). The values of basic fluorescence parameters were extracted from the recorded OJIP curve, and several structural and functional parameters were calculated and analyzed (Table 1). When salt content was less than 2.0 percent, area, φP_0 and φE_0 was greatly reduced under low temperature compared to the control, but significantly increased under LT+S stress compared to the LT treatment. All of these findings suggest that salt treatment can help plants recover from the effects of low temperature treatment. At salt concentrations of 1.0 percent and 1.5 percent, there was no difference in chlorophyll content between the LT+S treatment and the LT treatment, but at 2.0 percent, the chlorophyll content of the LT +S treatment was much lower than that of the LT treatment (Figure 2D). To summarize, combined stress affects photosynthetic performance by regulating PSII rather than chlorophyll content.

3.3 Effects on ionic homeostasis of bermudagrass under low temperature and salt stress

We measured the concentration of Na^+ and K^+ to further investigate the effects of salt and low temperature on bermudagrass. In leaves, the Na^+ concentration increased significantly under salt stress compared with the control, and there was no difference between LT+S and S treatments (Figure 3A). However, K^+ concentration in leaves increased remarkably under LT+S treatment, while there was no difference under low temperature and salt stress alone compared with the control (Figure 3C). In roots, Na^+ and K^+ concentration increased significantly under salt stress compared with the control, while them decreased significantly under LT+S treatment compared with the salt treatment (Figures 3B, 3D). Finally, compared with salt stress, the ratio of Na^+/K^+ in leaves was significantly decreased under combined stress and there was no difference in Na^+/K^+ ratio in roots under all stress conditions (Figures 3E, F).

3.4 Effects on resistance related genes under low temperature and salt stress

GLYI, *Cu-Zn/SOD*, *POD2* and *CAT1* expressions were measured to investigate the role of GLY and antioxidant system under low temperature and salt stress. *GLYI* was upregulated in both leaves and roots after 6 h of salt treatment, but it was no longer up-regulated after 17 d of salt treatment (Figures 4A, B). At 6 h or 17 d, LT treatment had no effect on *GLYI* in leaves but significantly reduced *GLYI* in roots (Figures 4A, B). *GLYI* expression in roots was significantly increased after 6 h and 17 d of LT+S treatment when compared to LT treatment (Figure 4B). Similarly, antioxidant-related genes (*Cu-Zn/SOD*, *POD2*, and *CAT1*) were

TABLE 2 Primer sequences for RT-PCR amplification analysis in bermudagrass.

Gene name	Forward primers	Reverse primers
GLY1	ATGTGTGTGACCGACTTTGCC	GAAGTCGTGCGTCTCGAAGGA
Cu-Zn/SOD	TAGCCCAGTTGTCGTGAGCCT	GGATTTGACCGTTGACTGGCG
POD2	TCGCTTCTGCTGGACGATGAC	GGGGGTCGAAGAAGTTGGGTA
CAT1	TCTCAGACAAGGACCGACTCA	GAGAAGCGGACGAATACTGGT
ACTIN	TCTGAAGGGTAAGTAGAGTAG	ACTCAGCACATTCCAGCAGAT

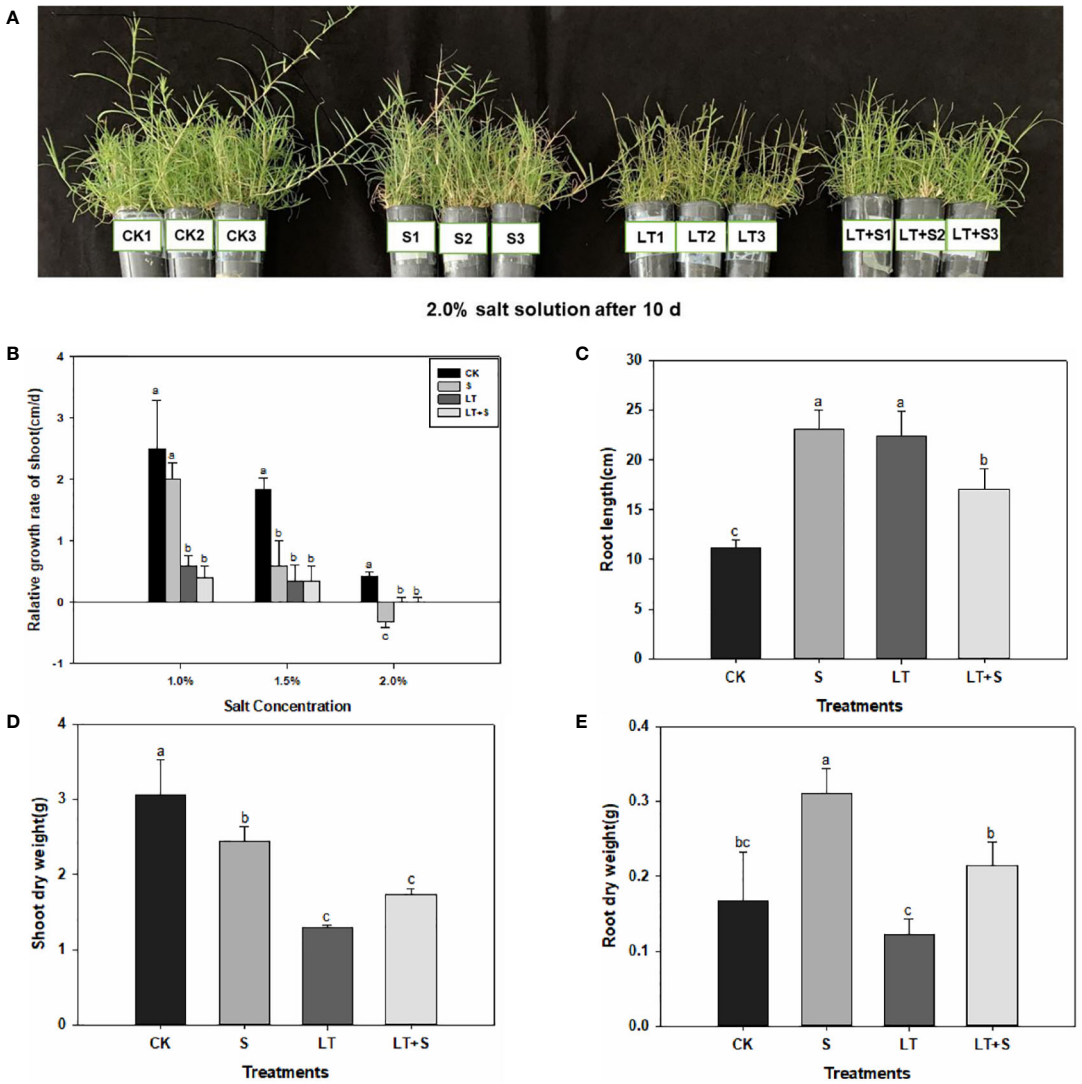

FIGURE 1
Bermudagrass phenotypic features under low temperature and salt stress. **(A)** Image of bermudagrass plants. **(B)** Relative growth rate of shoot. **(C)** Root length. **(D)** Shoot dry weight. **(E)** Root dry weight. Bermudagrass was transplanted into black plastic tubes after being clipped to a uniform length at the root. The plant height was reduced to the same height after a time of cultivation in a greenhouse. Duncan' s multiple range tests show that different letters above the same columns imply statistically significant differences at $P < 0.05$.

downregulated in roots after 6 h and 17 d of LT treatment (Figures 4D, F, H). The combination of salt and LT, on the other hand, suppressed the expression of antioxidant-related genes. *Cu-Zn/SOD* and *CAT1* expression levels in leaves exhibited no difference between control and low temperature treatment after 6 h, but were down-regulated after 17 d (Figures 4C, G). In comparison to the control treatment, the expression of *POD2* in leaves rose considerably after 17 d of low temperature treatment (Figure 4E). When compared to low temperature treatment alone, combined stress does not further the expression of these genes. In conclusion, combined stress reduces low temperature stress in roots *via* regulating these genes.

3.5 Effects on forage nutritive value of bermudagrass under low temperature and salt stress

We measured the quality indexes to further investigate the effects of salt and low temperature on bermudagrass. The effect of salt treatment alone on the nutritive value of forage was insignificant. The crude fat content was significantly lower in the LT and LT+S treatments compared to the control, but significantly higher in the LT+S treatment compared to the LT treatment alone, which was consistent with the fluorescence curve results (Figure 5A). Unlike crude fat, crude protein was

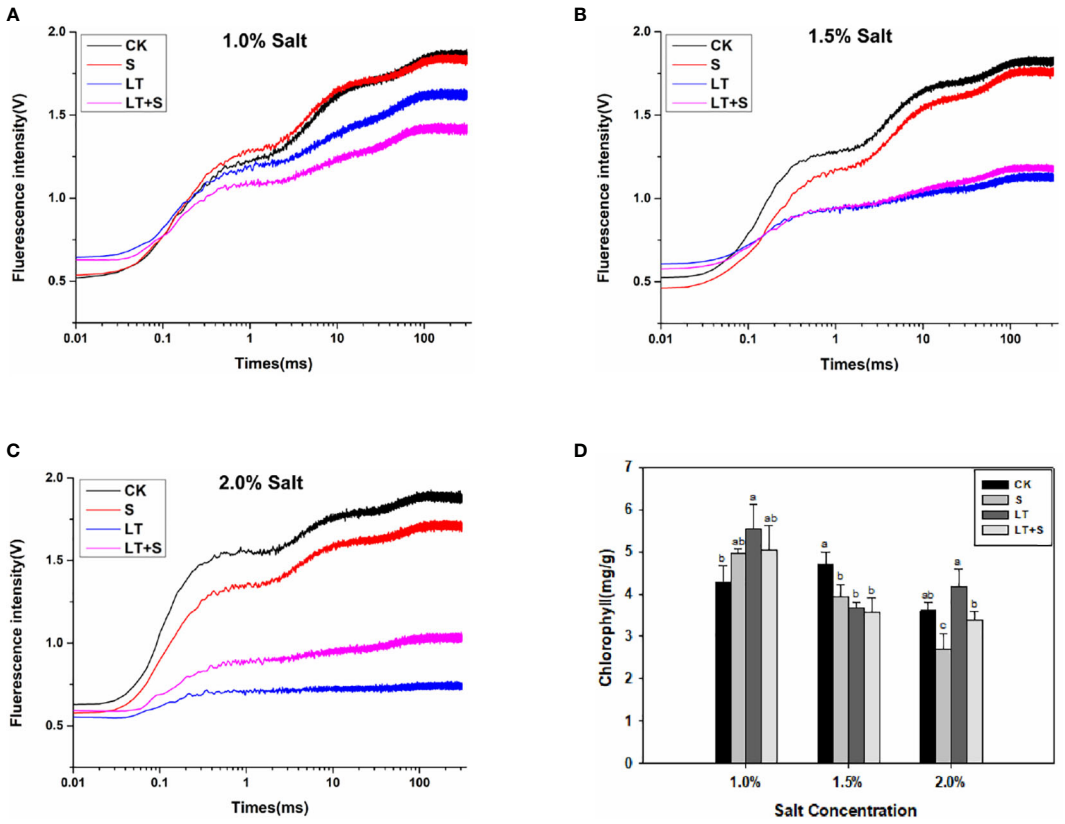

FIGURE 2
Effects of salt and cold treatment on photosynthetic parameters. **(A–C)**. Transient changes in chlorophyll fluorescence in bermudagrass leaves under 1.0 percent **(A)**, 1.5 percent **(B)** and 2.0 percent **(C)** salt treatment. **(D)** Chlorophyll content. Different letters above the same columns represent statistically significant differences at $P < 0.05$ (Duncan' s multiple range test).

significantly increased under LT+S conditions (Figure 5B). Only the LT+S treatment significantly reduced crude fiber (Figure 5C). It's worth mentioning that under the combined stress condition, the forage quality of the bermudagrass did not degrade any more compared to the low temperature treatment, but the crude fat rose.

4 Discussion

This article looked into the defensive mechanism of bermudagrass under low temperatures and salt stress. Plants response to stress is a complex process including morphology, physiology, and biochemistry (Huang et al., 2019). Low temperature-treated bermudagrass showed reduced relative growth rate in shoots, shoot dry weight, and increased root length in previous research (Esmaili and Salehi, 2012), which matched our findings (Figures 1B, E). From the standpoint of plant growth phenotype, bermudagrass under the LT+S treatment is superior to that of low temperature treatment, the root dry weight reflects the same situation. Relative growth rate, shoot dry weight and root length under low temperature and low temperature + salt treatment shows no discernible differences (Figures 1A-E). All of this suggests that the combined stress did not produce more substantial harm to the plants; rather, a moderate amount of salt may have mitigated the damage caused by low temperatures. Maintaining proper balance of Na^+/K^+ and higher K^+ concentration is considered as an important mechanism for plants to response to salt stress (Evelin et al., 2009). Lower Na^+/K^+ is a marker of salinity tolerance for plants (van Zelm et al., 2020). In salt-tolerant plants, K^+ efflux can be significantly inhibited to maintain stable Na^+/K^+ and reduce salt stress injury (Yang and Guo, 2018). In our study, Na^+/K^+ remained stable and K^+ concentration increased in root under salt stress (Figures 3D, F), so it can be inferred that bermudagrass A12359 has a certain salinity tolerance, which is the reason that it can alleviate the damage of low temperature to bermudagrass at the high salt concentration (2.0%).

Low temperature stress affects a variety of physiological processes in plants, the most susceptible of which is photosynthesis (Stitt and Hurry, 2002). We looked at

10.3389/fpls.2022.1042855

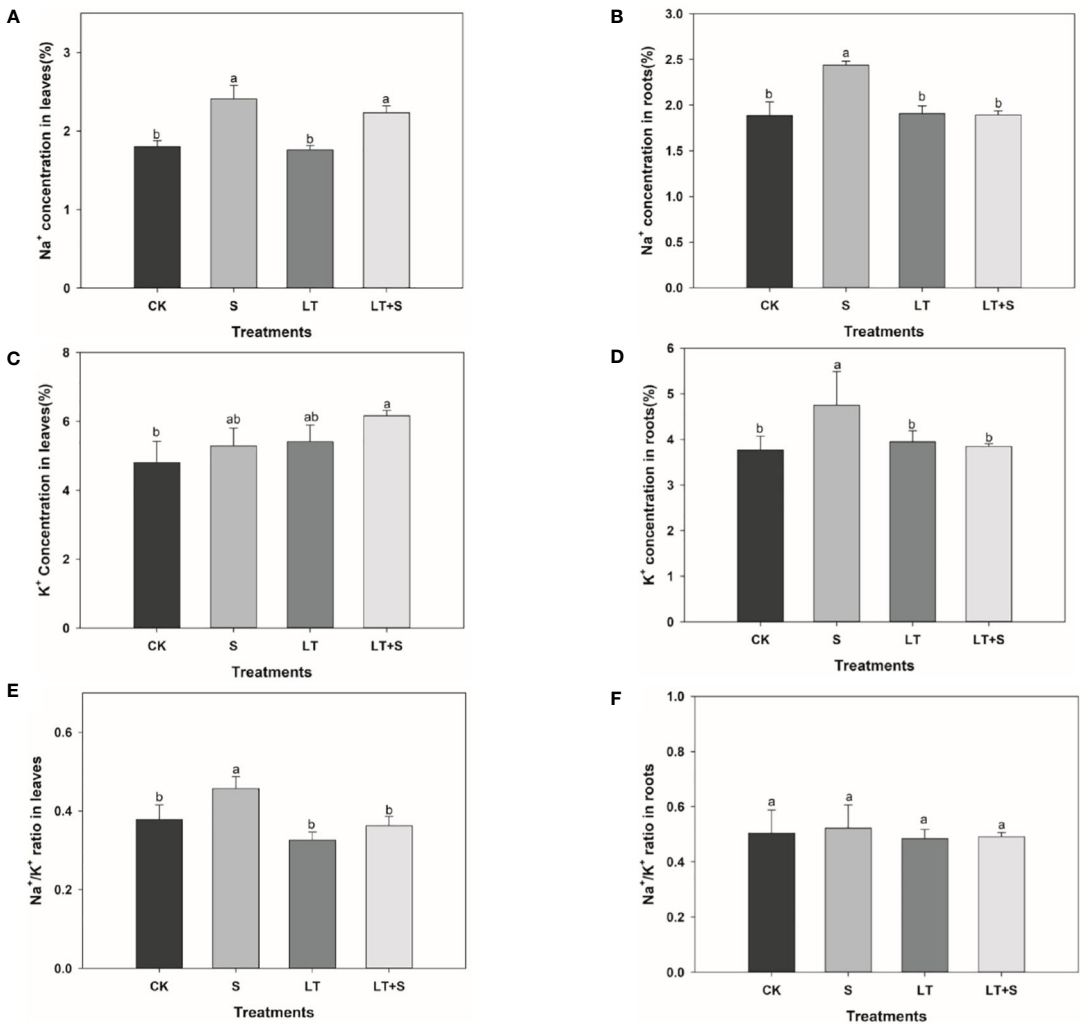

FIGURE 3
The bar chart shows the average Na+ concentration **(A, B)**, K+ concentration **(C, D)**, and Na+/K+ ratio **(E, F)** of bermudagrass under each treatment, with three replicates per treatment. Different letters above the same columns indicate statistic significant difference at $P < 0.05$ (Duncan' s multiple range test).

photosynthetic indexes at the third, sixth and seventeenth d to learn more about how bermudagrass protects itself under low temperatures and different salt concentrations. The PSII reaction center becomes sensitive under stress, and the OJIP fluorescence transient curves and chlorophyll fluorescence characteristics can accurately reflect PSII's physiological status (Chen et al., 2021). The electron transport activities (PSI and PSII) of the chloroplast thylakoid membrane were found to be dramatically reduced at low temperatures, with PSII being more vulnerable to cold pressure than PSI (Shi et al., 2016). The chlorophyll fluorescence transient response curve decreased under the three stress conditions as processing time at low temperature and salt concentration increased, compared to control, in our studies, but it decreased more noticeably under the LT treatment, and the fluorescence curve is higher under the LT +S treatment than the LT treatments when the salt concentration reaches 1.5 percent and 2.0 percent (Figures 2B, C).The findings revealed that an optimal salt concentration could help to relieve photosynthetic physiology in cold-stressed plants (Figures 2A, C). Low temperature stress causes a drop in E0, which is mostly influenced by alterations in the PSII receptor side (Van Heerden et al., 2003). φE_0 represents the reaction center of absorbed light quantum yield for electron transfer, and the higher the value, the more stressed the plants are. In this study, φE_0 significantly decreased under LT stress while improving under LT+S treatment, and the same changes were observed in area and φP_0. All of these results suggest that when LT+S was used instead of LT stress, electron transfer efficiency improved, and the effect of low temperature stress alone on plant photosynthesis was reduced.

10.3389/fpls.2022.1042855

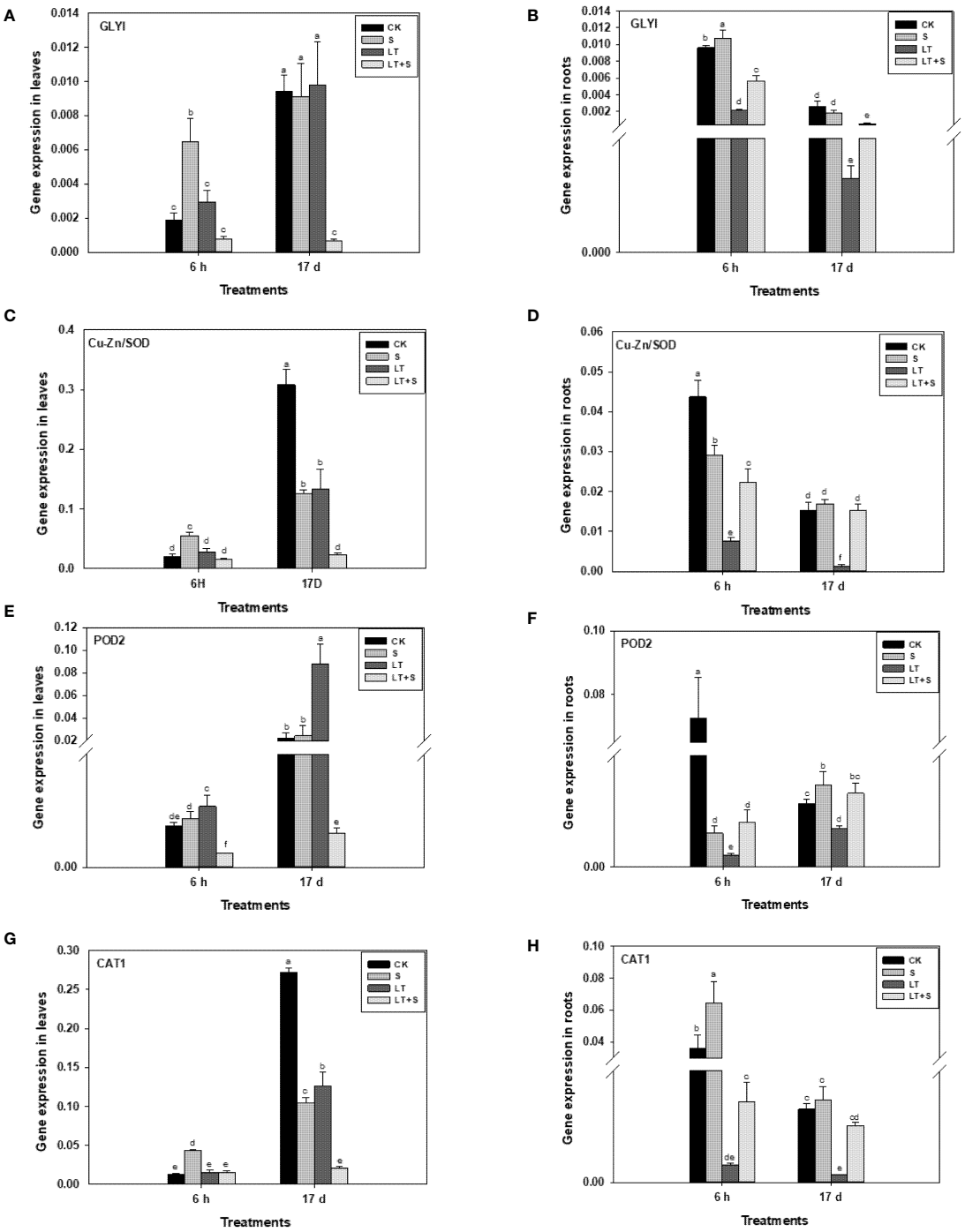

FIGURE 4
Glyoxalase and antioxidant enzyme related genes transcriptional level in bermudagrass under low temperature and salt stress. **(A, C, E, G)** represents genes transcriptional level in leaves and Figure **(B, D, F–H)** represents genes transcriptional level in roots. Different letters above the same columns indicate statistic significant difference at $P < 0.05$ (Duncan' s multiple range test).

Plants respond to salt, severe temperatures, and other factors through the GLY system, which consists of GlyI, GlyII, and GSH (coenzyme). The detoxification of methylglyoxal, a by-product of carbohydrate metabolism, is its primary physiological role (Roy et al., 2008). In this study, since the expression levels of GLYI and antioxidant oxidases related genes change early under stress conditions (Wang et al., 2020; Zhang et al., 2021), the gene expression levels were measured once after 6 h of treatment, and then again at the end of the experiment (17d), so as to observe the gene expression changes. Under salt, mannitol and heavy metal stress, *GLYI* expression in mustard was dramatically increased (Veena et al., 1999). *GLYI* was considerably elevated in both roots and leaves after 6 h of salt treatment in our experiment (Figures 4A, B), which is consistent with earlier research. Low temperature causes mechanical constraints-membrane damage, whereas salinity causes malignancy by disrupting the ion and osmotic balance of cells (Mahajan and Tuteja, 2005). Osmotic stress can particularly promote the production of GLYI, at which point the GLY system is triggered to repair the damage (Inoue et al., 1998). Low temperature stress was found to increase the levels of reactive oxygen species (ROS) and lower enzyme antioxidant activity in plants (Aroca et al., 2005; Sasaki et al., 2007), affecting the antioxidant system. In our study, antioxidant enzyme genes (*Cu-Zn/SOD*, *POD2*, and *CAT1*) in roots were significantly down-regulated under low temperature stress (Figures 4D, F, H). When exposed to low temperature stress alone, the expression of *GLYI* in leaves does not rise and even decreases dramatically in roots, and several indicators reveal that the injury to plants is highest at this time. However, when compared to low temperature treatment, the expression level of *GLYI* was higher during LT+S stress, indicating that the GLY system was activated again, reducing the damage caused by low temperature. Furthermore, the GLY system raises the level of free reduced glutathione, which is necessary for the removal of harmful reactive oxygen species (e.g., H_2O_2) and organic peroxides that accumulate in stressed plants, as well as the maintenance of other antioxidants (Frendo et al., 2013). Despite the roles of antioxidant enzymes and GLY in stress are clearly, we indicated that these genes may involve in stress acclimation to several different environmental adversity.

Crude protein and crude fiber are two important indexes for measuring the nutritional value of herbage, as well as important contents for improving herbage quality. The first selection

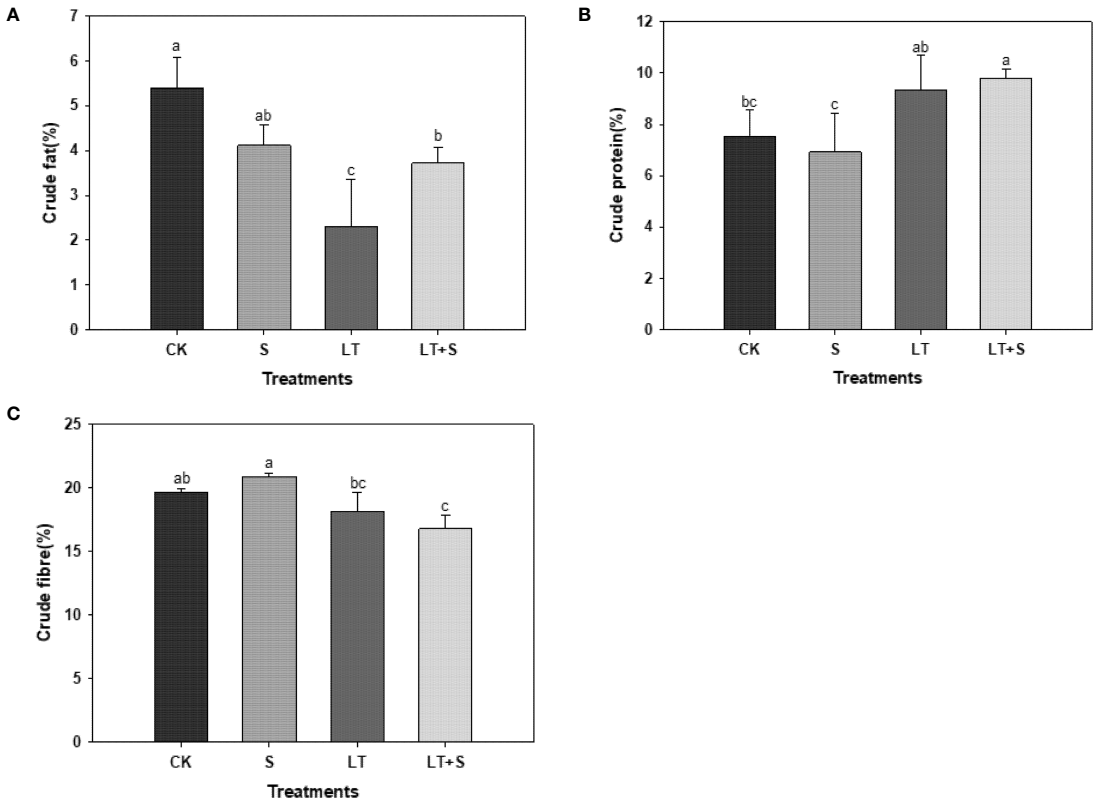

FIGURE 5
The bar chart shows the average of crude fat **(A)**, crude protein **(B)**, and crude fiber **(C)** content of bermudagrass under each treatment, with three replicates per treatment. Different letters above the same columns indicate statistic significant difference at $P < 0.05$ (Ducan' s multiple range test).

factors for high quality forage are high crude protein content and low crude fiber content (Barth, 2012). Previous research has shown that plants in low temperature environments reduce structural carbohydrate content while increasing soluble carbohydrate and protein content to minimize plant harm (Vo and Johnson, 2001). In our experiment, compared to the control, bermudagrass protein content increased significantly under LT and LT+S treatment (Figure 5B). This phenomenon could be explained by the fact that the LT treatment was set at 10 -15°C and the cells were subjected to low temperature stress but did not reach the point where the fluidity of the cell membrane becomes weak and rigidity increases. At this point, the cell membrane's phase transition reduces the ability of the membrane protein to bind to phospholipids and causes it to become free protein, resulting in an increase in protein content in the plant. Crude fat is a nutrient with a high calorific value that can enhance feed palatability (Li et al., 2019). According to the test results, the crude fat content was lowest under low temperature treatment and significantly higher under low temperature + salt treatment (Figure 5A), proving once again that appropriate salt can mitigate the damage caused by low temperature.

5 Conclusion

At present, plants are subjected to more and more abiotic stresses (Zulfiqar and Hancock, 2020b; Zulfiqar et al., 2021c), and the physiological responses under combined stress and single stress are completely different. Therefore, the changes of phenotype, photosynthesis, Na^+, K^+, gene expression and forage quality under single salt, low temperature stress and combined stress were analyzed in this study to explore the interaction between low temperature and salinity on bermudagrass. It was found that low temperatures cause more damage to bermudagrass, but moderate salt addition can mitigate the damage by enhancing photosynthesis, improving the expression of antioxidant system genes (*Cu-Zn/SOD*, *POD2* and *CAT1*) and glyoxalase system *GLYI* gene in roots and thus improves forage quality. This provides putative pathways improving turfgrass and forage tolerance to combination stress.

Data availability statement

The original contributions presented in the study are included in the article/supplementary material. Further inquiries can be directed to the corresponding author.

Author contributions

All authors contributed largely to the work presented in this article. Conceived and designed the experiments: JF. Performed the experiments XZ, GW, XL, YX. Analyzed the data: XZ, YY. Language modification: EA. Wrote the paper: XZ, YY. All authors contributed to the article and approved the submitted version.

Funding

This work was supported by National Key R&D Program of China (2019YFD0900702) and Agricultural Variety Improvement Project of Shandong Province (2019LZGC010).

Conflict of interest

The authors declare that the research was conducted in the absence of any commercial or financial relationships that could be construed as a potential conflict of interest.

Publisher's note

References

Abideen, Z., Koyro, H. W., Hussain, T., Rasheed, A., Alwahibi, M. S., Elshikh, M. S., et al. (2022). Biomass production and predicted ethanol yield are linked with optimum photosynthesis in phragmites karka under salinity and drought conditions. *Plants (Basel)* 11 (13), 1657. doi: 10.3390/plants11131657

Achuo, E. A., Prinsen, E., and Höfte, M. (2006). Influence of drought, salt stress and abscisic acid on the resistance of tomato to botrytis cinerea and oidium neolycopersici. *Plant Pathol.* 55, 178–186. doi: 10.1111/j.1365-3059.2006.01340.x

Allen, D. J., and Ort, D. R. (2001). Impacts of chilling temperatures on photosynthesis in warm-climate plants. *Trends Plant Sci.* 6 (1), 36–42. doi: 10.1016/s1360-1385(00)01808-2

Aroca, R., Amodeo, G., Fernández-Illescas, S., Herman, E. M., Chaumont, F., and Chrispeels, M. J. (2005). The role of aquaporins and membrane damage in chilling and hydrogen peroxide induced changes in the hydraulic conductance of maize roots. *Plant Physiol.* 137 (1), 341–353. doi: 10.1104/pp.104.051045

Bai, Y., Kissoudis, C., Yan, Z., Visser, R., and van der Linden, G. (2018). Plant behaviour under combined stress: tomato responses to combined salinity and pathogen stress. *Plant J.* 93 (4), 781–793. doi: 10.1111/tpj.13800

Banerjee, A., Tripathi, D. K., and Roychoudhury, A. (2018). Hydrogen sulphide trapeze: Environmental stress amelioration and phytohormone crosstalk. *Plant Physiol. Biochem.* 132, 46–53. doi: 10.1016/j.plaphy.2018.08.028

Barth, S. (2012). Breeding strategies for forage and grass improvement. *Ann. Bot.* 110 (6), 1261–1262. doi: 10.1093/aob/mcs219

Bela, K., Horváth, E., Gallé, Á., Szabados, L., Tari, I., and Csiszár, J. (2015). Plant glutathione peroxidases: emerging role of the antioxidant enzymes in plant development and stress responses. *J. Plant Physiol.* 176, 192–201. doi: 10.1016/j.jplph.2014.12.014

Biswas, D. K., and Jiang, G. M. (2011). Differential drought-induced modulation of ozone tolerance in winter wheat species. *J. Exp. Bot.* 62 (12), 4153–4162. doi: 10.1093/jxb/err104

Chen, X., Zhou, Y., Cong, Y., Zhu, P., Xing, J., Cui, J., et al. (2021). Ascorbic acid-induced photosynthetic adaptability of processing tomatoes to salt stress probed by fast OJIP fluorescence rise. *Front. Plant Sci.* 12. doi: 10.3389/fpls.2021.594400

Esmaili, S., and Salehi, H. (2012). Effects of temperature and photoperiod on postponing bermudagrass (cynodon dactylon [l.] pers.) turf dormancy. *J. Plant Physiol.* 169 (9), 851–858. doi: 10.1016/j.jplph.2012.01.022

Evelin, H., Kapoor, R., and Giri, B. (2009). Arbuscular mycorrhizal fungi in alleviation of salt stress: a review. *Ann. Bot.* 104, 1263–1280. doi: 10.1093/aob/mcp251

Frendo, P., Baldacci-Cresp, F., Benyamina, S. M., and Puppo, A. (2013). Glutathione and plant response to the biotic environment. *Free Radic. Biol. Med.* 65, 724–730. doi: 10.1016/j.freeradbiomed.2013.07.035

Fürtauer, L., Weiszmann, J., Weckwerth, W., and Nägele, T. (2019). Dynamics of plant metabolism during cold acclimation. *Int. J. Mol. Sci.* 20 (21), 5411. doi: 10.3390/ijms20215411

Hasanuzzaman, M., Bhuyan, M., Zulfiqar, F., Raza, A., Mohsin, S. M., Mahmud, J. A., et al. (2020a). Reactive oxygen species and antioxidant defense in plants under abiotic stress: Revisiting the crucial role of a universal defense regulator. *Antioxid. (Basel)* 9 (8), 681. doi: 10.3390/antiox9080681

Hasanuzzaman, M., Bhuyan, M., Parvin, K., Bhuiyan, T. F., Anee, T. I., Nahar, K., et al. (2020b). Regulation of ROS metabolism in plants under environmental stress: A review of recent experimental evidence. *Int. J. Mol. Sci.* 21 (22), 8695. doi: 10.3390/ijms21228695

Hasdai, M., Weiss, B., Levi, A., Samach, A., and Porat, R. (2006). Differential responses of arabidopsis ecotypes to cold, chilling and freezing temperatures. *Ann. Appl. Biol.* 148 (2), 113–120. doi: 10.1111/j.1744-7348.2006.00044.x

Henriet, C., Aimé, D., Térézol, M., Kilandamoko, A., Rossin, N., Combes-Soia, L., et al. (2019). Water stress combined with sulfur deficiency in pea affects yield components but mitigates the effect of deficiency on seed globulin composition. *J. Exp. Bot.* 70 (16), 4287–4304. doi: 10.1093/jxb/erz114

Huang, S., Jiang, S., Liang, J., Chen, M., and Shi, Y. (2019). Current knowledge of bermudagrass responses to abiotic stresses. *Breed Sci.* 69 (2), 215–226. doi: 10.1270/jsbbs.18164

Inoue, Y., Tsujimoto, Y., and Kimura, A. (1998). Expression of the glyoxalase I gene of saccharomyces cerevisiae is regulated by high osmolarity glycerol mitogen-activated protein kinase pathway in osmotic stress response. *J. Biol. Chem.* 273 (5), 2977–2983. doi: 10.1074/jbc.273.5.2977

Jabeen, R., Iqbal, A., Deeba, F., Zulfiqar, F., Mustafa, G., Nawaz, H., et al. (2022). Isolation and characterization of peroxidase P7-like gene and rab-GDI like gene from potential medicinal plants: A step toward understanding cell defense signaling. *Front. Plant Sci.* 13. doi: 10.3389/fpls.2022.975852

Kim, B. G., Waadt, R., Yong, H. C., Pandey, G. K., and Sheng, L. (2007). The calcium sensor cbl10 mediates salt tolerance by regulating ion homeostasis in arabidopsis. *Plant J.* 52 (3), 473–484. doi: 10.1111/j.1365-313X.2007.03249.x

Liang, W., Ma, X., Wan, P., and Liu, L. (2018). Plant salt-tolerance mechanism: A review. *Biochem. Biophys. Res. Commun.* 495 (1), 286–291. doi: 10.1016/j.bbrc.2017.11.043

Li, N., Du, C., Ma, B., Gao, Z., Wu, Z., Zheng, L., et al. (2019). Functional analysis of ion transport properties and salt tolerance mechanisms of RtHKT1 from the recretohalophyte reaumuria trigyna. *Plant Cell Physiol.* 60 (1), 85–106. doi: 10.1093/pcp/pcy187

Liu, C., Dai, Z., Xia, J., Chang, C., and Sun, H. (2018). Combined effect of salt and drought on boron toxicity in puccinellia tenuiflora. *Ecotoxicol. Environ. Saf.* 157, 395–402. doi: 10.1016/j.ecoenv.2018.03.061

Li, S., Wang, N., Ji, D., Zhang, W., Wang, Y., Yu, Y., et al. (2019). A GmSIN1/GmNCED3s/GmRbohBs feed-forward loop acts as a signal amplifier that regulates root growth in soybean exposed to salt stress. *Plant Cell* 31 (9), 2107–2130. doi: 10.1105/tpc.18.00662

Mahajan, S., and Tuteja, N. (2005). Cold, salinity and drought stresses: an overview. *Arch. Biochem. Biophys.* 444 (2), 139–158. doi: 10.1016/j.abb.2005.10.018

Meloni, D. A., Oliva, M. A., Martinez, C. A., and Cambraia, J. (2003). Photosynthesis and activity of superoxide dismutase, peroxidase and glutathione reductase in cotton under salt stress. *Environ. Exp. Bot.* 49 (1), 69–76. doi: 10.1016/s0098-8472(02)00058-8

Mittler, R., and Blumwald, E. (2010). Genetic engineering for modern agriculture: challenges and perspectives. *Annu. Rev. Plant Biol.* 61, 443–462. doi: 10.1146/annurev-arplant-042809-112116

Munns, R., Passioura, J. B., Colmer, T. D., and Byrt, C. S. (2020). Osmotic adjustment and energy limitations to plant growth in saline soil. *New Phytol.* 225 (3), 1091–1096. doi: 10.1111/nph.15862

Munshaw, G. C., Zhang, X., and Ervin, E. H. (2004). Effect of salinity on bermudagrass cold hardiness. *HortScience* 39, 420–423. doi: 10.1023/B:EJPP.0000021072.89968.de

Nowicka, B., Ciura, J., Szymańska, R., and Kruk, J. (2018). Improving photosynthesis, plant productivity and abiotic stress tolerance - current trends and future perspectives. *J. Plant Physiol.* 231, 415–433. doi: 10.1016/j.jplph.2018.10.022

Parvin, K., Hasanuzzaman, M., Bhuyan, M., Nahar, K., Mohsin, S. M., and Fujita, M. (2019). Comparative physiological and biochemical changes in tomato (Solanum lycopersicum l.) under salt stress and recovery: Role of antioxidant defense and glyoxalase systems. *Antioxid. (Basel)* 8 (9), 350. doi: 10.3390/antiox8090350

Ponce-Pineda, I. G., Carmona-Salazar, L., Saucedo-García, M., Cano-Ramírez, D., Morales-Cedillo, F., Peña-Moral, A., et al. (2021). MPK6 kinase regulates plasma membrane h^+-ATPase activity in cold acclimation. *Int. J. Mol. Sci.* 22 (12), 6338. doi: 10.3390/ijms22126338

Rong, Z., Yu, X., Ottosen, C. O., Rosenqvist, E., and Zhen, W. (2017). Drought stress had a predominant effect over heat stress on three tomato cultivars subjected to combined stress. *BMC Plant Biol.* 17 (1), 24. doi: 10.1186/s12870-017-0974-x

Roy, S. D., Saxena, M., Bhomkar, P. S., Pooggin, M., Hohn, T., and Bhalla-Sarin, N. (2008). Generation of marker free salt tolerant transgenic plants of arabidopsis thaliana using the gly i gene and cre gene under inducible promoters. *Plant Cell Tissue Organ Culture* 95 (1), 1–11. doi: 10.1007/s11240-008-9402-0

Sasaki, K., Kim, M. H., and Imai, R. (2007). Arabidopsis COLD SHOCK DOMAIN PROTEIN2 is a RNA chaperone that is regulated by cold and developmental signals. *Biochem. Biophys. Res. Commun.* 364 (3), 633–638. doi: 10.1016/j.bbrc.2007.10.059

Shao, A., Sun, Z., Fan, S., Xu, X., Wang, W., Amombo, E., et al. (2020). Moderately low nitrogen application mitigate the negative effects of salt stress on annual ryegrass seedlings. *PeerJ* 8, e10427. doi: 10.7717/peerj.10427

Shi, W., Wei, X., and Chen, G. X. (2016). Effects of low temperature on photosynthetic characteristics in the super-high-yield hybrid rice 'liangyoupeijiu' at the seedling stage. *Genet. Mol. Res.* 15 (4). doi: 10.4238/gmr15049021

Singla-Pareek, S. L., Yadav, S. K., Pareek, A., Reddy, M. K., and Sopory, S. K. (2008). Enhancing salt tolerance in a crop plant by overexpression of glyoxalase II. *Transgenic Res.* 17 (2), 171–180. doi: 10.1007/s11248-007-9082-2

Singla-Pareek, S. L., Yadav, S. K., Pareek, A., and Sopory, M. K. R. K. (2006). Transgenic tobacco overexpressing glyoxalase pathway enzymes grow and set viable seeds in zinc-spiked soils. *Plant Physiol.* 140 (2), 613–623. doi: 10.1104/pp.105.073734

Stitt, M., and Hurry, V. (2002). A plant for all seasons: alterations in photosynthetic carbon metabolism during cold acclimation in arabidopsis. *Curr. Opin. Plant Biol.* 5 (3), 199–206. doi: 10.1016/s1369-5266(02)00258-3

Suzuki, N., Rivero, R. M., Shulaev, V., Blumwald, E., and Mittler, R. (2014). Abiotic and biotic stress combinations. *New Phytol.* 203 (1), 32–43. doi: 10.1111/nph.12797

Thornalley, P. J. (1990). The glyoxalase system: new developments towards functional characterization of a metabolic pathway fundamental to biological life. *Biochem. J.* 269 (1), 1–11. doi: 10.1042/bj2690001

Van Heerden, P. D., Tsimilli-Michael, M., Krüger, G. H., and Strasser, R. J. (2003). Dark chilling effects on soybean genotypes during vegetative development: parallel studies of CO2 assimilation, chlorophyll a fluorescence kinetics O-J-I-P and nitrogen fixation. *Physiol. Plant* 117 (4), 476–491. doi: 10.1034/j.1399-3054.2003.00056.x

van Zelm, E., Zhang, Y., and Testerink, C. (2020). Salt tolerance mechanisms of plants. *Annu. Rev. Plant Biol.* 71, 403–433. doi: 10.1146/annurev-arplant-050718-100005

Veena,, Reddy, V. S., and Sopory, S. K. (1999). Glyoxalase i from brassica juncea: molecular cloning, regulation and its over-expression confer tolerance in transgenic tobacco under stress. *Plant J.* 17 (4), 385–395. doi: 10.1046/j.1365-313x.1999.00390.x

Vile, D., Pervent, M., Belluau, M., Vasseur, F., Bresson, J., Muller, B., et al. (2012). Arabidopsis growth under prolonged high temperature and water deficit: independent or interactive effects? *Plant Cell Environ.* 35 (4), 702–718. doi: 10.1111/j.1365-3040.2011.02445.x

Vo, S., and Johnson, E. A. (2001). Alpine plant life: Functional plant ecology of high mountain ecosystems. *MT Res. Dev.* 21 (2), 202–202. doi: 10.1659/0276-4741(2001)021[0202:APLFPE]2.0.CO;2

Wang, W., Shao, A., Amombo, E., Fan, S., Xu, X., and Fu, J. (2020). Transcriptome-wide identification of MAPKKK genes in bermudagrass (Cynodon dactylon l.) and their potential roles in low temperature stress responses. *PeerJ* 8, e10159. doi: 10.7717/peerj.10159

Xie, Y., Han, S., Li, X., Amombo, E., and Fu, J. (2017). Amelioration of salt stress on bermudagrass by the fungus aspergillus aculeatus. *Mol. Plant Microbe Interact.* 30 (3), 245–254. doi: 10.1094/MPMI-12-16-0263-R

Yadav, S. K., Singla-Pareek, S. L., Ray, M., Reddy, M. K., and Sopory, S. K. (2005). Methylglyoxal levels in plants under salinity stress are dependent on glyoxalase i and glutathione. *Biochem. Biophys. Res. Commun.* 337 (1), 61–67. doi: 10.1016/j.bbrc.2005.08.263

Yang, Y., and Guo, Y. (2018). Elucidating the molecular mechanisms mediating plant salt-stress responses. *New Phytol.* 217 (2), 523–539. doi: 10.1111/nph.14920

Yan, F., Mu, Y., Yan, G., Liu, J., Shen, J., and Luo, G. (2010). Antioxidant enzyme mimics with synergism. *Mini Rev. Med. Chem.* 10 (4), 342–356. doi: 10.2174/138955710791330972

Yusuf, M. A., Kumar, D., Rajwanshi, R., Strasser, R. J., Tsimilli-Michael, M., Govindjee,, et al. (2010). Overexpression of gamma-tocopherol methyl transferase gene in transgenic brassica juncea plants alleviates abiotic stress: physiological and chlorophyll a fluorescence measurements. *Biochim. Biophys. Acta* 1797 (8), 1428–1438. doi: 10.1016/j.bbabio.2010.02.002

Zhang, P., Duo, T., Wang, F., Zhang, X., Yang, Z., and Hu, G. (2021). *De novo* transcriptome in roots of switchgrass (Panicum virgatum l.) reveals gene expression dynamic and act network under alkaline salt stress. *BMC Genomics* 22 (1), 82. doi: 10.1186/s12864-021-07368-w

Zhang, J., Gao, F., Jia, H., Hu, J., and Feng, Z. (2019). Molecular response of poplar to single and combined ozone and drought. *Sci. Total Environ.* 655, 1364–1375. doi: 10.1016/j.scitotenv.2018.11.195

Zhao, S., Zhang, Q., Liu, M., Zhou, H., Ma, C., and Wang, P. (2021). Regulation of plant responses to salt stress. *Int. J. Mol. Sci.* 22 (9), 4609. doi: 10.3390/ijms22094609

Zulfiqar, F., Akram, N. A., and Ashraf, M. (2019). Osmoprotection in plants under abiotic stresses: new insights into a classical phenomenon. *Planta* 251 (1), 3. doi: 10.1007/s00425-019-03293-1

Zulfiqar, F., and Ashraf, M. (2021a). Bioregulators: unlocking their potential role in regulation of the plant oxidative defense system. *Plant Mol. Biol.* 105 (1-2), 11–41. doi: 10.1007/s11103-020-01077-w

Zulfiqar, F., and Ashraf, M. (2021b). Nanoparticles potentially mediate salt stress tolerance in plants. *PPB* 160, 257–268. doi: 10.1016/j.plaphy.2021.01.028

Zulfiqar, F., and Ashraf, M. (2022a). Antioxidants as modulators of arsenic-induced oxidative stress tolerance in plants: An overview. *J. Hazard Mater* 427, 127891. doi: 10.1016/j.jhazmat.2021.127891

Zulfiqar, F., Casadesús, A., Brockman, H., and Munné-Bosch, S. (2020a). An overview of plant-based natural biostimulants for sustainable horticulture with a particular focus on moringa leaf extracts. *Plant Sci.* 295, 110194. doi: 10.1016/j.plantsci.2019.110194

Zulfiqar, F., and Hancock, J. T. (2020b). Hydrogen sulfide in horticulture: Emerging roles in the era of climate change. *PPB* 155, 667–675. doi: 10.1016/j.plaphy.2020.08.010

Zulfiqar, F., Nafees, M., Chen, J., Darras, A., Ferrante, A., Hancock, J. T., et al. (2022b). Chemical priming enhances plant tolerance to salt stress. *Front. Plant Sci.* 13. doi: 10.3389/fpls.2022.946922

Zulfiqar, F., Russell, G., and Hancock, J. T. (2021c). Molecular hydrogen in agriculture. *Planta* 254 (3), 56. doi: 10.1007/s00425-021-03706-0

frontiers | Frontiers in Plant Science

TYPE Original Research
PUBLISHED 17 November 2022
DOI 10.3389/fpls.2022.1063436

OPEN ACCESS

EDITED BY
Jin-Lin Zhang,
Lanzhou University, China

REVIEWED BY
Liang Chen,
University of Chinese Academy of Sciences, China
Xiqing Ma,
China Agricultural University, China

*CORRESPONDENCE
Yu Chen
cyu801027@aliyun.com

†These authors have contributed equally to this work

SPECIALTY SECTION
This article was submitted to Plant Abiotic Stress, a section of the journal Frontiers in Plant Science

RECEIVED 07 October 2022
ACCEPTED 03 November 2022
PUBLISHED 17 November 2022

CITATION
Zheng Y, Zong J, Liu J, Wang R, Chen J, Guo H, Kong W, Liu J and Chen Y (2022) Mining for salt-tolerant genes from halophyte *Zoysia matrella* using FOX system and functional analysis of *ZmGnTL*. *Front. Plant Sci.* 13:1063436. doi: 10.3389/fpls.2022.1063436

Mining for salt-tolerant genes from halophyte *Zoysia matrella* using FOX system and functional analysis of *ZmGnTL*

Yuying Zheng[1†], Junqin Zong[2†], Jun Liu[1], Ruying Wang[3], Jingbo Chen[2], Hailin Guo[2], Weiyi Kong[2], Jianxiu Liu[2] and Yu Chen[1*]

[1]College of Agro-Grassland Science, Nanjing Agricultural University, Nanjing, China, [2]Institute of Botany, Jiangsu Province and Chinese Academy of Sciences, Nanjing, China, [3]Department of Horticulture, Oregon State University, Corvallis, OR, United States

Zoysia matrella is a salt-tolerant turfgrass grown in areas with high soil salinity irrigated with effluent water. Previous studies focused on explaining the regulatory mechanism of *Z. matrella* salt-tolerance at phenotypic and physiological levels. However, the molecular mechanism associated with salt tolerance of *Z. matrella* remained unclear. In this study, a high-efficient method named FOX (full-length cDNA overexpression) hunting system was used to search for salt-tolerant genes in *Z. matrella*. Eleven candidate genes, including several known or novel salt-tolerant genes involved in different metabolism pathways, were identified. These genes exhibited inducible expression under salt stress condition. Furthermore, a novel salt-inducible candidate gene *ZmGnTL* was transformed into *Arabidopsis* for functional analysis. *ZmGnTL* improved salt-tolerance through regulating ion homeostasis, reactive oxygen species scavenging, and osmotic adjustment. In summary, we demonstrated that FOX is a reliable system for discovering novel genes relevant to salt tolerance and several candidate genes were identified from *Z. matrella* that can assist molecular breeding for plant salt-tolerance improvement.

KEYWORDS

***Zoysia matrella*, FOX hunting, salt-tolerant genes, *ZmGnTL*, regulatory mechanism**

Introduction

Soil salinization has been an adverse environmental factor restricting plant growth and development, as well as limiting plant production and quality (Katerji et al., 2003; Zhang et al., 2013; Zhang and Shi, 2013; Zhang et al., 2022). Therefore, improving plant salt-tolerance will be crucial for crop production in large saline regions. Understanding the physiological and molecular mechanisms are beneficial for plant adaption to salt

stress (Van Zelm et al., 2020). Over the past two decades, scientists have described several regulatory pathways related to plant salt tolerance, including ion balance (Ji et al., 2013; Benito et al., 2014; Almeida et al., 2017), osmotic adjustment (Flowers et al., 2015; Slama et al., 2015), and reactive oxygen species (ROS) degradation (Yang and Guo, 2018a; Yang and Guo, 2018b). These pathways have been further verified through gene function analysis, such as *Salt Overly Sensitive 1-3* (*SOS1-3*) involved in Na^+ exclusion and ion homeostasis control in many plant species (Zhu, 2000; Shi et al., 2003; Han et al., 2022), antioxidant enzymes *GhSOD1* and *GhCAT1* in cotton (Luo et al., 2013), and *P5CS* related to proline metabolism conferring salt-inducible osmotic adjustment in rice (Igarashi et al., 1997), etc. As described above, most of these salt-tolerant genes were identified from model plants or crop species, very few salt-tolerant genes have been explored from halophytes that adapt to higher salinity.

Halophytes, such as non-salt secreting type *Thellungiella halophile*, *Salicornia brachiate*, *Suaeda corniculate* (Mishra and Tanna, 2017), *Suaeda maritima* (Zhang et al., 2013) and *Puccinellia tenuiflora* (Han et al., 2022), and salt secreting type *Limonium bicolor* (Gao et al., 2021), *Avicennia officinalis* (Jyothi-Prakash et al., 2014) and *Zoysia matrella* (Chen et al., 2015), can survive from high salinity conditions with some of them even directly irrigated with saline water. Systematic screening for salt-tolerant genes from halophytes will provide valuable information for explaining the underlying molecular mechanism of their salt tolerance. Several methods such as DNA seq, RNA seq, proteomics, and metabonomics have been successfully applied for gene mining in plants (Chen et al., 2015; Yuan et al., 2015). Genes involved in the special ultrastructure of salt glands were discovered in *L. bicolor* through RNA seq method (Yuan et al., 2015), which has been a primary approach in most non-model plants. However, functional genes can change in post-transcriptional level which could not be detected by RNA seq. FOX system as a gain-of-function method using heterologous overexpression of full-length cDNA libraries in model plant *Arabidopsis* has been successfully applied for gene mining in *Arabidopsis* and rice (Ichikawa et al., 2006; Higuchi et al., 2011; Higuchi-Takeuchi and Matsui, 2014). For example, *TsHsfA1d* from *Thellungiella salsuginea* identified *via* FOX hunting system functioned as a positive regulator of heat stress response in *Arabidopsis* (Higashi et al., 2013). Overexpressing rice *OsREX1-S* screened through FOX was confirmed to enhance tolerance of host plants to cadmium (Kunihiro et al., 2014). *OsCPK21* cloned from full-length cDNA overexpressed rice was involved in the positive regulation in response to abscisic acid (ABA) and salt stress (Asano et al., 2011).

Halophyte *Zoysia matrella* is an excellent warm season turfgrass that can growth in saline soils. Our previous research mainly focused on the salt tolerance evaluation and physiological responses of *Z. matrella* to salinity. Whereas the molecular mechanism of its salt tolerance is still unclear. Moreover, we identified several potential salt-genes from *Z. matrella* through yeast-based FOX system (Chen et al., 2015). In current study, we aimed to construct the *Arabidopsis*-based FOX system for further screening candidate salt-tolerant genes for future molecular breeding. In addition, we selected a novel salt-inducible candidate gene *ZmGnTL* (β-1,6-N-acetylglucosaminyltransferase like enzyme) for functional analysis.

Materials and methods

Full-length cDNA expression library construction of *Z. matrella*

The cDNA entry library plasmid was produced in our previous work (Chen et al., 2015). The library plasmid was inserted into plant expression vector pEarleyGate103 with recombination reaction system (Invitrogen, USA). The reaction products were transformed into ElectroMAX^{TM} DH10B^{TM} T1 competent cells by electroporation, and 50 μL of 100-fold diluted cells were plated on a LB solid medium containing 50 mg L^{-1} kanamycin. Kanamycin resistant bacterial colonies were counted after 12 h and transferred to 1 mL 50 mg L^{-1} kanamycin LB liquid medium for propagation. The recombination fragment size was estimated by polymerase chain reaction (PCR) with universal primer pair (TATC CTTCGCAAGACCCTTCCTCTA/GGTAAGTTTTCCGTATG TTGCATCA) of pEarleyGate103 vector.

Transformation of *Arabidopsis*, screening of salt-tolerant plants, and functional analysis of *ZmGnTL*

The expression library plasmid was transformed into *Agrobacterium tumefaciens EHA105* competent cells by electroporation, and the transformed cells were grown in LB solid medium containing 50 mg L^{-1} kanamycin for three days. All kanamycin resistant colonies were collected and suspended in 5% sucrose solution plus 0.5% Silwet-L77, and then introduced into *Arabidopsis thaliana* accession Columbia (Col-0) *via* floral dip method. The T1 generation seeds were obtained and screened in Murashige and Skoog (MS) solid medium containing 25 mg L^{-1} ampicillin, 20 mg L^{-1} glufosinate ammonium and 150 mM NaCl. Salt-tolerant transgenic plants were selected and transplanted into the soil. Leaves of those transgenic plants were used for extracting DNA, and PCR was performed using universal primer pair (F1/R1: TATCCTTCGCAAGACCCTTCCTCTA/GGTAAGTTTTCC GTATGTTGCATCA) of pEarleyGate103 vector. Each PCR product was sequenced and BLASTX (http://blast.ncbi.nlm.nih.gov/Blast.cgi) was performed using these DNA sequences to

identify putative salt tolerant genes.

ZmGnTL gene was reamplified from the cDNA template of *Z. matrella* using ORF primer pair (ccggtcgacATGACGTCAC CGGCGCCGGCGTACA/agtgaattcgtGTCACGTAGGATGACC GAGTCCGC) and then inserted into expression vector pEarleyGate103 with recombination reaction system. For further gene functional analysis, *ZmGnTL* was retransformed into *Arabidopsis* and the transgenic plants overexpressing *ZmGnTL* were screened following the methods of MS solid medium containing 20 mg L^{-1} glufosinate. gDNA-PCR and RT-PCR was detected using primer pair (F1/R1, shown in above). The seeds of WT and T3 generation homozygous lines were sterilized and planted in MS solid medium containing 0 or 120 mM NaCl, and the growth and biomass of seedlings were measured for salt tolerance analysis. In addition, the 18d old plants of WT and T3 generation transgenic Arabidopsis were treated with 150 mM and 200 mM NaCl in pots containing nutrient soil for 15d, and the phenotype was observed and physiological indexes were analyzed following the methods below.

Expression analysis of candidate salt-tolerant genes

Z. matrella were hydroponic planted in Hoagland nutrient solution and treated with 300 mM NaCl concentration. The leaves were collected at 0, 1, 3, 6, 24, 48 h and RNA were extracted using Trizol RNA Kit (Invitrogen, USA). For the reverse transcription reaction, 0.5 μg RNA was used in the reaction with PrimeScript RT reagent Kit and treated with gDNA Eraser (TaKaRa, USA). Primer pairs of candidate salt-tolerant genes and *ZmACT* (GenBank Number: GU290545) as a reference gene are displayed in Table 1. LightCycler 480 SYBR I master (Roche, Switzerland) was used for each 15 μL reaction, which contained 5 μL of diluted cDNA (60 ng/μl), 7.5 μL 2×SYBR I master, 0.4 μL each primer (10 μM), and 1.7 μL ddH_2O. The qRT-PCR reactions were performed using a LightCycler 480 II (Roche, Switzerland) with the following cycling conditions: an initial denaturation at 95°C for 10 min, followed by 40 cycles of 95°C/15 s, 58°C/15 s and 72°C/30 s, and thereafter melting curves were produced at 60-95°C. Gene relative expression levels were measured by $2^{-\Delta\Delta Ct}$ method. Each qRT-PCR analysis was performed in triplicate.

TABLE 1 qPCR primers for candidate salt-tolerance genes.

Salt-tolerant genes	Primer sequences 5'-3'(RT-Forward/RT-Reverse)
ZmSAP8	AAGGCAAATCCAGTGGTGAAG/ AAAGGGAAAGGCATGGGTAAA
ZmASR	TTCCACGAGCACCACGAGA/ CAGAGAGAAGAGGGCCAACAC
ZmDUF1644	GACAACGAAGAAGATGATAACCC/ CCAACTCCCACACGACAGT
ZmGnTL	CACCCGAGTGTCTTGAGCCA/ CAACCTAATAATCCCGTGTTTC
ZmSANT	CAAGAGAAAGCACAGAAAGAACC/ CAAGGGAAACATTACAACAAGG
ZmZAT	CCAGTAGGCTAATCTCAGGCTTC/ CAACGACAGGATAGACAGACACC
ZmLectin	CATGGTGGTGTGCGTGATG/ AAGACAGGAGCGGGTTGGA
ZmDBTNBT	TCATCCTCAAGGCTCCGTT/ CCTGCCGTCAATTTTTTCC
ZmGRX	CAAGGAAAACTGAGAGAGAGGC/ AGGAACAGGGGAAACAAAGAA
ZmUBP	AAGGACGACCTGACAGGCAG/ CGCTGTGATCCGAACCTAAAG
ZmUAM	GCTTGGGATGAGCTGAACCC/ CCACCTGCATGACAACAGAATT

Measurement of electrolyte leakage (EL) and relative water content (RWC)

Electrolyte leakage (EL) of leaves was measured according to the method of Blum and Ebercon (1981). Briefly, about 0.2 g fresh leaves were weighed and placed into a 50 mL centrifuge tube containing 30 mL ultrapure water. The centrifuge tubes were agitated on a shaker for 24 h at room temperature, and the initial conductivity (C_0) was measured with conductivity meter (Thermo, New York, USA). The tubes containing the same leaf tissue samples were then autoclaved at 121°C for 15 mins and agitated for another 24 h to measure the final conductivity (C_l). The EL was calculated as $C_0/C_l \times 100\%$. About 0.2 g fresh leaves were collected to measure leaf fresh weight (FW), submerged in water for 12 h to measure leaf turgid weight (TW), then dried at 80°C for 72 h to measure leaf dry weight (DW). The RWC was calculated as (FW–DW)/(TW–DW) × 100%.

Ion content analysis

Ten days after salt stress treatment, about 0.1 g fresh leaf or root tissue of *Arabidopsis* was oven-dried at 80°C to a constant weight. The oven-dried tissue was then decomposed for 45 min at 160°C by a microwave (ETHOS ONE, Milestone, Italy) in a digestion solution of 3 mL 65% nitric acid. After that, the liquid was diluted to 30 mL with ultrapure water. The contents of K^+ and Na^+ were determined by an ICP-OES (Optima 8000, Perkin Elmer, USA).

Quantification of superoxide O_{2^-} and hydrogen peroxide (H_2O_2)

The O_{2^-} production rate was measured according to Zhang et al. (2016). Briefly, leaf tissue (0.1 g) was frozen using liquid nitrogen and ground to powder, homogenized in 3 mL 65 mM phosphate buffer (PBS, pH 7.8), and centrifuged at 10000 × g for 15 min at 4°C. In the meantime, a 5:1 ratio of PBS (pH 7.8) and 10 mM hydroxylamine hydrochloride mixture was incubated at 25°C for 10 min. Then, 0.5 mL of the supernatant obtained from centrifugation was transferred to 0.5 mL mixture and incubated at 25°C for 20 min. After incubation, 1 mL 58 mM sulfonamides and 1 mL 7 mM naphthylamine were added to the mixture, and incubated at 25°C for another 20 min. Finally, 3 mL of chloroform was added to the reaction mixture, vortexed, then centrifuged at 10000 × g for 3 min. The absorbance was measured at 530 nm using a spectrophotometer (Spectronic Instruments, NY, USA). The production rate of O_2^- was calculated according to the formula described by Elstner and Heupel (1976).

Each 0.5 g leaf tissue sample was frozen using liquid nitrogen and ground to powder, then 5 mL cold 0.1% trichloroacetic acid (TCA) was added and homogenized. The homogenate was centrifuged at 12000 × g for 15 min and 0.5 mL of the supernatant was mixed with 0.5 mL 10 mM PBS buffer (pH 7.0) and 1 mL 1 M KI. The mixture was incubated at 28°C for 15 min in dark. The absorbance was measured at 390 nm. The content of H_2O_2 was calculated based on a standard curve generated with known H_2O_2 concentrations.

The analysis of enzymatic antioxidant activity

The enzymatic antioxidant activities of superoxide dismutase (SOD), peroxidase (POD), catalase (CAT), and ascorbate peroxidase (APX) were quantified using the methods described by Zhang et al. (2016). About 0.3 g leaf tissue was frozen using liquid nitrogen, ground to powder, then homogenized in 3 mL precooled 50 mM PBS (pH 7.8) containing 1% polyvinylpyrrolidone (PVP) and 0.2 mM EDTA. Homogenates were centrifuged at 15000 × g at 4°C for 20 min, and the supernatant was saved for the following enzyme activity analyses. SOD activity was measured at 560 nm absorbance. It is defined as the amount of enzyme required to cause 50% inhibition of nitroblue tetrazolium chloride reduction (Meloni et al., 2003). POD activity was measured by determining guaiacol oxidation by H_2O_2 at 470 nm (Lacan and Baccou, 1998). CAT activity was measured by monitoring the disappearance of H_2O_2 at 240 nm (Maehly and Chance, 1954). APX activity was measured by the decrease in absorbance at 290 nm for 1 min (Nakano and Asada, 1981).

Quantification of proline, glycine betaine and soluble sugar

The proline content was measured according to the description of Abrahám et al. (2010). About 0.1 g leaf or root tissue was ground to powder using liquid nitrogen and then homogenized in 0.5 mL 3% sulfosalicylic acid. Homogenates were centrifuged at 15000 × g at room temperature for 5 min. The plant extract supernatant (100 µL) was transferred to a 1.5 mL centrifuge tube, mixed with 500 µL reaction mixture (3% sulfosalicylic acid: glacial acetic acid: Acidic ninhydrin=1: 2: 2), and incubated at 96°C for 60 min. After incubation, 1 mL toluene was added to the reaction mixture and vortexed for 20 s; the organic layer was transferred into a fresh tube after allowing the separation of the organic and water phases without disturbance for a minimum of 5 mins. The absorbance of those samples was measured at 520 nm, and proline concentration was determined by referencing to a standard curve.

The glycine betaine content was measured according to the description of Wu et al. (2018). Freeze-dried plant leaf or root (1.0 g) was ground and suspended in 25 mL 60% methanol. The extraction process was facilitated by treating the samples in an ultrasonic cleaner (Bilon, Shanghai, China) for 30 mins. Then samples were centrifuged at 15,000 × g for 8 min, and the supernatant were transferred to a new 25 mL volumetric flask and brought to volume with 60% methanol. Ten µL of each glycine betaine standard and sample was used for liquid chromatograph (Thermo fisher, Shanghai, USA) quantification at 192 nm wavelength. The glycine betaine content was determined by referencing to the standard curve.

Freeze-dried plant materials (50 mg leaf or root) were homogenized in 5 mL 80% alcohol, incubated at 30°C for 30 mins, and then centrifuged at 4500 × g at 20°C for 10 mins. The supernatant was transferred to a 50 mL centrifuge tube, mixed with 2.5 mL 80% alcohol, incubated at 30°C for 30 mins, and then centrifuged at 4500 × g at 20°C for 10 mins. This extraction step was repeated. The supernatant was transferred to a 25 mL volumetric flask and brought to volume by purified water. Then, 1 mL from the 25 mL volumetric flask was transferred to a fresh glass tube and mixed with 1 mL 23% phenol, subsequently, 5 mL 98% sulfuric acid was added and homogenized. After 15 mins, the reaction solution was cooled down to room temperature and then incubated at 30°C for 30 mins. Finally, the absorbance was measured at 490 nm, and each soluble sugar concentration was determined by referencing to its standard curve (glucose,

fructose, or sucrose); and soluble sugar concentration was the sum of the three sugar contents.

Results

cDNA expression library

To evaluate the cDNA library quality, bacteria containing the library plasmid were cultured overnight on solid medium (LB + 50 mg L^{-1} kanamycin) resulting in 520 colonies on a plate (Figure 1A). Subsequently, 24 colonies were randomly selected for PCR to determine the inserted fragment size, and the result showed that the recombination rate was 100% and the average fragment size was 1.64 kb (Figure 1B).

Salt-tolerant screening and gene mining of *Arabidopsis*

The constructed expression library plasmid was transformed into *Arabidopsis* by floral dip method, and around 5000 T1 transgenic seedlings were obtained. The harvested seeds were used to screen salt tolerant seedlings in NaCl solid medium (MS + 20 mg L^{-1} Basta +150 mM NaCl). Finally, 25 T2 salt-tolerant plants were obtained (Figure 2). We extracted the DNA from these T2 transgenic lines for PCR and identified 11 candidate salt-tolerance genes by sequencing (Table 2).

Analysis of the expression of salt-tolerant genes with qRT-PCR

We analyzed the expression pattern of 11 candidate salt-tolerance genes response to salt stress in *Z. matrella* by qRT-PCR. The result showed that salt stress induced the gene expression of *ZmSAP8, ZmASR, ZmDUF1644, ZmGnTL, ZmSANT, ZmZAT, ZmLectin, ZmGRX*, and *ZmUBP*, whereas the expression of *ZmDBTNBT* and *ZmUAM* remained relatively stable (Figure 3). The expression level of *ZmSAP8, ZmASR, ZmDUF1644, ZmGnTL, ZmGRX*, and *ZmUBP* peaked at 6 h after salt stress, while the expression of *ZmSANT* and *ZmZAT* peaked at 24 h (Figure 3). *ZmLectin* significantly increased in expression after 1 h of salt stress, and highest expression level was observed at 48 h (Figure 3). Interestingly, the relative expression of *ZmGnTL* declined at 24 h after reaching the highest expression at 6 h and increased again at 48 h (Figure 3).

Sequence analysis of *ZmGnTL*

To elucidate the potential role of *ZmGnTL* in the abiotic stress response of *Arabidopsis*, we cloned the sequence of *ZmGnTL*. The sequence length of *ZmGnTL* is 1089 bp, encoding 362 amino acids. Clustering analysis with related genes from rice and *Arabidopsis* suggested that those gene sequences can be divided into three groups (Group I, II, and III). In Group III, ZmGnTL was shown to have high sequence homology with Os03g44580 and AtGnTL (AT3G52060) (Figure 4A). A multiple sequence alignment revealed that ZmGnTL contained an amino-terminal signal peptide and a catalytic domain (GnT), which is important for glycosylation. In addition, Pfam database (http://pfam.xfam.org) analysis revealed that a conserved acid Glu^{279} site in the GnT domain may be critical for its activity (Figures 4B, C).

Overexpression of *ZmGnTL* enhances salt-tolerance of *Arabidopsis*

The expression of *ZmGnTL* increased substantially in *Arabidopsis* subjected to salt stress (Figure 3). It is plausible that *ZmGnTL* plays an important role in salt adaptation. To further confirm this hypothesis, we re-transformed *ZmGnTL* into *Arabidopsis*, and further evaluated the salt tolerance of transgenic *Arabidopsis* lines. The gDNA-PCR and RT-PCR

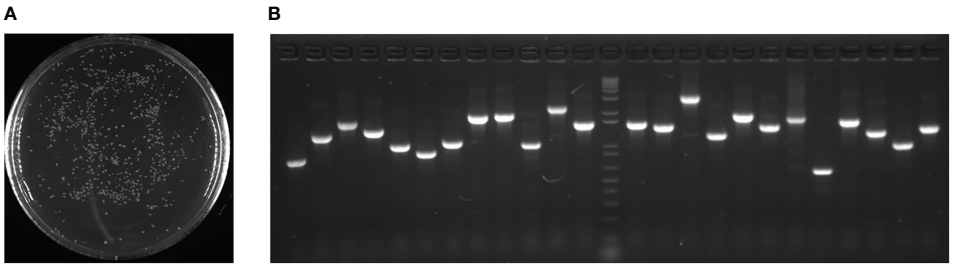

FIGURE 1
cDNA expression library quality assays. **(A)** 100-fold diluted bacteria with transformed cDNA library plasmid were cultured overnight on solid medium (LB + 50 mg L^{-1} kanamycin). **(B)** Twenty-four colonies were randomly selected for PCR to determine the size of the inserted fragment.

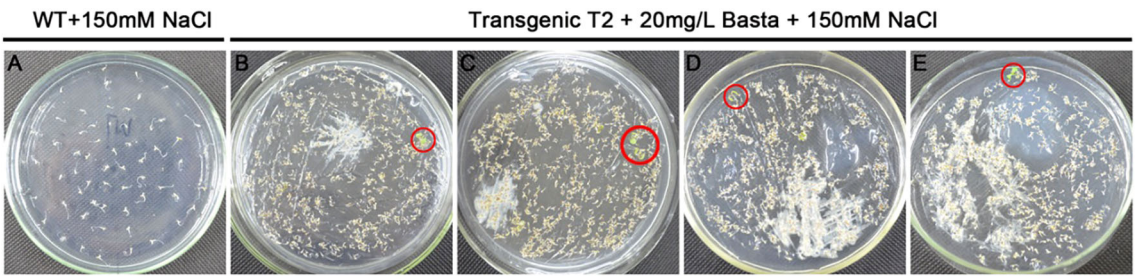

FIGURE 2
Screening of salt-tolerant *Arabidopsis* on MS plates. **(A)** Germination was completely inhibited with wildtype (WT) at 150 mM NaCl. **(B–E)** Screening transgenic lines on 20 mg L^{-1} Basta +150 mM NaCl MS plates, and salt-tolerant seedlings were circled in red.

analysis indicated that *ZmGnTL* successfully transformed into *Arabidopsis* (Figure 5A). The overexpressed lines (OX) under salt stress exhibited healthier phenotypes than wildtype (WT) in both MS medium and soil matrix. Whereas *ZmGnTL*-OX and WT were similar in growth under normal condition (Figures 5B, D). The biomass of OX lines was higher than WT under salt stress (Figure 5C), and the RWC content was also significantly higher in *ZmGnTL*-OX plants (Figure 5F). Additionally, both OX3 and OX4 exhibited lower EL levels compared with WT under salt stress (Figure 5E).

The physiological changes of *ZmGnTL* transgenic *Arabidopsis* under salt stress

To clarify the physiological changes of *ZmGnTL*-OX plants under salt stress, we measured the change of Na^+ and K^+ of *ZmGnTL*-OX and WT plants under different salinity treatments (0, 150, and 200 mM). Under control condition, the K^+ and Na^+ contents were not significantly different between *ZmGnTL*-OX lines and WT *Arabidopsis* plants. Whereas the K^+ content was increased observably in *ZmGnTL*-OX plants, while there is no significant difference in Na^+ content between *ZmGnTL*-OX plants and WT. (Figure 6). Therefore, the K^+/Na^+ ratio was higher in *ZmGnTL*-OX lines than that in WT under salt stress (Figure 6).

We also analyzed the change of antioxidation system and osmolytes of *ZmGnTL*-OX and WT plants under salt stress. The result showed that the overexpression of *ZmGnTL* significantly decreased the contents of O_2^- and H_2O_2 under salt stress (Figure 7). The enzyme activities of SOD, POD, CAT and APX were not different between *ZmGnTL*-OX lines and WT under normal growth condition (Figure 7). However, the activity levels of antioxidant enzymes SOD and APX were substantially higher in *ZmGnTL*-OX lines than those in WT *Arabidopsis* under salt stress, although the activities of POD and CAT were not affected by the overexpression (Figure 7). Proline and glycine betaine contents were also not significantly different in roots and leaves between *ZmGnTL*-OX lines and WT under normal condition (Figure 8). On the contrary, the accumulation of proline and glycine betaine was increased in leaves of *ZmGnTL*-OX plants under both 150 and 200 mM NaCl compared with WT. The contents of proline and glycine in root were significantly different under 150 mM NaCl but not

TABLE 2 Sequence analysis and function prediction of candidate salt-tolerance genes.

Salt-tolerant genes	ORF (bp/aa)	Predicted function
FOX-ST1	516/171	A20/AN1 domain-containing stress-associated protein8(SAP8)
FOX-ST2	399/132	ABA-, stress-and fruit-ripening inducible-like protein(ASR)
FOX-ST3	1026/341	DUF1644 family Protein(DUF1644)
FOX-ST4	1089/362	GnT-Like family protein(GnTL)
FOX-ST5	975/324	SANT domain protein(SANT)
FOX-ST6	1185/395	zinc transporter(ZAT)
FOX-ST7	981/327	Ricin B-related lectin domain containing protein(Lectin)
FOX-ST8	1251/417	3-N-debenzoyl-2-deoxytaxolN-benzoyl transferase(DBTNBT)
FOX-ST9	582/194	Glutaredoxin family(GRX)
FOX-ST10	1704/568	U-box domain-containing protein 39(UBP)
FOX-ST11	1098/366	UDP-arabinopyranosemutase 1(UAM)

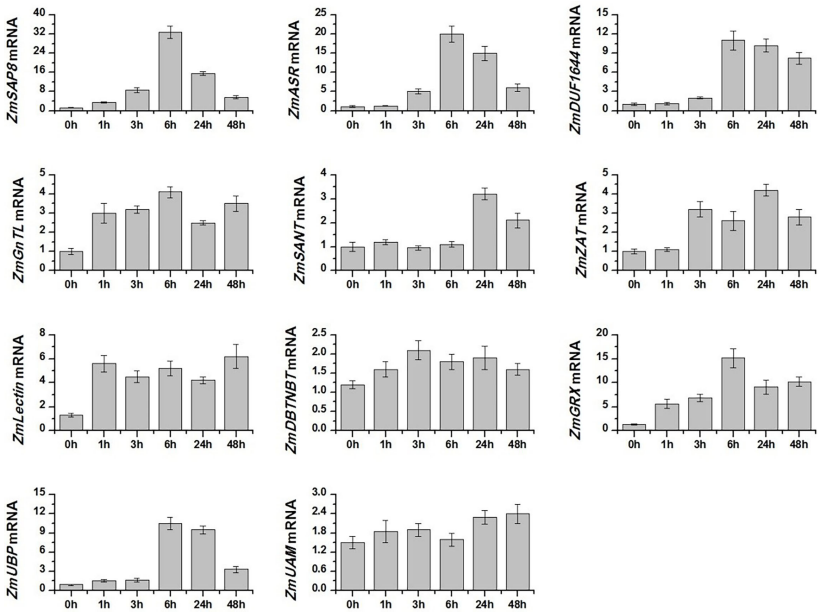

FIGURE 3
Relative expression levels of candidate salt-tolerant genes of *Zoysia matrella* treated with 300 mM NaCl. Data are shown as means ± SE of five biological replicates.

under 200 mM NaCl (Figure 8). There was not significantly difference in soluble sugar contents in both roots and leaves between *ZmGnTL*-OX lines and WT under both normal and salt stress conditions (Figure 8).

ZmGnTL influenced the expression of salt tolerant genes

To explore the molecular mechanism of *ZmGnTL* in regulating salt stress, WT and *ZmGnTL*-OX *Arabidopsis* plants were subjected to 24 h of salt stress to analyze the expression of genes associated with ion transport (*AKT1, NHX1, VP1*, and *KUP7*) (Hirsch et al., 1998; Apse et al., 2003; Li et al., 2005; Han et al., 2016), antioxidation (*APX1* and *Mn-SOD*) (Li et al., 2019; Chen et al., 2022), and osmotic adjustment (*PDH, P5CS, CMO*, and *BADH*) (Peng et al., 1996; Strizhov et al., 1997; Fitzgerald et al., 2009; Luo et al., 2012). The expression of *AtNHX1* was significantly higher in *ZmGnTL*-OX lines than that in WT roots and leaves under salt stress, while the expression was similar under normal condition (Figure 9). In the roots, the expression of *AtAKT1* was significantly higher in *ZmGnTL*-OX lines compared with that in WT under salt stress (Figure 9). Overexpression of *ZmGnTL* increased the expression of *AtAPX1* under 150 mM NaCl and *AtMn-SOD* under both 150 and 200 mM NaCl conditions, but their expression levels were lower and similar between *ZmGnTL*-OX lines and WT under normal condition (Figure 10). Under salt stress, genes related to osmotic stress regulation, such as *AtP5CS* and *AtBADH*, were also up-regulated in *ZmGnTL*-OX transgenic lines, the expression of *AtPDH* was similar between *ZmGnTL*-OX lines and WT under both 0 and 200 mM NaCl conditions but significantly lower in *ZmGnTL*-OX lines under 100 mM NaCl (Figure 10).

Discussion

Candidate salt-tolerant genes from *Z. matrella*

Salt stress leads to various physiological and molecular changes and impedes plant growth. To alleviate the damage of high concentrations of sodium, many genes are involved in regulating the salt stress under various mechanisms. In this study, 11 salt-tolerant genes from *Z. matrella* were identified. Many of these genes have been reported in various important biological processes.

The stress-associated protein 8 (SAP8) was reported as an osmotic stress-responsive transcription factor (Kanneganti and Gupta, 2008). Previous research showed that several SAP proteins are regulated by drought and salinity stress (Kanneganti and Gupta, 2008). Another gene ASR was associated with ABA in regulating stress and fruit ripening (Yoon et al., 2021); this gene family has been identified to responding to abiotic stresses and ABA in maize and rice but

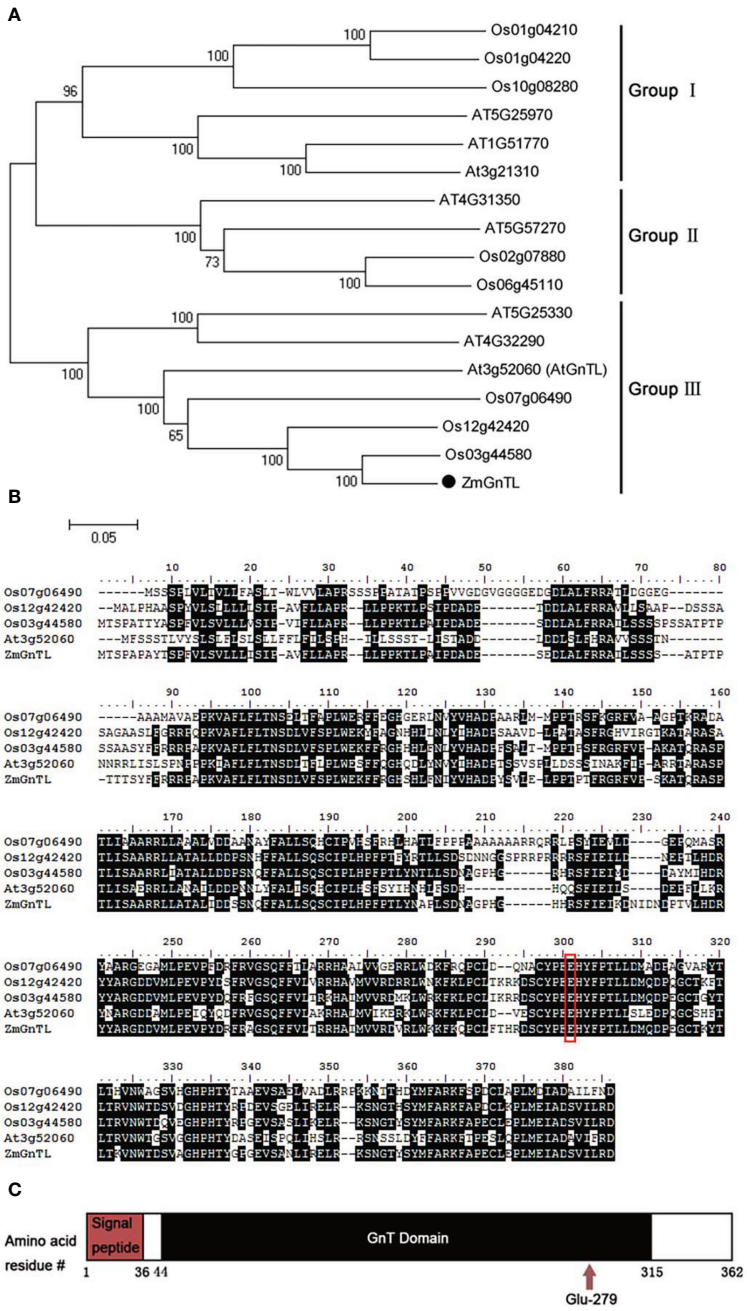

FIGURE 4
Sequence analysis of *ZmGnTL*. **(A)** Clustering analysis with related genes from rice and *Arabidopsis*. **(B)** Multiple sequence alignment analysis. **(C)** Pfam database predicted conserved domain.

is absent in *Arabidopsis* (Zhang et al., 2015; Yoon et al., 2021). For example, a study has demonstrated that overexpression of *OsASR1* and *OsASR3* improved drought and salinity tolerance in transgenic rice (Joo et al., 2013). Glutaredoxins (GRXs) are small disulfide oxidoreductases that catalyze the reduction of disulfide bridges (Rouhier et al., 2008). Studies on the function of GRXs in plants have mainly focused on model plants, and it has been shown that GRXs are involved in the stress response and hormone signaling (Morita et al., 2015; El-Kereamy et al., 2015; Verma et al., 2016; Li et al., 2021). Zinc transporter (ZAT) is a type of zinc finger proteins (ZFPs) which are transcriptional regulators in plants (Han et al., 2020). In rice, ZAT was reported to regulate the expression of several genes that involved in ROS signaling when plants were under salt stress

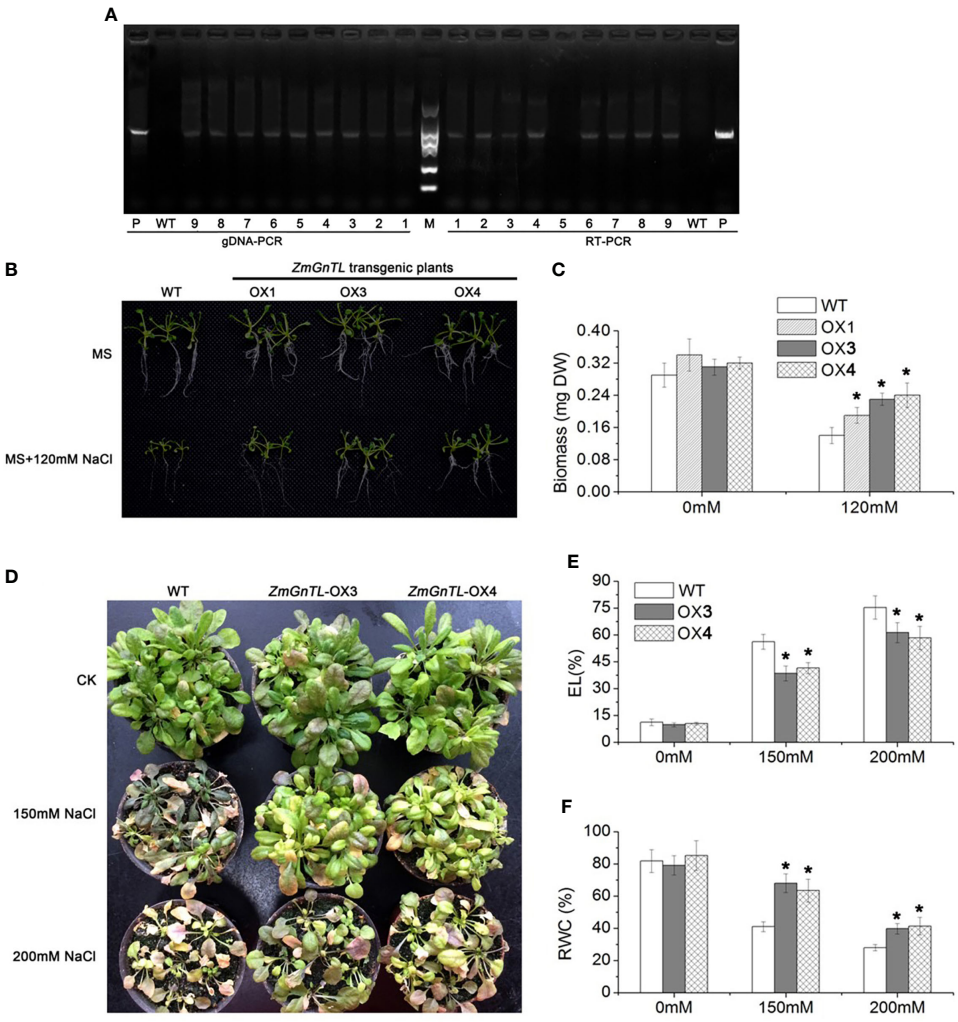

FIGURE 5
Overexpression of *ZmGnTL* enhanced the salt-tolerance in *Arabidopsis*. **(A)** gDNA -PCR and RT-PCR analysis of transgenetic lines, P (*ZmGnTL* plasmid), WT (wild type), 1-9 (transgenetic lines). **(B)** A comparison of salt-tolerant phenotypes and wildtype (WT) grown on MS medium. **(C)** Biomass of *Arabidopsis* seedlings grown on MS medium. **(D)** A comparison of salt-tolerant phenotypes and WT in soil matrix. **(E, F)** Electrolytic leakage (EL) and relative water content (RWC) of *Arabidopsis* plants. Data are shown as means ± SE of three to five biological replicates, and * indicated statistical significance at P< 0.05.

(Sun et al., 2010). Recently, *GhZAT34* and *GhZAT79* genes from *Gossypium hirsutum* were found to enhance salt tolerance in *Arabidopsis* and cotton (Rehman et al., 2021).

Lectins are a group of structurally diverse proteins which are defined as carbohydrate binding proteins and further divided into 25 subfamilies. Lectin plays an important role in response to abiotic or biotic stimuli (Vierbuchen, 1991; Naithani et al., 2021). In this study, we also identified a Glycosyltransferases (GTs) family gene *GnTL* in *Z. matrella*. GTs family protein is required for protein glycosylation (Vogt and Jones, 2000), and studies have shown that overexpressing genes (UGT85A5 and UGT87A2) from this family increased salt-tolerance in *Arabidopsis* and tobacco (Sun et al., 2013; Li et al., 2017). The protein encoded in *Arabidopsis AtGnTL* (AT3G52060) is involved in plasmodesmata interaction (Zalepa-King and Citovsky, 2013), but the function of *AtGnTL* related to salt tolerance has not been fully described.

Using the FOX system, we also identified an interesting gene, *DUF1644*, which belong to DUFs (domains of unknown functions) families (Bateman et al., 2010). The DUF1644 gene family is highly conserved in plants, but the biological function is unclear. Recently, a salt-induced gene, *OsSIDP366* (stress induced DUF1644 family protein), was found in rice, and overexpressing *OsSIDP366* significantly improved the salt tolerance of rice (Guo et al., 2016). Additionally, we identified *ZmSANT* gene. SANT domain

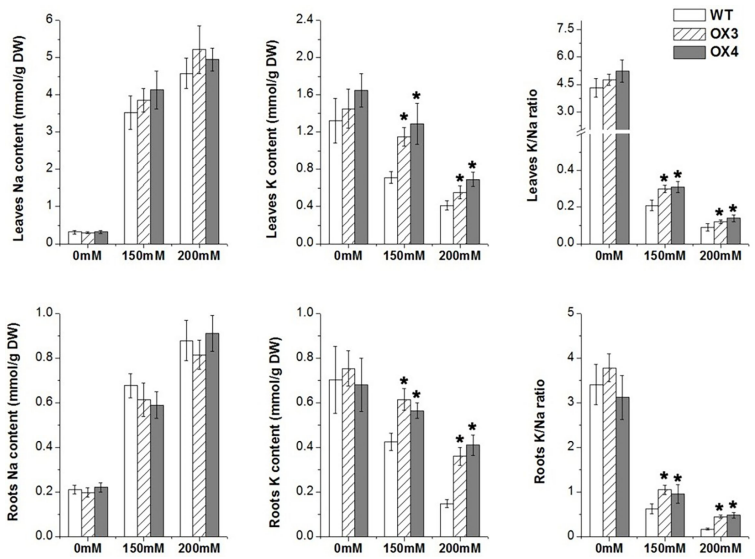

FIGURE 6
Contents of Na^+ and K^+ in leaves and roots of *ZmGnTL* transgenic *Arabidopsis*. *ZmGnTL*-OX plants and WT were treated with 0 mM, 150 mM, and 200 mM NaCl for 10 days. Data are shown as means ± SE of three to five biological replicates, and * indicated statistical significance at *P< 0.05.

protein was reported to be associated with chromatin remodeling, histone acetylation and deacetylation, but the biological function is unknown (Boyer et al., 2004; Marcum and Radhakrishnan, 2019). Fox system is reliable and efficient for screening up-regulated genes under salt stress or other abiotic stresses. Using this method, we successfully identified many candidate genes for further studying the mechanism of salt tolerance in halophytes.

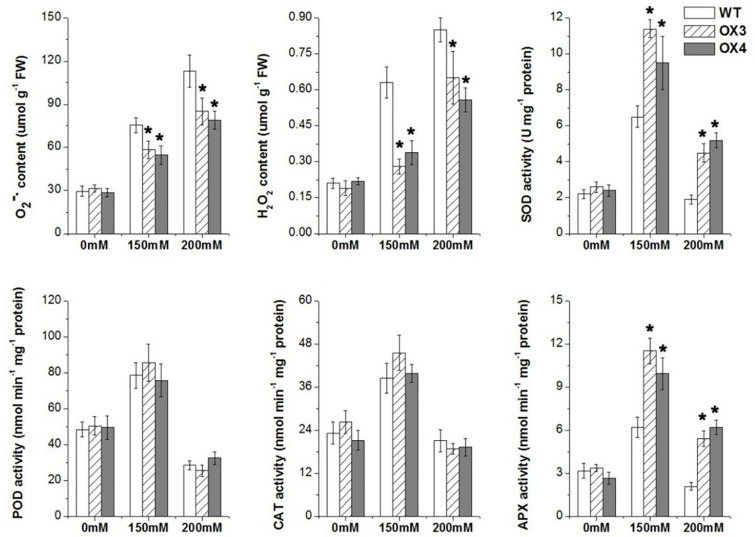

FIGURE 7
Reactive oxygen species contents and antioxidant enzyme activities of *ZmGnTL* transgenic *Arabidopsis*. *ZmGnTL*-OX plants and WT were treated with 0 mM, 150 mM, and 200 mM NaCl for 10 days. Data are shown as means ± SE of three to five biological replicates, and * indicated statistical significance at *P< 0.05.

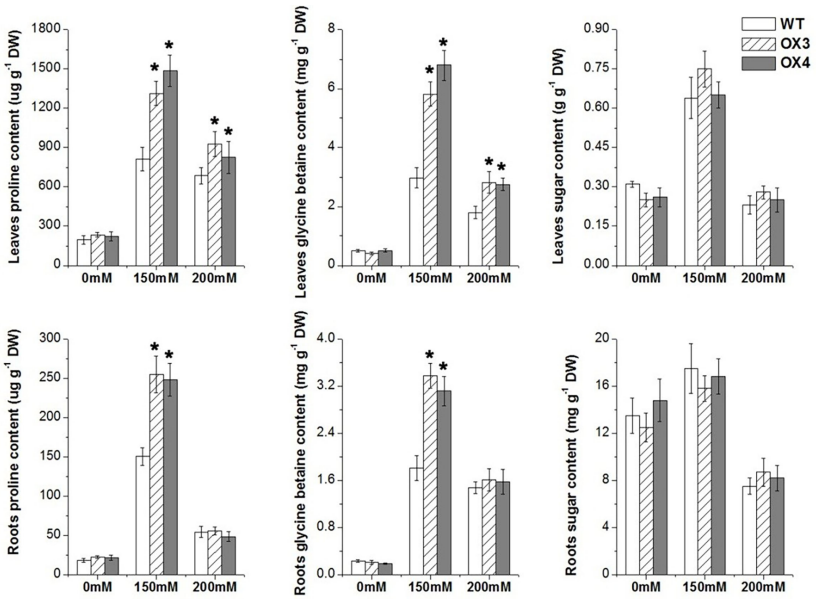

FIGURE 8
Osmolyte contents in leaves and roots of *ZmGnTL* transgenic *Arabidopsis*. *ZmGnTL*-OX plants and WT were treated with 0 mM, 150 mM, and 200 mM NaCl for 10 days. Data are show as means ± SE of three to five biological replicates, and * indicated statistical significance at *P< 0.05.

Overexpression of *ZmGnTL* improved the salt tolerance of *Arabidopsis*

GnTL genes belong to the glycosyltransferase superfamily and are crucial in glycan synthesis (Fukuda and Hindsgaul, 1994) by adding the oligosaccharide side chains to glycoproteins (Siddiqui et al., 2005). This protein has been found in more than 19 plant species (Zalepa-King and Citovsky, 2013). However, many of the GnTL genes are not clearly characterized in their functions. In this study, we identified a gene *ZmGnTL* using a plant cDNA library screening method (FOX) under salt stress. Furthermore, we demonstrated the function of *ZmGnTL* in *Arabidopsis* salt tolerance. Salt stress severely inhibited the growth of *Arabidopsis*. The overexpression of *ZmGnTL* alleviated the

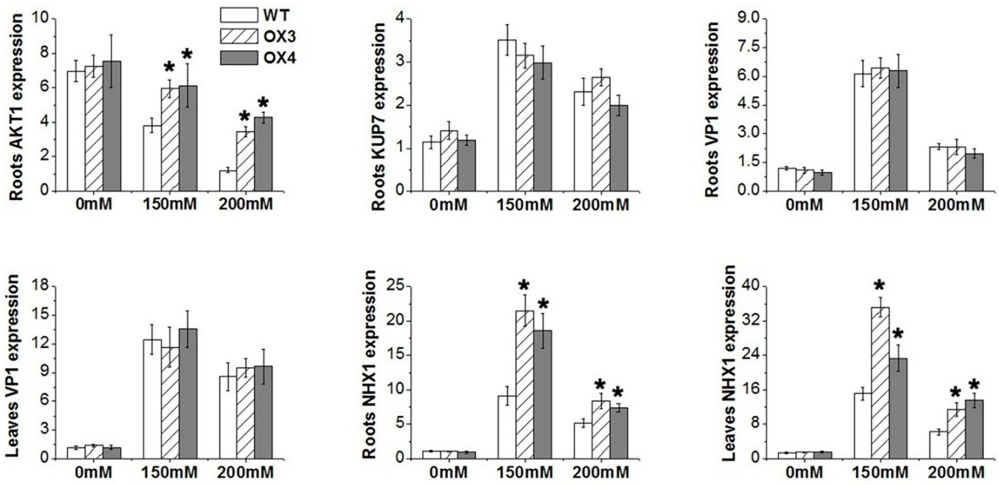

FIGURE 9
The relative expression of genes regulating ions balance in *Arabidopsis* under salt stress. *ZmGnTL*-OX plants and WT were treated with 0 mM, 150 mM, and 200 mM NaCl for 48 h. Data are shown as means ± SE of five biological replicates, and * indicated statistical significance at *P< 0.05.

damage of salt stress (Figure 5C), and the transgenic plants showed greater seedlings biomass and RWC content under salt treatment than WT (Figures 5B, E). Based on the data from the current study, we did not observe any advantages of the transgenic *Arabidopsis* lines overexpressing *ZmGnTL* growing under non-stress condition; those transgenic plants showed normal growth and similar genotypes as WT under non-salt stress condition, which was further supported by our results of similar physiological and gene expression measurements.

Under salt stress, higher Na^+ accumulation in plant leads to the disruption of ion homeostasis. Since excessive Na^+ often leads to K^+ deficiency, plants need to modulate the Na^+/K^+ homeostasis through maintaining high K^+/Na^+ ratio (Park et al., 2016). The potassium transporters, such as the inward-rectifier K^+ channel *Arabidopsis* K transporter (AKT1) plays an important role in K^+ uptake and transport in the root (Nieves-Cordones et al., 2014). In this study, we found that overexpression of *ZmGnTL* increased K^+ content and K^+/Na^+ ratio (Figure 6) through up-regulating the expression of *AtAKT1* and *AtNHX1* (a Na^+/H^+ antiporter, which transports Na^+ away from the cytosol to vacuolar) under salt stress to maintain the ion balance (Figure 9).

Under salt stress, ion imbalance and water deficiency in the plant cell cause osmotic stress. Salt stress induces the reduction in cell turgor pressure, shrinkage of the plasma membrane, and physical alteration of the cell wall (Park et al., 2016). In order to alleviate the damage of osmotic stress, plants activate the osmolyte (such as proline, polyols, and sugars) accumulation under salt stress (Yang and Guo, 2018a). Our results demonstrated that overexpression of *ZmGnTL* increased proline and glycine betaine contents in response to salt stress (Figure 8). In addition, gene expression experiment also revealed that the increased expression of *AtP5CS* (proline biosynthesis) and *AtBADH* (betaine aldehyde dehydrogenase) in transgenic lines compared with WT under salt stress; however, the expression of *AtPDH* was decreased (Figure 10). Proline dehydrogenase (PDH) is functioned to remove free proline and prevent excessive proline accumulation after salt stress. A reciprocal regulation of P5CS and PDH was previously described to control the levels of proline during and after osmotic stress (Peng et al., 1996).

In plants, salt-stress-triggered ion stress and osmotic stress cause metabolism imbalance and toxic accumulation of ROS, which lends to oxidative damages (Yang and Guo, 2018b). Plant cells sense the accumulated ROS and respond rapidly by using regulatory mechanisms to scavenge ROS and activate a series of downstream adaptive responses (Park et al., 2016; Van Zelm et al., 2020). Several studies have shown that the activities of ROS scavenging enzymes and antioxidants are triggered by salt stress stimuli. For example, the APX and CAT are activated by salt stress to alleviate oxidative stresses (Sofo et al., 2015; Choudhury et al., 2017). In our study, the content of ROS O_2^- and H_2O_2 were significantly lower in transgenic *Arabidopsis* compared to WT. These findings were also supported by the increased expression of SOD and APX genes in synthesizing ROS detoxifying proteins under salt stress (Figure 6). Therefore, our results indicated that *ZmGnTL* could effectively increase the content of antioxidant enzymes and help plants to alleviate the ROS toxicity caused by salt stress.

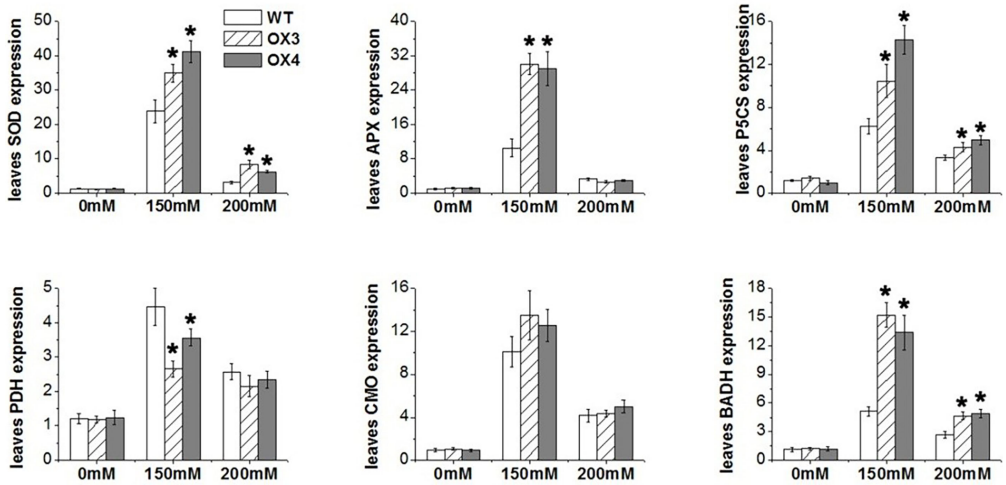

FIGURE 10
The relative expression of genes regulating antioxidant enzyme and osmolytes in *Arabidopsis* under salt stress. *ZmGnTL*-OX plants and WT were treated with 0 mM, 150 mM, and 200 mM NaCl for 48 h. Data are shown as means ± SE of five biological replicates, and * indicated statistical significance at *P< 0.05.

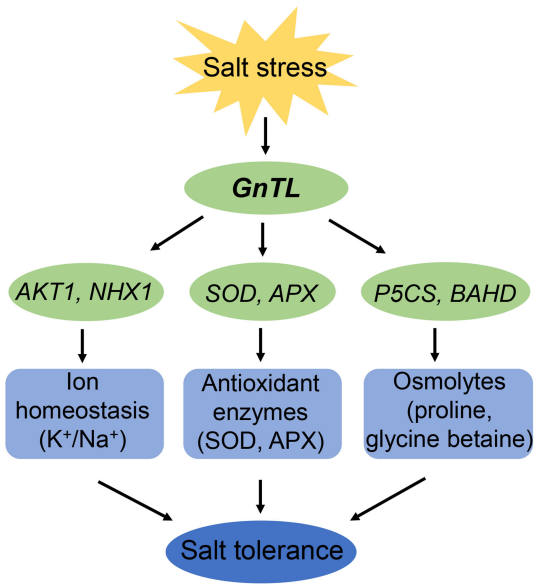

FIGURE 11
Proposed model for functional process of *GnTL* in improving plant salt tolerance.

Conclusion

In summary, 11 new salt tolerance candidate genes from *Z. matrella* were identified by FOX system. Among those genes, we analyzed the function of *ZmGnTL* in *Arabidopsis* in response to salt stress. Overexpression of *ZmGnTL* significantly up-regulated the expression of K^+ transporter gene, *AKT1*, tonoplast Na^+/H^+ antiporter gene, *NHX1*, *SOD*, *APX*, *P5CS*, and *BADH*, and down-regulated the expression of proline dehydrogenase gene, *PDH*. Our results suggested that *ZmGnTL* was involved in alleviating ion toxicity, and oxidative and osmotic stress under salt stress (Figure 11). *ZmGnTL* could be an important target gene for improving crop salt tolerance through genetic engineering.

Data availability statement

The original contributions presented in the study are included in the article/supplementary material. Further inquiries can be directed to the corresponding author.

Author contributions

YC, JiL, and JZ designed the experiments. YZ, JZ, and JuL performed the experiments. YZ, YC, and WK analyzed the data with suggestions by JC, HG, and JuL. YZ, YC, and RW wrote the manuscript. All authors contributed to the article and approved the submitted version.

Funding

This work was supported by the National Natural Science Foundation of China (31301806, 31872953 and 31672193).

Conflict of interest

The authors declare that the research was conducted in the absence of any commercial or financial relationships that could be construed as a potential conflict of interest.

Publisher's note

References

Abrahám, E., Hourton-Cabassa, C., Erdei, L., and Szabados, L. (2010). Methods for determination of proline in plants. *Methods Mol. Biol.* 639, 317–331. doi: 10.1007/978-1-60761-702-0_20

Almeida, D. M., Oliveira, M. M., and Saibo, N. J. M. (2017). Regulation of na+ and k+ homeostasis in plants: towards improved salt stress tolerance in crop plants. *Genet. Mol. Biol.* 40, 326–345. doi: 10.1590/1678-4685-GMB-2016-0106

Apse, M. P., Sottosanto, J. B., and Blumwald, E. (2003). Vacuolar cation/H+ exchange, ion homeostasis, and leaf development are altered in a T-DNA insertional mutant of AtNHX1, the arabidopsis vacuolar Na+/H+ antiporter. *Plant J.* 36, 229–239. doi: 10.1046/j.1365-313x.2003.01871.x

Asano, T., Hakata, M., Nakamura, H., Aoki, N., Komatsu, S., Ichikawa, H., et al. (2011). Functional characterisation of OsCPK21, a calcium-dependent protein kinase that confers salt tolerance in rice. *Plant Mol. Biol.* 75, 179–191. doi: 10.1007/s11103-010-9717-1

Bateman, A., Coggill, P., and Finn, R. D. (2010). DUFs: families in search of function. *Acta Crystallogr. Sect. F. Struct. Biol. Cryst. Commun.* 66, 1148–1152. doi: 10.1107/S1744309110001685

Benito, B., Haro, R., Amtmann, A., Cuin, T. A., and Dreyer, I. (2014). The twins k+ and na+ in plants. *J. Plant Physiol.* 171, 723–731. doi: 10.1016/j.jplph.2013.10.014

Blum, A., and Ebercon, A. (1981). Cell membrane stability as a measure of drought and heat tolerance in wheat1. *Crop Sci.* 21, 43–47. doi: 10.2135/cropsci1981.0011183X002100010013x

Boyer, L. A., Latek, R. R., and Peterson, C. L. (2004). The SANT domain: a unique histone-tail-binding module? *Nat. Rev. Mol. Cell Biol.* 5, 158–163. doi: 10.1038/nrm1314

Chen, H., Lee, J., Lee, J. M., Han, M., Emonet, A., and Lee, J. (2022). MSD2, an apoplastic Mn-SOD, contributes to root skotomorphogenic growth by modulating ROS distribution in arabidopsis. *Plant Sci.* 317, 111192. doi: 10.1016/j.plantsci.2022.111192

Chen, Y., Zong, J., Tan, Z., Li, L., Hu, B., and Chen, C. (2015). Systematic mining of salt-tolerant genes in halophyte-zoysia matrella through cDNA expression library screening. *Plant Physiol. Biochem.* 89, 44–52. doi: 10.1016/j.plaphy.2015.02.007

Choudhury, F. K., Rivero, R. M., Blumwald, E., and Mittler, R. (2017). Reactive oxygen species, abiotic stress and stress combination. *Plant J.* 90, 856–867. doi: 10.1111/tpj.13299

El-Kereamy, A., Bi, Y. M., Mahmood, K., Ranathunge, K., Yaish, M. W., and Nambara, E. (2015). Overexpression of the CC-type glutaredoxin, OsGRX6 affects hormone and nitrogen status in rice plants. *Front. Plant Sci.* 6. doi: 10.3389/fpls.2015.00934

Elstner, E. F., and Heupel, A. (1976). Inhibition of nitrite formation from hydroxylammonium-chloride: a simple assay for superoxide dismutase. *Anal. Biochem.* 70, 616–620. doi: 10.1016/0003-2697(76)90488-7

Fitzgerald, T. L., Waters, D. L., and Henry, R. J. (2009). Betaine aldehyde dehydrogenase in plants. *Plant Biol.* 11, 119–130. doi: 10.1111/j.1438-8677.2008.00161.x

Flowers, T. J., Munns, R., and Colmer, T. D. (2015). Sodium chloride toxicity and the cellular basis of salt tolerance in halophytes. *Ann. Bot.* 115, 419–431. doi: 10.1093/aob/mcu217

Fukuda, M., and Hindsgaul, O. (1994). *Molecular glycobiology* (New York: Oxford University Press).

Gao, Y. G., Zhao, B. Q., Jiao, X. M., Chen, M., Wang, B. S., and Yuan, F. (2021). Coupled development of aalt glands, stomata, and pavement cells in limonium bicolor. *Front. Plant Sci.* 12. doi: 10.3389/fpls.2021.745422

Guo, C., Luo, C. K., Guo, L. J., Li, M., Guo, X. L., Zhang, Y. X., et al. (2016). OsSIDP366, a DUF1644 gene, positively regulates responses to drought and salt stresses in rice. *J. Integr. Plant Biol.* 58, 492–502. doi: 10.1111/jipb.12376

Han, G. L., Lu, C. X., Guo, J. R., Qiao, Z. Q., Sui, N., Qiu, N. W., et al. (2020). C2H2 zinc finger proteins: master regulators of abiotic stress responses in plants. *Front. Plant Sci.* 11. doi: 10.3389/fpls.2020.00115

Han, Q. Q., Wang, Y. P., Li, J., Li, J., Yin, X. C., Jiang, X. Y., et al. (2022). The mechanistic basis of sodium exclusion in puccinellia tenuiflora under conditions of salinity and potassium deprivation. *Plant J.* 112, 322–338. doi: 10.1093/mp/sst024

Han, M., Wu, W., Wu, W. H., and Wang, Y. (2016). Potassium transporter KUP7 is involved in k+ acquisition and translocation in arabidopsis root under k +-limited conditions. *Mol. Plant* 9, 437–446. doi: 10.1016/j.molp.2016.01.012

Higashi, Y., Ohama, A., Ishikawa, T., Katori, T., Shimura, A., Kusakabe, K., et al (2013). HsfA1d, a protein identified via FOX hunting using Thellungiella salsuginea cDNAs, improves heat tolerance by regulating heat stress responsive gene expression. *Mol. Plant* 6, 411–22. doi: 10.1093/mp/sst024

Higuchi, M., Kondou, Y., Ichikawa, T., and Matsui, M. (2011). Full-length cDNA overexpressor gene hunting system (FOX hunting system). *Methods Mol. Biol.* 678, 77–89. doi: 10.1007/978-1-60761-682-5_7

Higuchi-Takeuchi, M., and Matsui, M. (2014). Screening for gene function using the FOX (full-length cDNA overexpressor gene) hunting system. *Methods Mol. Biol.* 1056, 201–210. doi: 10.1007/978-1-62703-592-7_19

Hirsch, R. E., Lewis, B. D., Spalding, E. P., and Sussman, M. R. (1998). A role for the AKT1 potassium channel in plant nutrition. *Science* 280, 918–921. doi: 10.1126/science.280.5365.918

Ichikawa, T., Nakazawa, M., Kawashima, M., Iizumi, H., Kuroda, H., Kondou, Y., et al. (2006). The FOX hunting system: an alternative gain-of-function gene hunting technique. *Plant J.* 48, 974–985. doi: 10.1111/j.1365-313X.2006.02924.x

Igarashi, Y., Yoshiba, Y., Sanada, Y., Yamaguchi-Shinozaki, K., Wada, K., and Shinozaki, K. (1997). Characterization of the gene for delta1-pyrroline-5-carboxylate synthetase and correlation between the expression of the gene and salt tolerance in oryza sativa l. *Plant Mol. Biol.* 33, 857–865. doi: 10.1023/a:1005702408601

Ji, H. T., Pardo, J. M., Batelli, G., Van Oosten, M. J., Bressan, R. A., and Li, X. (2013). The salt overly sensitive (SOS) pathway: established and emerging roles. *Mol. Plant* 6, 275–286. doi: 10.1093/mp/sst017

Joo, J., Lee, Y. H., Kim, Y. K., Nahm, B. H., and Song, S. I. (2013). Abiotic stress responsive rice ASR1 and ASR3 exhibit different tissue-dependent sugar and hormone-sensitivities. *Mol. Cells* 35, 421–435. doi: 10.1007/s10059-013-0036-7

Jyothi-Prakash, P. A., Mohanty, B., Wijaya, E., Lim, T. M., Lin, Q., Loh, C. S., et al. (2014). Identification of salt gland-associated genes and characterization of a dehydrin from the salt secretor mangrove avicennia officinalis. *BMC Plant Biol.* 14, 291. doi: 10.1186/s12870-014-0291-6

Kanneganti, V., and Gupta, A. K. (2008). Overexpression of OsiSAP8, a member of stress associated protein (SAP) gene family of rice confers tolerance to salt, drought and cold stress in transgenic tobacco and rice. *Plant Mol. Biol.* 66, 445–462. doi: 10.1007/s11103-007-9284-2

Katerji, N., van Hoorn, J. M., Hamdy, A., and Mastrorilli, M. (2003). Salinity effect on crop development and yield, analysis of salt tolerance according to several classification methods. *Agric. Water Manag.* 62, 37–66. doi: 10.1016/S0378-3774(03)00005-2

Kunihiro, S., Kowata, H., Kondou, Y., Takahashi, S., Matsui, M., Berberich, T., et al. (2014). Overexpression of rice OsREX1-s, encoding a putative component of the core general transcription and DNA repair factor IIH, renders plant cells tolerant to cadmium- and UV-induced damage by enhancing DNA excision repair. *Planta* 239, 1101–1111. doi: 10.1007/s00425-014-2042-1

Lacan, D., and Baccou, J. C. (1998). High levels of antioxidant enzymes correlate with delayed senescence in nonnetted muskmelon fruits. *Planta* 204, 377–382. doi: 10.1007/s004250050269

Li, Z. Q., Li, J. T., Bing, J., and Zhang, G. F. (2019). The role analysis of APX gene family in the growth and developmental processes and in response to abiotic stresses in arabidopsis thaliana. *Hereditas* 41, 534–547. doi: 10.16288/j.yczz.19-026

Li, T. T., Li, M. Z., Jiang, Y. M., and Duan, X. W. (2021). Genome-wide identification, characterization and expression profile of glutaredoxin gene family in relation to fruit ripening and response to abiotic and biotic stresses in banana (Musa acuminata). *Int. J. Biol. Macromol.* 170, 636–651. doi: 10.1016/j.ijbiomac.2020.12.167

Li, P., Li, Y. J., Wang, B., Yu, H. M., Li, Q., and Hou, B. K. (2017). The arabidopsis UGT87A2, a stress-inducible family 1 glycosyltransferase, is involved in the plant adaptation to abiotic stresses. *Physiol. Plant* 159, 416–432. doi: 10.1111/ppl.12520

Li, J. S., Yang, H. B., Peer, W. A., Richter, G., Blakeslee, J., Bandyopadhyay, A., et al. (2005). Arabidopsis h+-PPase AVP1 regulates auxin-mediated organ development. *Science* 310, 121–125. doi: 10.1126/science.1115711

Luo, D., Niu, X. L., Yu, J. D., Yan, J., Gou, X. J., Lu, B. R., et al. (2012). Rice choline monooxygenase (OsCMO) protein functions in enhancing glycine betaine biosynthesis in transgenic tobacco but does not accumulate in rice (Oryza sativa l. ssp. japonica). *Plant Cell Rep.* 31, 1625–1635. doi: 10.1007/s00299-012-1276-2

Luo, X. L., Wu, J. H., Li, Y. B., Nan, Z. R., Guo, X., Wang, Y. X., et al. (2013). Synergistic effects of GhSOD1 and GhCAT1 overexpression in cotton chloroplasts on enhancing tolerance to methyl viologen and salt stresses. *PloS One* 8, e54002. doi: 10.1371/journal.pone.0054002

Maehly, A. C., and Chance, B. (1954). The assay of catalases and peroxidases. *Methods Biochem. Anal.* 1, 357–424. doi: 10.1002/9780470110171.ch14

Marcum, R. D., and Radhakrishnan, I. (2019). Inositol phosphates and core subunits of the Sin3L/Rpd3L histone deacetylase (HDAC) complex up-regulate deacetylase activity. *J. Biol. Chem.* 294, 13928–13938. doi: 10.1074/jbc.RA119.009780

Meloni, D. A., Oliva,, Marco, A., Martinez, C. A., and Cambraia, J. (2003). Photosynthesis and activity of superoxide dismutase, peroxidase and glutathione reductase in cotton under salt stress. *Environ. Exp. Bot.* 49, 69–76. doi: 10.1016/S0098-8472(02)00058-8

Mishra, A., and Tanna, B. (2017). Halophytes: Potential resources for salt stress tolerance genes and promoters. *Front. Plant Sci.* 8. doi: 10.3389/fpls.2017.00829

Morita, S., Yamashita, Y., Fujiki, M., Todaka, R., Nishikawa, Y., Hosoki, A., et al. (2015). Expression of a rice glutaredoxin in aleurone layers of developing and mature seeds: subcellular localization and possible functions in antioxidant defense. *Planta* 242, 1195–1206. doi: 10.1007/s00425-015-2354-9

Naithani, S., Komath, S. S., Nonomura, A., and Govindjee, G. (2021). Plant lectins and their many roles: Carbohydrate-binding and beyond. *J. Plant Physiol.* 266, 153531. doi: 10.1016/j.jplph.2021.153531

Nakano, Y., and Asada, K. (1981). Hydrogen peroxide is scavenged by ascorbate specific peroxidase in spinach chloroplasts. *Plant Cell Physiol.* 22, 867–880. doi: 10.1093/oxfordjournals.pcp.a076232

Nieves-Cordones, M., Alemán, F., Martínez, V., and Rubio, F. (2014). K+ uptake in plant roots. the systems involved, their regulation and parallels in other organisms. *J. Plant Physiol.* 171, 688–695. doi: 10.1016/j.jplph.2013.09.021

Park, H. J., Kim, W. Y., and Yun, D. J. (2016). A new insight of salt stress signaling in plant. *Mol. Cells* 39, 447–459. doi: 10.14348/molcells.2016.0083

Peng, Z., Lu, Q., and Verma, D. P. S. (1996). Reciprocal regulation of delta 1-pyrroline-5-carboxylate synthetase and proline dehydrogenase genes controls proline levels during and after osmotic stress in plants. *Mol. Gen. Genet.* 253, 334–341. doi: 10.1007/pl00008600

Rehman, A., Wang, N., Peng, Z., He, S. P., Zhao, Z. B., Gao, Q., et al. (2021). Identification of C2H2 subfamily ZAT genes in gossypium species reveals GhZAT34 and GhZAT79 enhanced salt tolerance in arabidopsis and cotton. *Int. J. Biol. Macromol.* 184, 967–980. doi: 10.1016/j.ijbiomac.2021.06.166

Rouhier, N., Lemaire, S. D., and Jacquot, J. P. (2008). The role of glutathione in photosynthetic organisms: emerging functions for glutaredoxins and glutathionylation. *Annu. Rev. Plant Biol.* 59, 143–166. doi: 10.1146/annurev.arplant.59.032607.092811

Shi, H., Lee, B. H., Wu, S. J., and Zhu, J. K. (2003). Overexpression of a plasma membrane na+ /H+ antiporter gene improves salt tolerance in arabidopsis thaliana. *Nat. Biotechnol.* 21, 81–85. doi: 10.1038/nbt766

Siddiqui, S. F., Pawelek, J., Handerson, T., Lin, C. Y., Dickson, R. B., Rimm, D. L., et al. (2005). Coexpression of beta1,6-n-acetylglucosaminyltransferase V glycoprotein substrates defines aggressive breast cancers with poor outcome. *Cancer Epidemiol. Biomarkers Prev.* 14, 2517–2523. doi: 10.1158/1055-9965

Slama, I., Abdelly, C., Bouchereau, A., Flowers, T., and Savouré, A. (2015). Diversity, distribution and roles of osmoprotective compounds accumulated in halophytes under abiotic stress. *Ann. Bot.* 115, 433–447. doi: 10.1093/aob/mcu239

Sofo, A., Scopa, A., Nuzzaci, M., and Vitti, A. (2015). Ascorbate peroxidase and catalase activities and their genetic regulation in plants subjected to drought and salinity stresses. *Int. J. Mol. Sci.* 16, 13561–13578. doi: 10.3390/ijms160613561

Strizhov, N., Abrahám, E., Okrész, L., Blickling, S., Zilberstein, A., Schell, J., et al. (1997). Differential expression of two P5CS genes controlling proline accumulation during salt-stress requires ABA and is regulated by ABA1, ABI1 and AXR2 in arabidopsis. *Plant J.* 12, 557–569. doi: 10.1046/j.1365-313x.1997.00557.x

Sun, S. J., Guo, S. Q., Yang, X., Bao, Y. M., Tang, H. J., Sun, H., et al. (2010). Functional analysis of a novel Cys2/His2-type zinc finger protein involved in salt tolerance in rice. *J. Exp. Bot.* 61, 2807–2818. doi: 10.1093/jxb/erq120

Sun, Y. G., Wang, B., Jin, S. H., Qu, X. X., Li, Y. J., and Hou, B. K. (2013). Ectopic expression of arabidopsis glycosyltransferase UGT85A5 enhances salt stress tolerance in tobacco. *PloS One* 8, e59924. doi: 10.1371/journal.pone.0059924

Van Zelm, E., Zhang, Y. X., and Testerink, C. (2020). Salt tolerance mechanisms of plants. *Annu. Rev. Plant Biol.* 71, 403–433. doi: 10.1146/annurev-arplant-050718-100005

Verma, P. K., Verma, S., Pande, V., Mallick, S., Deo Tripathi., R., Dhankher, O. P., et al. (2016). Overexpression of rice glutaredoxin OsGrx_C7 and OsGrx_C2.1 reduces intracellular arsenic accumulation and increases tolerance in arabidopsis thaliana. *Front. Plant Sci.* 7. doi: 10.3389/fpls.2016.00740

Vierbuchen, M. (1991). Lectin receptors. *Curr. Top. Pathol.* 83, 271–361. doi: 10.1007/978-3-642-75515-6_10

Vogt, T., and Jones, P. (2000). Glycosyltransferases in plant natural product synthesis: characterization of a supergene family. *Trends Plant Sci.* 5, 380–386. doi: 10.1016/s1360-1385(00)01720-9

Wu, Y. J., Pang, L., Li, M., and Li, L. X. (2018). Determination of betaine in lycii fructus by HPLC-CAD. *Shandong. Chem. Industry.* 47, 67–69. doi: 10.19319/j.cnki.issn.1008-021x.2018.12.026

Yang, Y. Q., and Guo, Y. (2018a). Elucidating the molecular mechanisms mediating plant salt-stress responses. *New Phytol.* 217, 523–539. doi: 10.1111/nph.14920

Yang, Y. Q., and Guo, Y. (2018b). Unraveling salt stress signaling in plants. *J. Integr. Plant Biol.* 60, 796–804. doi: 10.1111/jipb.12689

Yoon, J. S., Kim, J. Y., Kim, D. Y., and Seo, Y. W. (2021). A novel wheat ASR gene, TaASR2D, enhances drought tolerance in brachypodium distachyon. *Plant Physiol. Biochem.* 159, 400–414. doi: 10.1016/j.plaphy.2020.11.014

Yuan, F., Lyu, M. J., Leng, B. Y., Zheng, G. Y., Feng, Z. T., Li, P. H., et al. (2015). Comparative transcriptome analysis of developmental stages of the limonium bicolor leaf generates insights into salt gland differentiation. *Plant Cell Environ.* 38, 1637–1657. doi: 10.1111/pce.12514

Zalepa-King, L., and Citovsky, V. (2013). A plasmodesmal glycosyltransferase-like protein. *PloS One* 8, e58025. doi: 10.1371/journal.pone.0058025

Zhang, Y. T., Hou, K., Qian, H., Gao, Y. Y., Fang, Y., Xiao, S., et al. (2022). Characterization of soil salinization and its driving factors in a typical irrigation area of Northwest China. *Sci. Total. Environ.* 837, 155808. doi: 10.1016/j.scitotenv.2022.155808

Zhang, L. L., Hu, W., Wang, Y., Feng, R. J., Zhang, Y. D., Liu, J. H., et al. (2015). The MaASR gene as a crucial component in multiple drought stress response pathways in arabidopsis. *Funct. Integr. Genomics* 15, 2472–2460. doi: 10.1007/s10142-014-0415-y

Zhang, J., Li, H. B., Xu, B., Li, J., and Huang, B. R. (2016). Exogenous melatonin suppresses dark-induced leaf senescence by activating the superoxide dismutase-catalase antioxidant pathway and down-regulating chlorophyll degradation in excised leaves of perennial ryegrass (Lolium perenne l.). *Front. Plant Sci.* 7. doi: 10.3389/fpls.2016.01500

Zhang, J. L., and Shi, H. Z. (2013). Physiological and molecular mechanisms of plant salt tolerance. *Photosynth. Res.* 115, 1–22. doi: 10.1007/s11120-013-9813-6

Zhang, J. L., Wang, S. M., and Flowers, T. J. (2013). Differentiation of low-affinity na+ uptake pathways and kinetics of the effects of k+ on na+ uptake in the halophyte suaeda maritima. *Plant Soil.* 368, 629–640. doi: 10.1007/s11104-012-1552-5

Zhu, J. K. (2000). Genetic analysis of plant salt tolerance using arabidopsis. *Plant Physiol.* 124, 941–948. doi: 10.1104/pp.124.3.941

frontiers | Frontiers in Plant Science

TYPE Original Research
PUBLISHED 08 December 2022
DOI 10.3389/fpls.2022.1052640

OPEN ACCESS

EDITED BY
Jing Zhang,
Nanjing Agricultural University, China

REVIEWED BY
Caixiang Liu,
University of Chinese Academy of Sciences, China
Yuxia Guo,
Henan Agricultural University, China

*CORRESPONDENCE
Zhe Chen
chenzhe@qhnu.edu.cn
Zunji Shi
shizj@lzu.edu.cn

†These authors have contributed equally to this work

SPECIALTY SECTION
This article was submitted to Plant Abiotic Stress, a section of the journal Frontiers in Plant Science

RECEIVED 24 September 2022
ACCEPTED 22 November 2022
PUBLISHED 08 December 2022

CITATION
Lei L, Yuan X, Fu K, Chen Y, Lu Y, Shou N, Wu D, Chen X, Shi J, Zhang M, Chen Z and Shi Z (2022) Pseudotargeted metabolomics revealed the adaptive mechanism of *Draba oreades* Schrenk at high altitude.
Front. Plant Sci. 13:1052640.
doi: 10.3389/fpls.2022.1052640

Pseudotargeted metabolomics revealed the adaptive mechanism of *Draba oreades* Schrenk at high altitude

Ling Lei[1†], Xuefeng Yuan[2†], Keyi Fu[2], Yuan Chen[2], Yijun Lu[1], Na Shou[2], Dandan Wu[2], Xi Chen[2], Jian Shi[3], Minjuan Zhang[3], Zhe Chen[4*] and Zunji Shi[2*]

[1]Clinical Psychology, Maternal and Child Health Hospital of Guangxi Zhuang Autonomous Region, Guangxi Key Laboratory of Reproductive Health and Birth Defect Prevention, Nanning, China, [2]State Key Laboratory of Herbage Improvement and Grassland Agro-ecosystems, Center for Grassland Microbiome, College of Pastoral Agriculture Science and Technology, Lanzhou University, Lanzhou, China, [3]Metabolomics Detection Department, Wuhan Metware Biotechnology Co., Ltd, Wuhan, China, [4]Academy of Plateau Science and Sustainability, Qinghai Normal University, Xining, China

Strong ultraviolet radiation and low temperature environment on Gangshika Mountain, located in the eastern part of the Qilian Mountains in Qinghai Province, can force plants to produce some special secondary metabolites for resisting severe environmental stress. However, the adaptive mechanism of *Draba oreades* Schrenk at high altitude are still unclear. In the current study, *Draba oreades* Schrenk from the Gangshika Mountain at altitudes of 3800 m, 4000 m and 4200 m were collected for comprehensive metabolic evaluation using pseudotargeted metabolomics method. Through KEGG pathway enrichment analysis, we found that phenylpropanoid biosynthesis, phenylalanine, tyrosine and tryptophan biosynthesis and phenylalanine metabolism related to the biosynthesis of flavonoids were up-regulated in the high-altitude group, which may enhance the environmental adaptability to strong ultraviolet intensity and low temperature stress in high altitude areas. By TopFc20 distribution diagram, the content of flavonoids gradually increased with the elevation of altitude, mainly including apigenin, luteolin, quercetin, hesperidin, kaempferol and their derivatives. Based on the random forest model, 10 important metabolites were identified as potential biomarkers. L-phenylalanine, L-histidine, naringenin-7-O-Rutinoside-4'-O-glucoside and apigenin related to the flavonoids biosynthesis and plant disease resistance were increased with the elevation of altitude. This study provided important insights for the adaptive mechanism of *Draba oreades* Schrenk at high altitude by pseudotargeted metabolomics.

KEYWORDS

***Draba oreades* Schrenk, flavonoids, high altitude, machine learning, pseudotargeted metabolomics**

Introduction

Many commercially available drugs are obtained directly or indirectly from plant secondary metabolites (Adhikari et al., 2020). The protection and sustainable utilization of medicinal plants are crucial to the development of the traditional Chinese medicine industry, and most of China's medicinal plants come from wild plant resources (Shan et al., 2022). The efficacy of medicinal plants mainly depends on natural secondary metabolites. In the past century, the research on natural secondary metabolites has achieved some important results, such as artemisinin for malaria, huperzine A for Alzheimer's disease, ephedrine for cold and camptothecin for cancer, which were separated from *Artemisia annua*, *Huperzine serrata*, *Ephedra sinica* and *Camptotheca acuminate*, respectively (Qiu, 2007). However, natural secondary metabolites are susceptible to environmental factors (Setyawati et al., 2021), and the types and quantities of natural secondary metabolites vary with geographical location and altitude (Jugran et al., 2016; Cirak et al., 2017; Senica et al., 2017; Dong et al., 2020). Studies have shown that the antioxidant capacity of natural secondary metabolites are related to altitude (Ni et al., 2013; Knuesting et al., 2018; Pandey et al., 2018). Ultraviolet radiation and low temperature conditions promote the biosynthesis of flavonoids, resulting in the accumulation of flavonoids in plants (Liu et al., 2018; Dong et al., 2020).

In terms of adaptation strategies for other plants to different altitudes, Rius et al. found that the local varieties of maize adapted to high altitude in the Andes Mountains accumulated flavonoids in their leaves and other green tissues under ultraviolet radiation (Rius et al., 2012). Berardi et al. found that flavonoids were increased with elevated altitude in *Silene vulgaris* (Berardi et al., 2016). Du et al. found that the flavonoid content was higher and the flavonoid composition was markedly different in the leaves of *Cyclocarya paliurus* collected at high altitude (Du et al., 2021). Here, *Draba oreades* Schrenk is a perennial herb with wide adaptability. It mainly grows at the edge of high mountain rocks and cracks at the edge of high mountain gravel ditches with an altitude of 2300-5500 meters. It is distributed in Inner Mongolia, Shaanxi, Gansu, Qinghai, Xinjiang and other places in China, and in Central Asia, Kashmir, India and other places abroad. Up to now, the effect of altitude on the synthesis of natural secondary metabolites in *Draba oreades* Schrenk remains undetermined.

In view of this, based on liquid chromatography-mass spectrometry (LC-MS/MS) platform and sequencing platform, this study detected the shoot tissues of *Draba oreades* Schrenk at different altitudes by pseudotargeted metabolomics method, compared and analyzed the metabolome differences in the composition and quality of natural secondary metabolites of *Draba oreades* Schrenk at different altitudes, and clarified the effects of different altitudes on the accumulation of natural secondary metabolites and related regulatory mechanisms. The results of this study can provide scientific basis for the adaptive mechanism and the sustainable utilization of *Draba oreades* Schrenk at high altitude.

Materials and methods

Site description

Plant samples were collected from Gangshika Mountain (37° 41'51.23"N~ 37°40'58.03"N, 101°28'8.11"E~101°26'49.11"E, 3800 m~4200 m a.s.l.), located in the eastern part of the Qilian Mountains in Qinghai Province. The area had a typical plateau continental climate, with a long cold winter and short warm summer. The annual average temperature was -1.6°C, with the maximum monthly mean temperature in July (10.1°C) and the minimum monthly mean temperature in January (-15.0°C). The historical extreme maximum and minimum temperatures were 26.8°C and -37.1°C, respectively. The number of days with a daily minimum temperature below 0°C during the year was as high as 280 days. The annual precipitation was 560 mm on average, of which 85% was concentrated in May to September. The regional annual mean evaporation was 1238.0 mm (Dai et al., 2019). The vegetation type of the sampling area was alpine screes cushion vegetation, and the dominant species was Thylacospermum caespitosum (Cambess.) Schischk. It was associated with Saussurea, Potentilla, Leontopodium, Gentian, Saxifraga, Poa, Oxytropis, and Polygonum. The average height of vegetation was less than 10 cm, and the aboveground dry biomass averages 210 $g{\cdot}m^{-2}$. The soil was a part of transition zone of seasonal permafrost and spot permafrost. The topsoil (0-10 cm) organic matter, bulk density, pH and soil volume water content in K. humilis meadow were 138.52 ± 13.82 $g{\cdot}kg^{-1}$, 0.75 ± 0.05 $g{\cdot}cm^{-3}$, 7.50 ± 0.22 and 32.7% ± 5.17%, respectively (Li et al., 2013). The site froze from late October to mid-November. A stable thin permafrost layer began to form in late November, and the thickness of the permafrost continued to increase, and reached the maximum freezing depth of 0.5-1 m in mid-February of the following year. The soil began to enter the thawing period in early March, and the thaw depth continued to increase until thawing was complete by late April (Dai et al., 2019).

Sample collection

In this study, *Draba oreades* Schrenk was used as the experimental material. Samples were collected from three altitude gradients, 3800 m, 4000 m and 4200 m respectively. Eight complete plants were randomly selected at each altitude, and a total of 24 plant samples were collected. The samples were washed with distilled water immediately after collection, then frozen with liquid nitrogen, and then brought back to the

laboratory for storage at - 80°C until further use. For the metabolome analysis, eight plants selected from each of the three altitude gradients were used for metabolome detection, separately.

Metabolites extraction and detection

Metabolomics analysis of metabolites was conducted by pseudotargeted metabolomics, which can monitor hundreds to thousands of metabolites by dynamic multiple reaction monitoring, merging the advantages of untargeted and targeted metabolomics with high sensitivity, high specificity and excellent quantification ability. The standards were used to confirm the chemical identities of metabolites, which were based on the self-built target standard database MWDB (metware database) by widely target UPLC-MS/MS platform. Qualitative analysis was carried out according to the retention time RT, the information of the precursor ion pair and the secondary spectrum data of the detected metabolites. The quantification was more accurate and the repeatability was better.

The shoots of *Draba oreades* Schrenk were extracted overnight at 4°C with 70% aqueous methanol. Following centrifugation at 10000 g for 10 min, the extracts of *Draba oreades* Schrenk were absorbed (CNWBOND Carbon-GCB SPE Cartridge, 250 mg, 3 ml; ANPEL Laboratory Technologies Co., Ltd, Shanghai, China) and filtrated (SCAA-104, 0.22 μm pore size; ANPEL Laboratory Technologies Co., Ltd, Shanghai, China) before LC-ESI-MS/MS based pseudotargeted metabolomics analysis. The sample extracts were analyzed using an LC-ESI-MS/MS system (HPLC, Shim-pack UFLC SHIMADZU CBM30A system, Kyoto, Japan; MS, Applied Biosystems 4500 QTRAP, Foster City, California, USA). The analytical conditions were as follows: column, Waters ACQUITY UPLC HSS T3 C18 (1.8 μm, 2.1 mm*100 mm); solvent system, water (0.04% acetic acid): acetonitrile (0.04% acetic acid); gradient program,100: 0 V/V at 0 min, 5: 95 V/V at 11.0 min, 5: 95 V/V at 12.0 min, 95: 5 V/V at 12.1 min, 95: 5 V/V at 15.0 min; flow rate, 0.40 ml/min; temperature, 40°C; injection volume: 5μl. The effluent was connected to an ESI-triple quadrupole-linear ion trap (QTRAP)-MS (Applied Biosystems Co., Ltd, Foster City, California, USA). Triple quadrupole (QQQ) scans were acquired on a triple quadrupole-linear ion trap mass spectrometer (QTRAP). The ESI source operation parameters were as follows: ion source, turbo spray; source temperature 550°C; ion spray voltage (IS) 5500 V; ion source gas I (GSI), gas II (GSII), and curtain gas (CUR) were set at 55, 60, and 25.0 psi, respectively; the collision gas (CAD) was high. Instrument tuning and mass calibration were performed with 10 μmol/l polypropylene glycol solutions in QQQ modes. QQQ scans were acquired as MRM experiments with collision gas (i.e., nitrogen) set to 5 psi. DP and CE for individual MRM transitions were done with further DP and CE optimization. A specific set of MRM transitions was monitored for each period according to the metabolites eluted within this period.

Metabolomics data analysis

For metabolomics data analysis, the metabolomics data obtained by LC-ESI-MS/MS system were normalized with $\log_2$ transformation and standard with z-score, which were then exported into SIMCA 14.1 software to analyze the differential metabolites of samples. Quality control (QC) samples were a mixture of all sample extracts, which were inserted into the queue to monitor the stability of the detection method. Unsupervised principal component analysis (PCA) was performed to estimate the degree of variability and the overall metabolic difference. The metabolomics data were analyzed according to the orthogonal partial least structures discriminant analysis (OPLS-DA) model. The scores of each group were plotted to display the differences between each group. A combination of Fold change (FC) values, *P*-values, and Variable important in projection (VIP) values from the OPLS-DA model can be used to screen for differential metabolites, and the validity of OPLS-DA models was further confirmed by permutation tests. Volcano plot and Venn diagram were used to illustrate the number of differential metabolites. The pathway enrichment analysis of differential metabolites was conducted based on the Kyoto Encyclopedia of genes and genomes (KEGG) pathway database (http://www.kegg.jp/kegg/pathway.html) (Kanehisa and Goto, 2000).

Statistical analysis

We used R Programming Language (R 4.1.0, New Zealand) and GraphPad software (8.0 version, United States) for graphic illustration and statistical analysis. The differential metabolites between groups were screened by VIP values, *P*-values, and FC values (VIP > 1, $P < 0.05$, FC ≥ 2 or ≤ 0.5). One-way ANOVA analysis or two-tailed Student's t test were conducted for calculating the significant difference between the two groups.

Results

Characterization of soil samples and measurement of total ultraviolet intensity

The soil samples and plant samples were collected from the Gangshika Mountain at altitudes of 3800 m (E 101°26'49.11", N 37°40′58.03"), 4000 m (E 101°27'4.56", N 37°41′40.05") and 4200 m (E 101°28'8.11", N 37°41′51.23"). The physicochemical properties of the soil samples were presented in Table S1. In the

low-altitude group, the average water content was 39.5%, the average salinity was 50.5 mg/L, and the average conductivity was 92.4 us/cm, all which were higher than the mid-altitude and high-altitude groups. Notably, the average soil temperature at 4200 m was 1.9°C, which was lower than the average soil temperature at 4000 m and at 3800 m. Moreover, total ultraviolet intensity of plant growing season from May to September showed the increasing trend with the elevation of altitudes (Table S2).

Quality control analysis of metabolomics data

QC samples were used to determine the state of the instrument and balance the LC-MS system to evaluate the stability of the system during the whole experiment. Through the QC analysis of the original LC-MS data, the variation coefficient distribution of the three groups of samples and QC samples were obtained. The abscissa represented the CV value, the ordinate represented the proportion of the number of metabolites smaller than the corresponding CV value to the total number of metabolites. The higher the proportion of metabolites with lower CV values in QC samples, the more stable the experimental data was. The proportion of metabolites with CV value less than 0.3 in QC samples (mix samples were used for QC) was higher than 85%, indicating the reliability of the measurement technology (Figure S1A). The stability of the determination method was evaluated by superimposing the total ion current (TIC) of the four groups of samples, the ordinate represented the peak intensity and the abscissa represented the retention time. The results showed that the TIC in the positive and negative ion mode were highly overlapped, the retention time was consistent with the peak intensity, indicating that the peak separation effect was good, and the signal was stable in the whole analysis process (Figures S1B, C). In addition, a total of 776 metabolites were detected by UHPLC-TQMS using hydrophilic and hydrophobic methods. PCA results of all metabolites showed that QC samples gathered together, further indicating the stability of the analytical method (Figure 1A).

Metabolomic analysis

PCA analysis can reflect the distribution of relative abundance of metabolites. The closer the distance was, the smaller the difference of substance content was. In this study, PCA results of three groups of samples and QC samples were all within the confidence interval, there were significant differences among groups (P=0.035), but no obvious separation of samples in the same group, indicating that the representativeness was good (Figure 1A). PCA was an unsupervised analysis method, which cannot ignore intra group errors and eliminate random errors irrelevant to the research purpose, so it was not conducive to the discovery of inter group differences. After that, the supervised method will be used for further research.

Through the supervised method OPLS-DA, the orthogonal variables that were not related to the classification variables in metabolites can be screened out, and the nonorthogonal variables and orthogonal variables can be analyzed respectively, so as to obtain more reliable information about the correlation between the inter group differences of metabolites and the experimental group. The low altitude samples in OPLS-DA model were mainly distributed on the left side of the confidence interval, and the high altitude samples were mainly distributed on the right side of the confidence interval. The separation effect of the two altitude samples was significant, R^2X=0.807, Q^2 = 0.999, and the two parameter values were greater than 0.5, indicating that the model was reliable (Figure 1B). The OPLS-DA model had a significant separation between the low-altitude group and the mid-altitude group, R^2X=0.777, Q^2 = 0.999 (Figure 1C). The mid-altitude group and the high-altitude group had also a significant separation, R^2X=0.641, Q^2 = 0.975 (Figure 1D). Moreover, P-values of CV-ANOVA of OPLS-DA models in pairwise comparisons were all less than 0.001, further indicating that there were significant differences among the three groups.

OPLS-DA permutation test can obtain R^2 and Q^2 values of the random model by randomly changing the arrangement order of classification variables Y and establishing the corresponding OPLS-DA model for many times. It played an important role in avoiding over fitting of the test model and evaluating the statistical significance of the model. Our results showed that all R^2 points of the three groups of samples were lower than the rightmost original R^2 point from left to right, and all Q^2 points were lower than the original Q^2 point on the right. Moreover, the regression line and ordinate of the points intersected the negative semi axis, indicating that the OPLS-DA model was reliable and robust without over fitting, which can better explain the difference between the two groups (Figure S2).

Screening of differential metabolites

The differential metabolites of *Draba oreades* Schrenk at different altitudes were screened through the volcano plot. The abscissa represented the logarithm of the difference multiple of the differential metabolites [$\log_2$(FC)], and the ordinate represented the negative logarithm of P-value [- $\log_{10}$ (P-value)]. The metabolites at low, middle and high altitudes were compared in pairs. In the comparison group of low-altitude vs high-altitude, there were 451 differential metabolites, 141 up-regulated metabolites and 310 down-regulated metabolites (Figure 2A). In the comparison group of low-altitude vs mid-altitude, there were 431 differential metabolites, 180 up-regulated metabolites and 251

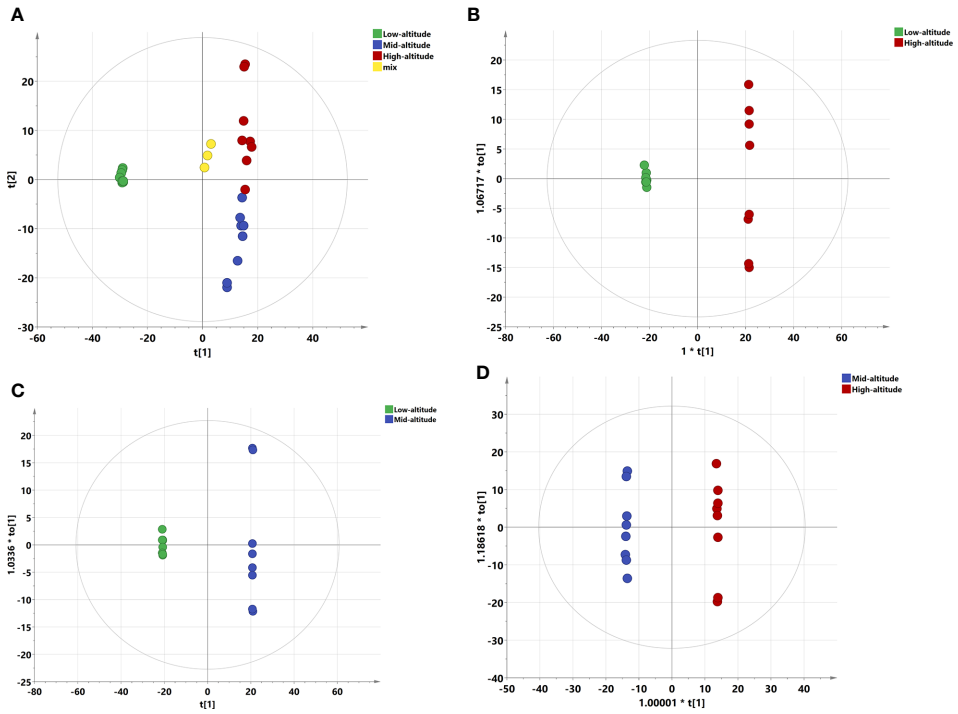

FIGURE 1
PCA and OPLS-DA scoring charts of *Draba oreades* Schrenk at different altitudes. **(A)** PCA plot. **(B)** OPLS-DA model score at Low-altitude vs High-altitude. **(C)** OPLS-DA model score at Low-altitude vs Mid-altitude. **(D)** OPLS-DA model score at Mid-altitude vs High-altitude. QC, quality control.

down-regulated metabolites (Figure 2B). In the comparison group of mid-altitude vs high-altitude, there were 235 differential metabolites, 38 up-regulated metabolites and 197 down-regulated metabolites (Figure 2C). Meanwhile, we found that the number of differential metabolites was the largest in the mid-altitude vs high-altitude comparison group, and the least in the low-altitude vs high-altitude comparison group, and the down-regulated differential metabolites were far more than the up-regulated differential metabolites in the three comparison groups. Venn analysis was carried out on the differential metabolites of *Draba oreades* Schrenk at different altitudes, 91 common differential metabolites were obtained by independent pairwise comparison. There were 39, 34 and 50 unique metabolites in the comparison of low-altitude vs high-altitude, low-altitude vs mid-altitude, mid-altitude vs high-altitude respectively (Figure 2D).

Analysis of metabolic pathways of differential metabolites

KEGG pathway enrichment analysis was performed for the up-regulated and down-regulated differential metabolites screened in the volcano plot, as shown in Figure 3. The ordinate was - $\log_{10}$ (P), and the abscissa was pathway impact. The size of the dot represented the number of differential metabolites enriched in the corresponding pathway, and the color of the dot represented the P value. The smaller the P value, the redder the color of the dot. The metabolic pathways of the up-regulated differential metabolites between the low-altitude and the high-altitude were mainly aminoacyl-tRNA biosynthesis, phenylpropanoid biosynthesis, pyrimidine metabolism and linoleic acid metabolism (Figure 3A), the metabolic pathways of the down-regulated differential metabolites were mainly purine metabolism, citrate cycle, one carbon pool by folate, and glyoxylate and dicarboxylate metabolism (Figure 3B). The metabolic pathways of the up-regulated differential metabolites between the low-altitude and the mid-altitude were mainly phenylpropanoid biosynthesis, aminoacyl-tRNA biosynthesis, beta-Alanine metabolism, pantothenate and CoA biosynthesis, and nicotinate and nicotinamide metabolism (Figure 3C), the metabolic pathways of the down-regulated differential metabolites were mainly purine metabolism, arginine biosynthesis, alanine, aspartate and glutamate metabolism and citrate cycle (Figure 3D). The metabolic pathways of the up-regulated differential metabolites between the mid-altitude and the high-altitude were mainly phenylalanine, tyrosine and tryptophan biosynthesis, starch and sucrose metabolism, purine metabolism and phenylalanine

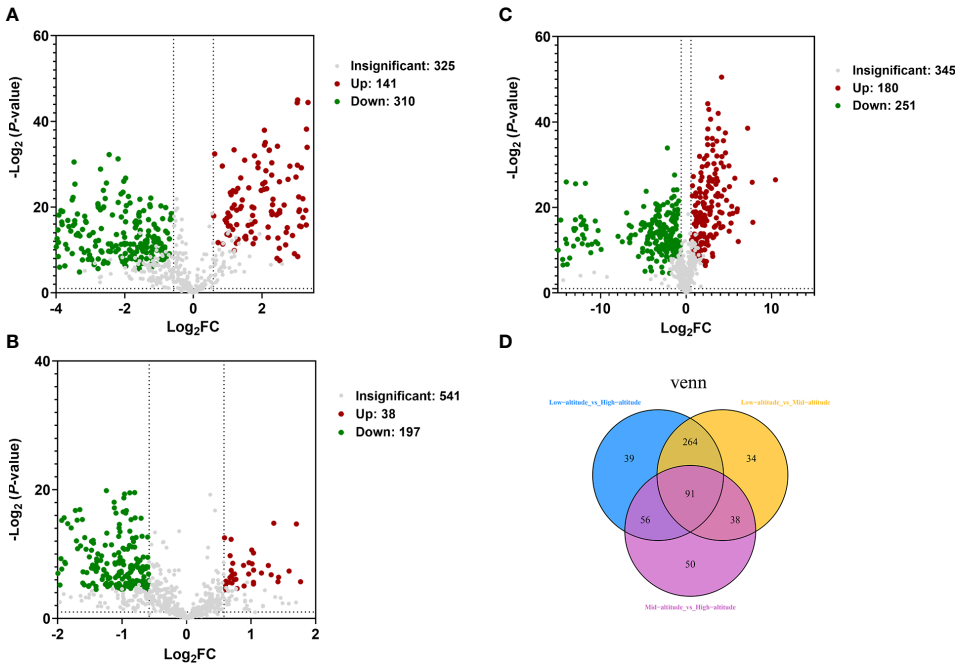

FIGURE 2
Volcano plot and Venn diagram were used to illustrate the number of differential metabolites. **(A)** Volcano plot of Low-altitude vs High-altitude. **(B)** Volcano plot of Low-altitude vs Mid-altitude. **(C)** Volcano plot of Mid-altitude vs High-altitude. **(D)** Venn diagram showed the common differential metabolites and unique differential metabolites at different altitudes.

metabolism (Figure 3E), the metabolic pathways of the down-regulated differential metabolites were mainly phenylpropanoid biosynthesis and citrate cycle (Figure 3F).

Analysis of the top 20 changed differential metabolites

In order to further understand the different metabolites with great differences in the comparison groups at different altitudes, the topFc20 distribution map screened the compounds with the top 20 changes in the relative content of different metabolites. Red represented the 10 compounds with increased relative content, and green represented the 10 compounds with decreased relative content. In the low-altitude and high-altitude comparison group, the flavonoids including luteolin-7-O-neohesperidoside (lonicerin), luteolin-7-O-rutinoside, hesperetin-7-O-rutin (hesperidin), kaempferol-3-O-arabinoside-7-O-rhamnoside, hesperetin-7-O-rutinoside (hesperidin), isorhamnetin-3-O-arabinoside-7-O-rhamnoside, luteolin-7-O-glucoside (cynaroside), apigenin-6-C-(2”-xylosyl) glucoside and the coumarin including 7-Hydroxycoumarin-7-O-glucoside (skimmin) were up-regulated at high altitude, which were important pharmacological compounds (Figure 4A). In the low-altitude and mid-altitude comparison group, the flavonoids including lonicerin, hesperidin, luteolin-7-O-rutinoside, isorhamnetin-3-O-arabinoside-7-O-rhamnoside, kaempferol-3-O-arabinoside-7-O-rhamnoside and the coumarin including skimmin were up-regulated in mid-altitude (Figure 4B). In the mid-altitude and high-altitude comparison group, the flavonoids including epicatechin, hesperetin, cynaroside and the organic acid including cinnamic acid were up-regulated at high altitude (Figure 4C).

Machine learning and receiver operating characteristic curve analysis

The machine learning method of random forest model was used to screen the biomarkers for the metabolites of *Draba oreades* Schrenk at different altitudes. In the random forest model, 10 important metabolites were separated as potential biomarkers according to the relative importance of metabolites (Figure 5A). The abscissa of the Receiver operating characteristic (ROC) curve of biomarkers represents specificity, the ordinate represents sensitivity, and the curves of different colors represented different metabolites. The area enclosed by the curve and the abscissa was a value called area under the curve (AUC) (Figure 5B). AUC value greater than 0.6 indicated that the machine learning model was effective. The higher the AUC

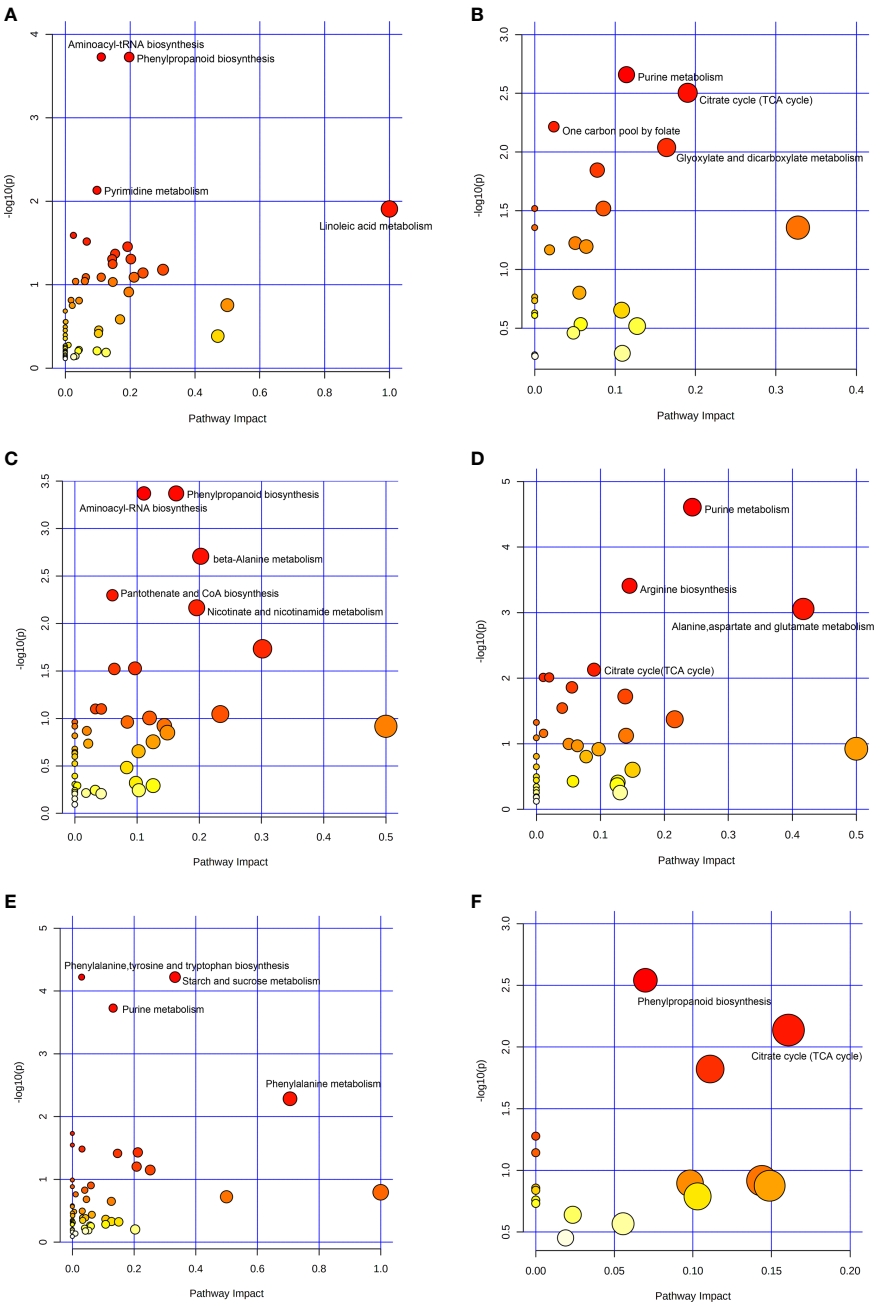

FIGURE 3
Bubble plot of KEGG pathway enrichment analysis. **(A)** Metabolic pathways of up-regulated differential metabolites at Low-altitude vs High-altitude. **(B)** Metabolic pathways of down-regulated differential metabolites at Low-altitude vs High-altitude. **(C)** Metabolic pathways of up-regulated differential metabolites at Low-altitude vs Mid-altitude. **(D)** Metabolic pathways of down-regulated differential metabolites at Low-altitude vs Mid-altitude. **(E)** Metabolic pathways of up-regulated differential metabolites at Mid-altitude vs High-altitude. **(F)** Metabolic pathways of down-regulated differential metabolites at Mid-altitude vs High-altitude.

value, the better the predictability of biomarkers. In the current study, Hmtp000776 (4,5,6-Trihydroxy-2-cyclohexen-1-ylideneacetonitrile), Lmzn001875 (naringenin-7-O-Rutinoside-4'-O-glucoside), L-phenylalanine, L-histidine, apigenin, linoleic acid, sedoheptulose, cycloleucine, trans-citridic acid and L-homomethionine were identified as potential biomarkers of *Draba oreades* Schrenk at high altitude (Figure 5A). The AUC values of these 10 potential biomarkers were all greater than 0.6, indicating that these metabolites were biomarkers to distinguish between different altitudes (Figure 5B). And the results showed

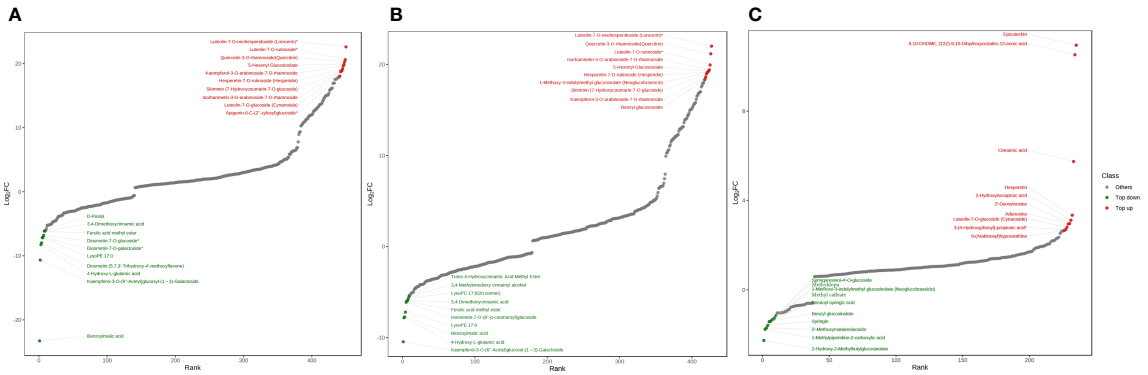

FIGURE 4
TopFc20 distribution diagram. **(A)** Low-altitude vs High-altitude. **(B)** Low-altitude vs Mid-altitude. **(C)** Mid-altitude vs High-altitude.

that the relative abundance of 10 biomarkers increased with the increase of altitude (Figure 5C).

Discussions

Previous studies have shown that natural secondary metabolites of plants have multiple functions (Shang et al., 2021). However, due to the limitations of natural resources or low contents in plants, the supply of natural secondary metabolites is often curtailed and the components of natural secondary metabolites remain unclear (Yang et al., 2016). Previous study found that the content of Salidroside in *Rhodiola sachalinensis* was related to the altitudes (Zhao et al., 2014; Dong et al., 2020), suggesting that altitude may be an important factor that affects phytochemicals. Thus, we need to study the impact of environmental factors on plant secondary metabolites, which will help to determine the favorable geographical location for the plants with important value (Adhikari et al., 2020). However, so far, the effect of altitude on the synthesis of natural secondary metabolites in *Draba oreades* Schrenk remains undetermined, suggesting that it may be of great significance to systematically analyze and screen the metabolites of *Draba oreades* Schrenk under different altitudes. In this study, based on the pseudotargeted metabolomics analysis of LC-MS, the global metabolites of *Draba oreades* Schrenk from three different altitudes were determined. The effects of altitude on the metabolites of *Draba oreades* Schrenk were discussed.

The samples were subjected to multivariate analysis such as PCA and OPLS-DA by pseudotargeted metabolomics, and 776 metabolites were identified in three different altitudes of *Draba oreades* Schrenk. The differential metabolites of *Draba oreades* Schrenk among low, middle or high altitudes were also compared. The results showed that the differential metabolites could be used to distinguish the samples from different altitudes, indicating that the species and relative abundance of metabolites in different altitudes were different, and the altitude had a significant effect on the metabolism of *Draba oreades* Schrenk. Farhat et al. found that the changes of altitude would lead to significant changes in phenolic content and antioxidant activity of *Salvia verbenaca L.* (Farhat et al., 2013). Setyawati et al. found that altitude had an impact on the content of secondary metabolites of turmeric and ginger, the content of secondary metabolites of turmeric and ginger was higher in high altitude areas and decreased with the decrease of altitude (Setyawati et al., 2021).

KEGG pathway enrichment analysis showed that the metabolic pathways of significant enrichment in *Draba oreades* Schrenk at different altitudes. Previous studies showed that phenylpropanoid biosynthesis was crucial to the development and survival of plants, it produced precursor metabolites with multiple functions, which can help plants cope with non-biological and biological stresses in the environment. Among the precursor metabolites, the most significant compounds were flavonoids which were related to UV protection and low temperature resistance, and other compounds were involved in the plant's defense response to pathogens (De Vries et al., 2021; Dong and Lin, 2021). Dong et al. found that the phenylpropanoid biosynthesis promoted the synthesis of flavonoids with the increase of altitude in *Rhodiola* (Dong et al., 2020). Aminoacyl-tRNA biosynthesis played an important role in protein synthesis (Jiang et al., 2020). Phenylalanine, tyrosine and tryptophan biosynthesis was involved in the synthesis of three aromatic amino acids including tryptophan, tyrosine and phenylalanine, tryptophan was the key precursor of the IAA biosynthetic pathway in plants (Zhao, 2012), tyrosine may help to improve the drought tolerance of plants (Ma et al., 2017), and phenylalanine was the key precursor of flavonoids production in plants (Meng et al., 2019). Beta-Alanine metabolism was involved in the synthesis of pantothenic acid, and beta-Alanine was methylated to beta-

10.3389/fpls.2022.1052640

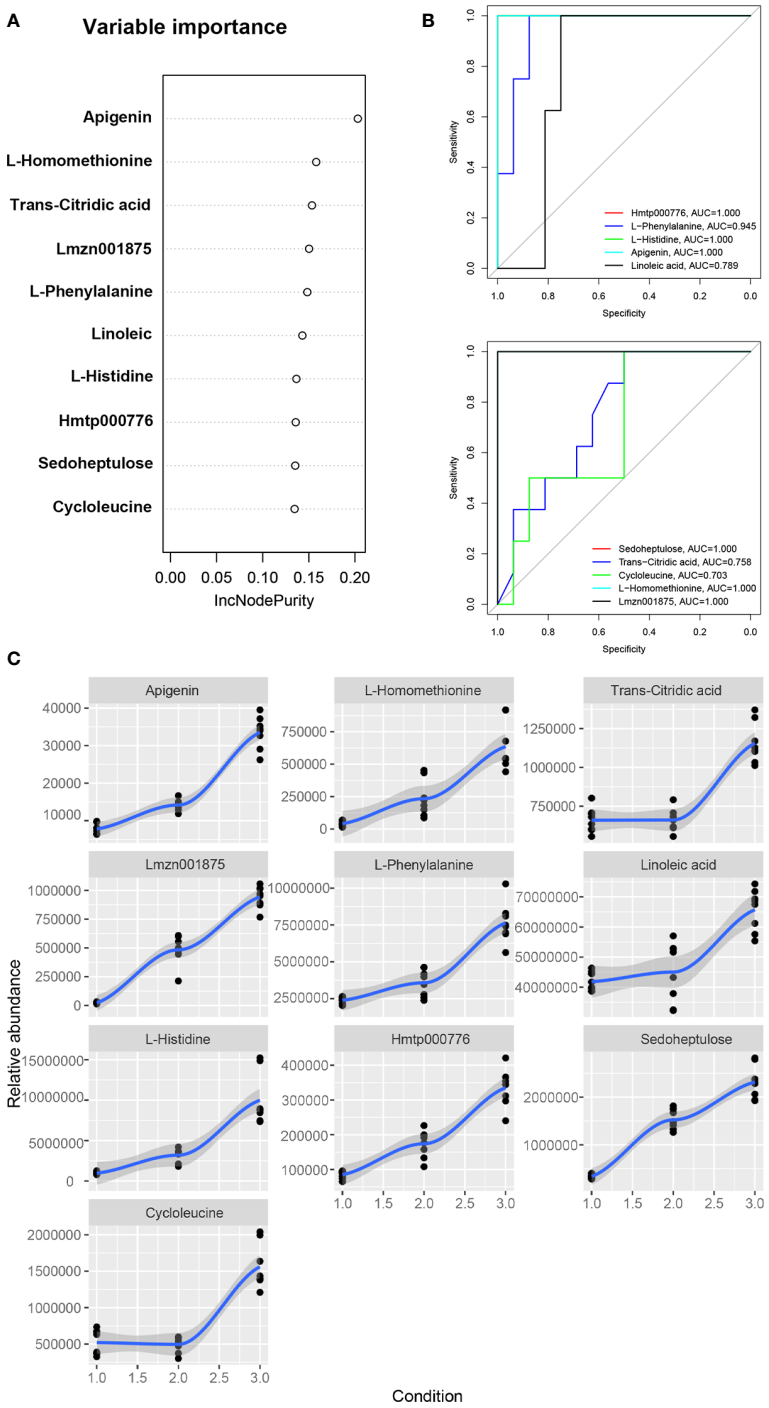

FIGURE 5
Machine learning and receiver operating characteristic curve analysis. **(A)** The random forest model was used to screen 10 metabolic biomarkers for *Draba oreades* Schrenk at different altitudes. **(B)** ROC curves of biomarkers. **(C)** Relative abundance trend charts of 10 biomarkers at different altitudes. The abscissa 1.0 represented low-altitude, 2.0 represented mid-altitude, and 3.0 represented high-altitude. Lmzn001875: Naringenin-7-O-Rutinoside-4'-O-glucoside, Hmtp000776: 4,5,6-Trihydroxy-2-cyclohexen-1-ylideneacetonitrile.

Alanine betaine in stress resistant plants which was an osmotic protective compound in response to high salt and hypoxia (Rathinasabapathi et al., 2001). Starch and sucrose metabolism was related to the tolerance and sensitivity of plants to abiotic stresses (Dev Sharma et al., 2021). In this study, we found that phenylpropanoid biosynthesis and aminoacyl-tRNA biosynthesis were up-regulated in the mid-altitude and high-altitude compared to the low-altitude. Phenylalanine, tyrosine and tryptophan biosynthesis, starch and sucrose metabolism and phenylalanine metabolism were up-regulated in the high-altitude compared to the mid-altitude. Beta-Alanine metabolism was up-regulated in the mid-altitude compared to the low-altitude. Collectively, *Draba oreades* Schrenk may enhance the biosynthesis of flavonoids through above important metabolic pathways to adapt to the environmental challenges brought by high altitude.

Purine metabolism retransported nitrogen for plant growth and development (Watanabe et al., 2014). Citrate cycle was a key pathway for cells to generate energy during metabolism and provide precursors for biosynthetic reaction, closely relating to plant growth (Zhang et al., 2018; Arnold et al., 2022). In this study, it can be seen that these metabolic pathways related to plant growth and development were down-regulated in the mid-altitude and high-altitude compared to the low-altitude, such as purine metabolism and citrate cycle, duo to the harsh high altitude environment. In addition, glyoxylate and dicarboxylate metabolism, pyrimidine metabolism, one carbon pool by folate, arginine metabolism, and linoleic acid metabolism showed the unstable trend at different altitudes.

TopFc20 distribution diagram screened the up-regulated differential metabolites in the three comparison groups of low, middle and high altitude, mainly including flavonoids with important pharmacological activities such as luteolin-7-O-neohesperidoside (lonicerin), luteolin-7-O-rutinoside, hesperetin-7-O-rutin (hesperidin), kaempferol-3-O-arabinoside-7-O-rhamnoside, hesperetin-7-O-rutinoside (hesperidin), isorhamnetin-3-O-arabinoside-7-O-rhamnoside, luteolin-7-O-glucoside (cynaroside), apigenin-6-C-(2"-xylosyl) glucoside, epicatechin, hesperetin, including organic acids such as cinnamic acid, and including coumarin components such as skimmin. In this study, with the increase of altitude, the more flavonoids including luteolin, quercetin, apigenin and their derivatives were accumulated. It was reported that luteolin had anti-tumor effects on a variety of human malignant tumors, such as lung cancer, breast cancer, glioblastoma, prostate cancer, colon cancer and pancreatic cancer (Imran et al., 2019). Quercetin was an antioxidant flavonoid widely distributed in plants and was a promising anticancer agent (Murakami et al., 2008; Li and Song, 2019). Apigenin had preventive and therapeutic effects on cardiovascular diseases and nervous system diseases (Shukla and Gupta, 2010). In addition, skimmin (7-Hydroxycoumarin-7-O-glucoside) had preventive effects on diabetes and nephropathy (Zhang et al., 2012; Zhang et al., 2013). Studies showed that ultraviolet radiation changed the secondary metabolism of plants, kaempferol had important protective effects against ultraviolet damage (Tripp et al., 2018). The concentrations of two flavonoids with the highest absorbance in the ultraviolet wavelength, apigenin and luteon, were positively correlated with high latitude areas (Tripp et al., 2018). This explained why the content of flavonoids in plant metabolites in high altitude areas was higher than that in low altitude areas.

Based on the random forest model, 10 important metabolites were identified as potential biomarkers of *Draba oreades* Schrenk in this study, and the relative abundance of the 10 biomarkers increased with the elevation of altitude. Among them, Lmzn001875 (naringenin-7-O-Rutinoside-4'-O-glucoside), Hmtp000776 (4,5,6-Trihydroxy-2-cyclohexen-1-ylideneacetonitrile), L-phenylalanine, L-histidine, apigenin, linoleic acid were the main biomarkers with pharmacological activities in SymMap database. Linoleic acid was the most abundant polyunsaturated fatty acid in human nutrition (Choque et al., 2014; Imran et al., 2019). Amino acids including L-phenylalanine and L-histidine, as substrates of protein biosynthesis, played a regulatory role in this process (Heinemann and Hildebrandt, 2021). Phenylalanine can be used as the starting substrate of flavonoid biosynthesis, which played a variety of functions in plants (Cheng et al., 2014). L-histidine can induce plants to enhance resistance to plant diseases (Yariyama et al., 2019). Some studies showed that the flavonoid content in plants was significantly positively correlated with altitude (Adhikari et al., 2020; Dong et al., 2020), which was correlated with the stronger ultraviolet radiation and low temperature stress in high altitude areas (Hectors et al., 2012; Emiliani et al., 2013). Under the stimulation of strong light, the most effective protective mechanism was the biosynthesis of flavonoids substances (Frohnmeyer and Staiger, 2003). In the current study, our results suggested that the more ultraviolet intensity and the lower temperature at 4200 m exhibited more severe environmental stress compared to at 4000 m and at 3800 m (Tables S1, S2). Notably, the flavonoids as potential biomarkers including naringenin-7-O-Rutinoside-4'-O-glucoside and apigenin, and the flavonoid synthesis related metabolic pathways were markedly up-regulated at 4200 m in the study.

In summary, it was found that there were significant differences in the metabolites of *Draba oreades* Schrenk at different altitudes through pseudotargeted metabolomics analysis. Phenylpropanoid biosynthesis, phenylalanine, tyrosine and tryptophan biosynthesis and phenylalanine metabolism related to the biosynthesis of flavonoids were up-regulated in the high-altitude group, which may enhance the environmental adaptability to strong ultraviolet intensity and low temperature stress in high altitude areas. Purine metabolism and citrate cycle related to plant growth and development were down-regulated in the mid-altitude and high-altitude groups, duo to the harsh high altitude environment. By TopFc20 distribution diagram, the

content of flavonoids gradually increased with the elevation of altitude, mainly including apigenin, luteolin, quercetin, hesperidin, kaempferol and their derivatives. Based on the random forest model, 10 important metabolites were identified as potential biomarkers. Notably, L-phenylalanine, L-histidine, naringenin-7-O-Rutinoside-4'-O-glucoside and apigenin related to the flavonoids biosynthesis and plant disease resistance were increased with the elevation of altitude. This study provides important insights for the environment adaptability of *Draba oreades* Schrenk to high altitude.

Data availability statement

The original contributions presented in the study are included in the article/Supplementary Material. Further inquiries can be directed to the corresponding authors.

Author contributions

ZS, project administration, supervision, experimental design, validation, visualization, writing-review and editing, and funding acquisition. ZC, supervision and funding acquisition. LL, investigation, resources, methodology, and data curation. XY, data curation, visualization, and writing-original draft. KF, investigation and visualization. YC, investigation. YL, resources, visualization. NS, visualization. DW and XC, validation. JS and MZ, methodology. All authors contributed to the article and approved the submitted version.

Funding

This study was financially supported by the Foundation of Guangxi Health Commission (S2021068), the Open Fund Project of Guangxi Key Laboratory of Precision Medicine for Genetic Diseases (GXWCH-ZDKF-2022-15, Maternal and Child Health Hospital of Guangxi Zhuang Autonomous Region), the Open Fund Project of Guangxi Key Laboratory of Reproductive Health and Birth Defect Prevention (GXWCH-ZDKF-2022-09, Maternal and Child Health Hospital of Guangxi Zhuang Autonomous Region), the Foundation of Science and Technology of Gansu Province (22JR5RA457), the Fundamental Research Funds for the Central Universities (lzujbky-2022-ct04), and the National Natural Science Foundation of China (32061123004).

Acknowledgments

The authors are very grateful for the valuable comments on manuscript revisions of the editor and referees. The authors are grateful to Metware Biotechnology Co., Ltd for their contribution and assistance in the pseudotargeted metabolomics analysis.

Conflict of interest

Authors JS and MZ were employed by Wuhan Metware Biotechnology Co., Ltd.

The remaining authors declare that the research was conducted in the absence of any commercial or financial relationships that could be construed as a potential conflict of interest.

Publisher's note

Supplementary material

The Supplementary Material for this article can be found online at: https://www.frontiersin.org/articles/10.3389/fpls.2022.1052640/full#supplementary-material

References

Adhikari, P., Joshi, K., Singh, M., and Pandey, A. (2020). Influence of altitude on secondary metabolites, antioxidants, and antimicrobial activities of Himalayan yew (Taxus wallichiana). *Plant Biosyst.* 156 (1), 187–195. doi: 10.1080/11263504.2020.1845845

Arnold, P. K., Jackson, B. T., Paras, K. I., Brunner, J. S., Hart, M. L., Newsom, O. J., et al. (2022). A non-canonical tricarboxylic acid cycle underlies cellular identity. *Nature* 603 (7901), 477–481. doi: 10.1038/s41586-022-04475-w

Berardi, A. E., Fields, P. D., Abbate, J. L., and Taylor, D. R. (2016). Elevational divergence and clinal variation in floral color and leaf chemistry in silene vulgaris. *Am. J. Bot.* 103 (8), 1508–1523. doi: 10.3732/ajb.1600106

Cheng, A. X., Han, X. J., Wu, Y. F., and Lou, H. X. (2014). The function and catalysis of 2-oxoglutarate-dependent oxygenases involved in plant flavonoid biosynthesis. *Int. J. Mol. Sci.* 15 (1), 1080–1095. doi: 10.3390/ijms15011080

Choque, B., Catheline, D., Rioux, V., and Legrand, P. (2014). Linoleic acid: Between doubts and certainties. *Biochimie* 96, 14–21. doi: 10.1016/j.biochi.2013.07.012

Cirak, C., Radusiene, J., Jakstas, V., Ivanauskas, L., Seyis, F., and Yayla, F. (2017). Altitudinal changes in secondary metabolite contents of hypericum androsaemum and hypericum polyphyllum. *Biochem. Systematics Ecol.* 70, 108–115. doi: 10.1016/j.bse.2016.11.006

Dai, L. C., Guo, X. W., Zhang, F. W., Du, Y. G., Ke, X., Li, Y. K., et al. (2019). Seasonal dynamics and controls of deep soil water infiltration in the seasonally-frozen region of the qinghai-Tibet plateau. *J. Hydrol.* 571, 740–748. doi: 10.1016/j.jhydrol.2019.02.021

De Vries, S., Furst-Jansen, J. M. R., Irisarri, I., Dhabalia Ashok, A., Ischebeck, T., Feussner, K., et al. (2021). The evolution of the phenylpropanoid pathway entailed pronounced radiations and divergences of enzyme families. *Plant J.* 107 (4), 975–1002. doi: 10.1111/tpj.15387

Dev Sharma, K., Patil, G., and Kiran, A. (2021). Characterization and differential expression of sucrose and starch metabolism genes in contrasting chickpea (Cicer arietinum l.) genotypes under low temperature. *J. Genet.* 100, 71. doi: 10.1007/s12041-021-01317-y

Dong, X., Guo, Y., Xiong, C., and Sun, L. (2020). Evaluation of two major rhodiola species and the systemic changing characteristics of metabolites of rhodiola crenulata in different altitudes by chemical methods combined with UPLC-QqQ-MS-Based metabolomics. *Molecules* 25 (18), 4062. doi: 10.3390/molecules25184062

Dong, N. Q., and Lin, H. X. (2021). Contribution of phenylpropanoid metabolism to plant development and plant-environment interactions. *J. Integr. Plant Biol.* 63 (1), 180–209. doi: 10.1111/jipb.13054

Du, Z., Lin, W., Yu, B., Zhu, J., and Li, J. (2021). Integrated metabolomic and transcriptomic analysis of the flavonoid accumulation in the leaves of cyclocarya paliurus at different altitudes. *Front. Plant Sci.* 12. doi: 10.3389/fpls.2021.794137

Emiliani, J., Grotewold, E., Ferreyra, M. L. F., and Casati, P. (2013). Flavonols protect arabidopsis plants against UV-b deleterious effects. *Mol. Plant* 6 (4), 1376–1379. doi: 10.1093/mp/sst021

Farhat, M. B., Landoulsi, A., Chaouch-Hamada, R., Sotomayor, J. A., and Jordán, M. J. (2013). Phytochemical composition and *in vitro* antioxidant activity of by-products of salvia verbenaca l. growing wild in different habitats. *Ind. Crops Prod.* 49, 373–379. doi: 10.1016/j.indcrop.2013.05.006

Frohnmeyer, H., and Staiger, D. (2003). Ultraviolet-b radiation-mediated responses in plants. balancing damage and protection. *Plant Physiol.* 133 (4), 1420–1428. doi: 10.1104/pp.103.030049

Hectors, K., van Oevelen, S., Guisez, Y., Prinsen, E., and Jansen, M. A. (2012). The phytohormone auxin is a component of the regulatory system that controls UV-mediated accumulation of flavonoids and UV-induced morphogenesis. *Physiol. Plant* 145 (4), 594–603. doi: 10.1111/j.1399-3054.2012.01590.x

Heinemann, B., and Hildebrandt, T. M. (2021). The role of amino acid metabolism in signaling and metabolic adaptation to stress-induced energy deficiency in plants. *J. Exp. Bot.* 72 (13), 4634–4645. doi: 10.1093/jxb/erab182

Imran, M., Rauf, A., Abu-Izneid, T., Nadeem, M., Shariati, M. A., Khan, I. A., et al. (2019). Luteolin, a flavonoid, as an anticancer agent: A review. *BioMed. Pharmacother.* 112, 108612. doi: 10.1016/j.biopha.2019.108612

Jiang, L., Jones, J., and Yang, X. L. (2020). Human diseases linked to cytoplasmic aminoacyl-tRNA synthetases. *Enzymes* 48, 277–319. doi: 10.1016/bs.enz.2020.06.009

Jugran, A. K., Bahukhandi, A., Dhyani, P., Bhatt, I. D., Rawal, R. S., and Nandi, S. K. (2016). Impact of altitudes and habitats on valerenic acid, total phenolics, flavonoids, tannins, and antioxidant activity of valeriana jatamansi. *Appl. Biochem. Biotechnol.* 179 (6), 911–926. doi: 10.1007/s12010-016-2039-2

Kanehisa, M., and Goto, S. (2000). KEGG: kyoto encyclopedia of genes and genomes. *Nucleic Acids Res.* 28 (1), 27–30. doi: 10.1093/nar/28.1.27

Knuesting, J., Brinkmann, M. C., Silva, B., Schorsch, M., Bendix, J., Beck, E., et al. (2018). Who will win where and why? an ecophysiological dissection of the competition between a tropical pasture grass and the invasive weed bracken over an elevation range of 1000 m in the tropical Andes. *PloS One* 13 (8), e0202255. doi: 10.1371/journal.pone.0202255

Li, Y., Dong, S., Wen, L., Wang, X., and Wu, Y. (2013). The effects of fencing on carbon stocks in the degraded alpine grasslands of the qinghai-Tibetan plateau. *J. Environ. Manage* 128, 393–399. doi: 10.1016/j.jenvman.2013.05.058

Li, Q., and Song, J. (2019). Analysis of widely targeted metabolites of the euhalophyte suaeda salsa under saline conditions provides new insights into salt tolerance and nutritional value in halophytic species. *BMC Plant Biol.* 19 (1), 388. doi: 10.1186/s12870-019-2006-5

Liu, Y., Liu, J., Wang, Y., Abozeid, A., Tian, D. M., Zhang, X. N., et al. (2018). The different resistance of two astragalus plants to UV-b stress is tightly associated with the organ-specific isoflavone metabolism. *Photochem. Photobiol.* 94 (1), 115–125. doi: 10.1111/php.12841

Ma, J. H., Gao, X. L., Liu, Q., Shao, Y., Zhang, D. J., Jiang, L. N., et al. (2017). Overexpression of TaWRKY146 increases drought tolerance through inducing stomatal closure in arabidopsis thaliana. *Front. Plant Sci.* 8. doi: 10.3389/fpls.2017.02036

Meng, J., Wang, B., He, G., Wang, Y., Tang, X. F., Wang, S. M., et al. (2019). Metabolomics integrated with transcriptomics reveals redirection of the phenylpropanoids metabolic flux in ginkgo biloba. *J. Agric. Food Chem.* 67 (11), 3284–3291. doi: 10.1021/acs.jafc.8b06355

Murakami, A., Ashida, H., and Terao, J. (2008). Multitargeted cancer prevention by quercetin. *Cancer Lett.* 269 (2), 315–325. doi: 10.1016/j.canlet.2008.03.046

Ni, Q. X., Wang, Z. Q., Xu, G. Z., Gao, Q. X., Yang, D. D., Morimatsu, F., et al. (2013). Altitudinal variation of antioxidant components and capability in indocalamus latifolius (Keng) McClure leaf. *J. Nutr. Sci. Vitaminol.* 59 (4), 336–342. doi: 10.3177/jnsv.59.336

Pandey, G., Khatoon, S., Pandey, M. M., and Rawat, A. K. S. (2018). Altitudinal variation of berberine, total phenolics and flavonoid content in thalictrum foliolosum and their correlation with antimicrobial and antioxidant activities. *J. Ayurveda Integr. Med.* 9 (3), 169–176. doi: 10.1016/j.jaim.2017.02.010

Qiu, J. (2007). Traditional medicine: a culture in the balance. *Nature* 448 (7150), 126–128. doi: 10.1038/448126a

Rathinasabapathi, B., Fouad, W. M., and Sigua, C. A. (2001). Beta-alanine betaine synthesis in the plumbaginaceae. purification and characterization of a trifunctional, s-adenosyl-L-methionine-dependent n-methyltransferase from limonium latifolium leaves. *Plant Physiol.* 126 (3), 1241–1249. doi: 10.1104/pp.126.3.1241

Rius, S. P., Grotewold, E., and Casati, P. (2012). Analysis of the P1 promoter in response to UV-b radiation in allelic variants of high-altitude maize. *BMC Plant Biol.* 12, 92. doi: 10.1186/1471-2229-12-92

Senica, M., Stampar, F., Veberic, R., and Mikulic-Petkovsek, M. (2017). The higher the better? differences in phenolics and cyanogenic glycosides in sambucus nigra leaves, flowers and berries from different altitudes. *J. Sci. Food Agric.* 97 (8), 2623–2632. doi: 10.1002/jsfa.8085

Setyawati, A., Komariah,, Pujiasmanto, B., Fatawi, A., and Batubara, I. (2021). "Secondary metabolites of turmeric and ginger on various altitudes and soil characteristics," in *IOP Conference Series: Earth and Environmental Science*, Vol. 724. doi: 10.1088/1755-1315/724/1/012020

Shang, X. H., Huang, D., Wang, Y., Xiao, L., Ming, R. H., Zeng, W. D., et al. (2021). Identification of nutritional ingredients and medicinal components of pueraria lobata and its varieties using UPLC-MS/MS-Based metabolomics. *Molecules* 26 (21), 6587. doi: 10.3390/molecules26216587

Shan, Z. J., Ye, J. F., Hao, D. C., Xiao, P. G., Chen, Z. D., and Lu, A. M. (2022). Distribution patterns and industry planning of commonly used traditional Chinese medicinal plants in China. *Plant Divers.* 44 (3), 255–261. doi: 10.1016/j.pld.2021.11.003

Shukla, S., and Gupta, S. (2010). Apigenin: A promising molecule for cancer prevention. *Pharm. Res.* 27 (6), 962–978. doi: 10.1007/s11095-010-0089-7

Tripp, E. A., Zhuang, Y. B., Schreiber, M., Stone, H., and Berardi, A. E. (2018). Evolutionary and ecological drivers of plant flavonoids across a large latitudinal gradient. *Mol. Phylogenet. Evol.* 128, 147–161. doi: 10.1016/j.ympev.2018.07.004

Watanabe, S., Matsumoto, M., Hakomori, Y., Takagi, H., Shimada, H., and Sakamoto, A. (2014). The purine metabolite allantoin enhances abiotic stress tolerance through synergistic activation of abscisic acid metabolism. *Plant Cell Environ.* 37 (4), 1022–1036. doi: 10.1111/pce.12218

Yang, L., Yang, C., Li, C., Zhao, Q., Liu, L., Fang, X., et al. (2016). Recent advances in biosynthesis of bioactive compounds in traditional Chinese medicinal plants. *Sci. Bull. (Beijing)* 61, 3–17. doi: 10.1007/s11434-015-0929-2

Yariyama, S., Ando, S., Seo, S., Nakaho, K., Miyashita, S., Kanayama, Y., et al. (2019). Exogenous application of l-histidine suppresses bacterial diseases and enhances ethylene production in rice seedlings. *Plant Pathol.* 68 (6), 1072–1078. doi: 10.1111/ppa.13037

Zhang, Y., Swart, C., Alseekh, S., Scossa, F., Jiang, L., Obata, T., et al. (2018). The extra-pathway interactome of the TCA cycle: Expected and unexpected metabolic interactions. *Plant Physiol.* 177 (3), 966–979. doi: 10.1104/pp.17.01687

Zhang, S., Xin, H. Q., Li, Y., Zhang, D. M., Shi, J., Yang, J. Z., et al. (2013). Skimmin, a coumarin from hydrangea paniculata, slows down the progression of membranous glomerulonephritis by anti-inflammatory effects and inhibiting immune complex deposition. *Evidence-Based Complementary Altern. Med* 2013, 819296. doi: 10.1155/2013/819296

Zhang, S., Yang, J. Z., Li, H. Y., Li, Y., Liu, Y., Zhang, D. M., et al. (2012). Skimmin, a coumarin, suppresses the streptozotocin-induced diabetic nephropathy in wistar rats. *Eur. J. Pharmacol.* 692 (1-3), 78–83. doi: 10.1016/j.ejphar.2012.05.017

Zhao, Y. (2012). Auxin biosynthesis: a simple two-step pathway converts tryptophan to indole-3-acetic acid in plants. *Mol. Plant* 5 (2), 334–338. doi: 10.1093/mp/ssr104

Zhao, W., Shi, X., Li, J., Guo, W., Liu, C., and Chen, X. (2014). Genetic, epigenetic, and HPLC fingerprint differentiation between natural and ex situ populations of rhodiola sachalinensis from changbai mountain, China. *PloS One* 9 (11), e112869. doi: 10.1371/journal.pone.0112869

frontiers | Frontiers in Plant Science

TYPE Original Research
PUBLISHED 15 December 2022
DOI 10.3389/fpls.2022.1071225

OPEN ACCESS

EDITED BY
Jin-Lin Zhang,
Lanzhou University, China

REVIEWED BY
Zhijian Chen,
Chinese Academy of Tropical Agricultural Sciences, China
Yu Chen,
Nanjing Agricultural University, China
Klára Kosová,
Crop Research Institute (CRI), Czechia

*CORRESPONDENCE
Lingyan Jiang
lyjiang@hainanu.edu.cn
Lijuan Luo
990908@hainanu.edu.cn

†These authors have contributed equally to this work and share first authorship

SPECIALTY SECTION
This article was submitted to Plant Abiotic Stress, a section of the journal Frontiers in Plant Science

RECEIVED 16 October 2022
ACCEPTED 30 November 2022
PUBLISHED 15 December 2022

CITATION
Yang L, Gao J, Gao M, Jiang L and Luo L (2022) Characterization of plasma membrane proteins in *stylosanthes* leaves and roots using simplified enrichment method with a nonionic detergent.
Front. Plant Sci. 13:1071225.
doi: 10.3389/fpls.2022.1071225

Characterization of plasma membrane proteins in *stylosanthes* leaves and roots using simplified enrichment method with a nonionic detergent

Liyun Yang†, Jing Gao†, Mengze Gao, Lingyan Jiang* and Lijuan Luo*

Hainan Key Laboratory for Sustainable Utilization of Tropical Bioresource, College of Tropical Crops, Hainan University, Haikou, China

Plant plasma membranes (PMs) play an important role in maintaining the stability of the intracellular environment and exchanging information with the external environment. Therefore, deciphering dynamics of PM proteome provides crucial information for elucidating cellular regulation in response to diverse stimuli. In the study, we developed a simplified method for enriching PM proteins in leaf and root tissues of a tropical forage *Stylosanthes* by combining differential centrifugation and Brij-58 treatment. Both immunoblot analysis and mass spectrometry demonstrated that the representation and abundance of PM proteins were increased in the enrichment fraction, and the contamination of other organellar proteins was decreased. A total of 426 and 388 proteins were predicted to be PM proteins in leaves and roots, respectively. Functional analysis classified these PM proteins into six major categories (transporter, enzyme, receptor, membrane structure protein, vesicular trafficking and chaperone), and orthologs of many PM proteins regulating the responses to abiotic and biotic stresses have been detected. In addition, the sequence analysis, subcellular localization and gene expression analyses of a newly identified receptor-like kinase, SgRKL1, has been performed. Together, these results show that the simplified PM enrichment method can be successfully applied to different plant tissue types and to study the dynamics of PM proteome of *Stylosanthes* in response to multiple stresses.

KEYWORDS

plasma membrane, proteomics, Brij-58 treatment, protein enrichment, *Stylosanthes*

1 Introduction

Due to the difficulties and complexities of whole-cell proteome analyses, subcellular fractionation is an important strategy for focusing on proteins that are of biological interest but present at relatively low levels. About 20-30% of all genes in an organism code for membrane proteins including plasma membrane (PM), and the PM forms the interface between the cytosol and extracellular environments, regulating a broad range of physiological responses, including plant growth and development, sensing and responding to environmental stresses, distribution and movement of biological molecules (ion, hormones, metabolites and etc.) and disease resistance (Chen and Weckwerth, 2020). Due to the unique roles of the PM, identification and functional characterization of plant PM proteome is of great importance.

However, the analyses of PM proteome are challenging due to the high hydrophobicity, heterogeneity and relatively low abundance of PM proteins in the total cellular protein pool (Yadeta et al., 2013; Chen and Weckwerth, 2020). To promote the separation and enrichment of PM proteins, several techniques have been developed, including density gradient centrifugation, free-flow electrophoresis, and phase polymer systems (Yadeta et al., 2013). Aqueous two-phase partitioning is one of the optimal method for isolating highly purified PMs, however, this method is time consuming, and the protocol needs to be optimized for different tissue types, cell types or species (Michele et al., 2016). Because the isolation of subcellular compartments by biochemical approaches can never reach 100% purity, it is of greater interest to develop the strategies that could detect a large number of PM proteins for comparisons rather than isolate highly purified PM proteins. Based on such rationale, a simplified enrichment method using differential centrifugation and Brij-58 treatment has been developed in *Arabidopsis* cell cultures and seedlings as well as maize roots (Zhang and Peck, 2011; Zhang et al., 2013; Collins et al., 2017). Although this method can not produce PM proteins as pure as those from aqueous two-phase partitioning, the strategy is very powerful to enrich sufficient PM fraction for the large-scale identification and quantitative comparisons (Voothuluru et al., 2016).

Stylo (*Stylosanthes* spp.) is a dominant leguminous forage crop cultivated in tropical and subtropical areas (Schultze-Kraft et al., 2018). It is widely used for livestock and soil improvement. Due to its excellent adaptation to acidic and infertile soils, stylo has shown the superior tolerance against phosphorus (P) deficiency, aluminium (Al) and manganese (Mn) toxicity (Sun et al., 2013; Chen et al., 2015; Jiang et al., 2018; Liu et al., 2019; Luo et al., 2020). Interestingly, PM proteins have been shown to play critical roles in regulating these processes. For instance, a transcriptomic analysis that investigated the responses of stylo to Al^{3+} stresses has revealed that the secretion of citrate could be the major mechanisms of Al^{3+} resistance, and anion channels in PM may play vital roles in regulating the secretion (Jiang et al., 2018). In addition, PM localized purple acid phosphatases, SgPAP7, SgPAP10, SgPAP23, SgPAP26, have been proved to mediate the extracellular phytate-P utilization in stylo, contributing to the tolerance of phosphorus deficiency (Liu et al., 2016; Liu et al., 2018). Although roles for several PM proteins of stylo have been identified, broader identification and functional analyses of PM proteins (and their complexes) regulating the resistance under various stresses remain an important area of investigation.

In this study, we evaluated the application of the simplified PM enrichment method of combining differential centrifugation and Brij-58 treatment in the leaf and root tissue of stylo. We demonstrated the easy and effective transfer of the method into new plant species and tissue types. Furthermore, we performed the classification of functions of the detected PM proteins and identified orthologs of many PM proteins with important function. In addition, we performed the sequence analysis, subcellular localization and gene expression analyses of a newly identified receptor-like kinase SgRKL1.

2 Materials and methods

2.1 Plant growth and tissue collection

The stylo (*Stylosanthes guianensis*) genotype Reyan No.2 seeds (provided by Chinese Academy of Tropical Agricultural Sciences) were used in all experiments. Seeds were peeled and washed by sterilized water, shaken evenly to remove the bubbles and heated at 85°C for 3 min. The heated seeds were germinated on sheets of germination paper moistened with sterilized water at room temperature and near-saturating humidity in the dark. After 3-day germination, seedlings were transferred into soil and grown in 10 cm × 10 cm pots with a density of 10 seedlings per pot. The aerial parts of one-week seedlings were used to collect the leaf tissues. Root tissues were collected from two-week seedlings with primary roots around 20 mm and grown under the hydroponic culture condition where seedlings post 3-day germination were transferred into 1.5 mL eppendorf tubes with culture medium (0.4% plant agar in Magnavaca's nutrient solution) (Famoso et al., 2010). The temperature for seedling growth ranged from 25°C to 32°C and relative humidity from 60% to 80%.

The inoculation of *Colletotrichum gloeosporioides* was performed as described by previous research (Jiang et al., 2021). Briefly, *C. gloeosporioides* was cultured in CM liquid medium at 200 rpm for 3 days at 28°C, and the mycelium was filtered with sterile gauze to obtain spore suspension. One-month-old stylo plants grown in soil were spray-inoculated of spore suspension with a conidial of 7.5×10^6 conidia/mL containing 0.02% Silwet L-77 (Solarbio, Beijing, China), and the inoculated plants were incubated in dark room at 28°C and

90% humidity for 12 h. Then, the plants were transferred to a growth chamber at 28°C, 90% humidity and 16 h/8 h light/dark photoperiod cycle. Leaf samples pooled from 9 plants were collected at 0 h, 12 h, 24 h, 36 h, 48 h, 60 h, 72 h and 96 h post inoculation. The tissue samples were collected from cotyledons of one-week-old stylo, leaves, stems and roots of one-month-old stylo. For one biological replicate, cotyledon, leaf, stem, root samples were pooled from 9 stylo plants. For low phosphorus (P) stress experiment, stylo seeds were pre-germinated on wet filter paper at 28°C. After germinated for 3 d, the uniform seedlings were transferred to blue plastic basin containing the modified Magnavaca's nutrient solution according to previous research (Luo et al., 2020). After 15-day growth, the seedlings were transferred to fresh modified Magnavaca's nutrient solution supplied with (HP) or without (LP) 300 μmol/L KH_2PO_4. After 15-day HP and LP treatments, root samples pooled from 9 stylo plants were harvested as one biological replicate. Three biological replicates were included for the following expression pattern analysis.

Nicotiana benthamiana plants were grown in a growth room at 22°C with a 16 h/8 h light/dark photoperiod cycle. Four-week-old plants with seven to eight leaves were used for *Agrobacterium tumefaciens* inoculation.

2.2 Protein extraction and plasma membrane enrichment

The process of protein extraction and plasma membrane enrichment were modified from the previously published protocol (Collins et al., 2017). Briefly, fresh leaf tissues were ground using 1 mL ice-cold buffer H (250 mM sucrose, 50 mM HEPES-KOH pH 7.5, 5% glycerol, 50 mM NaPP, 1 mM NaMo, 25 mM NaF, 10 mM EDTA, 0.5% PVP, 3 mM DTT, 1 mM PMSF) per 0.2 g, and frozen root tissues were ground to a fine powder with 1 mL buffer H per 0.5 g fresh weight. The homogenate was then centrifuged for 10 min (10000 × *g*, 4°C),and the resulting supernatant was collected and centrifuged in an ultracentrifuge (Thermo Sorvall WX 100) for 30 min (100000 × *g*, 4°C) to pellet the crude microsomal fractions. The pellets were suspended and incubated in 2 μL of buffer H with 0.02% w/v Brij-58 (Sigma-Aldrich, America) per μg of microsomal protein on ice for 30 min, and then ultracentrifuged for 30 min (100000 × *g*, 4°C). The Brij-58 treatment and ultracentrifugation were repeated one more time to obtain the final enriched plasma membrane protein fraction.

2.3 Immunoblotting

Proteins samples (20-30 μg) were separated by 10% SDS-PAGE and transferred to PVDP membrane for 2 h at 65 V on ice. The immunoblotting was performed with primary rabbit antibody anti-AHA (H^+-ATPase plasma membrane marker, Agrisera), anti-AOX1/2 (alternative oxidase isoforms 1/2, mitochondrial inner membrane marker, Agrisera), and anti-β-actin (cytosolic maker, Agrisera) (Slajcherová et al., 2012). Chemiluminescent detection (Pierce) was performed using horseradish peroxidase-linked goat anti-rabbit antibody (Cell Signaling and Technologies). Coomassie Brilliant Blue R-250 staining (0.1% w/v CBB R-250 in 10% v/v acetic acid and 40% v/v methanol) was used after antibody probing, to visualize levels of total protein on the membrane.

2.4 SDS-PAGE analysis and tryptic digestion

Total protein and PM fraction were resuspened in sample-loading buffer and heated to 65°C for 7 min. The protein samples were separated by 10% SDS-PAGE, stained with colloidal Coomassie G-250 overnight and destained in distilled water the following day. Each lane was then cut into 3 gel slices with a razor blade. The proteins from gel slices were reduced with 10 mM DTT, alkylated with 55 mM iodoacetamide and digested within the gel using 0.01 μg/μL trypsin in 25 mM NH_4HCO_3 buffer at 37°C overnight. After digestion, peptides were eluted twice with 50% ACN. The extracted peptide mixture was dried by lyophilization.

2.5 LC-MS/MS analysis

Lyophilized peptides were dissolved in 0.1% FA and 2% ACN for MS analysis. Peptides were first separated through UltiMate 3000 UHPLC (Thermo) and eluted into the nanoelectrospray ion source of a Q-Exactive HF X LC-MS/MS mass spectrometer (Thermo Fisher Scientific, San Jose, CA), which is operating in data-dependent mode. The buffer solutions used for HPLC were 2% ACN, 0.1% FA (buffer A) and 98% ACN, 0.1% FA (buffer B) with a velocity of 300 nL per minute through the following increment: 0-5 min, 5% buffer B; 5-45 min, 5% to 25% buffer B; 45-50 min, 25% to 35% buffer B; 50-52 min, 35% to 80% buffer B; 52-54 min, 80% buffer B; 54-60 min, 5% buffer B. Survey scans covered the range 350-1500 m/z, and the range for MS/MS spectra was 100-1500 m/z. Charge state rejection was enabled for +2 to +6 with a peak detection window of 10 ppm. Dynamic exclusion was enabled with one count for 30 s.

2.6 Peptide and protein identification

All MS/MS spectra were analyzed using MASCOT (server version 2.3) (Perkins et al., 1999) searching against Papilionoideaethe Uniprot database (http://www.uniprot.org/, updated on Jan, 2020) which contained 925535 sequences and

Arabidopsis database (https://www.arabidopsis.org/, updated on Mar 31, 2005). Carbamidomethyl was specified as a fixed modification, and oxidized methionine, deamidated glutamine were specified as a variable modification. The peptide mass tolerance was set as 20 ppm, and the fragment mass tolerance was 0.05 Da. Peptide and protein identifications were assigned by the Percolator (https://www.elastic.co/guide/en/elasticsearch/reference/7.7/percolator.html, updated on July 28, 2014) at FDR ≤ 0.01 (Käll et al., 2007). The relative abundance of identified peptide was calculated based on IBAQ algorithm (Schwanhäusser et al., 2011).

2.7 Domain, phylogenetic and motif analysis of RKL1

The coding sequence of SgRKL1 was determined by sequence alignment between the peptide sequence identified from mass spectrometry and *de novo* transcriptome sequence of stylo previously published in our lab (Jiang et al., 2021). The Conserved Domains (https://www.ncbi.nlm.nih.gov/Structure/cdd/wrpsb.cgi) was used for predicting conserved domain of SgRKL1 protein. The DeepTMHMM (https://dtu.biolib.com/DeepTMHMM) was used for predicting signal peptide and transmembrane domain of SgRKL1. A total of 27 homology sequences of RKL1 were downloaded from NCBI, and the phylogenetic tree was constructed using the MEGA v7.0 by neighbour-joining (NJ) method with 500 bootstrap replicates. The MEME (https://meme-suite.org/meme/doc/meme.html) website was used to predict the motif composition of the RKL1 protein. The maximum motif parameter of the gene was 10, the rest of the parameters remained unchanged.

2.8 Subcellular localization of SgRKL1

Full length coding sequence of *SgRKL1* gene was amplified from cDNA of stylo leaf using primer pairs (Fw: CAAGGGTCTAGACCCGGGAATGGTGGCCATTAGCATT; Rv: CGATCAATCAGGATCCTAACTCTACAAGATCATGTTGTT) and Phanta Max Master Mix (Vazyme, Nanjing, China). The amplified sequence was gel purified by FastPure Gel DNA Extraction Mini Kit (Vazyme, Nanjing, China) and cloned into the pCAMBIA2300 plasmid by XhoI and SpeI digestion site and ClonExpress Ultra one step cloning kit (Vazyme, Nanjing, China). The expression vector of SgRKL1 was verified by sequencing and introduced into *Agrobacterium tumefaciens* strain GV3101. The sequence of *SgRKL1* was deposited in NCBI data base with accession number OP837387.

Agrobacterium cultures harboring pCAMBIA-SgRKL1-GFP/pCAMBIA-GFP and pEG100-PIP2A-mCherry constructs were mixed in a 1:1 ratio to a final OD_{600} of 1.0 in infiltration buffer (10 mM $MgCl_2$, 10 mM MES, pH 5.7) that was infiltrated into four-week-old *N. benthamiana* plants. Two days post infiltration, the leaf tissues were collected for detection of GFP and mCherry fluorescence signals at 488 nm and 587 nm using confocal microscopy (A1RHD25 + N-SIM +N-STORM, Nikon) and protein isolation. Different fractions of leaf of *N. benthamiana* were isolated using the same method as stylo described in section 2.2.

2.9 Quantitative real-time PCR analysis

Total RNA was extracted from leaf and root tissues of stylo using TRizol reagent (Invitrogen, Waltham, MA, United States) according to the manufacturer's protocol. First-strand cDNA was synthesized from 1 μg of total RNA using HiScript II 1st Strand cDNA Synthesis Kit (+gDNA wiper) (Vazyme, Nanjing, China). Quantitative real-time PCR (qRT-PCR) was carried out using ChamQ Universal SYBR qPCR Master Mix (Vazyme, Nanjing, China) on Applied Biosystems QuantStudio™ 7 Flex System (Applied Biosystems, USA). Reaction mixtures of 10 μL contained 5 μL of 2× ChamQ Universal SYBR qPCR Master Mix, 0.2 μL of each primer (0.2 μmol/L, Fw: CCTTCCGGCGACATTACCAA; Rv: GCAGAAGACACACCACGGAT), 1 μL of cDNA template, and 3.6 μL of ddH_2O. The amplification program was set at 95°C for 3 min, followed by 40 cycles of 95°C for 15 s and 60°C for 1 min, and a melt-curve program (60–95°C, with a temperature increase of 0.05°C after every 1 s). Signal threshold levels were set automatically by the system. The housekeeping gene, *ribosomal protein L19 (RPL19)*, was used as reference gene to normalize gene expression (Jiang et al., 2021). Three biological replicates were included in this study, and the relative expression levels calculated using $2^{-\Delta\Delta Ct}$ (Schmittgen and Livak, 2008).

2.10 Statistical analysis

The experimental data was analyzed using SPSS software (Version 20; SPSS Inc., Chicago, IL, USA) with the ANOVA procedures, the relative expression level was displayed with mean ± standard error (SE). Dancan's method was used for multiple comparison, and Student's t-test was used for comparison between two groups, $P < 0.05$ was considered statistically significant.

3 Results

3.1 Development of PM-enrichment method in *Stylosanthes* leaves and roots

3.1.1 Outline of procedures

In this study, we have developed a simplified method to enrich PM proteins in stylo leaf and root tissues using differential centrifugation and Brij-58 treatment (Figure 1). Briefly, frozen

leaf or root tissues were ground with a motar and pestle. Following homogenization, protein extracts were pre-cleared by a low-speed centrifugation to remove cell debris and intact organelles. The resulting supernatant total protein (T) was used to pellet the crude microsomal fraction (CM) by ultracentrifugation. The CM fraction was resuspended in buffer H containing Brij-58, and the suspension was pelleted by ultracentrifugation followed by buffer wash to remove loosely bound membrane-associated proteins. After the final round of ultracentrifugation, the resulting pellet was hereafter referred to as the enriched plasma membrane fraction (PM) (Figure 1).

3.1.2 Immunoblot analysis of different fractions

To test the effect of this method for enriching PM proteins, we performed the immunoblot analysis using equal amounts of protein from total protein fraction (T), the supernatant fraction of first ultracentrifugation (Cyto), the CM fraction and the PM fraction (Figures 2A, B). The integral PM H^+-ATPases (AHAs), mitochondrial inner membrane protein (AOX1/2), β-actin and cytosolic rubisco proteins were used as markers (Slajcherová et al., 2012; Evans and Clarke, 2019). For leaf tissues, the AHA proteins were strongly enriched in the PM as compared to the T, Cyto or CM fraction, and the AOX1/2 proteins were enriched in the CM fraction and depleted in the PM fraction. Conversely, cytosolic markers, β-actin and rubisco proteins, were strongly depleted in PM fraction (Figure 2A). For root tissues, the AHAs and AOX1/2 proteins were enriched in the CM and PM faction, and the AOX1/2 proteins were decreased in the PM fraction. The β-actin proteins were depleted in the PM fraction (Figure 2B). These results demonstrate that, at least for the markers used, the strategy combining differential centrifugation and Brij-58 treatment has effectively enriched the plasma membrane proteins and reduced the proteins from cytosol and other membrane organelles.

3.1.3 Analysis of total and PM faction by MS

To further test the enrichment effect, we applied mass spectrometry (MS) to look at a wider range of proteins. For both leaves and roots, proteins from the total fraction and PM fraction were separated by SDS-PAGE. Each lane was cut into three slices, and peptides were recovered by in-gel digestion, the proteins in the gels were reduced, alkylated, and digested with trypsin. The digested proteins were analyzed by liquid chromatography tandem mass spectrometry (LC-MS/MS) (Figure 3A), and all the identified proteins and peptides were summarized in the Table S1. The identified proteins were further filtered based on minimum of two unique peptides, resulting in 2135 and 2025 proteins in leaves and roots, respectively (Table S2). The PCA analysis of T and PM proteome in leaves and roots showed the clear separation between enrichment treatment (16.06%) and different organs (12.51%) (Figure 3B). In leaf tissues, 752 (35%) and 978 (46%) unique proteins were identified in T and PM fraction, respectively, and 405 (19%) proteins overlapped between the T and PM fraction. In root tissues, 746 (37%) and 906 (45%) unique proteins were identified in T and PM fraction, respectively, and 373 (18%) proteins overlapped between the T and PM fraction (Figure 3C).

To examine the consistency of the mass spectrometry and immunoblotting results for PM enrichment, we checked the iBAQ values of several representative proteins, of which the localization has been previously published (Tables 1, 2). The results showed that the iBAQ value of the PM marker (AHA) was significantly increased in the PM fraction both in leaves and roots. Similarly, the amount of other classic PM proteins such as aquaporin, LRR receptor-like kinase and calcium-transporting ATPase was also significantly increased after enrichment. Conversely, the representative proteins in MI, ER, Cyto were almost depleted after enrichment. These results clearly demonstrate the ability of this method to enrich PM proteins in both leaves and roots of stylo, we next performed a more extensive analysis to identify the organellar composition in the T and PM fraction.

3.2 Analysis of organellar composition of total versus PM fractions

Protein locations were assigned based on WoLF PSORT (Horton et al., 2007), and proteins with multiple location assignments were excluded from our lists. We first examined T and PM fraction for the percentage of proteins predicted to be in different locations (Table 3; Table S2). In leaf tissues, we found that the proteins with increased representation in PM fraction were predicted to be localized in the plasma membrane (PM, 2.08-fold enrichment), vacuole (VU, 1.22-fold enrichment), golgis apparatus (GO, 1.26-fold enrichment) and mitochondria (MI, 1.18-fold enrichment) while proteins with decreased number were from cytosol (CY), plastid (PL), extracellular space (EX), peroxisome (PR), cytoskeleton (CS). Proteins from nucleus (NU) and endoplasmic reticulum (ER) were distributed relatively evenly between two fractions. In root tissues, the PM enriched for proteins in the PM (2.00-fold enrichment) and VU (1.18-fold enrichment) while decreased the number of proteins from GO, ER, CY, PL, EX, PR and CS. Proteins from MI and NU were distributed relatively evenly between two fractions (Table 3). The results showed that this method has a similar effect of enrichment in leaves and roots, and the representation of PM proteins was increased by more than 2-fold in PM fraction.

To compare the abundance of proteins assigned to specific compartments in T and PM fraction, we performed pair-wise comparisons of iBAQ values using log2 ratio. For these

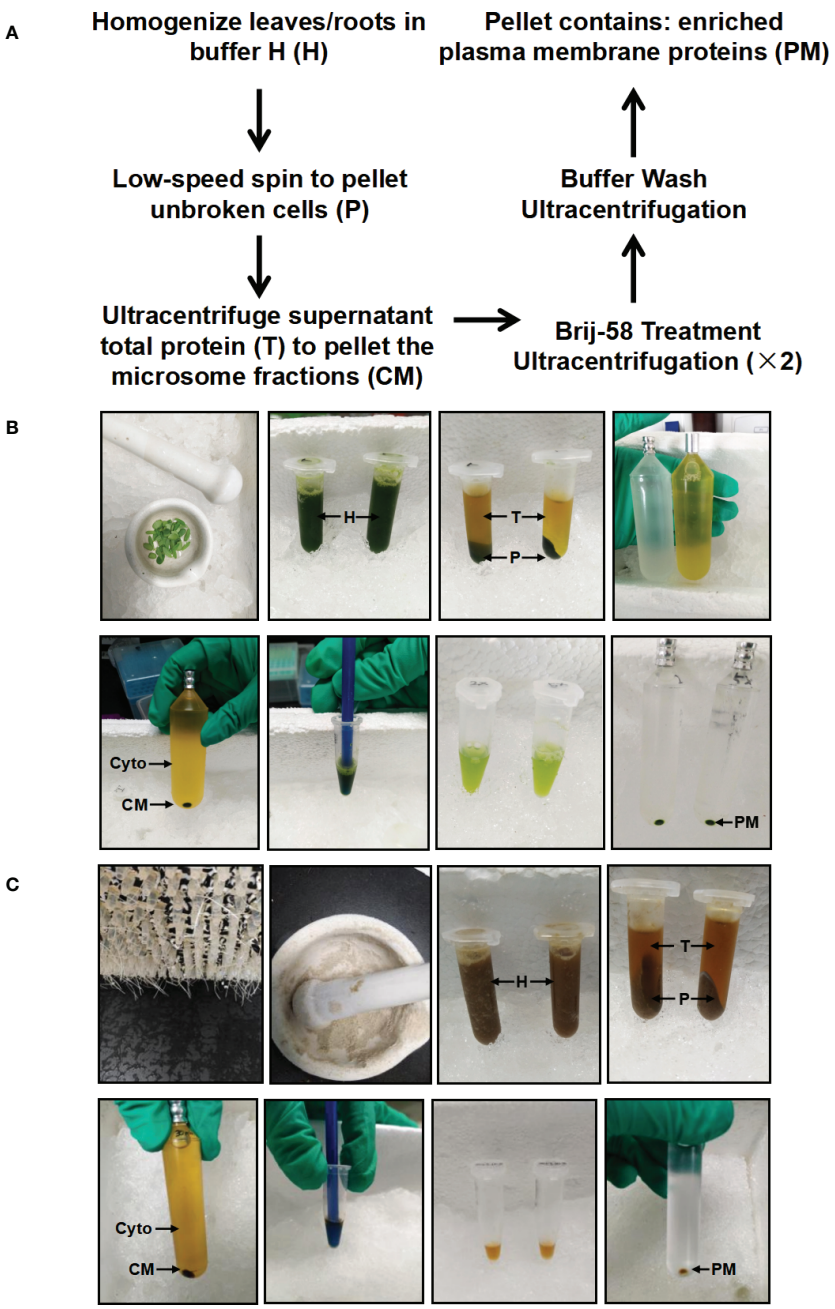

FIGURE 1
Schematic and image representation of the simplified plasma membrane enrichment procedure in leaf and root tissue of *Stylosanthes*. **(A)** Schematic representation of the procedure. **(B)** Images showing the key procedures in leaf tissue. **(C)** Images showing the key procedures in root tissue. After homogenization in Buffer H, the total homogenate (H) is subjected to low-speed spin to separate the supernatant (T: containing cytosolic and microsomal proteins) from the pellet (P: containing cell debris). The total protein fraction (T) is transferred to ultracentrifugation tube to pellet the crude microsome (CM) by ultracentrifugation, and the resulting supernatant contains cytosolic proteins (Cyto). The CM is resuspended in Buffer H with Brij-58, incubated on ice and subjected to ultracentrifugation to yield an enriched plasma membrane fraction (PM).

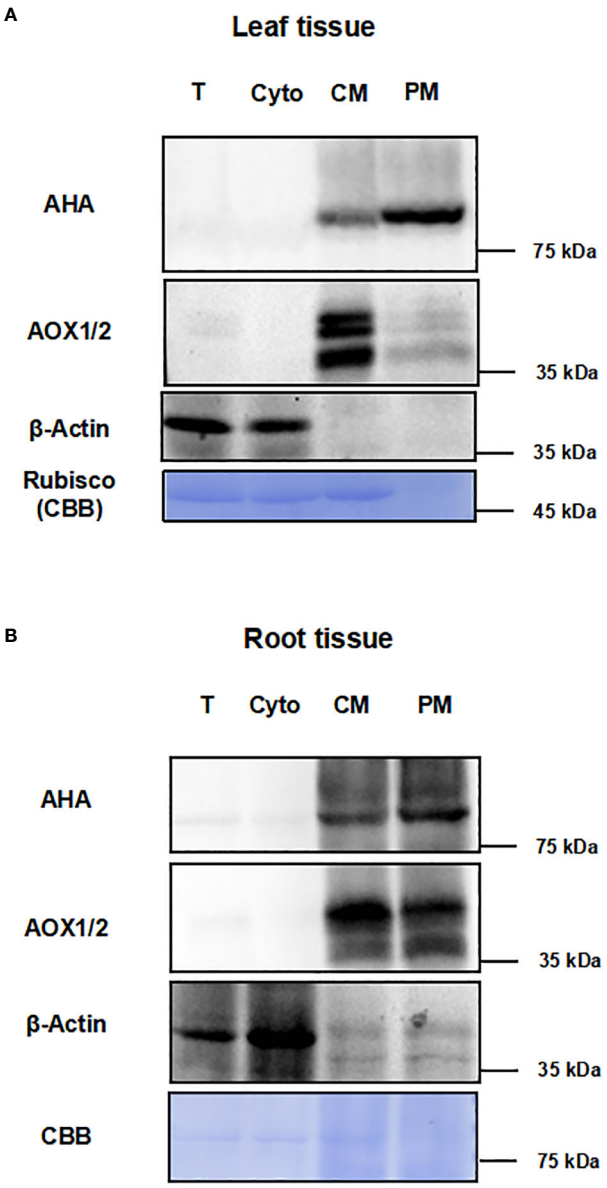

FIGURE 2
Immunoblot analysis for different fractions with antibodies against subcellular marker proteins. The proteins of leaf and root tissue from steps of the enrichment procedure were analyzed by immunoblotting with organelle specific markers (T, total homogenate; Cyto, cytosolic fraction; CM, crude microsomal fraction; PM, plasma membrane-enriched fraction). **(A)** Equal amounts of proteins of leaves from each fraction were analyzed by immunoblotting with two antibodies against organellar marker proteins (PM marker: AHA; mitochondrial marker: AOX1/2; cytosolic maker: β-actin). **(B)** Equal amounts of proteins of roots from each fraction were analyzed by immunoblotting with antibodies against AHA, AOX1/2 and β-actin. PM, plasma membrane; AHA, H+-ATPase; AOX1/2, Plant alternative oxidase 1 and 2. Total protein loads were detected by coomassie blue staining (CBB).

comparisons, proteins not identified in one fraction (having zero iBAQ) were assigned 0.2 to allow inclusion in the calculations. For each compartment, the calculated mean values of log2 are shown in Figure 4. In both leaf and root tissue, the fold increase of PM protein was significantly higher than that of proteins in other compartments, and proteins in CY, PL, EX, PR and CS were decreased in PM fraction. In general, the representation differences detected in different locations is consistent with the abundance comparisons, and both results support the capability of the technique for enriching the PM proteins.

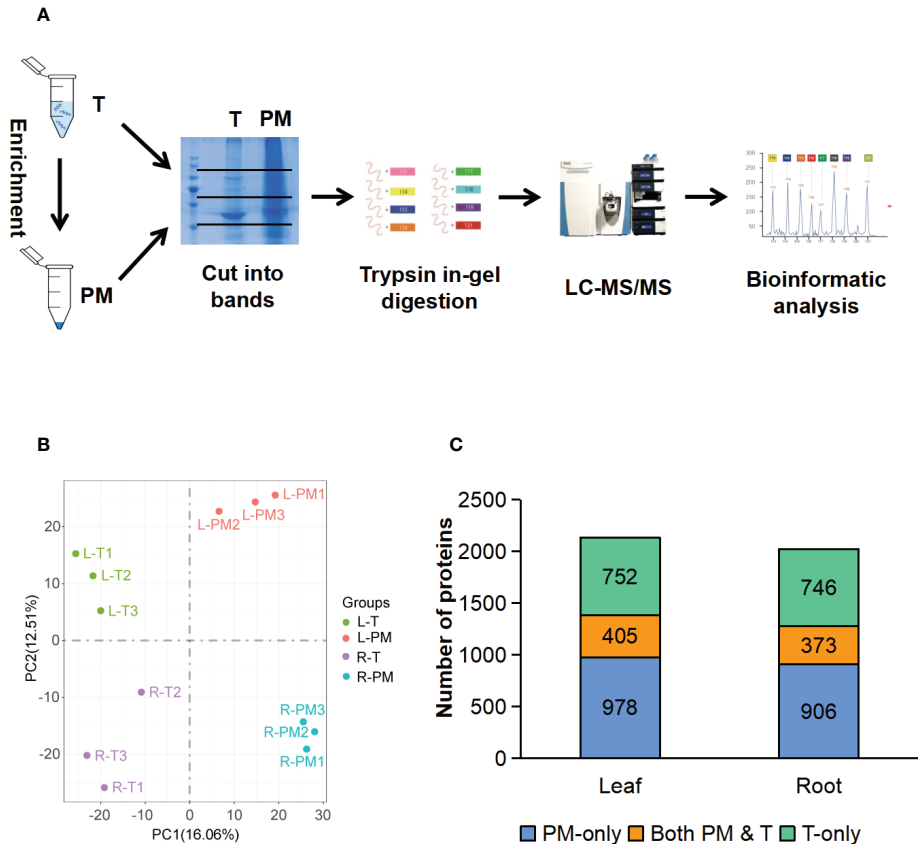

FIGURE 3
LC-MS/MS analysis of the total fraction and enriched plasma membrane fraction. **(A)** Workflow of MS analysis of total and enriched PM fraction. **(B)** PCA analysis of proteome data from the total and enriched PM fraction of leaf and root tissue, three biological replicates for each fraction of each tissue type. **(C)** Comparison of proteins identified in total fraction alone (green blocks), enriched PM fraction alone (blue blocks), and shared by both fraction (orange blocks). T, total fraction; PM, enriched plasma membrane fraction; L-T, total fraction of leaves; L-PM, enriched plasma membrane fraction of leaves; R-T, total fraction of roots; R-PM, enriched plasma membrane fraction of roots.

3.3 Analysis of PM proteins identified in PM fractions

3.3.1 Analysis of transmembrane domain of PM proteins

In total, 426 and 388 proteins were predicted to be PM proteins in leaves and roots, respectively. Among identified PM proteins, 174 proteins were shared by leaves and roots, whereas 252 and 214 proteins were leaf- and root-specific. (Figure 5A; Table S3). To investigate the presence of transmembrane domain in these identified PM proteins, the analysis was performed using the TMHMM prediction programs. The results showed that 91.78% of proteins in leaves and 87.11% of proteins in roots had at least one transmembrane domain, and these proteins could be integral proteins (Figure 5B). The proteins without transmembrane domain could be peripheral proteins or lipid-anchored proteins.

3.3.2 Functional classification of PM proteins

PM proteins are involved in many important biological processes. To investigate the functions of the identified PM proteins, functional classification has been performed using the PANTHER classification system (Mi et al., 2019). The results showed that the functions of proteins could be divided into six major categories: transporter, enzyme, receptor, membrane structure protein, vesicular trafficking and chaperone (Figure 6; Table S4). Transporter proteins dominated in the identified proteins, and ABC transporters constituted the largest group. A total of 53 and 49 ABC transporters were characterized in leaf and root, respectively, including members in ABCA, ABCB, ABCC and ABCG subfamily. Other major transporters included nitrate transporter (NRT1/2 ortholog), inorganic phosphate transporter (PHT1 ortholog), potassium transporter (POT4/5/7/11/12 ortholog), sulfate transporter (SULTR4.2 ortholog), metal-nicotianamine transporter (YSL6/7 ortholog), sucrose transporter (SUC2 and STP1 ortholog) and auxin

10.3389/fpls.2022.1071225

TABLE 1 Representative list of PM, ER, MI and Cyto proteins in PM and T fractions of leaves measured by mass spectrometry.

Accessionnumber (a)	Arabidopsis ID (b)	Description	iBAQ (Leaf)(c)		Compartment(d)
			PM	T	
A0A445C0K6	AT2G24520	Plasma membrane ATPase	860954.80	11790.07	PM
A0A371HFL0	AT3G16240	Aquaporin TIP2-1	64291040.66	0	PM
A0A2K3PLU7	AT5G10290	LRR receptor-like kinase resistance protein	143487.49	0	PM
A0A444WPI3	AT5G49360	Fn3_like domain-containing protein	0	1829698.35	ER
A0A445KRZ9	AT5G42020	Luminal-binding protein 4 isoform D	0	29890.76	ER
A0A371IGU2	AT4G38630	26S proteasome non-ATPase regulatory subunit 4-like protein	10990.20	387695.32	ER
A0A1S2XXJ3	AT3G23990	chaperonin CPN60-2	0	120063.77	MI
A0A444ZVK9	AT4G37930	Serine hydroxymethyltransferase	0	300434.54	MI
A0A445DTY1	AT1G63940	Pyr_redox_2 domain-containing protein	0	314465.04	MI
A0A445E0V9	AT1G05180	NEDD8-activating enzyme E1 regulatory subunit	0	314501.02	Cyto
A0A4D6N6X8	AT5G38830	Cysteinyl-tRNA synthetase	0	497946.91	Cyto
A0A392S5X8	AT1G65350	Ubiquitin 11	0	1575497.93	Cyto

(a) Database accession number from UniProt; (b) Database Arabidopsis ID from Tair; (c) The iBAQ value is the average of three replicates; (d) Compartment assignment based on publication. PM, plasma membrane; ER, endoplasmic reticulum; MI, mitochondria; Cyto, cytosol.

transporter (PIN3 ortholog). Interestingly, nitrate and inorganic phosphate transporters were mainly identified from root PM proteome, while sucrose transporters were only identified from leaf. Primary active transporter was also the major category which included H^+-ATPases, maganese-transporting ATPase, calcium-transporting ATPase and phospholipid-transporting ATPase. Enzyme proteins were the second largest class, in which glycosyltransferase contained the largest number. There were 13 and 14 glycosyltransferase proteins detected in the leaf and root PM proteome, respectively, and 23 of them were

TABLE 2 Representative list of PM, ER, MI and Cyto proteins in PM and T fractions of roots measured by mass spectrometry.

Accessionnumber (a)	Arabidopsis ID (b)	Description	iBAQ (Root)(c)		Compartment(d)
			PM	T	
A0A444ZI65	AT2G24520	Plasma membrane ATPase	681078.44	0	PM
A0A445GUH7	AT5G57110	Calcium-transporting ATPase	168601.27	0	PM
A0A445DU07	AT4G11220	Reticulon-like protein	3590495.91	0	PM
A0A151SQ13	AT1G77510	Protein disulfide-isomerase	0	265827.62	ER
A0A445KTK0	AT2G32730	26S proteasome non-ATPase regulatory subunit 1 homolog	76757.07	191063.76	ER
A0A0L9V3F1	AT1G53240	Malate dehydrogenase	0	108372.81	MI
A0A445CGM8	AT5G26780	Serine hydroxymethyltransferase	38394.02	647188.72	MI
A0A444ZMJ2	AT3G61440	Cysteine synthase	0	212915.78	MI
A0A445CYF4	AT3G24170	Glutathione reductase	0	216379.56	Cyto
A0A445DN91	AT2G44100	Guanosine nucleotide diphosphate dissociation inhibitor	0	399519.35	Cyto

(a) Database accession number from UniProt; (b) Database Arabidopsis ID from Tair; (c) The iBAQ value is the average of three replicates; (d) Compartment assignment based on publication. PM, plasma membrane; ER, endoplasmic reticulum; MI, mitochondria; Cyto, cytosol.

TABLE 3 Comparison of organelle proteomes between total protein and enrichment fraction.

Cellular compartments	Leaf			Root		
	% of proteins identified in PM fraction	% of proteins identified in T fraction	Fold change of protein representation (PM/T)	% of proteins identified in PM fraction	% of proteins identified in T fraction	Fold change of protein representation (PM/T)
PM	26.53%	12.75%	2.08	24.65%	12.34%	2.00
VU	2.11%	1.73%	1.22	1.81%	1.53%	1.18
MI	5.23%	4.42%	1.18	5.35%	5.23%	1.02
NU	7.99%	7.29%	1.10	8.82%	7.93%	1.11
GO	0.22%	0.17%	1.26	0.08%	0.09%	0.87
ER	1.24%	1.21%	1.02	1.10%	1.44%	0.76
CY	24.78%	31.22%	0.79	29.37%	34.41%	0.85
PL	28.71%	36.77%	0.78	26.46%	32.25%	0.82
EX	1.31%	1.73%	0.75	0.94%	1.80%	0.52
PR	0.58%	0.78%	0.74	0.24%	0.63%	0.37
CS	1.31%	1.91%	0.69	1.18%	2.34%	0.50

The ratio of the total number of proteins in each subcellular compartment to the total number of proteins identified. The average of three biological replicates is mean percentage of exclusive proteins identified for each cellular compartment. PM, plasma membrane; VU, vacuole; MI, mitochondria; NU, nucleus; GO, golgis apparatus; ER, endoplasmic reticulum; CY, cytosol; PL, plastid; EX, extracellular space; PR, peroxisome; CS, cytoskeleton.

transmembrane proteins. A couple of important signal receptor proteins were characterized, including 18 Leucine-rich repeat (LRR) receptor protein kinases, 3 Lectin receptor kinases, 1 Cysteine-rich receptor-like protein kinases, 4 G-protein coupled receptors, Somatic embryogenesis receptor kinase 4 (SERK4) ortholog/BRASSINOSTEROID INSENSITIVE 1-associated receptor kinase 1 (BAK1) ortholog, Chitin elicitor receptor kinase 1 (CERK1) ortholog, Glutamate receptor 3.6 (GLR3.6) ortholog, and 15 other transmembrane signal receptors. Additionally, proteins involved in vesicular trafficking were also detected in the PM proteome, such as vesicle coat proteins (Clathrin heavy chain 1/2 ortholog) and SNARE proteins (Syntaxin-132 ortholog). In summary, the PM proteome has characterized the major type proteins localized on the PM, and many orthologs of functional PM proteins previously identified in other plant species have also been detected.

3.4 Identification and functional analysis of PM protein SgRKL1

3.4.1 Identification and sequence analysis of PM protein SgRKL1

In order to verify the PM localization of proteins identified from PM proteomics and also to investigate the potential involvement of PM proteins in biotic and abiotic stresses, we chose a newly identified receptor-like kinase, SgRKL1, for investigation. SgRKL1 was identified from both leaf and root PM proteomics of stylo, and its homolog in *Arabidopsis* was previously reported to regulate plant immunity and root growth (Tarutani et al., 2004; ten Hove et al., 2011; Zhao et al., 2019; Demirjian et al., 2022; Zhao et al., 2019). The sequence analysis showed that the coding sequence of SgRKL1 was 2010 bp in length, which encoded 669 amino acid residues (Table S5). The conserved domains analysis showed that SgRKL1 protein contained a signal peptide, 4 Leucine-rich repeats, a transmembrane domain and a protein kinase domain, belonging to the receptor-like kinases (RLKs) (Figure 7A). To investigate the conservation of RKL1 protein, phylogenetic analysis was performed using protein sequences of 28 plant species (Table S6). The results showed that RKL1 proteins from 26 species (except *Arabidopsis* and *Cannabis sativa*) contained 10 identical motifs, and *Arabidopsis* and *Cannabis sativa* also shared 9 common motifs with other plant species, indicating that RKL1 proteins were highly conserved across different species. SgRKL1 was clustered in the branch of leguminosa and had the highest homology with RKL1 of *Arachis ipaensis, Arachis hypogaea, Arachis duranensis* (Figure 7B).

3.4.2 Validation of the subcellular localization of SgRKL1

To verify the subcellular localization, we performed the co-localization and immunoblot analysis for SgRKL1. For co-localization analysis, the SgRKL1-GFP fusion protein and PM marker protein PIP2A-mCherry were transiently expressed in *N. benthamiana* leaves, and the fluorescent signals were observed using confocal microscopy. The results showed that the signal of

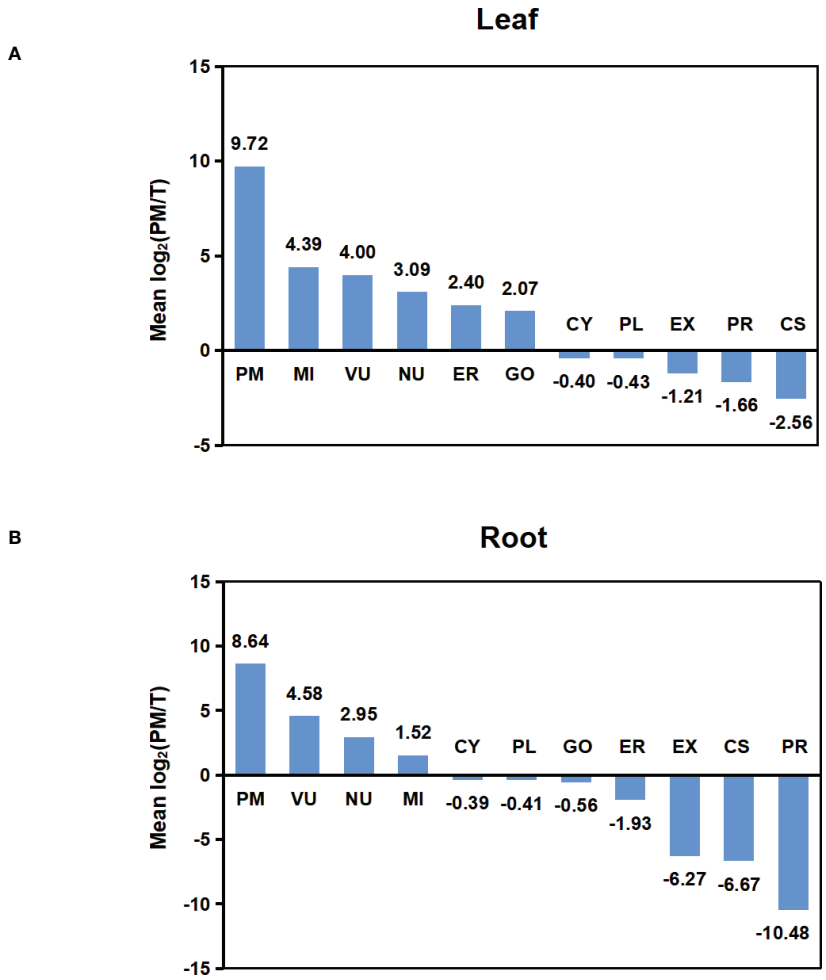

FIGURE 4
Abundance comparison of organelle proteomes between total and PM enriched fraction. **(A)** Abundance comparison of organelle proteomes between two fractions in leaf. **(B)** Abundance comparison of organelle proteomes between two fractions in root. Log2 values were calculated for the ratio of IBAQ value of proteins assigned to specific compartments in PM or total fraction [i.e. log2(PM/T)]. The mean log2(PM/T) was calculated by using the average log2 values of all three biological replicas for each subcellular compartment.

SgRKL1-GFP was localized at PM and overlapped with PIP2A-mCherry, while the free GFP signal was mainly localized at cytoplasm and nuclues (Figure 8A). Meanwhile, the protein extracts of *N. benthamina* transiently expressed with SgRKL1-GFP and GFP were separated into total protein, cytosol and PM fraction using the same enrichment method, and the immunoblot analysis was performed to examine the localization of SgRKL1-GFP and GFP proteins. The results showed that the AHA proteins (PM marker) were significantly enriched in the PM fraction and depleted in the cytosol fraction, and the rubisco proteins (cytosolic marker) were depleted in the PM fraction, suggesting the successful separation of the protein extracts. SgRKL1-GFP proteins were detected in the total and PM fraction (significantly enriched in the PM fraction), while the GFP proteins were in the total and cytosol fraction, which was consistent with the results of co-localization analysis (Figure 8B). Both co-localization and immunoblot analysis have validated the PM localization of SgRKL1. These results also demonstrate that the enrichment method could be applied in the *N. benthamiana* system.

3.4.3 Expression pattern analysis of *SgRKL1*

To investigate the potential functions of *SgRKL1*, we performed the qPCR analysis to detect the expression patterns of *SgRKL1* in different tissue types of stylo (roots, stems, leaves, cotyledons) under normal growth condition and in response to biotic stress (inoculation with *C. gloeosporioides*) and abiotic stress (low phosphorus stress). The results showed that *SgRKL1* gene had highest expression in root and lowest expression in leaf (Figure 9A). The time-course expression pattern analysis of stylo

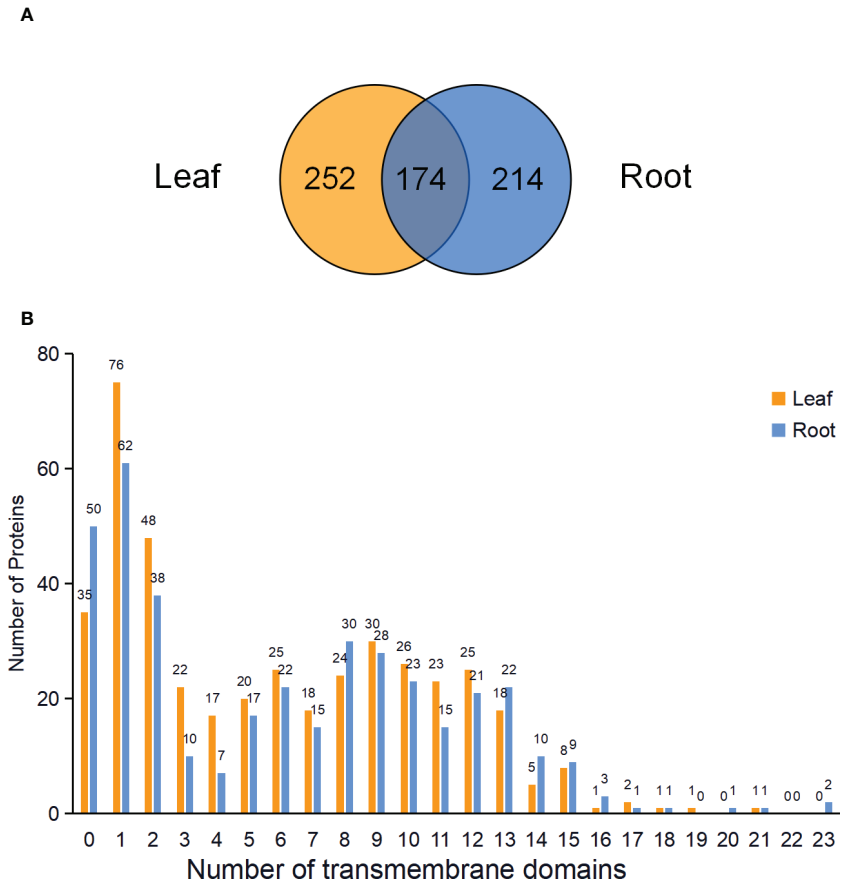

FIGURE 5
Venn diagram and analysis of transmembrane domains of identified PM proteins in leaves and roots. **(A)** Venn diagram showing the common and specific PM proteins in leaves and roots. **(B)** Predicted transmembrane domains of PM proteins in the leaves and roots.

post inoculation of *C. gloeosporioides* showed that the expression levels of *SgRKL1* in leaf were significantly down-regulated from 12 h to 96 h post inoculation (Figure 9B), whereas the expression levels of *SgRKL1* in root were up-regulated by the treatment of 15-day phosphorus starvation (Figure 9C). These results suggest that SgRKL1 may be involved in the responses against *C. gloeosporioides* infection and low phosphorus stress.

4 Discussion

Plasma membrane proteins play important roles in sensing signals and controlling solute transport. However, the identification of PM proteins is typically under-represented in the large-scale proteomics datasets because of the relatively low abundance and hydrophobicity of PM proteins (Yadeta et al., 2013). Plant PM proteins are even more challenging to isolate compared to those from mammalian cells due to the complexities and variation of plant species and tissue types. Improvement of PM protein identification could be achieved by removal of highly abundant soluble proteins (such as the RuBisCo large subunit) and other non-PM membrane proteins (Chen and Weckwerth, 2020). The method of isolating total microsomal membranes by differential centrifugation followed by treatment with nonionic detergent Brij-58 has greatly enriched PM proteins in cell culture and seedlings of *Arabidopsis* and root tissue of maize (Zhang and Peck, 2011; Zhang et al., 2013; Collins et al., 2017). Our results have also shown the successful application of such PM enrichment method in both leaf and root tissue of tropical forage stylo. For the immunoblot analysis of marker proteins in different fractions, the results in both leaf and root tissues of stylo have shown that the AHA proteins (PM marker) were strongly enriched in the PM fraction. The AOX1/2 proteins (mitochondrial marker) were enriched in the CM fraction in both leaf and root tissue of stylo but depleted in the PM fraction in leaf and decreased in the PM fraction in root. These results are consistent with those from the cell culture and seedlings of *Arabidopsis* and roots of maize (Zhang and Peck, 2011; Zhang et al., 2013; Collins et al., 2017). For the MS analysis of organellar

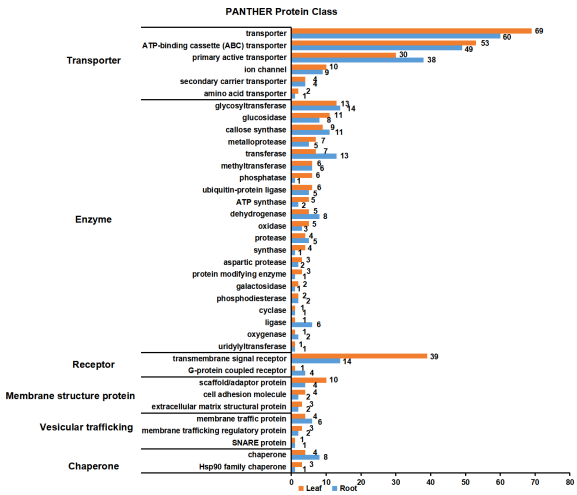

FIGURE 6
Functional classification of PM proteins in leaves and roots. The function of PM proteins are classified according to PANTHER classification system. The PM proteins were divided into six major categories: transporter, enzyme, receptor, membrane structure protein, vesicular trafficking and chaperone. Orange and blue blocks indicate the number of PM proteins in leaves and roots, respectively.

composition in PM fractions, both our results in stylo and previous results in *Arabidopsis* have shown the increased representation of PM proteins in the PM fraction. Additionally, the PM fraction in stylo has also slightly increased the number of proteins from vacuole (VU), mitochondria (MI), golgis apparatus (GO) in leaf and VU in root, respectively. The number of proteins in cytosol (CY), plastid (PL), extracellular space (EX), peroxisome (PR), cytoskeleton (CS) has been decreased in PM fraction. In *Arabidopsis*, the PM fraction has enriched for proteins in CY and EX while decreased the number of proteins from VU, PL, MI and PR (Zhang and Peck, 2011). The difference in the organellar composition may be caused by different fraction comparison (PM versus total fraction in stylo whereas PM versus CM fraction in *Arabidopsis*) or different buoyancy of proteins in different plant species. The leaf tissue of stylo is rich in polysaccharides and polyphenols, which makes the protein extraction and enrichment process more complicated. The successful application in leaf and root tissues of stylo has further broaden the possible application of such enrichment method in tissues rich in polysaccharides and polyphenols, such as many tropical crops. In addition, we have also shown the method could successfully enrich the PM fraction in the leaf tissue of *N. benthamiana*. Therefore, it is suggested that this technology may be broadly applicable to PM protein studies in diverse plant species and tissue types.

Although the effect of this method for enriching PM proteins is conclusive, the mechanism by which the Brij-58 performs such role is not clear. The Brij-58 is also called polyethylene glycol hexadecyl ether with the chemical formula of $HO(CH_2CH_2O)_{20}C_{16}H_{33}$. The Brij-58 may invert the PM vesicle inside-out and release other contaminants such as membrane organelles and/or cytosolic proteins (Zhang and Peck, 2011). It is also possible that Brij-58 selectively solubilizes other non-PM membrane proteins (Kaakinen et al., 2008). In addition, the enrichment method can not unequivocally assign the location of a protein to PM or isolate highly purified PM samples as two-phase partitioning method. However, it serves as a rapid, cheap and simple method to increase the representation of PM proteins in proteomic studies. Especially, the method is easier to handle when many samples need to be processed at the same time. Moreover, the enrichment for PM proteins will be sufficient to obtain meaningful information for many proteomic comparison. For instance, quantitative proteomic analysis of the PM-enriched protein fractions have identified the proteins with differential abundance in different growth zone of maize primary root and under water stress condition (Voothuluru et al., 2016).

In previous stylo proteomic studies, only 23 and 37 PM proteins have been detected in the leaf and root proteome, respectively (Liu et al., 2019). Our studies have identified 426 and 388 PM proteins in the enrichment fraction of leaf and root tissue, greatly increasing the identification of PM protein. In addition to PM protein purple acid phosphatases, many proteins that may play important biological functions in biotic and abiotic stress have been characterized. For instance, ABC transporters, nitrate transporter (NRT1/2 ortholog), inorganic phosphate transporter (PHT1 ortholog), potassium transporter (POT4/5/7/11/12 ortholog), sulfate transporter (SULTR4.2 ortholog), metal-nicotianamine transporter (YSL6/7 ortholog), sucrose transporter (SUC2 and STP1 ortholog), auxin transporter (PIN3 ortholog) and many primary active transporters have been characterized. As been demonstrated to

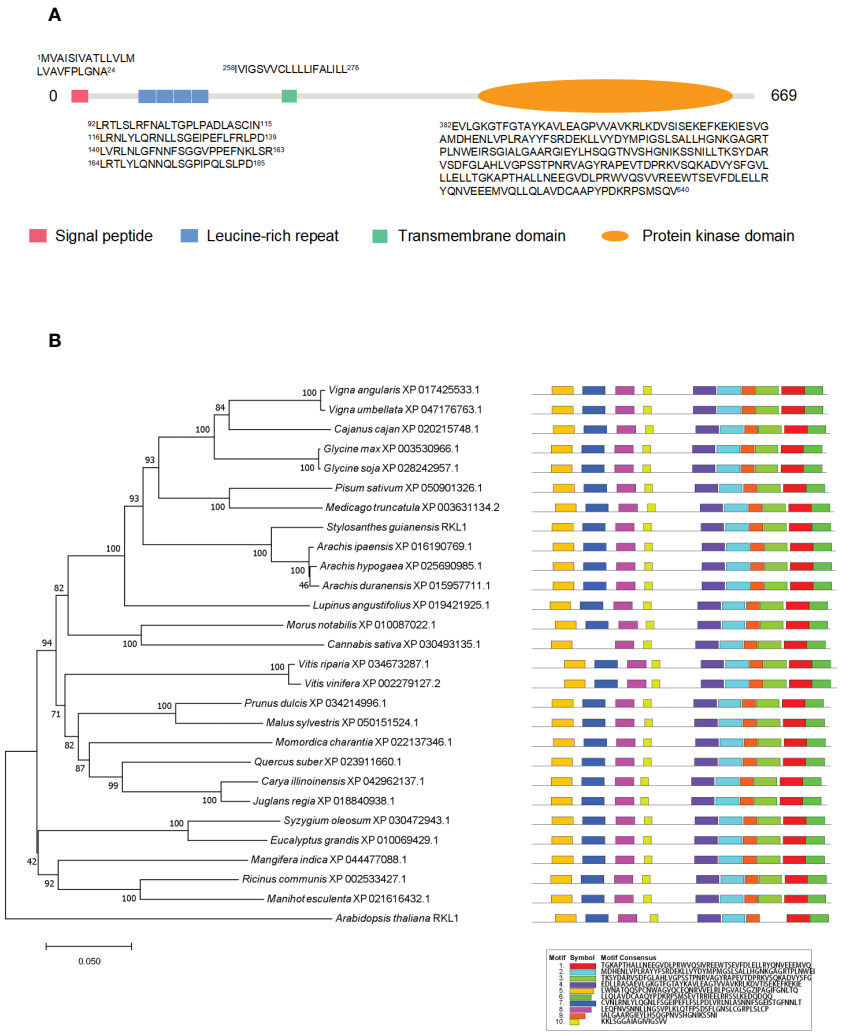

FIGURE 7
The domain, phylogenetic and motif analysis of SgRKL1. **(A)** The domain analysis of SgRKL1. The red box represents the signal peptide, blue box represents Leucine-rich repeat, green box represents the transmembrane domain, and the orange oval represents the protein kinase domain. The sequences of amino acid of each domain were listed correspondingly. **(B)** Phylogenetic tree and motif analysis of RKL1 protein sequences from 28 plant species. The legend represents the sequence of amino acids in the corresponding motifs.

drive the efflux or influx of a variety of substances including auxin, ABA, heavy metals and antimicrobial compounds in other plant species (Lane et al., 2016; Ye et al., 2021), these proteins may contribute to the adaptation of stylo to acidic and infertile soils. Therefore, it would be interesting to perform extensive proteomic analysis using the PM enrichment method to investigate resistance mechanisms of stylo against P deficiency as well as Al and Mn toxicity. In addition to transporters, many important receptor proteins that are essential in pathogen perception and resistance have also been characterized, such as LRR receptor protein kinases, Lectin receptor kinases, Cysteine-rich receptor-like protein kinases, G-protein coupled receptors, SERK4/BAK1 ortholog, CERK1 ortholog and GLR3.6 ortholog (Tang et al., 2017). These results also suggest the possible application of the PM enrichment method to study the stylo-pathogen interaction.

A newly identified receptor-like kinase, SgRKL1, has been characterized in both leaf and root PM proteome of stylo. To investigate the possible functions of SgRKL1, we have performed the sequence analysis, subcellular localization analysis and expression pattern analysis. The results have shown that SgRKL1 localizes on PM and may involve in regulating the responses against *C. gloeosporioides* and low phosphorus stress. Studies in *Arabidopsis* have also shown the role of *Arabidopsis RKL1 (AtRKL1)* in regulating plant immunity and root growth. For instance, the expression levels of *AtRKL1* in leaf are suppressed by the infection of *Pseudomonas syringae* pv. *Maculocola* (Tarutani et al., 2004). A genome-wide association

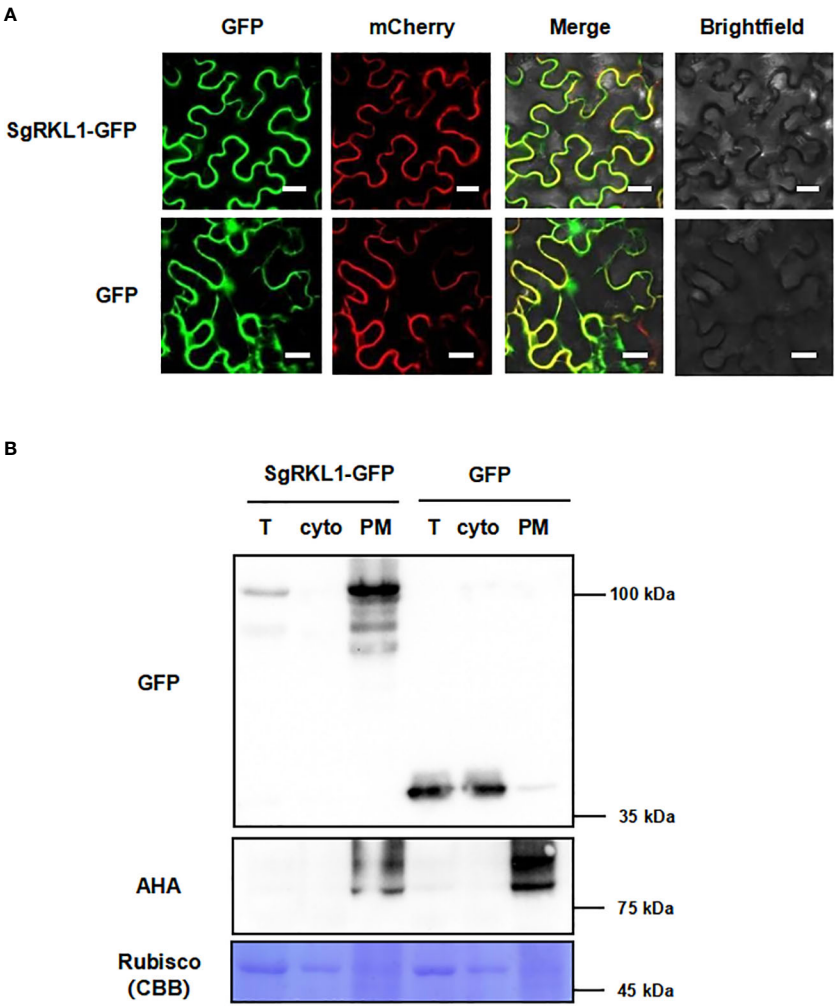

FIGURE 8
Subcellular localization of the identified PM protein SgRKL1. **(A)** Co-localization of SgRKL1-GFP and PM marker protein PIP2A-mCherry. Images were taken using confocal microscopy 2 days after infiltration in *N. benthamiana*. Bars, 20 μM. **(B)** Immunoblot analysis of SgRKL1-GFP transiently expressed in *N. benthamiana*. Total protein (T), cytosolic fraction (cyto), plasma membrane enriched fraction (PM) were collected 2 days after infiltration. Immunoblot analysis was performed using anti-GFP and anti-AHA antibodies to detect the distribution of SgRKL1-GFP/free GFP and PM marker protein AHA, respectively. Coomassie blue staining CBB was performed to show the distribution of Rubisco protein. The experiments were repeated three times with similar results as shown.

analysis of two *Arabidopsis* mapping population has also identified AtRKL1 as the susceptibility factors targeted by *Ralstonia solanacearum*, and knocking out *AtRKL1* increases the resistance against *R. solanacearum* (Demirjian et al., 2022). Consistent with results in *Arabidopsis*, our results have also shown that the expression levels of *SgRKL1* decrease in response to the inoculation of *C. gloeosporioides*. All these results, together with high conservation of RKL1 proteins across different plant species, indicate that RKL1 proteins may be an important targets of pathogens and negatively regulate the plant immunity. In addition to the role in disease resistance, RKL1 may also be an important regulator in roots. In *Arabidopsis*, *AtRKL1* is expressed in vascular tissues throughout the root system, and *Atrkl1* mutants show reduced root length (ten Hove et al., 2011). Our studies also show that *SgRKL1* is highly expressed in root of stylo under normal growth conditions, suggesting the role of *SgRKL1* in regulating the root growth of stylo. The adjustment of root morphology is a common strategy in many plants to adapt to low phosphorus stress (Liu, 2021). Our studies show that the expression levels of *SgRKL1* in roots are significantly up-regulated by low phosphorus treatment, suggesting that *SgRKL1* may be involved in regulating the root adaptation to low phosphorus stress, but the mechanisms need further investigation.

10.3389/fpls.2022.1071225

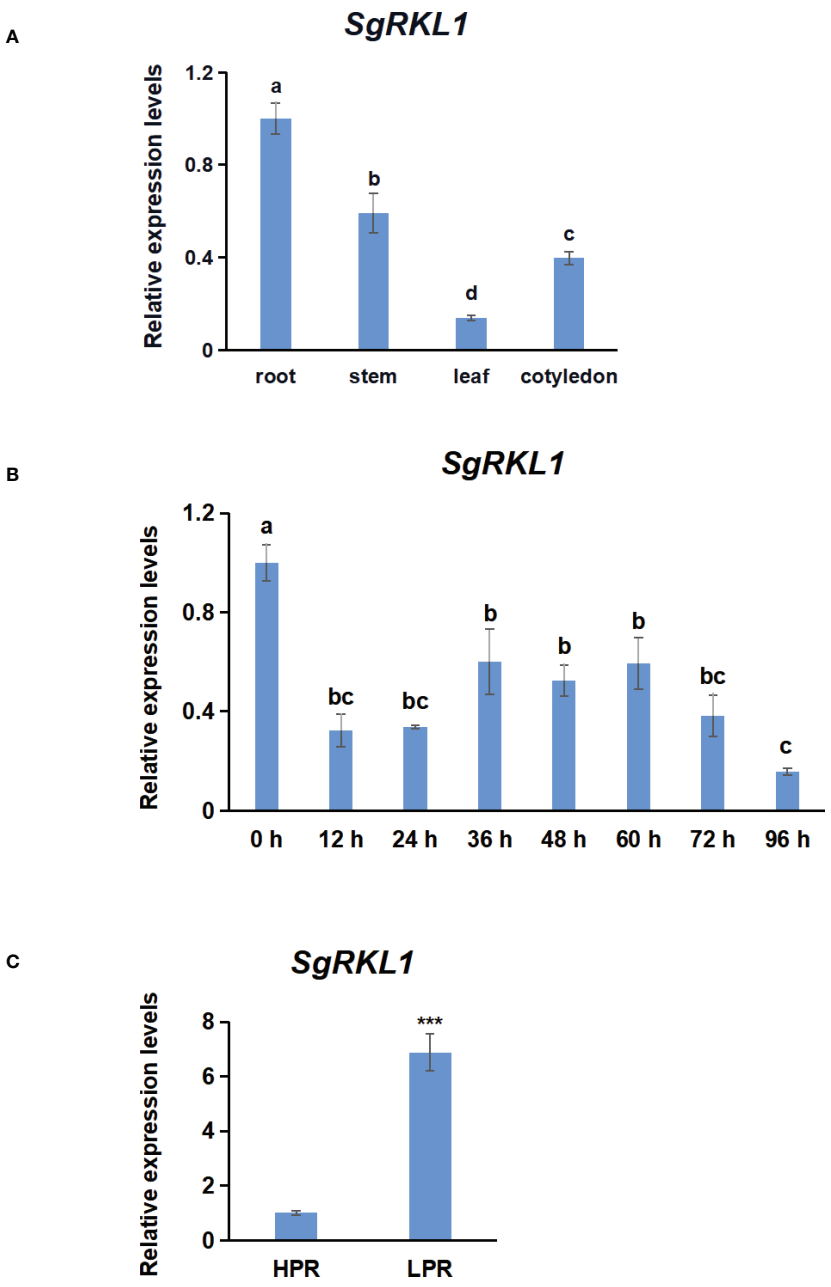

FIGURE 9
Analysis of expression pattern of *SgRKL1* by qPCR. **(A)** Expression pattern analysis of *SgRKL1* gene in different tissues of stylo under normal growth condition. **(B)** Expression pattern analysis of *SgRKL1* gene in leaves of stylo post inoculation with *C gloeosporioides*. Leaves samples were collected at 0 h,12 h,24 h, 36 h, 48 h, 60 h, 72 h and 96 h post inoculation of *C gloeosporioides*. **(C)** Expression pattern analysis of *SgRKL1* gene in roots of stylo under low phosphorus treatment. HPR represents the treatments with a phosphorus concentration of 300 μmol/L, and LPR represents the treatments with a phosphorus concentration of 0 μmol/L. Data are means ± SE pooled from three biological replicates, n = 3. Different letters in **(A)** and **(B)** indicate significant differences using Dancan's test ($P < 0.05$). Asterisks in **(C)** indicate significant differences using the Student's t-test (***$P < 0.001$).

Data availability statement

The datasets presented in this study can be found in online repositories. The name of the repository and accession number can be found below: ProteomXchange; PXD037423.

Author contributions

LY: Performed the experiments, analyzed the data, wrote the manuscript. JG: Performed the experiments, analyzed the data. MG: Performed the experiments. LJ: Conceived and designed the experiment, analyzed the data, wrote and revised the manuscript. LL: Revised the manuscript. All authors contributed to the article and approved the submitted version.

Funding

This work was supported by grants from the National Natural Science Foundation of China (31960342 to L.J., 31872409 to L.L.), Hainan Provincial Natural Science Foundation of China (320RC466 to L.J.), Young Elite Scientists Sponsorship Program by CAST (Project No. 2020QNRC001 to L.J.) and Young Talents' Science and Technology Innovation Project of Hainan Association for Science and Technology (QCXM202001 to L.J.), the Key Research and Development Projects of Hainan Province (ZDYF2020211 to L.L.).

Conflict of interest

The authors declare that the research was conducted in the absence of any commercial or financial relationships that could be construed as a potential conflict of interest.

Publisher's note

All claims expressed in this article are solely those of the authors and do not necessarily represent those of their affiliated organizations, or those of the publisher, the editors and the reviewers. Any product that may be evaluated in this article, or claim that may be made by its manufacturer, is not guaranteed or endorsed by the publisher.

Supplementary material

The Supplementary Material for this article can be found online at: https://www.frontiersin.org/articles/10.3389/fpls.2022.1071225/full#supplementary-material

References

Chen, Z., Sun, L., Liu, P., Liu, G., Tian, J., and Liao, H. (2015). Malate synthesis and secretion mediated by a manganese-enhanced malate dehydrogenase confers superior manganese tolerance in *Stylosanthes guianensis*. *Plant Physiol.* 167, 176–188. doi: 10.1104/pp.114.251017

Chen, Y., and Weckwerth, W. (2020). Mass spectrometry untangles plant membrane protein signaling networks. *Trends Plant Sci.* 25, 930–944. doi: 10.1016/j.tplants.2020.03.013

Collins, C. A., Leslie, M. E., Peck, S. C., and Heese, A. (2017). Simplified enrichment of plasma membrane proteins from *Arabidopsis thaliana* seedlings using differential centrifugation and brij-58 treatment. *Methods Mol. Biol.* 1564, 155–168. doi: 10.1007/978-1-4939-6813-8_13

Demirjian, C., Razavi, N., Desaint, H., Lonjon, F., Genin, S., Roux, F., et al. (2022). Study of natural diversity in response to a key pathogenicity regulator of *Ralstonia solanacearum* reveals new susceptibility genes in *Arabidopsis thaliana*. *Mol. Plant Pathol.* 23 (3), 321–338. doi: 10.1111/mpp.13135

Evans, J. R., and Clarke, V. C. (2019). The nitrogen cost of photosynthesis. *J. Exp. Bot.* 70 (1), 7–15. doi: 10.1093/jxb/ery366

Famoso, A. N., Clark, R. T., Shaff, J. E., Craft, E., McCouch, S. R., and Kochian, L. V. (2010). Development of a novel aluminum tolerance phenotyping platform used for comparisons of cereal aluminum tolerance and investigations into rice aluminum tolerance mechanisms. *Plant Physiol.* 153 (4), 1678–1691. doi: 10.1104/pp.110.156794

Horton, P., Park, K. J., Obayashi, T., Fujita, N., Harada, H., Adams-Collier, C. J., et al. (2007). WoLF PSORT: protein localization predictor. *Nucleic Acids Res.* 35, W585–W587. doi: 10.1093/nar/gkm259

Jiang, C., Liu, L., Li, X., Han, R., Wei, Y., and Yu, Y. (2018). Insights into aluminum-tolerance pathways in *Stylosanthes* as revealed by RNA-seq analysis. *Sci. Rep.* 8, 6072. doi: 10.1038/s41598-018-24536-3

Jiang, L., Wu, P., Yang, L., Liu, C., Guo, P., Wang, H., et al. (2021). Transcriptomics and metabolomics reveal the induction of flavonoid biosynthesis pathway in the interaction of *Stylosanthes-Colletotrichum gloeosporioides*. *Genomics* 113 (4), 2702–2716. doi: 10.1016/j.ygeno.2021.06.004

Kaakinen, M., Papponen, H., and Metsikkö, K. (2008). Microdomains of endoplasmic reticulum within the sarcoplasmic reticulum of skeletal myofibers. *Exp. Cell Res.* 314, 237–245. doi: 10.1016/j.yexcr.2007.10.009

Käll, L., Canterbury, J. D., Weston, J., Noble, W. S., and MacCoss, M. J. (2007). Semi- supervised learning for peptide identification from shotgun proteomics datasets. *Nat. Methods* 4, 923–925. doi: 10.1038/nmeth1113

Lane, T. S., Rempe, C. S., Davitt, J., Staton, M. E., Peng, Y., Soltis, D. E., et al. (2016). Diversity of ABC transporter genes across the plant kingdom and their potential utility in biotechnology. *BMC Biotechnol.* 16, 47. doi: 10.1186/s12896-016-0277-6

Liu, D. (2021). Root developmental responses to phosphorus nutrition. *J. Integr. Plant Biol.* 63 (6), 1065–1090. doi: 10.1111/jipb.13090

Liu, P., Cai, Z., Chen, Z., Mo, X., Ding, X., Liang, C., et al. (2018). A root-associated purple acid phosphatase, SgPAP23, mediates extracellular phytate-p utilization in *Stylosanthes guianensis*. *Plant Cell Environ.* 41, 2821–2834. doi: 10.1111/pce.13412

Liu, P., Huang, R., Hu, X., Jia, Y., Li, J., Luo, J., et al. (2019). Physiological responses and proteomic changes reveal insights into *Stylosanthes* response to manganese toxicity. *BMC Plant Biol.* 19, 212. doi: 10.1186/s12870-019-1822-y

Liu, P., Xue, Y., Chen, Z., Liu, G., and Tian, J. (2016). Characterization of purple acid phosphatases involved in extracellular dNTP utilization in *Stylosanthes*. *J. Exp. Bot.* 67, 4141–4154. doi: 10.1093/jxb/erw190

Luo, J., Liu, Y., Zhang, H., Wang, J., Chen, Z., Luo, L., et al. (2020). Metabolic alterations provide insights into *Stylosanthes* roots responding to phosphorus deficiency. *BMC Plant Biol.* 20, 85. doi: 10.1186/s12870-020-2283-z

Michele, R. D., McFarlane, H. E., Parsons, H. T., Meents, M. J., and Heazlewood, J. L. (2016). Free-flow electrophoresis of plasma membrane vesicles enriched by

two-phase partitioning enhances the quality of the proteome from *Arabidopsis* seedlings. *J. Proteome Res.* 15, 900–913. doi: 10.1021/acs.jproteome.5b00876

Mi, H., Muruganujan, A., Huang, X., Ebert, D., Mills, C., Guo, X., et al. (2019). Protocol update for large-scale genome and gene function analysis with the PANTHER classification system (v.14.0). *Nat. Protoc.* 14, 703–721. doi: 10.1038/s41596-019-0128-8

Perkins, D. N., Pappin, D. J., Creasy, D. M., and Cottrell, J. S. (1999). Probability-based protein identification by searching sequence databases using mass spectrometry data. *Electrophoresis* 20, 3551–3567. doi: 10.1002/(SICI)1522-2683(19991201)20:183.0.CO;2-2

Schmittgen, T. D., and Livak, K. J. (2008). Analyzing real-time PCR data by the comparative C(T) method. *Nat. Protoc.* 3 (6), 1101–1108. doi: 10.1038/nprot.2008.73

Schultze-Kraft, R., Rao, I. M., Peters, M., Clements, R. J., Bai, C., and Liu, G. D. (2018). Tropical forage legumes for environmental benefits: an overview. *Trop. Grassl. Forrajes Trop.* 6, 1. doi: 10.17138/tgft(6)1-14

Schwanhäusser, B., Busse, D., Li, N., Dittmar, G., Schuchhardt, J., Wolf, J., et al. (2011). Global quantification of mammalian gene expression control. *Nature* 473, 337–342. doi: 10.1038/nature10098

Slajcherová, K., Fišerová, J., Fischer, L., and Schwarzerová, K. (2012). Multiple actin isotypes in plants: diverse genes for diverse roles? *Front. Plant Sci.* 3. doi: 10.3389/fpls.2012.00226

Sun, L., Liang, C., Chen, Z., Liu, P., Tian, J., Liu, G., et al. (2013). Superior aluminium (Al) tolerance of *Stylosanthes* is achieved mainly by malate synthesis through an Al-enhanced malic enzyme, SgME1. *New Phytol.* 202, 209–219. doi: 10.1111/nph.12629

Tang, D., Wang, G., and Zhou, J. M. (2017). Receptor kinases in plant-pathogen interactions: More than pattern recognition. *Plant Cell.* 29, 618–637. doi: 10.1105/tpc.16.00891

Tarutani, Y., Sasaki, A., Yasuda, M., Nakashita, H., Yoshida, S., Yamaguchi, I., et al. (2004). Identification of three clones which commonly interact with the kinase domains of highly homologous two receptor-like kinases, RLK902 and RKL1. *Biosci. Biotechnol. Biochem.* 68 (12), 2581–2587. doi: 10.1271/bbb.68.2581

ten Hove, C. A., Bochdanovits, Z., Jansweijer, V. M., Koning, F. G., Berke, L., Sanchez-Perez, G. F., et al. (2011). Probing the roles of LRR RLK genes in *Arabidopsis thaliana* roots using a custom T-DNA insertion set. *Plant Mol. Biol.* 76 (1-2), 69–83. doi: 10.1007/s11103-011-9769-x

Voothuluru, P., Anderson, J. C., Sharp, R. E., and Peck, S. C. (2016). Plasma membrane proteomics in the maize primary root growth zone: novel insights into root growth adaptation to water stress. *Plant Cell Environ.* 39, 2043–2054. doi: 10.1111/pce.12778

Yadeta, K. A., Elmore, J. M., and Coaker, G. (2013). Advancements in the analysis of the *Arabidopsis* plasma membrane proteome. *Front. Plant Sci.* 4. doi: 10.3389/fpls.2013.00086

Ye, J. Y., Tian, W. H., Zhou, M., Zhu, Q. Y., Du, W. X., Zhu, Y. X., et al. (2021). STOP1 activates NRT1.1-mediated nitrate uptake to create a favorable rhizospheric pH for plant adaptation to acidity. *Plant Cell.* 33, 3658–3674. doi: 10.1093/plcell/koab226

Zhang, Z. J., and Peck, S. C. (2011). Simplified enrichment of plasma membrane proteins for proteomic analyses in *Arabidopsis thaliana*. *Proteomics* 11, 1780–1788. doi: 10.1002/pmic.201000648

Zhang, Z., Voothuluru, P., Yamaguchi, M., Sharp, R. E., and Peck, S. C. (2013). Developmental distribution of the plasma membrane-enriched proteome in the maize primary root growth zone. *Front. Plant Sci.* 4. doi: 10.3389/fpls.2013.00033

Zhao, Y., Wu, G., Shi, H., and Tang, D. (2019). RECEPTOR-LIKE KINASE 902 associates with and phosphorylates BRASSINOSTEROID-SIGNALING KINASE1 to regulate plant immunity. *Mol. Plant* 12 (1), 59–70. doi: 10.1016/j.molp.2018.10.008

frontiers | Frontiers in Plant Science

TYPE Original Research
PUBLISHED 20 February 2023
DOI 10.3389/fpls.2023.1104070

OPEN ACCESS

EDITED BY
Jin-Lin Zhang,
Lanzhou University, China

REVIEWED BY
Haijun Gong,
Northwest A&F University, China
Mohamed Magdy F. Mansour,
Ain Sham University, Egypt

*CORRESPONDENCE
Jinbiao Ma
majinbiao@ms.xjb.ac.cn
Xiaorong Fan
xiaorongfan@njau.edu.cn

SPECIALTY SECTION
This article was submitted to Plant Abiotic Stress, a section of the journal Frontiers in Plant Science

RECEIVED 21 November 2022
ACCEPTED 06 February 2023
PUBLISHED 20 February 2023

CITATION
Haxim Y, Wang L, Pan Z, Fan X and Ma J (2023) A novel high-affinity potassium transporter SeHKT1;2 from halophyte *Salicornia europaea* shows strong selectivity for Na^+ rather than K^+. *Front. Plant Sci.* 14:1104070. doi: 10.3389/fpls.2023.1104070

A novel high-affinity potassium transporter SeHKT1;2 from halophyte *Salicornia europaea* shows strong selectivity for Na^+ rather than K^+

Yakupjan Haxim[1,2,3], Lei Wang[1], Zhendong Pan[1,3], Xiaorong Fan[4]* and Jinbiao Ma[1,2,3]*

[1]State Key Laboratory of Desert and Oasis Ecology, Key Laboratory of Ecological Safety and Sustainable Development in Arid Lands, Xinjiang Institute of Ecology and Geography, Chinese Academy of Sciences, Ürümqi, China, [2]Xinjiang Key Laboratory of Conservation and Utilization of Plant Gene Resources, Xinjiang Institute of Ecology and Geography, Chinese Academy of Sciences, Ürümqi, China, [3]Turpan Eremophytes Botanical Garden, Chinese Academy of Sciences, Turpan, China, [4]State Key Laboratory of Crop Genetics and Germplasm Enhancement, MOA Key Laboratory of Plant Nutrition and Fertilization in Low-Middle Reaches of the Yangtze River, Nanjing Agricultural University, Nanjing, China

High-affinity K^+ transporters (HKTs) are known as transmembrane cation transporters and are involved in Na^+ or Na^+-K^+ transport in plants. In this study, a novel HKT gene *SeHKT1;2* was isolated and characterized from the halophyte, *Salicornia europaea*. It belongs to subfamily I of HKT and shows high homology with other halophyte HKT proteins. Functional characterization of *SeHKT1;2* indicated that it contributes to facilitating Na^+ uptake in Na^+-sensitive yeast strains G19, however, cannot rescue the K^+ uptake-defective phenotype of yeast strain CY162, demonstrating SeHKT1;2 selectively transports Na^+ rather than K^+. The addition of K^+ along with NaCl relieved the Na^+ sensitivity. Furthermore, heterologous expression of *SeHKT1;2* in *sos1* mutant of *Arabidopsis thaliana* increased salt sensitivity and could not rescued the transgenic plants. This study will provide valuable gene resources for improving the salt tolerance in other crops by genetic engineering.

KEYWORDS

***Salicornia europaea*, salt tolerance, high-affinity K^+ transporters, HKT, ion selectivity**

Introduction

Globally, soil salinity remains a significant abiotic stress for plants and constraints agriculture development. In order to solve the current problems of salt stress, we must understand how salt stress tolerance works and develop salt-tolerant crops. In addition to osmotic stress, high salinity can cause plant death and growth inhibition. A primary consequence of ionic stress is sodium disequilibrium in many plants, especially gramineous

crops, which can adversely affect plant nutrition, enzyme activity, photosynthesis, and metabolism (Tester and Davenport, 2003; Mahajan and Tuteja, 2005). Na^+ is attracted to the plasma membrane in saline environments due to high external Na^+. A number of mechanisms are involved in plants acquiring salt tolerance, including the outright exclusion of Na^+ and vacuolar compartmentalization. Na^+ is extruded out of salt-stressed cells by plasma membrane Na^+/H^+ antiporters, also called SOS1 or NHA-type transporters. NHX-type antiporters, also known as Na^+/H^+ antiporters, sequestrate Na^+ from the cytosol into vacuoles when salt stress is applied to the cell (Hasegawa et al., 2003; Zhu, 2003; Mahajan et al., 2008). In addition to controlling Na^+ influx, salt tolerance can also be improved by reducing the amount of sodium absorbed. A number of studies have indicated that toxic Na^+ influx into roots is mediated by nonselective cation channels (NSC) or voltage-independent channels (VIC) under high external Na^+ concentrations (Amtmann and Sanders, 1998; Schachtman and Liu, 1999; Blumwald et al., 2000). In spite of this, NSC/VIC remains mysterious in terms of their detailed molecular identities. As a result, plant cells may be able to uptake Na^+ through high-affinity K^+ transporters (HKT-type transporters).

Based on amino acid in the first pore domain, the HKT transporters can be classified into two subclasses. Class I HKT transporters possess a serine (S) whereas members of class II have a glycine (G) residue at first pore forming region (Mäser et al., 2002b; Almeida et al., 2013). A single amino acid at this position determines the ion selectivity of the transporter. The class I HKT transporters showed preference for Na^+ conductance over that of other cations whereas the class II HKT transporters select either Na^+ and/or K^+ (Mäser et al., 2002b; Almeida et al., 2014). A variety of plant species have been shown to have HKT-type transporters (Schachtman and Schroeder, 1994; Nieves-Cordones et al., 2016), and their functions have been studied in different ways. A heterologous expression system of *TaHKT2;1* in wheat, for example, showed dual modes of action. In other words, when the Na^+-K^+ exchange rate was low, it acted as a Na^+- K^+ symporter, while when the exchange rate was high, it acted as a Na^+-uniporter (Rubio et al., 1995; Gassmann et al., 1996). Transgenic wheat plants increased in growth under salinity when *TaHKT2;1* was knocked down genetically (Laurie et al., 2002), indicating that TaHKT2;1 can be a Na^+-uptake pathway in wheat roots. Several heterologous expression systems have also characterized Arabidopsis *AtHKT1;1* and Rice *OsHKT2;1* as Na^+-uniporters (Uozumi et al., 2000; Horie et al., 2001; Garciadeblás et al., 2003). The genetic mutations of *AtHKT1;1* in Arabidopsis roots showed that it does not mediate Na^+ influx (Mäser et al., 2002a; Berthomieu et al., 2003; Horie et al., 2006); however, OsHKT2;1 mediates Na^+ uptake in roots with low K^+ levels (Horie et al., 2007). The salt-tolerance mechanisms of monocotyledonous halophytes can be used as a tool to improve salt tolerance crops.

It has been increasingly clear how halophytes have adapted to high salinity conditions over the past few decades. The morphological and biochemical adaptations of halophytes allow them to cope with high soil salinity (Flowers et al., 2010). *Salicornia europaea* is a salt marsh halophyte belonging to the *Amaranthaceae* family that is one of the most salt-tolerant plants on the planet (Patel, 2016). *S. europaea* imparted a higher salt tolerance. In *S. europaea*, salt tolerance may be attributed to its ability to restrict Na^+ influx unidirectionally to roots, leading to a large concentration gradient between roots and shoots (Bressan et al., 2013). As the uptake of K^+ is maintained in *S. europaea* roots, it has been proposed that the endodermal barrier to Na^+ restricts Na^+ uptake. The molecular identity of the channel or transporter associated with the restriction of unidirectional Na^+ influx has not been disclosed (Xu et al., 2016).

In this study, we cloned a novel gene encoding a potassium transporter of the HKT type from *S. europaea* (SeHKT1;2). The gene expression pattern of *SeHKT1;2* under K^+-starvation and salt stress was analyzed and its function was characterized in yeast and Arabidopsis.

Materials and methods

Plant materials, growth conditions, and stress treatments

Seeds of *S. europaea* were collected from an alkaline soil area of Xinjiang, China. Plants were germinated in tap water for 14 days and then transferred to half-strength Hoagland's nutrient solution and allowed to grow for another 14 days before stress treatments. The temperatures of the growth chamber were maintained at 28°C during the day (16 h) and 22°C at night (8 h) under a photoperiod (350-400 μmol m^{-2} s^{-1}). For the salt-stress treatment, NaCl was added to half-strength Hoagland's nutrient solution with 0 mM, 10 mM, 200 mM, 500 mM, and 800 mM separately. For the K^+-starvation treatment, KCl was removed from the standard solution. Under 200 mM NaCl treatment, plants tissue samples were harvested at 0, 6, 24, 48, 72, and 120 h after stress treatments and preserved at −80°C for further analyses.

Cloning of SeHKT1;2 from *S. europaea*

Total RNA was extracted from the shoots of *S. europaea* using RNeasy plant extraction Mini Kit (Qiagen, Germany) according to the manufacturer's instructions. Total RNA was reverse transcribed by using an oligo dT primer and MMLV-reverse transcriptase (TaKaRa, China). Full-length cDNA was obtained using 5'- and 3'-RACE (Rapid Amplification of cDNA Ends) techniques. The partial cDNA fragment was amplified by PCR, using a degenerate primer (Table S1) deduced from the conserved regions of HKT and a reverse transcription product as a template. The full-length cDNA of *SeHKT1;2* was amplified using primers (Table S1). The PCR product was sub-cloned into the pMD-19 T vector and sequenced.

Bioinformatic analysis of *SeHKT1;2* sequence

Transmembrane domains were predicted by DeepTMHMM (https://biolib.com/damgaard/DeepTMHMM-testing). A

maximum-likelihood phylogenetic tree of plant HKT proteins was constructed using the MEGA program (version 7.0, Auckland, NewZealand). The accession numbers of genes utilized in the present study are listed in Table S2. The protein secondary structure was predicted using NetSurfP - 3.0 online program (Høie et al., 2022). The 3D model of SeHKT1;2 protein was build using SWISS-MODEL online program (Waterhouse et al., 2018).

RNA extraction and cDNA synthesis for real-time RT-PCR

For real-time RT-PCR, total RNA was extracted from the shoots and roots of *S. europaea* subjected to 0 mM Na^+, 10 mM Na^+, 200 mM Na^+, 500 mM Na^+, and 800 mM Na^+, K^+-starvation, time-course using the RNeasy plant extraction Mini Kit (Qiagen, Germany) according to the manufacturer's instructions. Two micrograms of DNase-treated RNA were transcribed to cDNA using the Reversal Transcription Reagent Kit (TaKaRa) following the manufacturer's instructions. The cDNA was diluted 10 times and 1μl of the diluted cDNA was used as the template in each well for quantitative real-time PCR analysis. The cDNA was amplified using Power SYBR Green PCR Master Mix (Applied Biosystems, USA) on CFX96 Real-Time PCR Detection System (Bio-Rad, USA). A *α-tubulin* gene from *S. europaea* has been used as internal reference (Lv et al., 2012; Ma et al., 2013; Xiao et al., 2015) and served as an internal standard to normalize the expression data for the *SeHKT1;2* gene. The qRT-PCR was performed using sequence specific primers (Table S2). The thermal profile for qRT-PCR was as follows: 2 min at 95°C, 40 cycles of 15 s at 95°C and 30 s at 60°C, and a melting curve protocol (plates read when increased 0.5°C every 5 s from 65°C to 95°C). The melting curve verified the amplification specific and confirmed that there were no primer dimers. All of the samples were run with replicates. The threshold cycle (Ct) values were measured according to the setting of an auto-calculated baseline threshold in Bio-Rad CFX Manager software (Bio-Rad, USA).

Functional characterization of *SeHKT1;2* in yeast

The ORF of *SeHKT1;2* was inserted into the yeast protein expression vector pYES2. To test the Na^+ Absorption and efflux function of *SeHKT1;2*, the *Saccharomyces cerevisiae* yeast mutant strain AXT3K (*enal::Hls3::ena4,nhal::LEuZ,nhxl::KanMx4*), which lacks the main plasma membrance Na^+ transporters, and G19 (*MATa ade2ura3leu2his3trp1 ena1Δ::HIS3Δ::ena4Δ*) disrupted in the *ENA1-4* genes encoding Na^+ export pumps were used. The plasmids were introduced by PEG/LiAc method. Positive transformants were selected on Ura-selective medium [0.67% (w/v) yeast nitrogen base without amino acids, 0.077% (w/v) DO supplement-Ura, 2% (w/v) galactose, and 1.5% (w/v) agar]. Growth at variable Na^+ concentrations with 0, 25, 30, 60, 100 or 150 mM for AXT3K and 0, 60, 100, 150, 300 mM for G19 were tested in arginine phosphate (AP) medium [8 mM phosphoric acid, 10 mM L-Arginine, 2 mM $MgSO_4$, 0.2 mM $CaCl_2$, 2% glucose, plus vitamins and trace elements, and 1.5% (w/v) agar, pH 6.5].

Meanwhile, Yeast (Saccharomyces cerevisiae) strain CY162 (*MATa, △trk1, trk2:: pCK64, his3, leu2, ura3, trp1, ade2*), which is a K^+-uptake-defective mutant and cannot grow without supplement K^+ was used to test K^+-uptake function of *SeHKT1;2* gene. Positive transformants were selected on Ura-selective medium with 100 mM KCl. Yeast growth experiments were performed on arginine-phosphate (AP) medium with added K^+ (1 mM, 10 mM) and supplemented with 100 mM, 150 mM and 300 mM Na^+ concentrations. Control experiments were performed with the yeast modified with vector pYES2 and pYES2-*SeHKT1;2* growing under 100 mM KCl.

For the yeast growth test experiment, all transformed yeasts were cultured overnight at 30°C in AP medium until the OD_{600} reached 0.8, and 10-fold serial diluted cultures were incubated on AP plates containing the indicated concentrations of K^+ and Na^+. The plates were incubated at 30°C for 5 days. Control experiments were performed with the yeast wild type modified with vector pYES2.

Generation of transgenic Arabidopsis plants over-expressing the *SeHKT1;2* gene

The coding regions of *SeHKT1;2* was sub-cloned into the plant transformation binary vector pBI121 (Clontech, Japan) under the control of CaMV35S promoters. The constructs were introduced into *Agrobacterium tumefaciens* strain GV3101 and Arabidopsis salt-hypersensitive mutant *sos1* was transformed by the floral dip method (Clough and Bent, 1998). Transgenic plants were selected on half-strength Murashige & Skoog medium containing 25 mg/L kanamycin. qRT-PCR showed the introduced gene transcript in 10 out of 15 lines of *SeHKT1;2* with varied expression levels among the lines. Two lines transgenic plants with higher expression level were used for phenotype assays of salt stresses. All of the lines used in these experiments were homozygous. Wild type and transgenic *Arabidopsis* seeds were surface-sterilized with 70% (v/v) ethanol for 2 min and 1% (v/v) NaCl solution for 15 min. The seeds were rinsed three times with water and sown on an MS medium containing 1.5% (w/v) sucrose, 0.8% (w/v) agar, and 50 mg/L kanamycin. Seven-day-old seedlings were transferred from germination medium to soil, supplemented with the indicated amounts of 300 mM NaCl after ten days.

Results

Identification of *SeHKT1-like* gene from *S. europaea*

By using degenerate primers deduced from several *HKT* sequences and standard reverse transcription (RT)-PCR methods, a cDNA homolog of an HKT high-affinity K^+ transporter from *S. europaea* was cloned. The length of the amplified cDNA fragment was about 1500-bp long. The full-length cDNA was obtained by 5′

and 3′ RACE (Rapid Amplification of cDNA Ends) which contains an ORF of 1611-bp long (Figure S1A). The translated amino acid sequence of this gene exhibited 44.31% amino acid sequence identity with SeHKT1;1 (AKS12114.1) (Figure S1B) therefore it was designated as *SeHKT1*;2 (AKS2645929). Subsequently the evolutionary relationships of SeHKT1;2 with HKT proteins from other plant species. An unrooted phylogenetic tree was generated based on full-length amino acid sequences. Results showed that SeHKT1;2 was grouped into subfamily I of HKT transporters (Figure 1).

Structural characteristic of SeHKT1;2

The *SeHKT1;2* encoding a 536 amino acid polypeptide with 8 predicted transmembrane domains (Figure 2). SMART domain architecture analysis showed that SeHKT1;2 protein has single TrkH conservative domain (pfam ID: PF02386) between amino acids 70-524 (Figure S2A). The secondary structure of the SeHKT1;2 protein was predicted, and it was found to have a complex helical folding structure (Figure S2B). The 3D models of SeHKT1;2 showed the presence of three glycine residues (Gly244, Gly368 and Gly480) and one serine residue (Ser119) forming an ion selectivity filter, which belong to subfamily I (Figures 2, S3).

Tissue specific expression of *SeHKT1;2* gene

The expression pattern of *SeHKT1;2* gene under the salt stress conditions was determined. The *SeHKT1;2* gene expression patterns in *S. europaea* seedlings were completely different between shoots and roots. In a time-course experiment, the *SeHKT1;2* was induced by NaCl (200mM) and reached the peak at 48h in shoot, but it was gradually reduced in root (Figure 3). Subsequently, we quantified expression level of *SeHKT1;2* gene under the presence of NaCl. As a result, the 10 mM NaCl significantly increased the expression of *SeHKT1;2* in shoot, but it remained same in the presence of high concentration (200mM, 500mM, 800 mM) of NaCl (Figure 3). In addition, we also examined the *SeHKT1;2* gene expression under K^+ starved condition. In our experiments, *SeHKT1;2* showed a very low expression level in roots while showed 10 folds higher in shoots (Figure 3). The expression of *SeHKT1;2* in root was not affected by NaCl.

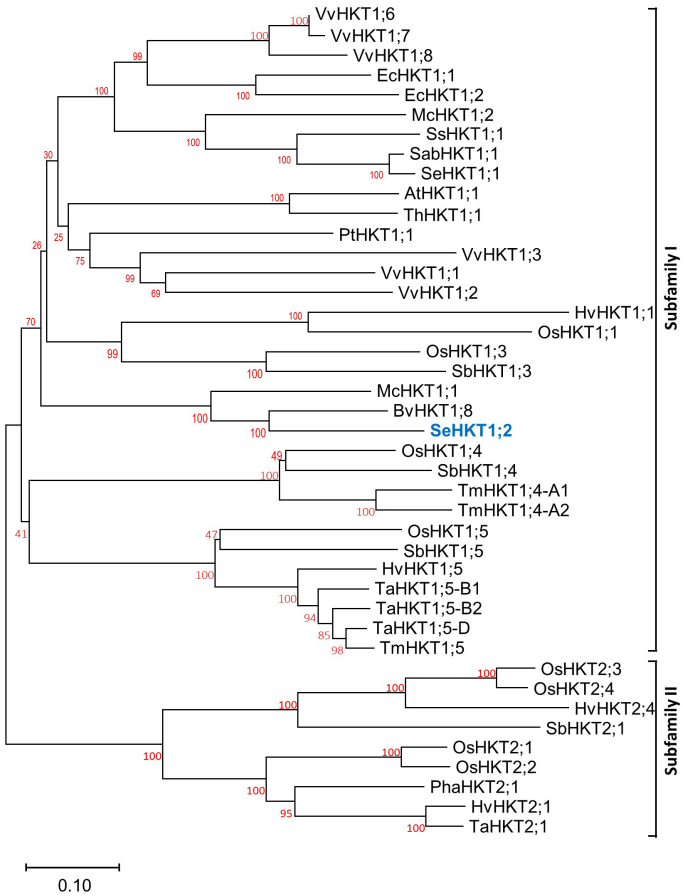

FIGURE 1
The phylogenetic relationship of SeHKT1;2 with HKTs from other plant species. Full length of HKT proteins form different plant species were used and the tree was generated by using neighbor-joining method with 1000 bootstrap replicates. Accession numbers and species for all sequences are listed in Supplemental Table S1.

10.3389/fpls.2023.1104070

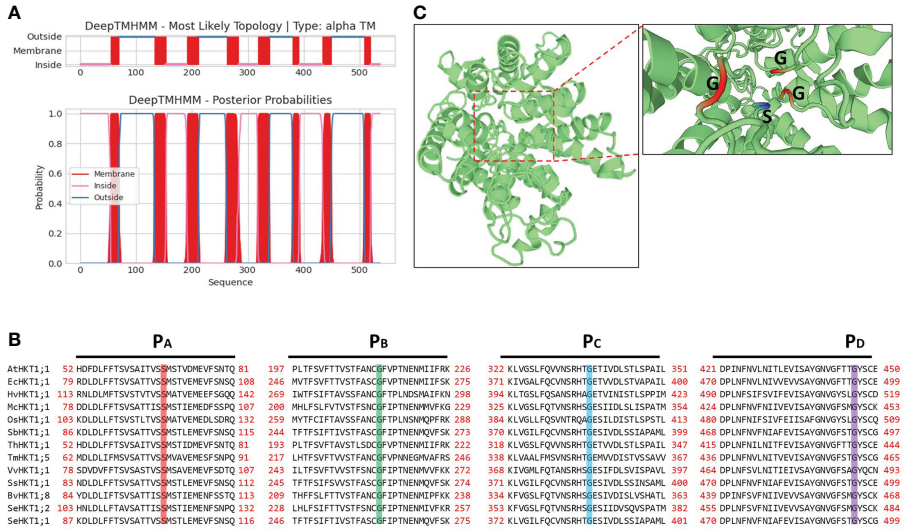

FIGURE 2
Structure analysis of SeHKT1;2 protein. **(A)** Prediction of the transmembrane domain of SeHKT1;2 protein. Blue lines are pore loop regions, and red boxes are transmembrane regions. **(B)** Multiple sequence alignment of the four conserved selectivity-filter-pore regions of HKT proteins. Amino acid sequences were aligned using Clustal W and visualized using BioEdit. Conserved residues in pore loops were indicated with colored lines. **(C)** Predicted 3D model of SeHKT1;2 protein. The first P-loop (PA, S/G) and the other P-loop (PB-D, G) are shown in magenta and orange (Color figure online).

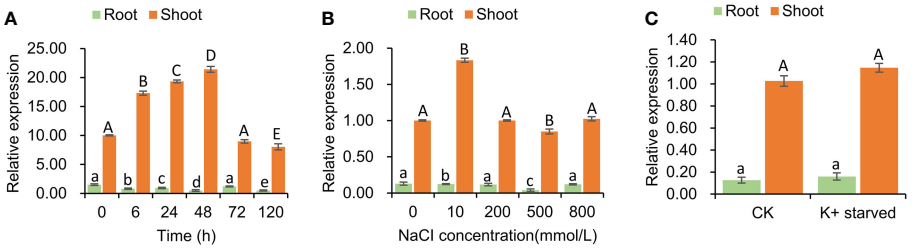

FIGURE 3
Tissue specific expression of *SeHKT1;2* gene. **(A)** Time course expression level of *SeHKT1;2* gene in shoots and roots. **(B)** The relative expression level of *SeHKT1;2* gene under 0, 10, 200, 500, 800 mmol NaCl concentration treatment. Plant samples were taken after 72h of NaCl treatment. **(C)** Expression pattern of *SeHKT1;2* gene under K^+ starved condition. After the seedlings were pre-cultured with standard Hoagland nutrient solution for 30 days, the seedlings were divided two groups. One group were continue cultured with standard Hoagland nutrient solution as CK group. Another group were cultured with NO_3^- - free Hoagland nutrient as K^+-starved group. Plant samples were taken after 72h of K^+ starvation treatment. *α-tubulin* was used as the internal reference for data processing. Values indicated the mean and standard deviation of biological repetitions (n = 3).

Functional characterization of SeHKT1;2 in yeast

Previous functional characterization in yeasts showed that SaHKT1 from the *Suaeda salsa* functions as a Na^+ selective transporter (Wang et al., 2020). To determine whether SeHKT1;2 is involved in Na^+ uptake, we expressed *SeHKT1;2* proteins in a Na^+-sensitive mutant yeast strain, G19 (Quintero et al., 1996). Results showed that under the low concentration of K^+ (1Mm), the increasing of Na^+ concentration in the growth medium caused severe growth defects in both SeHKT1;2-expressing cells and empty vector-harboring control cells (Figure 4 left panel). Interestingly, higher K^+ concentration (10mM) improved the growth of both control and SeHKT1;2-expressing cells (Figure 4 right panel). Moreover, the higher concentration (300mM) of Na^+ restricted cell growth of both control and SeHKT1;2-expressing cells (Figure S4). These data indicate that Na^+ toxicity was reduced by K^+ uptake, and that cells expressing SeHKT1;2 has a selective advantage under K^+ limitation suggesting that SeHKT1;2 have a higher affinity for K^+.

To investigate the transporter activity of SeHKT1;2, we performed complementation assay by ectopic expression of *SeHKT1;2* in the K^+ transporter-deficient yeast strain CY162 (Anderson et al., 1992). We observed no significant differences between *SeHKT1;2* and empty vector control in their growth supplied with various concentration of KCl, and both grew well on the medium containing 100 mM KCI (Figure 5A). This indicates that *SeHKT1;2* failed to complement K^+ uptake. Additionally, the

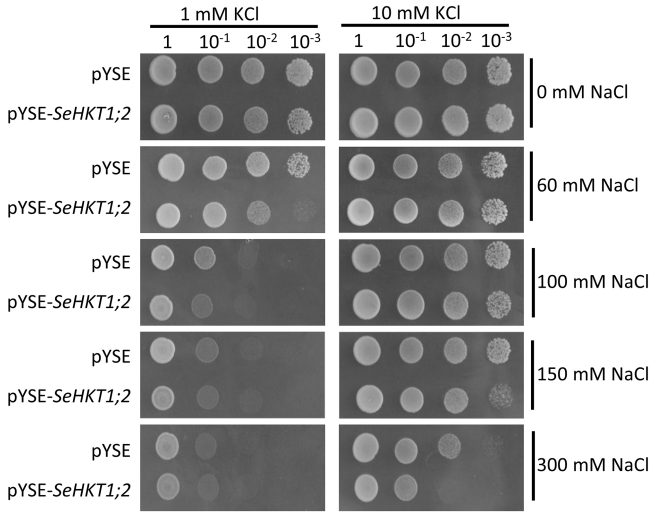

FIGURE 4
Functional characterizations of *SeHKT1;2* in G19 yeast strain. Growth of G19 yeast cells transformed by empty vector (pYSE) control and pYSE-SeHKT1;2. Each G19 transformants on solid arginine phosphate (AP) medium supplemented with various concentrations (1mM,10 mM) of KCl with combination of different salt concentrations (0, 60, 100, 150, and 300 mM NaCl) were incubated at 30°C for 3 days. Numbers (1, 10^{-1}, 10^{-2}, 10^{-3}) on the top of each panel indicated serial dilutions of yeast cells placed on the medium.

transformants growth was completely impacted as the non-transformed strain when K^+ and Na^+ were applied in combined form, in the CY162 with increased K^+ (10Mm KCl) in combination with Na^+, the transformants growth was somehow recovered (Figure 5B). These results suggested that a trend toward K^+ selectivity by SeHKT1;2.

Heterologous expression of *SeHKT1;2* in Arabidopsis *sos1* mutant

In an attempt to validate the function of *SeHKT1;2* in salt tolerance, we over expressed the *SeHKT1;2* in Arabidopsis *sos1* mutants. As expected, the whole phenotypes of *SeHKT1;2*-expressing in *sos1* and wild type Col-0 plants showed the same growth vigor and had no obvious difference under the normal condition. The growth of *sos1* plant, however, was restricted by imposing of salt stresses (300 mM NaCl) and attenuated by overexpression of *SeHKT1;2* (Figure 6). Interestingly, the overexpression of *SeHKT1;2* cannot restore the salt tolerance of *sos1* mutant plant.

Discussion

HKT transporters are one of the well-studied cation transporters in plant species. From an *S. europaea* halophyte, a homolog of HKT, *SeHKT1;2*, was isolated and the amino acids at the four pore-loop conservative sites of SeHKT1;2 protein are Ser-Gly-Gly-Gly, which belong to subfamily I (Figure 2). The presence of a Ser (serine) in the first pore-lope regions of HKT protein is associated with Na^+ selectivity, and is associated with Na^+ and/or K^+ selectivity only when the serine at this position is changed to Gly (glycine) (Horie et al., 2009). Although the rice OsHKT2;1 has Ser residue at the filter position of the first P-loop but exhibits features of class I transporters such as poor K^+ permeability (Horie et al., 2001; Yao et al., 2010).

The AtHKT1, EsHKT1;2(TsHKT1;2) and EpHKT1;2 belong to subfamily I and contain the conserved serine residue in the first pore-lope region (Ali et al., 2012; Ali et al., 2018). Unlike the AtHKT1, the EsHKT1;2 and EpHKT1;2 show significantly higher affinity for K^+ than for Na^+ (Ali et al., 2018). Presence of aspartic acid residue (D) in the second pore-loop domain of EpHKT1;2 (D207,D238) and EsHKT1;2 (D205,D236) determines their cation specificity (Na^+ or K^+) (Ali et al., 2016; Ali et al., 2018) suggesting that glycine residues are not the only amino acids involved in K^+ transport in HKT proteins. SeHKT1;2 contains asparagine residue (N) instead of aspartic acid residue (D) in the second pore-loop domain at the corresponding positions (D242, D273) in which same with AtHKT1 (Figure S5) and supposed to has functional similarity with AtHKT1. In contrast, SeHKT1;2 exhibited higher affinity for K^+ (Figures 4, 5), whereas AtHKT1 showed a higher affinity for Na^+. Although SeHKT1;2 shared similarity with AtHK1 in key amino acids but functionally different form AtHK1 indicating that other structural differences, presently unknown, may enhance K^+ uptake of SeHKT1;2.

Plant HKT gene expression is always affected by salt stresses. *PtHKT1;5* from a halophytic grass, *Puccinellia tenuiflora*, was up regulated in root cells by salt (NaCl) stress. Unlike *PtHKT1;5*, the *SsHKT1;1* from another halophyte, *Suaeda salsa*, was downregulated under NaCl treatment. It seems that the expression of HKT1 is up-regulated in salt-excluding while down-regulated salt-accumulating halophyte species under salt stress. *S. europaea* is a salt-accumulating halophyte, and transcript of *SeHKT1;2* in root was also decreased by the time under salt stress (Figure 3). In contrast, salt stress induced the *SeHKT1;2* gene expression in shoot of *S. europaea* (Figure 3). The differential

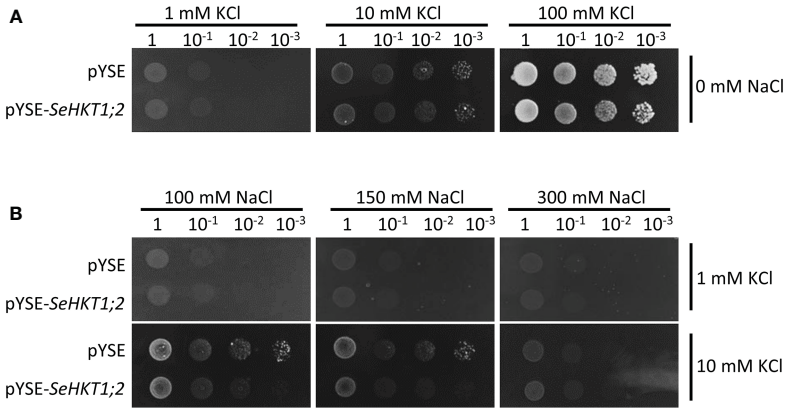

FIGURE 5
Complementation assay in yeast CY162 strain. **(A)** Growth of yeast strain CY162 cells harboring the empty vector (pYSE) control and pYSE-SeHKT1;2. Growth of each CY162 transformant on solid arginine phosphate (AP) medium supplemented with various concentrations (1mM,10 mM, 100 mM) of KCl and 0 mM NaCl incubated at 30°C for 3 days. Numbers (1, 10^{-1}, 10^{-2}, 10^{-3}) on the top of each panel indicated serial dilutions of yeast cells placed on the medium. **(B)** Growth status of the yest cell lines in **(A)** on AP medium containing different concentration of KCl (1 mM,10 mM) and NaCl (100mM,150mM,300mM). Each yest cell lines were incubated at 30°C for 3 days. Numbers (1, 10^{-1}, 10^{-2}, 10^{-3}) on the top of each panel indicated serial dilutions of yeast cells placed on the medium.

FIGURE 6
Phenotypes of transgenic and wild type Arabidopsis lines under salt stress. The *sos1* mutant Arabidopsis were infiltrated by *Agrobacterium tumefaciens* harbored the *SeHKT1;2* construct. Four-week-old Arabidopsis plants were treated with watered with 300 mM NaCl for 14 days.

expression of *SeHKT1;2* gene in root and shoot may reduce Na^+ retrieval from the xylem and facilitate Na^+ transport into its shoots so *S. europaea* could adjust to high external salinity and exhibit better growth under saline environment. Hence, SeHKT1;2 is key protein in salt accumulation in *S. europaea*.

Plants maintain sodium homeostasis by Salt Overly Sensitive (SOS) pathway (Yang and Guo, 2018). AtSOS1 is the key sodium transporter in Arabidopsis SOS pathway. The *sos1* mutant Arabidopsis plants are even more sensitive to Na^+ stresses compared with *sos3* mutant plants (Zhu et al., 1998; Shi et al., 2000). A previous study demonstrated that Na^+ efflux rate significantly decreased by 16% in *sos1* compared with WT (Wang et al., 2019). In our study, *sos1* exhibited more sensitivity to salt stress and heterologous expression of *SeHKT1;2* could not rescue the *sos1* mutant plants but increased the sensitivity of the *sos1* mutant plants (Figure 6). In the *sos1* mutant plants the impairment of AtSOS1 mediated efflux of cytoplasmic Na^+ resulting in accumulation of cytoplasmic Na^+ and showed salt sensitivity (Figures 6, 7). The salt overly sensitive phenotype caused by heterologous expression of SeHKT1;2 can be explained that the *SeHKT1;2* in *sos1* Arabidopsis influx Na^+ so that further accumulate cytoplasmic Na^+ and eventually

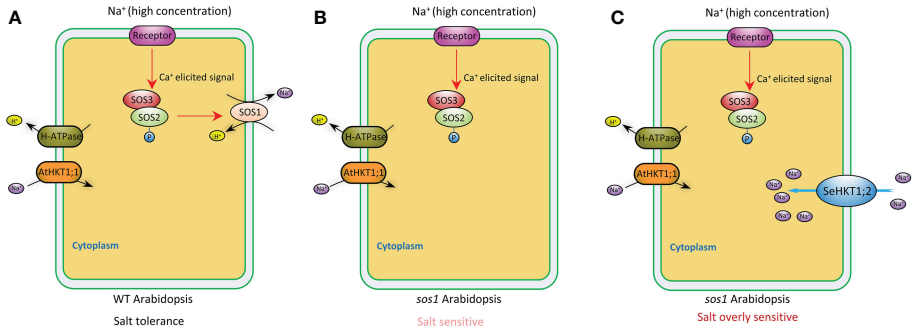

FIGURE 7
A proposed model depicting the putative function of SeHKT1;2 contributing to Na^+ uptake across the plasma membrane. In wild type Arabidopsis, high Na^+ concentration elicits a $Ca2^+$ signal that activates SOS3-SOS2 complex, which in turn stimulates cytoplasmic Na^+ efflux activity of SOS1 across the plasma membrane **(A)**. Efflux of cytoplasmic Na^+ was reduced in *sos1* Arabidopsis, making the plants salt sensitive **(B)**. Na^+ uptake across the plasma membrane by SeHKT1;2 increased the cytoplasmic Na^+ concentration, making the plants salt overly sensitive **(C)**.

inhibits plant growth and increases salt sensitivity of *sos1* plant (Figures 6, 7). This study suggested that SeHKT1;2 play very important roles in synergistically regulating Na^+ homeostasis by controlling Na^+ transport in Arabidopsis.

Data availability statement

The original contributions presented in the study are included in the article/Supplementary Material. Further inquiries can be directed to the corresponding authors.

Author contributions

The experimental design, data analyzation, manuscript organization were completed by JM and YH and ZP were assistant with RNA quantification. JM and LW conceived the project, supervised the analysis, and critically revised the manuscript. XF revised the manuscript. All authors contributed to the article and approved the submitted version.

Funding

This work was funded by the Xinjiang Uygur Autonomous Region regional coordinated innovation project (Shanghai cooperation organization science and technology partnership program) (No. 2022E01022), Introduction Project of High-level Talents in Xinjiang Uygur Autonomous Region.

Conflict of interest

The authors declare that the research was conducted in the absence of any commercial or financial relationships that could be construed as a potential conflict of interest.

Publisher's note

All claims expressed in this article are solely those of the authors and do not necessarily represent those of their affiliated organizations, or those of the publisher, the editors and the reviewers. Any product that may be evaluated in this article, or claim that may be made by its manufacturer, is not guaranteed or endorsed by the publisher.

Supplementary material

The Supplementary Material for this article can be found online at: https://www.frontiersin.org/articles/10.3389/fpls.2023.1104070/full#supplementary-material

References

Ali, A., Khan, I. U., Jan, M., Khan, H. A., Hussain, S., Nisar, M., et al. (2018). The high-affinity potassium transporter EpHKT1;2 from the extremophile eutrema parvula mediates salt tolerance. *Front. Plant Sci.* 9. doi: 10.3389/fpls.2018.01108

Ali, Z., Park, H. C., Ali, A., Oh, D.-H., Aman, R., Kropornicka, A., et al. (2012). TsHKT1;2, a HKT1 homolog from the extremophile arabidopsis relative thellungiella salsuginea, shows k+ specificity in the presence of NaCl. *Plant Physiol.* 158, 1463–1474. doi: 10.1104/pp.111.193110

Ali, A., Raddatz, N., Aman, R., Kim, S., Park, H. C., Jan, M., et al. (2016). A single amino-acid substitution in the sodium transporter HKT1 associated with plant salt tolerance. *Plant Physiol.* 171, 2112–2126. doi: 10.1104/pp.16.00569

Almeida, P. M. F., de Boer, G.-J., and de Boer, A. H. (2014). Assessment of natural variation in the first pore domain of the tomato HKT1;2 transporter and characterization of mutated versions of SlHKT1;2 expressed in xenopus laevis oocytes and *via* complementation of the salt sensitive athkt1;1 mutant. *Front. Plant Sci.* 5. doi: 10.3389/fpls.2014.00600

Almeida, P., Katschnig, D., and de Boer, A. H. (2013). HKT transporters–state of the art. *Int. J. Mol. Sci.* 14, 20359–20385. doi: 10.3390/ijms141020359

Amtmann, A., and Sanders, D. (1998). Mechanisms of na+ uptake by plant cells. *Adv. Bot. Res.* 29, 75–112. doi: 10.1016/S0065-2296(08)60310-9

Anderson, J. A., Huprikar, S. S., Kochian, L. V., Lucas, W. J., and Gaber, R. F. (1992). Functional expression of a probable arabidopsis thaliana potassium channel in saccharomyces cerevisiae. *Proc. Natl. Acad. Sci. U. S. A.* 89, 3736. doi: 10.1073/PNAS.89.9.3736

Berthomieu, P., Conéjéro, G., Nublat, A., Brackenbury, W. J., Lambert, C., Savio, C., et al. (2003). Functional analysis of AtHKT1 in arabidopsis shows that na(+) recirculation by the phloem is crucial for salt tolerance. *EMBO J.* 22, 2004–2014. doi: 10.1093/EMBOJ/CDG207

Blumwald, E., Aharon, G. S., and Apse, M. P. (2000). Sodium transport in plant cells. *Biochim. Biophys. Acta* 1465, 140–151. doi: 10.1016/S0005-2736(00)00135-8

Bressan, R. A., Park, H. C., Orsini, F., Oh, D. h., Dassanayake, M., Inan, G., et al. (2013). Biotechnology for mechanisms that counteract salt stress in extremophile species: A genome-based view. *Plant Biotechnol. Rep.* 7, 27–37. doi: 10.1007/S11816-012-0249-9/FIGURES/3

Clough, S. J., and Bent, A. F. (1998). Floral dip: A simplified method for agrobacterium-mediated transformation of arabidopsis thaliana. *Plant J.* 16, 735–743. doi: 10.1046/J.1365-313X.1998.00343.X

Flowers, T. J., Galal, H. K., and Bromham, L. (2010). Evolution of halophytes: Multiple origins of salt tolerance in land plants. *Funct. Plant Biol.* 37, 604–612. doi: 10.1071/FP09269

Garciadeblás, B., Senn, M. E., Bañuelos, M. A., and Rodríguez-Navarro, A. (2003). Sodium transport and HKT transporters: The rice model. *Plant J.* 34, 788–801. doi: 10.1046/J.1365-313X.2003.01764.X

Gassmann, W., Rubio, F., and Schroeder, J. I. (1996). Alkali cation selectivity of the wheat root high-affinity potassium transporter HKT1. *Plant J.* 10, 869–882. doi: 10.1046/J.1365-313X.1996.10050869.X

Høie, M. H., Kiehl, E. N., Petersen, B., Nielsen, M., Winther, O., Nielsen, H., et al. (2022). NetSurfP-3.0: Accurate and fast prediction of protein structural features by protein language models and deep learning. *Nucleic Acids Res.* 50, W510–W515. doi: 10.1093/NAR/GKAC439

Hasegawa, P. M., Bressan, R. A., Zhu, J. K., and Bohnert, H. J. (2003). Plant cellular and molecular responses to high salinity. *Annu. Rev. Plant Physiol. Plant Mol. Biol.* 51, 463–499. doi: 10.1146/ANNUREV.ARPLANT.51.1.463

Horie, T., Costa, A., Kim, T. H., Han, M. J., Horie, R., Leung, H. Y., et al. (2007). Rice OsHKT2;1 transporter mediates large na+ influx component into k+-starved roots for growth. *EMBO J.* 26, 3003–3014. doi: 10.1038/SJ.EMBOJ.7601732

Horie, T., Hauser, F., and Schroeder, J. I. (2009). HKT transporter-mediated salinity resistance mechanisms in arabidopsis and monocot crop plants. *Trends Plant Sci.* 14, 660. doi: 10.1016/J.TPLANTS.2009.08.009

Horie, T., Horie, R., Chan, W. Y., Leung, H. Y., and Schroeder, J. I. (2006). Calcium regulation of sodium hypersensitivities of sos3 and athkt1 mutants. *Plant Cell Physiol.* 47, 622–633. doi: 10.1093/PCP/PCJ029

Horie, T., Yoshida, K., Nakayama, H., Yamada, K., Oiki, S., and Shinmyo, A. (2001). Two types of HKT transporters with different properties of na+ and k+ transport in oryza sativa. *Plant J.* 27, 129–138. doi: 10.1046/J.1365-313X.2001.01077.X

Laurie, S., Feeney, K. A., Maathuis, F. J. M., Heard, P. J., Brown, S. J., and Leigh, R. A. (2002). A role for HKT1 in sodium uptake by wheat roots. *Plant J.* 32, 139–149. doi: 10.1046/J.1365-313X.2002.01410.X

Lv, S., Jiang, P., Chen, X., Fan, P., Wang, X., and Li, Y. (2012). Multiple compartmentalization of sodium conferred salt tolerance in salicornia europaea. *Plant Physiol. Biochem.* 51, 47–52. doi: 10.1016/J.PLAPHY.2011.10.015

Ma, J., Zhang, M., Xiao, X., You, J., Wang, J., Wang, T., et al. (2013). Global transcriptome profiling of salicornia europaea l. shoots under NaCl treatment. *PloS One* 8, e65877. doi: 10.1371/JOURNAL.PONE.0065877

Mahajan, S., Pandey, G. K., and Tuteja, N. (2008). Calcium- and salt-stress signaling in plants: shedding light on SOS pathway. *Arch. Biochem. Biophys.* 471, 146–158. doi: 10.1016/J.ABB.2008.01.010

Mahajan, S., and Tuteja, N. (2005). Cold, salinity and drought stresses: An overview. *Arch. Biochem. Biophys.* 444, 139–158. doi: 10.1016/J.ABB.2005.10.018

Mäser, P., Eckelman, B., Vaidyanathan, R., Horie, T., Fairbairn, D. J., Kubo, M., et al. (2002a). Altered shoot/root na+ distribution and bifurcating salt sensitivity in arabidopsis by genetic disruption of the na+ transporter AtHKT1. *FEBS Lett.* 531, 157–161. doi: 10.1016/S0014-5793(02)03488-9

Mäser, P., Hosoo, Y., Goshima, S., Horie, T., Eckelman, B., Yamada, K., et al. (2002b). Glycine residues in potassium channel-like selectivity filters determine potassium selectivity in four-loop-per-subunit HKT transporters from plants. *Proc. Natl. Acad. Sci. U. S. A.* 99, 6428. doi: 10.1073/PNAS.082123799

Nieves-Cordones, M., Ródenas, R., Chavanieu, A., Rivero, R. M., Martinez, V., Gaillard, I., et al. (2016). Uneven HAK/KUP/KT protein diversity among angiosperms: Species distribution and perspectives. *Front. Plant Sci.* 7. doi: 10.3389/FPLS.2016.00127/BIBTEX

Patel, S. (2016). Salicornia: Evaluating the halophytic extremophile as a food and a pharmaceutical candidate. *3 Biotech.* 6. doi: 10.1007/S13205-016-0418-6

Quintero, F. J., Garciadeblás, B., and Rodríguez-Navarro, A. (1996). The SAL1 gene of arabidopsis, encoding an enzyme with 3'(2'),5'-bisphosphate nucleotidase and inositol polyphosphate 1-phosphatase activities, increases salt tolerance in yeast. *Plant Cell* 8, 529–537. doi: 10.1105/TPC.8.3.529

Rubio, F., Gassmann, W., and Schroeder, J. I. (1995). Sodium-driven potassium uptake by the plant potassium transporter HKT1 and mutations conferring salt tolerance. *Science* 270, 1660–1663. doi: 10.1126/SCIENCE.270.5242.1660

Schachtman, D., and Liu, W. (1999). Molecular pieces to the puzzle of the interaction between potassium and sodium uptake in plants. *Trends Plant Sci.* 4, 281–287. doi: 10.1016/S1360-1385(99)01428-4

Schachtman, D. P., and Schroeder, J. I. (1994). Structure and transport mechanism of a high-affinity potassium uptake transporter from higher plants. *Nature* 370, 655–658. doi: 10.1038/370655A0

Shi, H., Ishitani, M., Kim, C., and Zhu, J.-K. (2000). The arabidopsis thaliana salt tolerance gene SOS1 encodes a putative Na+/H+ antiporter. *Proc. Natl. Acad. Sci.* 97, 6896–6901. doi: 10.1073/pnas.120170197

Tester, M., and Davenport, R. (2003). Na+ tolerance and na+ transport in higher plants. *Ann. Bot.* 91, 503–527. doi: 10.1093/AOB/MCG058

Uozumi, N., Kim, E. J., Rubio, F., Yamaguchi, T., Muto, S., Tsuboi, A., et al. (2000). The arabidopsis HKT1 gene homolog mediates inward na(+) currents in xenopus laevis oocytes and na(+) uptake in saccharomyces cerevisiae. *Plant Physiol.* 122, 1249–1259. doi: 10.1104/PP.122.4.1249

Wang, Q., Guan, C., Wang, P., Ma, Q., Bao, A.-K., Zhang, J.-L., et al. (2019). The effect of AtHKT1;1 or AtSOS1 mutation on the expressions of na+ or k+ transporter genes and ion homeostasis in arabidopsis thaliana under salt stress. *Int. J. Mol. Sci.* 20. doi: 10.3390/ijms20051085

Wang, W. Y., Liu, Y. Q., Duan, H. R., Yin, X. X., Cui, Y. N., Chai, W. W., et al. (2020). SsHKT1;1 is coordinated with SsSOS1 and SsNHX1 to regulate na+ homeostasis in suaeda salsa under saline conditions. *Plant Soil* 449, 117–131. doi: 10.1007/S11104-020-04463-X/FIGURES/10

Waterhouse, A., Bertoni, M., Bienert, S., Studer, G., Tauriello, G., Gumienny, R., et al. (2018). SWISS-MODEL: Homology modelling of protein structures and complexes. *Nucleic Acids Res.* 46, W296–W303. doi: 10.1093/NAR/GKY427

Xiao, X., Ma, J., Wang, J., Wu, X., Li, P., and Yao, Y. (2015). Validation of suitable reference genes for gene expression analysis in the halophyte salicornia europaea by real-time quantitative PCR. *Front. Plant Sci.* 5. doi: 10.3389/fpls.2014.00788

Xu, C., Tang, X., Shao, H., and Wang, H. (2016). Salinity tolerance mechanism of economic halophytes from physiological to molecular hierarchy for improving food quality. *Curr. Genomics* 17, 207. doi: 10.2174/1389202917666160202215548

Yang, Y., and Guo, Y. (2018). Unraveling salt stress signaling in plants. *J. Integr. Plant Biol.* 60, 796–804. doi: 10.1111/jipb.12689

Yao, X., Horie, T., Xue, S., Leung, H. Y., Katsuhara, M., Brodsky, D. E., et al. (2010). Differential sodium and potassium transport selectivities of the rice OsHKT2;1 and OsHKT2;2 transporters in plant cells. *Plant Physiol.* 152, 341. doi: 10.1104/PP.109.145722

Zhu, J. K. (2003). Regulation of ion homeostasis under salt stress. *Curr. Opin. Plant Biol.* 6, 441–445. doi: 10.1016/S1369-5266(03)00085-2

Zhu, J.-K., Liu, J., and Xiong, L. (1998). Genetic analysis of salt tolerance in arabidopsis: Evidence for a critical role of potassium nutrition. *Plant Cell* 10, 1181–1191. doi: 10.1105/tpc.10.7.1181

frontiers | Frontiers in Plant Science

TYPE Original Research
PUBLISHED 09 March 2023
DOI 10.3389/fpls.2023.1100601

OPEN ACCESS

EDITED BY
Jing Zhang,
Nanjing Agricultural University, China

REVIEWED BY
Boon Chin Tan,
University of Malaya, Malaysia
Qiguo Sun,
Jiangsu Vocational College of Agriculture and Forestry, China

*CORRESPONDENCE
Jihong Xie
xiejihong223@163.com
Linqing Yu
linqing_yu@126.com

SPECIALTY SECTION
This article was submitted to Plant Abiotic Stress, a section of the journal Frontiers in Plant Science

RECEIVED 17 November 2022
ACCEPTED 17 February 2023
PUBLISHED 09 March 2023

CITATION
Wang Y, Sun Z, Wang Q, Xie J and Yu L (2023) Transcriptomics and metabolomics revealed that phosphate improves the cold tolerance of alfalfa.
Front. Plant Sci. 14:1100601.
doi: 10.3389/fpls.2023.1100601

Transcriptomics and metabolomics revealed that phosphate improves the cold tolerance of alfalfa

Yuntao Wang[1], Zhen Sun[2], Qiqi Wang[1], Jihong Xie[1]* and Linqing Yu[3]*

[1]Grassland Research Institute, Chinese Academy of Agricultural Science, Hohhot, Inner Mongolia, China, [2]College of Grassland, Qingdao Agricultural University, Qingdao, Shandong, China, [3]College of Life Science, Inner Mongolia University, Hohhot, Inner Mongolia, China

Introduction: Alfalfa (*Medicago sativa L.*) is a highly nutritious leguminous forage that plays an essential role in animal husbandry. In the middle and high latitudes of the northern hemisphere, there are problems with its low rates of overwintering and production. The application of phosphate (P) is an important measure to improve the cold resistance and production of alfalfa, but little is known about the mechanism of P in improving the cold resistance of alfalfa.

Methods: This study integrated the transcriptome and metabolome to explain the mechanism of alfalfa in response to low-temperature stress under two applications of P (50 and 200 mg kg^{-1}) and a control of none applied.

Results: The application of P fertilizer improved the root structure and increased the content of soluble sugar and soluble protein in the root crown. In addition, there were 49 differentially expressed genes (DEGs) with 23 upregulated and 24 metabolites with 12 upregulated when 50 mg kg^{-1} of P was applied. In contrast, there were 224 DEGs with 173 upregulated and 12 metabolites with 6 upregulated in the plants treated with 200 mg kg^{-1} of P compared with the Control Check (CK). These genes and metabolites were significantly enriched in the biosynthesis of other secondary metabolites and the metabolic pathways of carbohydrates and amino acids. The integration of the transcriptome and metabolome indicated that P affected the biosynthesis of N-acetyl-L-phenylalanine, L-serine, lactose, and isocitrate during the period of increasing cold. It could also affect the expression of related genes that regulate cold tolerance in alfalfa.

Discussion: Our findings could contribute to a deeper understanding of the mechanism that alfalfa uses to tolerate cold and lay a theoretical foundation for breeding alfalfa that is highly efficient at utilizing phosphorus.

KEYWORDS

alfalfa, transcriptomics, metabolomics, cold tolerance, phosphorus

1 Introduction

As a cool-season perennial forage crop, alfalfa (*Medicago sativa* L.) plays a variety of beneficial roles for livestock, soil coverage, soil fertility, and human health (Gaafar et al., 2019). It has a high biomass yield, excellent nutritional quality, and wide adaption, and it can fix nitrogen (N) (Summers and Putnam, 2008). Alfalfa is grown on approximately 30 million ha of land worldwide (Acharya et al., 2020; Diatta et al., 2021), and the global production of alfalfa hay was 210.9 million metric tons (Edde, 2022). North America is the primary producer of alfalfa in the world; the United States has the largest planting area with more than 7.23 million ha of alfalfa grown annually, with Canada and Mexico close behind (Putnam et al., 2001; Wechsler et al., 2017; Edde, 2022). The cultivated area of alfalfa in China is approximately 3.77×10^6 hm^2, which is approximately 13% of the world's total arable land used to grow alfalfa. The growth of alfalfa is primarily distributed in northeastern, northwestern, and northern China (Yang et al., 2021). In these northern regions, the inability of alfalfa to withstand low subfreezing temperatures remains one of its biggest challenges (Castonguay et al., 2006; Rocher et al., 2015), which hampers the development of the alfalfa industry and animal husbandry.

The morphological and physiological characteristics of the roots are strongly associated with the cold resistance of alfalfa. The root types of alfalfa primarily include four types: tap, branch, rhizomatous, and creeping roots (Goplen, 1987; Hong et al., 1987). Tap-rooted types have a main root and a narrow, protruding crown; the branch-rooted types of alfalfa have a moderately wide crown and a number of primary roots; the rhizomatous- and creeping-rooted types have a protected crown, develop new roots readily, and can also develop stems from the roots. The shoots can separate from the maternal parent plant and become independent plants to survive; thus, they more easily regrow after freezing damage and show strong cold resistance (Goplen, 1987; Dou, 2011). A substantial amount of research has documented that the root crown, lateral roots, and root biomass affect the winter survival and persistence of alfalfa (Castonguay et al., 2006; Liu et al., 2015b; Xu et al., 2022). Previous studies have primarily focused on the root crown. It is a transitional plant structure that is located between the shoots and the root system. It is also the uppermost dormant organ of the winter plant body, which is crucial to overwintering and regeneration in the spring (Marquez-Ortiz et al., 1999; Liu et al., 2015b). The overwintering rate of alfalfa is closely related to the size and depth of the root crown; they grow more deeply and thicker in the soil, which helps the plants to successfully survive the winter (Wang, 2021b). This is considered to be a cold-sensitivity escape mechanism to prevent the exposure of the overwintering organ to low temperature. The major alfalfa varieties with strong cold resistance have more lateral roots because they help alfalfa plants to absorb more water and nutrient elements from the soil to supply the demand of overwintering plants for nutrients (Johnson et al., 1996; Wang et al., 2023). The root biomass is related to the accumulation of organic matter, and the herringbone branching is conducive to the absorption of deeper water by alfalfa, which contributes to improve the plant's cold resistance (Viands, 1988). Its physiology, including the contents of soluble sugar and protein, is also closely related to cold resistance. Soluble sugar acts as an osmotic regulator, a cryoprotectant, and a signaling molecule to stabilize the cell membrane and scavenge reactive oxygen species (ROS) under low-temperature stress, and its contents increase during the freezing process to protect the plant cells (Trischuk et al., 2014). Therefore, the accumulation of sugar at the root crown before winter is related to the cold resistance of alfalfa (Cunningham et al., 1998; Bertrand et al., 2017). Soluble proteins are strongly hydrophilic and can enhance the water-holding capacity of cells. The accumulation of soluble proteins can bind more water to the cells and reduce the damage caused by low temperatures (Kontunen-Soppela et al., 2002; Moieni-Korbekandi et al., 2013). The increase in the soluble protein content of alfalfa in autumn and winter helps to enhance its resistance to low temperatures.

As an important means of regulating cultivation, nutrient management not only can improve the production of alfalfa, but it is also an essential measure to improve its stress resistance (Wang, 2021a). Phosphorus is one of the three essential nutrients for plant growth and development, which is absorbed in the form of phosphate (P) (Bhosale et al., 2018). It is an essential macroelement that plays a role in an array of processes, including energy generation, nucleic acid synthesis, photosynthesis, glycolysis, respiration, membrane synthesis and stability, respiration, carbohydrate metabolism, and N fixation (Vance et al., 2003; Raghothama and Karthikeyan, 2005). In addition, it plays a vital role in enhancing the adaptability of plants to the external environment (Yan et al., 2022). P is also an important component of phospholipids and ATP, which affect the resistance of plants to low temperatures (Li et al., 2016). Phospholipids in the plant cell membranes can interact with proteins, sugars, and other substances to alleviate the cell dehydration caused by low-temperature stress and protect the stability of cell membranes (Cheng, 2008). Plants can be negatively affected by the low levels of phosphorus that affect a variety of growing environments, particularly in soils that are calcareous or alkaline (Yue et al., 2019). A deficiency in P will affect plant photosynthesis, such as by limiting the distribution and utilization of carbohydrates and the absorption and transport of P (Terry and Tao, 1991). This can also cause an imbalance in the production and clearance of ROS and an array of physiological, biochemical, and metabolic changes resulting in damage to the plants (Lin et al., 2010). The application of P can increase the contents of soluble sugar in plants, and sucrose transport in the phloem requires ATP hydrolysis to provide energy so that P can regulate the metabolism and transport of sucrose in plant leaves (Tian et al., 2017). Current studies have shown that the application of moderate P fertilizer can promote the root growth of alfalfa and increase the content of cold-resistant substances, such as starch and soluble proteins, in the root crown of alfalfa to some extent (Shen et al., 2017). However, the related molecular mechanism remains unclear.

The recently developed technologies of high-throughput sequencing, high-resolution mass spectrometry, and information processing have made systems biology (omics) research a major

focus of scientific investigation (Xin et al., 2019). The integrated analyses of transcriptomic and metabolic data obtained from two biological levels, i.e., transcript and metabolite levels, respectively, can serve as a useful way to study complex biological phenomena (Agarrwal et al., 2016). In addition, these integrated analyses have been applied to various plant biological processes, including the evolutionary adaption of poplar species (*Populus* L.) to salinity stress (Janz et al., 2010), rice (*Oryza sativa* L.) insect interaction research (Agarrwal et al., 2016), and the response of wild soybean (*Glycine max* L.) to N starvation (Liu et al., 2020). However, to our knowledge, there are few studies that have examined the mechanisms of the effect of P fertilizer on the cold resistance of alfalfa by integrating the analyses of transcriptomic and metabolic data.

In this study, alfalfa was exposed to three P treatments for 90 days. We measured the contents of the soluble sugar and protein of root crowns and some root indices. In addition, we performed transcriptomic and metabolomic studies among the three P treatments under cold temperature. Our integrated transcriptome–metabolome analysis allowed us to gain a deeper understanding of alfalfa's response to the application of P in terms of cold tolerance. We sought to identify the strategies used by alfalfa to respond to the application of P during the increase in cold stress, which could be used to improve the cold tolerance and yield of alfalfa and breed new alfalfa varieties.

2 Materials and methods

2.1 Field design and sampling

The variety of alfalfa used in this study was Zhongcao No. 3, which was provided by the Grassland Research Institute of the Chinese Academy of Agricultural Sciences (GRI of CAAS) (Beijing, China). On September 5, 2020, an alfalfa plant that had grown for 5 years in the Agro-pastoral Experiment Station (40°34′E; 111°45′N; 1,050 m a.s.l.) of the GRI of CAAS was transferred to the greenhouse, and the seedlings were raised by stem cuttings in seedling trays on May 10, 2021. On July 15, 2021, cloned plants were selected and transplanted into pots that were 18 cm in diameter and 19 cm in depth. Each pot had only one plant and 5 kg of gray cinnamon soil from the field as a substrate. The physiochemical properties of the soil included an organic matter content of 6.25 g kg^{-1}, total N content of 1.09 g kg^{-1}, available N content of 69.45 mg g^{-1}, available P content of 20.5 mg kg^{-1}, available potassium content of 425.0 mg kg^{-1}, and a pH of 8.5. Three levels of P levels were established according to P_2O_5 contents of 0, 50, and 200 mg kg^{-1} (designated CK, P1, and P4, respectively). Each treatment had 10 pots, which were placed into the field. The root crowns of alfalfa were collected on October 15, 2021. Three clones served as biological replicates. The root crowns were rinsed with clean water, wiped with absorbent paper, cut into small pieces of 3–5 mm, quickly placed into frozen tubes, stored in liquid N, and then preserved in at -80°C for further analysis (Ye et al., 2018). The temperature during the sampling period is shown in Figure S1.

2.2 Analyses of morphological and physiological indices

The phenotypic characteristics of alfalfa were measured as previously described (Wang et al., 2022). The root dry weight was measured by weighing the dried roots, which were oven-dried at 105°C for 30 min and then at 65°C for 48 h. The contents of soluble sugar were determined using anthrone–sulfuric acid colorimetry (Yemm and Willis, 1954). The contents of soluble protein were determined using Coomassie brilliant blue (Wu et al., 2013). Three plants were used as biological replicates for each treatment.

2.3 RNA extraction and sequencing

Samples treated with different levels of P were fully ground in liquid N. Total RNA was extracted using the TRIzol reagent (Life Technologies, Carlsbad, CA, USA) according to the manufacturer's instructions. The RNA was purified, reverse-transcribed, used to construct a library, and sequenced according to the manufacturer's instructions. To prepare Illumina RNA-seq libraries, the poly(A) mRNA was isolated from purified total RNA using biotin-Oligo (dT) magnetic beads and fragmented into small pieces using an RNA fragmentation kit according to the manufacturer's instructions (Illumina, San Diego, CA, USA) (Hu et al., 2020). Fragmented RNA was then used as a template, and random oligonucleotides were used as primers to synthesize single-stranded complementary DNA (cDNA) by reverse transcription (Du, 2021). RNase H was then used to degrade the RNA strands, and a QiaQuick PCR extraction kit (Qiagen, Venlo, The Netherlands) was used to synthesize double-stranded cDNA (Du, 2021). The purified double-stranded cDNA was repaired by terminal repair. A tail was added and connected to the sequencing junction, and the cDNA that was approximately 200 bp was screened by ampure (AM) Pure Extraction-Purification (XP) beads. PCR amplification was conducted, and the PCR product was purified by AM Pure XP beads, which provided the cDNA library used for sequencing (Bao et al., 2020). To ensure the sequencing quality, a library quality inspection kit, the DNA 1000 assay kit (Agilent Technologies, Santa Clara, CA, USA), was used to inspect the library. The amplified fragments were sequenced using an Illumina Hi-Seq 4000 platform.

The reads obtained from the sequencing machines included raw reads that contained adapters or low-quality bases that would affect the following assembly and analysis. Thus, the reads were further filtered using an ultra-fast all-in-one FASTQ preprocessor (FASTP) (version 0.18.0) to obtain high-quality clean reads (Chen et al., 2018). An index of the reference genome was built, and paired-end clean reads were mapped to the reference genome using HISAT2. 2.4 with "-RNA-strandness RF" and other parameters set as the default (Kim et al., 2015; Chen et al., 2020). By comparing the value of the transcript on each Unigene, the value was standardized to the fragments per kilobase of transcript per million fragments mapped (FPKM) to represent the level of gene expression (Zhao et al., 2021). RNA differential expression analysis was performed using DESeq2

and edgeR (Robinson et al., 2010; Love et al., 2014). Genes with a false discovery rate below 0.05 and an absolute fold change ≥2 were considered to be differentially expressed genes (DEGs). Based on the expression information, we used R[1] to conduct principal component analysis (PCA) and hierarchical clustering analyses. Gene Ontology (GO) functional and Kyoto Encyclopedia of Genes and Genomes (KEGG) pathway enrichment analyses were performed using GOATOOLS and KoBAS software, which can determine the primary biological functions of DEGs and identify the main biological pathways in which the DEGs are involved (Zhang et al., 2021). All the RNA sequencing data reported in this study have been deposited in National Center for Biotechnology Information (NCBI) under the sequence read archive with the accession number PRJNA909902.

The same batch of samples used in transcriptome sequencing was used for quantitative PCR (qPCR) detection. The qPCR primers and genes are shown in Table S1. The *AKR4C9* gene was used as a reference. Real-time quantitative reverse transcription PCR (qRT-PCR) was conducted using a qTOWER 2.2 PCR System (Jena, Germany) and SYBR Green PCR Master Mix (TaKaRa, Shiga, Japan). The amplification program was as follows: 90 s at 95°C, and 40 cycles × (95°C, 5 s, 60°C, 15 s, and 72°C, 20 s). The dissolution curve of the amplified product was analyzed at 65°C–95°C. Each reaction was performed three times. The levels of the expression of candidate genes were measured using the $2^{-(\Delta\Delta Ct)}$ method.

2.4 Metabolite extraction and ultra-high-performance liquid chromatography–quadrupole time-of-flight mass spectrometry

The samples treated with different levels of P were removed from storage at -80°C, vacuum frozen-freeze dried, and then crushed using a mixer mill (MM 400, RETSCH, Haan, Germany) with a zirconia bead for 1.5 min at 30 Hz. The sample (100 mg powder) was extracted overnight at 4°C with 1.0 ml of 70% aqueous methanol that contained 0.1 mg/L lidocaine as an internal standard. The supernatant was absorbed after centrifugation at 10,000 g for 10 min (CNWBOND Carbon-GCB SPE Cartridge, 250 mg, 3 ml; ANPEL, Shanghai, China, www.anpel.com.cn/cnw) and filtered (SCAA-104, 0.22 μm pore size; ANPEL) before liquid chromatography with tandem mass spectrometry (LC-MS/Metabolites (MS)) analysis (Chen et al., 2013). After the metabolites were extracted, 10 μl of each sample were mixed to serve as quality control (QC) samples, and 60 μl were evaluated by ultra-high-performance liquid chromatography–quadrupole time-of-flight mass spectrometry (UPLC-QTOF-MS) to monitor the stability of the instrument during the whole analytical process (Zhang et al., 2021).

The metabolites of the samples were qualitatively analyzed by mass spectrometry based on the metabolite database assembled by Guangzhou Chideo Biotechnology Co., Ltd. (Guangzhou, China). The structural analysis of some metabolites refers to the secondary Metabolites (MS) information in the existing mass spectrometry public databases, such as MassBank[2], HMDB[3] (Wishart et al., 2013), MoToDB[4], and METLIN[5] (Zheng et al., 2013). The quantification of metabolites was conducted by integrating the peak area of the mass spectra of all the substances and correcting the mass spectrometry peaks of the same metabolite in different samples to ensure the accuracy of quantification. The metabolites were analyzed by a PCA, partial least squares discriminant analysis, and orthogonal partial least squares discriminant analysis. The differences in metabolites between the different treatments were analyzed by a *t*-test and one-way analysis of variance (ANOVA; Zhao et al., 2020). The metabolites were mapped to the KEGG metabolic pathways for pathway and enrichment analyses.

2.5 Statistical analysis

The data were analyzed statistically with Statistical analysis System (SAS) 9.20 (SAS Institute, Cary, NC, USA) using a one-way analysis of variance (ANOVA), and multiple comparisons were performed based on the results of significance tests with the least significant difference method. Those with a *P*-value of *t*-test <0.05 and VIP ≥ 1 were considered differential metabolites between the two groups, and all the treatments had three biological replicates.

3 Results

3.1 Phosphate fertilizer affects the phenotypic and physiological characteristics of alfalfa

The phenotypes of alfalfa roots varied under different P treatments, and the growth and development of alfalfa roots were improved by the application of P (Figure 1A). The application of P reduced the depth of the root crown by 12.3% and 21.4% at P1 and P4 compared with the CK, respectively (Figure 1BI). The morphological indices of alfalfa increased during the P1 and P4 treatments compared with the CK. For example, the diameter of the root crown in the P1 and P4 treatments increased by 13.5% and 32.8%, respectively, while the number of branch roots from root crowns increased by 35.3% and 47.1%, respectively (Figure 1BII, III). The root dry weight increased by 48.8% and 59.3% at P1 and P4 compared with the CK, respectively (Figure 1BIV). The physiological indices of soluble sugar and soluble protein of the alfalfa roots increased following the application of P. The contents of soluble sugar in the P1 and P4 treatments increased by

1 http://www.r-project.org/

2 http://www.massbank.jp/

3 http://www.hmdb.ca/

4 http://www.ab.wur.nl/moto/

5 http://metlin.scripps.edu/index.php

10.3389/fpls.2023.1100601

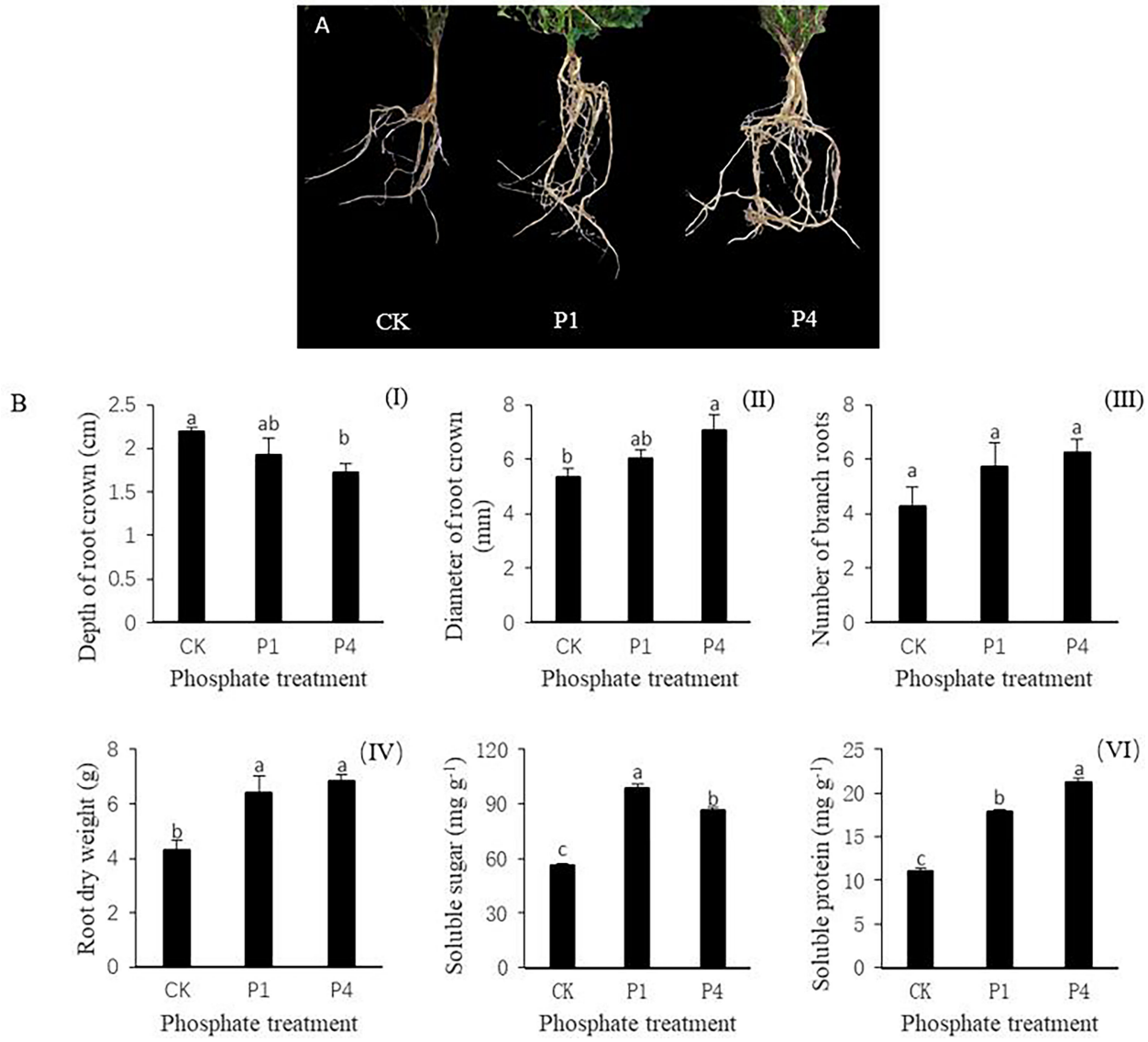

FIGURE 1
The responses of alfalfa phenotypic and physiological indices to phosphate (P) application under low temperature. **(A)** Alfalfa roots exposed to P application showed improved root growth. **(B)** Changes in the morphological and physiological indices of alfalfa roots, including (I) the depth of the root crown into the soil surface, (II) the diameter of the root crown, (III) the number of branch roots, (IV) root dry weight, (V) soluble sugar, and (IV) soluble protein. Values labeled with different lowercase letters indicate a significant difference between the P treatments at $P< 0.05$. CK, P1, and P4 represent 0, 50, and 200 P_2O_5 mg kg^{-1}.

76.6% and 54.5%, respectively, while those of the soluble protein increased by 62.5% and 92.7% compared with the CK, respectively (Figure 1BV, VI).

3.2 RNA Sequencing profiles of alfalfa roots in response to phosphate at low temperature

The analysis of DEGs was performed using edge R software under different P conditions. The results are shown in Figure 2. Compared with the CK, 49 genes were differentially expressed under the P1 conditions, with 23 genes upregulated and 26 genes downregulated. Compared with the CK, there were 224 DEGs under the P4 conditions, with 173 genes upregulated and 51 genes downregulated. Compared with P1, there were 392 DEGs under the P4 conditions, with 329 upregulated and 63 downregulated.

To further understand the functions and the related biological process that the DEGs participated in, GO enrichment analyses were conducted, and the results are shown in Figure 3. The DEGs were classified into cellular components, molecular functions, and biological processes. With the cellular component, the enriched GO terms of the three comparison groups were the cell, cell part, organelle, and membrane, membrane part, and organelle part. In addition, CK-*vs*-P4 and P1-*vs*-P4 were enriched in the cell junction, extracellular region, and macromolecular complex. Within the molecular function, the

10.3389/fpls.2023.1100601

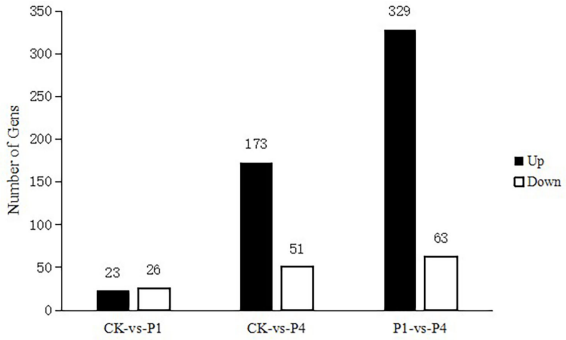

FIGURE 2
The total number of differentially expressed genes (DEGs) and upregulated and downregulated DEGs under different P treatments. DEGs, differentially expressed genes; P, phosphate.

enriched GO terms of three comparison groups were catalytic activity and binding. In addition, P1-*vs*-P4 was also enriched in antioxidant activity and transporter activity. Within the biological process, the enriched GO terms of three comparison groups were metabolic process, cellular process, single-organism process, response to stimulus, biological regulation, and localization. In addition, CK-*vs*-P4 and P1-*vs*-P4 were enriched in the developmental process, multicellular organismal process, multi-organism process,

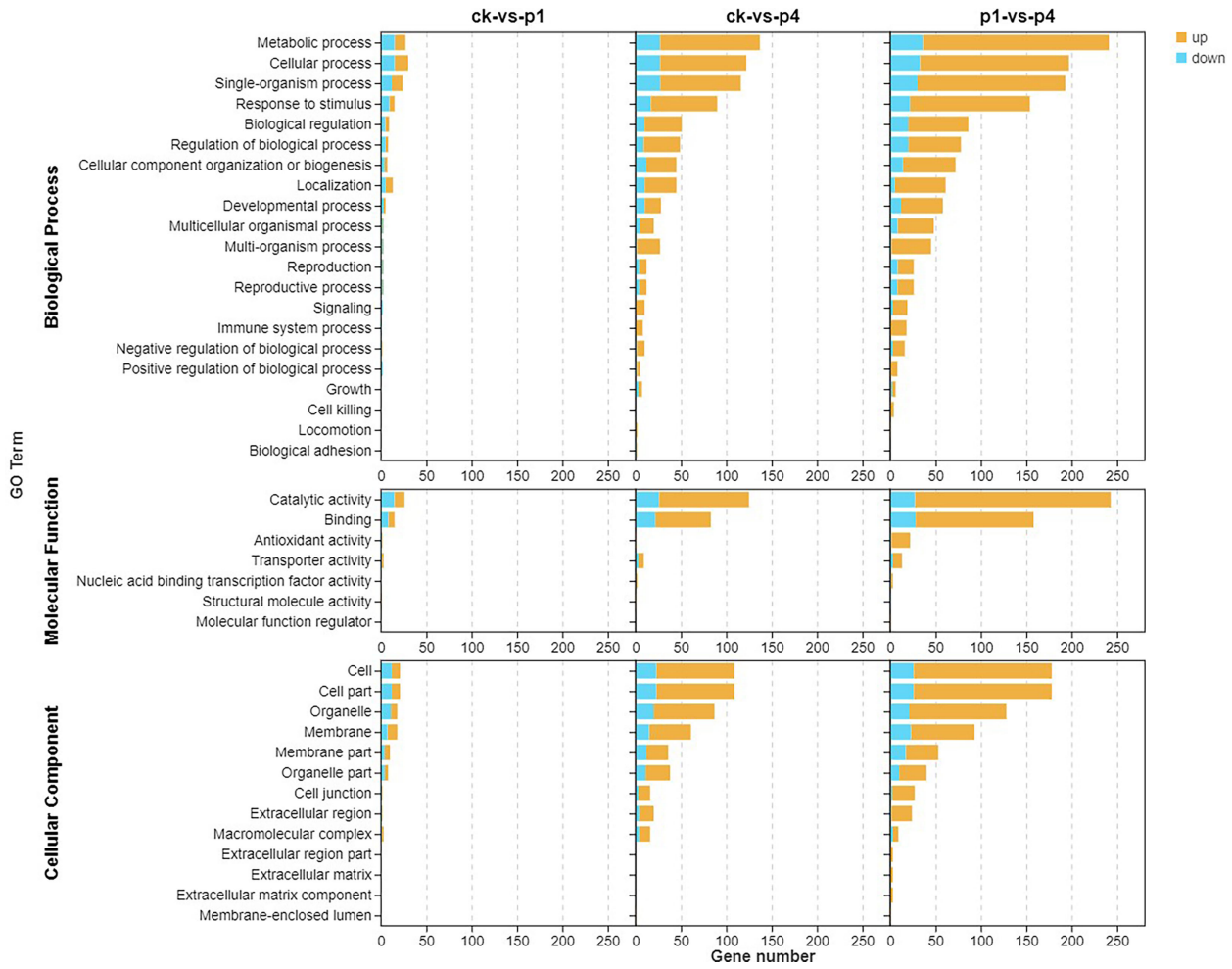

FIGURE 3
Gene Ontology (GO) enrichment analysis of the DEGs after cooling under different P treatments. DEGs, differentially expressed genes; GO, Gene Ontology; P, phosphate.

reproduction, reproductive process, signaling, immune system process, and negative and positive regulation of the biological process. These results indicated that the DEGs induced by P could be enriched into multiple GO terms, and the number of GO terms and upregulated genes increased with the increase in the application of P.

The pathway enrichment of the DEGs was analyzed using KEGG, and results are shown in Figure 4. The DEGs of CK-*vs*-P1 were primarily enriched in the biosynthesis of other secondary metabolites, carbohydrate metabolism, amino acid metabolism, and metabolism of other amino acids. The DEGs of CK-*vs*-P4 were enriched in not only the metabolic pathways described above but also the folding, sorting and degradation, transcription, and translation of genetic information processing and signal transduction and transport and catabolism. The DEGs of P1-*vs*-P4 were enriched in not only the same pathways of CK-*vs*-P4 but also the metabolism of terpenoids and polyketides and lipid metabolism. These results indicated that the number of KEGG pathways increased with the increase in P application.

3.3 Verification by real-time quantitative reverse transcription PCR

In addition to detecting metabolites to verify the RNA-Seq results, we used qRT-PCR to analyze six key upregulated genes to verify the results of the detection of transcriptional gene expression. The results are shown in Figure S2. The qRT-PCR verification results of the selected genes obtained using qRT-PCR were consistent with the expression data obtained by the corresponding RNA-seq, indicating that the RNA-seq expression data obtained are accurate and reliable.

3.4 Metabolite profiles of alfalfa roots in response to phosphate at low temperature

To obtain an overview of metabolic changes in response to the availability of P, a non-targeted metabolic analysis was performed. As shown in Figure 5, 24 metabolites were determined as having differential levels under P1 treatment compared with the CK. Among them, 12 metabolites increased, and 12 metabolites decreased. Compared with the CK, 12 metabolites were differentially produced under P4 treatment, and six of these metabolites increased, while six metabolites decreased. Compared with P1, 23 metabolites were determined as having differential levels under the P4 treatment. Among them, 10 metabolites increased, and 13 metabolites decreased. The primary types of metabolites that changed after the application of P were as follows: amino acids and derivatives, flavonoids, lipids, nucleotides and derivatives, organic acids, sugar, phenolic acids, and terpenoids. The types of variation in the specific metabolites and the main profile of metabolites that changed under the different P treatments are shown in Table S2.

KEGG metabolic pathway enrichment analysis classified the differential metabolites identified under low and high P treatments into metabolism, genetic information processing, environmental information processing, and human diseases (Figure 6). Within the metabolism, all three comparison groups were enriched in the biosynthesis of other secondary metabolites, amino acid metabolism, and lipid metabolism. In addition to these pathways, CK-*vs*-P4 and P1-*vs*-P4 were enriched in carbohydrate metabolism, energy metabolism, and the metabolism of other amino acids. These results indicated that the metabolic progress of alfalfa was significantly affected by P fertilizer at low temperature, and the application of increased amounts of P had a greater effect on metabolism.

3.5 Integrated metabolome and transcriptome analyses of alfalfa

The integration of the DEGs and metabolites obtained from different P levels of alfalfa identified several metabolic pathways of coenrichment (Figure 7). The DEGs and metabolites of the CK and P1 had three common annotated metabolic pathways, including fatty acid degradation, phenyl propionic acid biosynthesis, and the biosynthesis of secondary metabolites. The DEGs and metabolites

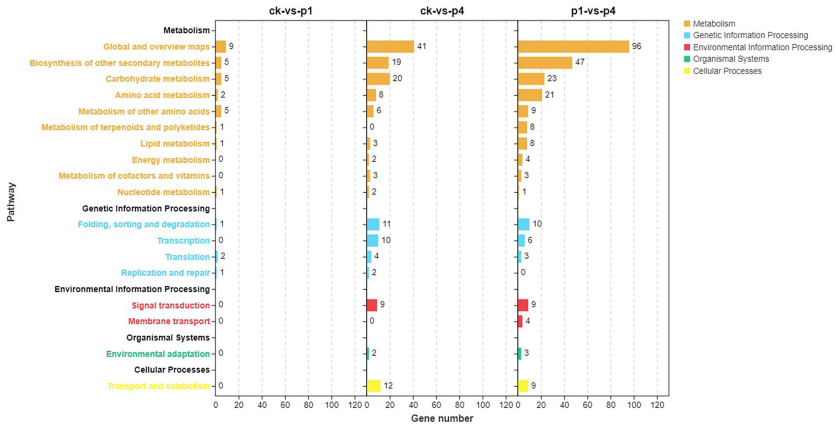

FIGURE 4
Kyoto Encyclopedia of Genes and Genomes (KEGG) pathway analysis of DEGs after cooling under different P treatments. DEGs, differentially expressed genes; KEGG, Kyoto Encyclopedia of Genes and Genomes; P, phosphate.

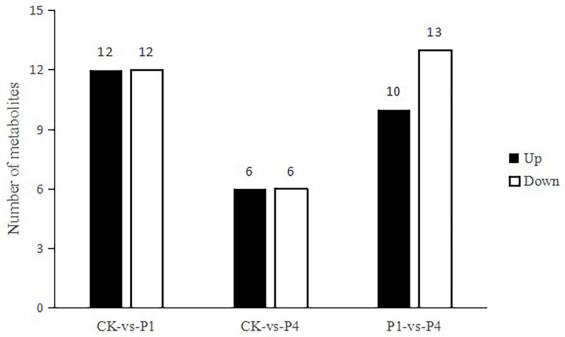

FIGURE 5
The total number of differential metabolites with differential levels, upregulated and downregulated, under different P treatments.

of CK and P4 had 12 common metabolic pathways, including the biosynthesis of secondary metabolites, biosynthesis of amino acids, sulfur metabolism, cyanoamino acid metabolism, ATP-binding cassette (ABC) transporters, cysteine and methionine metabolism, galactose metabolism, 2-oxocarboxylic acid metabolism, carbon metabolism, glyoxylate and dicarboxylate metabolism, aminoacyl-tRNA biosynthesis, and phenylalanine metabolism. The DEGs and metabolites of P1 and P4 had 15 common annotated metabolic pathways, including the biosynthesis of secondary metabolites, cysteine and methionine metabolism, biosynthesis of flavonoid, biosynthesis of isoflavone, biosynthesis of amino acid, sulfur metabolism, cyanoamino acid metabolism, ABC transporter, flavonoid and flavonol biosynthesis, 2-oxocarboxylic acid metabolism, aminoacyl-tRNA biosynthesis, phenylalanine metabolism, citrate cycle, and glyoxylate and dicarboxylate metabolism. The metabolic pathways of phenyl propionic acid biosynthesis and the biosynthesis of secondary metabolites were shared by the three groups.

The related genes and metabolites in carbohydrate metabolism, amino acid metabolism, and the carbon metabolism pathway were combined in the three comparison groups with different rates of P applied, and the correlation between metabolites and genes was analyzed (Figure 8). Among them, N-acetyl-L-phenylalanine and L-serine are the primary metabolites that are related to amino acid metabolism, and there are 21 related genes. The level of production of N-acetyl-L-phenylalanine positively correlated with the following genes: *methionine gamma-lyase* (*MGL*) and *homocysteine S-methyltransferase 3* (*HMT3*, MS. gene006429 and MS. gene34360). The production of L-serine positively correlated with *methionine gamma-lyase* (*MGL*), *homocysteine S-methyltransferase 3*(*HMT3*, MS. gene006429 and MS. gene34360), *beta-cyanoalanine synthase* (*CAS1*, MS. gene054826, MS. gene058651 and MS. gene023918), *1-aminocyclopropane-1-carboxylate oxidase 1* (*ACO1*, MS. gene98564, MS. gene75722, and MS. gene79848), *beta glucosidase 11* (*BGLU11*, MS. gene70075, MS. gene037510, and MSTRG.1088), *protein PAT1 homolog* (*PAT*), *cysteine synthase/L-3-cyanoalanine synthase* (*CAS2*), and *S-adenosylmethionine synthase* (*SAMS2*). The primary metabolites related to carbon metabolism were lactose, isocitrate, and L-serine, and there were five related genes in which the production of lactose positively correlated with the gene *RFS6* (r = 0.62). The level of production of isocitrate did not significantly correlate with the genes, and the production of L-serine positively correlated with *RFS1* (r = 0.76).

4 Discussion

4.1 Effect of P fertilizer on the phenotypical and physiological indices of alfalfa during the increase in cold weather

Roots are the source of all the mineral elements required for plant growth; thus, root growth and development are highly plastic and vary substantially depending upon numerous soil factors

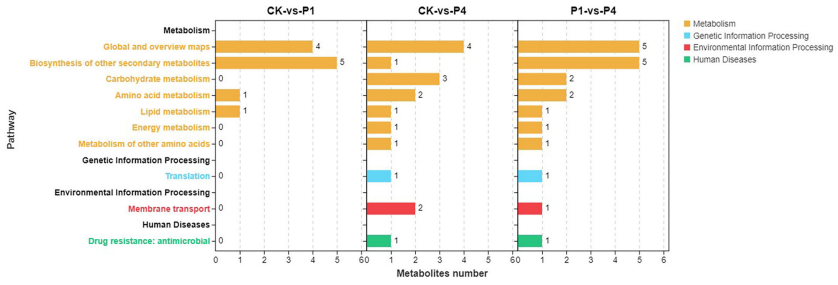

FIGURE 6
KEGG pathway enrichment analysis of the changed metabolites under different P treatments. KEGG, Kyoto Encyclopedia of Genes and Genomes.

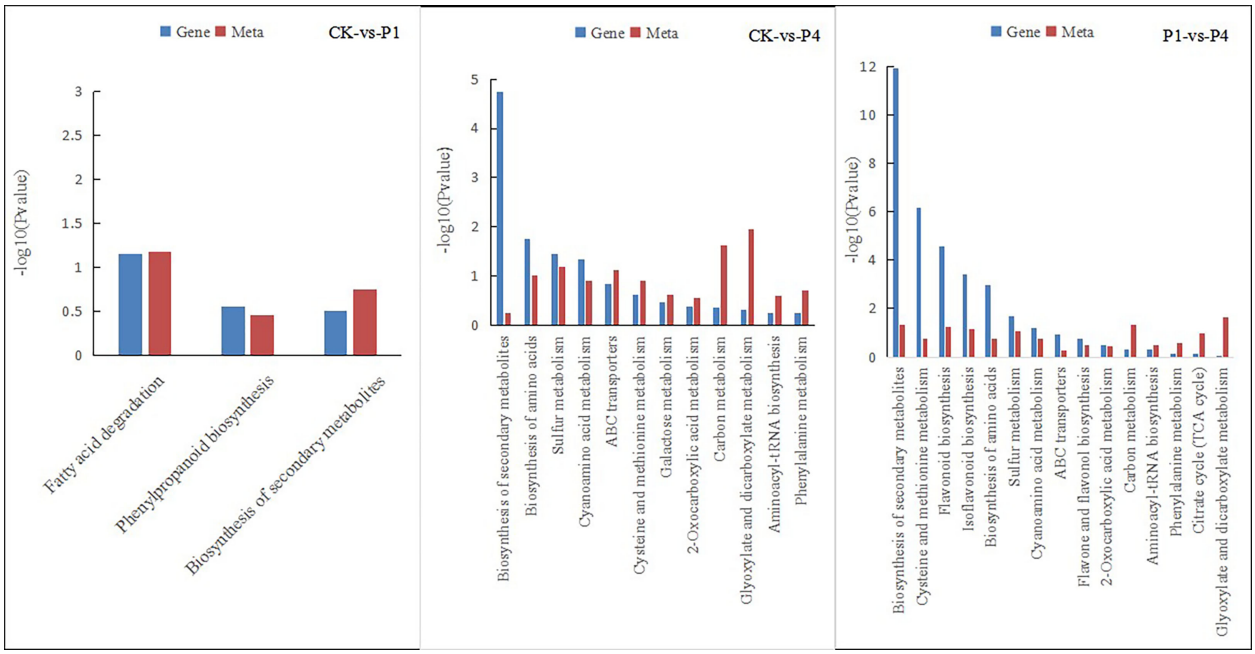

FIGURE 7
Pathways of the simultaneous annotation of differential metabolites and DEGs for different P treatments. DEGs, differentially expressed genes; P, phosphate.

(Vance et al., 2003). The root biomass is related to the accumulation of organic matter, which can contribute to improve the cold resistance of plants (Li et al., 2021). The root crown is the transitional plant structure located between the shoots and the root system, and it can influence photosynthate translocation, water transport, winter hardiness, and spring regrowth (Marquez-Ortiz et al., 1999). Alfalfa plants with deep and large root crowns survived the winter better than the plants with shallow and small root crowns (Marquez-Ortiz et al., 1999; Liu et al., 2015b; Wang et al., 2023). In addition, alfalfa with more lateral roots have strong cold resistance,

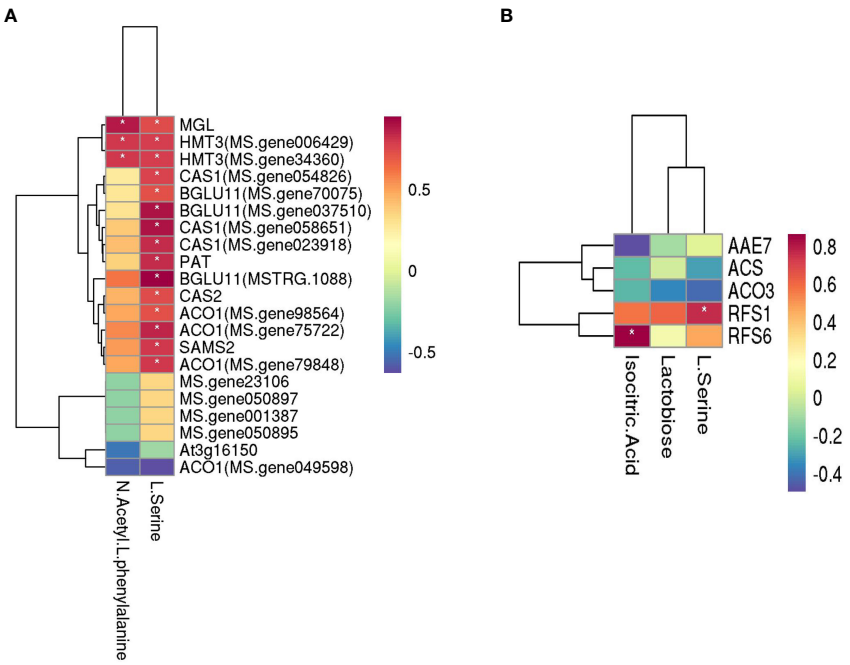

FIGURE 8
Heatmaps of amino acid metabolism and carbohydrate metabolism with the genes of three P comparison group units. **(A)** Amino acid metabolism and **(B)** carbohydrate metabolism. The darker the color (red or blue), the stronger the correlation. * means that the correlation between metabolite and gene was significant.

and the possession of more lateral roots facilitates the absorption of more nutrients and water from the soil to meet the nutritional needs of overwintering alfalfa plants (Liu et al., 2015b). Previous research had proven the effect of a localized supply of soil P on the root proliferation of plants (Vance et al., 2003; Gruber et al., 2013). In this study, the cutting seedings had no obvious taproot, and the branch roots grew directly from the lower end of the root crown. The application of P fertilizer promoted the development of the root crown, widened the root crown, and increased the dry root weight. However, the increase in the number of branch roots was not apparent, and the depth of root crown was reduced. Our results showed that the application of P fertilizer can promote the development of the root system, particularly the root crown to some extent, and improve the cold resistance of alfalfa, which also facilitates the growth and development of alfalfa.

Soluble sugars and soluble proteins are intracellular osmotic regulators, which can be increased by stress, thus, improving the adaptability of plants to respond to stress (Zhao et al., 2015). Under low-temperature stress, amino acids, such as proline, arginine, and methionine, and soluble sugars, such as sucrose, glucose, and raffinose, accumulate in the root crowns, roots, and leaves of alfalfa (Zhang et al., 2015). In addition to reducing water loss, the enormous accumulation of these solutes can also prevent the cells from freezing and help to stabilize membrane integrity (Duca and Maria, 2015). As the amount of low-temperature stress increased, the contents of soluble protein and soluble sugar in the alfalfa root crown increased (Tao et al., 2009; Zhu et al., 2021) and improved the cold resistance of alfalfa. When the temperature increased, the resistance disappeared, and the sugar and protein content decreased (Zhang, 2008). P is an essential element in the composition of cells, which can participate in the composition of nuclear protein, lecithin, enzymes, ATP, and ADP among others and has an important impact on the synthesis, transport, and storage of sugar (Chen et al., 2013). P can enhance N fixation by legumes, promote fat metabolism, and enhance the stress resistance of crops. These changes occur because P can increase the content of soluble sugar and phospholipids in plants. Soluble sugar can reduce the freezing point of cell cytoplasm, and phospholipid can improve the adaptability of cells to temperature changes, thus, enhancing the cold resistance of crops (Wang et al., 2016). We found that the contents of soluble sugar and soluble protein both increased during exposure to increasing amounts of cold when P was applied, which is consistent with the findings of Shen et al. (2017).

4.2 Effect of P on the transcriptome of alfalfa roots under low-temperature stress

In general, when plants are subjected to low-temperature stress, they will change at the transcriptome level to resist the damage caused by low temperatures (Qi, 2017). Plant-specific upregulated DEGs under low-temperature stress play a more critical role in determining plant cold resistance than downregulated DEGs, and a higher percentage of upregulated genes increases the resistance of plants to cold (Zhang, 2015). In this study, we found that the P fertilizer had a substantial effect on the expression of alfalfa genes at low temperatures, and the number of DEGs and upregulated DEGs increased with the increase in P application.

Several key genes were detected in alfalfa following the application of P (Table S1). Cold regulated (*COR*) genes are genes that respond to low temperatures and are expressed by the regulation of a specific signal transduction pathway, and the products of *COR* genes are cryoprotective proteins that act by reducing membrane permeability during freezing and increasing the ability of membranes to expand during thawing (Wu et al., 2012). Thus, the constitutive expression of the *COR* genes could improve the freezing tolerance of plants. The novel cold-regulated genes *CsCOR1* and *CbCOR15* enhance dehydration tolerance in tobacco (*Nicotiana benthamiana*) (Li et al., 2010; Wu et al., 2012). Sangwan et al. (2001) proved that the rigidification of the plasma membrane could induce *COR* genes and result in cold acclimation. In this study, the expression of *COR* was upregulated under the application of P, which enhanced the cold resistance of alfalfa. *CYP71D10* (*P450*) is a protein-coding gene present in plants, which have an immense variety of P450s that act on different substrates. The differential activities of P450s are believed to represent one of the mechanisms that enables certain crops species to be more tolerant of abiotic stress than other crops, particularly following herbicide treatment (Siminszky et al., 1999). Our research proved that the application of P under low temperatures could enrich the expression of a *P450* that plays a vital role in cold tolerance. *PAT* is a photonuclear aspartate aminotransferase, which has not only the activity of ASPAT but also the activity of prephenate transaminase. It is primarily located in the cytoplasm, mitochondria, and plastids and is involved in not only plant metabolism but also the abiotic stress response pathways of plants (Wei et al., 2022). *PAT* reduces the accumulation of ROS and protects the structural integrity of cell membranes, which improves the abiotic tolerance stress of plants (Tian, 2021). *S-adenosyl methionine synthetase* (*SAMS*) uses L-methionine as a substrate, and ATP provides the energy to catalyze the synthesis of S-adenosylmethionine, which plays a very important role in the responses of plants to stress (Roje, 2006). Zhang et al. (2020) confirmed that the overexpression of *SlSAMS1* significantly reduced the accumulation of superoxide (O_2^-), hydrogen peroxide (H_2O_2) and malondialdehyde and enhanced the contents of abscisic acid and the enzymes that scavenge ROS, including superoxide dismutase, catalase, and ascorbate peroxidase, and plays an important role in improving the drought and salt tolerance of transgenic tomato (*Solanum lycopersicum* L.). Guo et al. (2014) showed that the overexpression of *MfSAMS1* promoted polyamine synthesis and oxidation, which, in turn, improved the induction of protection against antioxidants by H_2O_2. As a result, this enhanced the tolerance to freezing and chilling stress in transgenic alfalfa plants. Our study proved that the expression of *SAMS* in the root crown of alfalfa treated with P was enhanced, which improved the plant's resistance to cold. *HSP70* plays an important role in plant growth and development and responds to various abiotic stresses, such as heat, drought, salinization, hormones, and other environmental perturbations (Cho and Choi, 2009; Montero-Barrientos et al., 2010; Usman et al., 2017). In heat-

tolerant varieties of pepper (*Capsicum annuum* L.), the level of expression of *CaHsp70* was rapidly upregulated upon heat stress, and the thermal stability of biofilm was simultaneously enhanced (Usman et al., 2015). Lv et al. (2022) found that the expression of *JcHsp70s* and its corresponding miRNAs, which are highly responsive to low temperature, is generally negatively regulated, and the interaction between *JcHsp70s* and miRNAs may be involved in the process of improving the cold tolerance of purging nut (*Jatropha curcas* L.) under low temperatures. In this study, treatment with P fertilizer also increased the expression of *HSP70* in the root crown of alfalfa under low-temperature stress. In addition, there are other DEGs owing to the application of P fertilizer. These DEGs were enriched in three metabolic pathways, including the biosynthesis of other secondary metabolites, carbohydrate metabolism, and amino acid metabolism. They can also be involved in scavenging excess ROS, supplying energy, and maintaining cell osmotic pressure under low-temperature stress, which are very important for alfalfa to survive over the winter.

4.3 Effects of phosphate on the metabolism of alfalfa roots under low-temperature stress

The changes in plant metabolites under stress can reflect the ability of plants to adapt to stress. Plants accumulate different sugars and amino acids under low-temperature stress, such as trehalose, glucose, fructose, inositol, galactitol, raffinose, sucrose, putrescine, ascorbate, phenylalanine, and alanine (Jin et al., 2017). Under the influence of external substances, the expression of metabolites in plants will also change after responding to low-temperature stress (Zhou et al., 2017). Flavonoids are important secondary metabolites, which can enhance plant resistance and chemical defenses, thus, improving the tolerance of plants to abiotic stress (Zhu et al., 2007; Liu et al., 2015a). When plants are injured, secondary metabolites, such as alkaloids and polyphenolic acids, will gradually accumulate and form defense structures, thus, enhancing plant resistance (Hu et al., 2012). Terpenoids can directly or indirectly participate in a series of biological processes, such as hormone synthesis, cell membrane stability, and photosynthesis in plants. Plants can improve their ability to protect and defend themselves by regulating the content of terpenoids. Sugar metabolism is a critical metabolic cycle process in plant growth and development, and providing energy is the primary function of sugar metabolism. Secondly, sugar synthesis metabolism can also play an important role in the response of plants to abiotic stress (Sambe et al., 2015). Plants with low external levels of Pi have serious problems maintaining a balanced ratio of sugars, lipids, amino acids, organic acids, terpenes, and flavonoids, but the application of P can improve this situation (Mo et al., 2019; Ding et al., 2021; Nasr Esfahani et al., 2021). In this experiment, the application of P could regulate the types and contents of metabolites. When a small amount of P fertilizer is applied, it primarily affects the biosynthesis of secondary metabolites, while the application of more P fertilizer primarily affects the biosynthesis of secondary metabolites, amino acid metabolism, carbohydrate metabolism, and others.

4.4 Integrated metabolome and transcriptome analysis revealed the mechanism used by phospate to improve cold tolerance

The mechanism of cold resistance of alfalfa is very complex and involves morphology, physiology and biochemistry, molecular, transcription, and metabolism. Hence, it is crucial to integrate a variety of combinatorial techniques to comprehensively analyze the mechanism of the cold resistance of alfalfa (Wang and Xu, 2021). During cold acclimation, root morphology and the synthesis of compatible solutes were closely related to the cold resistance of alfalfa. Less root mass and lower concentrations of root total non-structural carbohydrates can minimize the survival of plants over the winter when the plants are subjected to low temperatures (Castonguay et al., 2006). The crown depth below the soil surface is viewed as a key morphological adaptation for forage legumes to overwinter successfully. The alfalfa varieties that have more branch rooting in general were better able to resist cold than the varieties that have a taproot or fewer types of branch roots (Johnson et al., 1998). The accumulation of soluble sugars under low temperature plays an important role in the acquisition of cold tolerance in plants (Guy, 1990). Several proteins were increasingly or newly synthesized during the acclimation of alfalfa to the cold (Mohapatra et al., 1987). Simultaneously, free amino acids were shown to accumulate in the taproots and crowns (Hendershot and Volenec, 1993; Dhont et al., 2003). The increase in free proline was notable, and the concentrations of arginine and histidine were also markedly increased (Dhont et al., 2003). In this study, the application of P fertilizer significantly changed the traits of root system architecture and increased the contents of soluble sugar and protein during the cold accumulation period. In addition, there were commonly annotated pathways shared by the transcriptome and metabolome. Thus, the application of P fertilizer influences the cold tolerance of alfalfa. With the increase in the application of P, the common metabolic pathways for the enrichment of DEGs and metabolites affected by P gradually increased. The biosynthesis of amino acids is regulated by a compound metabolic network that links N assimilation with carbon metabolism (Hans et al., 2008). Carbohydrate metabolism is the most important basic metabolism in the plant, which provides the necessary carbon frame and energy to synthesize amino acids, proteins, and nucleic acids in N metabolism. Under low-temperature stress, the application of P primarily affected the contents of L-serine, N-acetyl-L-phenylalanine, isocitrate, and lactobiose. A correlation analysis revealed that the production of L-serine positively correlated with *MGL*, *HMT3*, *CAS1*, *BGLU11*, *PAT*, *CAS2*, *ACO1*, *SAMS2*, and *RFS1*. N-acetyl-L-phenylalanine positively correlated with *MGL* and *HMT3*, and lactobiose positively correlated with *RFS6*. Among them, *RFS1* and *RFS6* are related to the synthesis of raffinose synthase, which is a crucial enzyme in the raffinose metabolism pathway. This pathway can catalyze the reaction of inositol galactoside and sucrose to raffinose, and they can also catalyze the reaction of inositol galactoside and raffinose to synthesize stachyose. Its expression can be regulated by various

stress response signals and transcription factors (Nishizawa et al., 2008; Cho et al., 2010). *SAMS2* facilitates the synthesis of S-adenosyl methionine synthetase and can be induced by a variety of stress factors; its overexpression can significantly improve the resistance to plant stress (Guo et al., 2014). The overexpression of *PAT* increased the contents of proline and soluble sugar in transgenic *Arabidopsis thaliana* and improved the cold, drought, and saline–alkali tolerance of plants (Yuan et al., 2016). Other genes also play essential roles in the synthesis and metabolism of amino acids and carbohydrates. Thus, the moderate application of P fertilizer can improve the cold resistance of alfalfa by regulating the synthesis and metabolism of amino acids and sugars.

5 Conclusion

Low-temperature stress affects the growth and development of alfalfa, leading to morphological, physiological, metabolic, and molecular changes and, thus, limits the overwintering and production of alfalfa. The application of P can improve the cold resistance and forage yield of alfalfa. In this study, we analyzed the changes of alfalfa under low-temperature stress by transcriptomic and metabolomic approaches after the application of P. We found that the application of P fertilizer improved the root structure and increased the content of soluble sugar and soluble protein in the root crown, and there were 49 DEGs (23 genes upregulated) and 24 metabolites (12 upregulated) following 50 mg kg^{-1} of P applied and 224 DEGs (173 genes upregulated) and 12 metabolites (6 upregulated) following 200 mg kg^{-1} of P applied, respectively, compared with the CK. These genes and metabolites were significantly enriched in the biosynthesis of other secondary metabolites, carbohydrate metabolism, and amino acid metabolism pathways. The integration of the transcriptomic and metabolomic analyses showed that P could affect the biosynthesis of N-acetyl-L-phenylalanine, L-serine, lactose, and isocitrate and the expression of related genes to regulate the cold tolerance of alfalfa. Our findings could contribute to a deeper understanding of the mechanism that alfalfa uses to respond to cold tolerance and lay a theoretical foundation for breeding highly P-efficient alfalfa.

Data availability statement

The data presented in the study are deposited in the NCBI repository, accession number PRJNA909902. The data has been released.

Author contributions

YW, LY and JX designed the experiment. YW, ZS and QW collected the samples in the field, and YW and ZS conducted laboratory analyses. YW analyzed the data, interpreted the results, and wrote the manuscript. All authors reviewed and edited the manuscript and approved the submitted version.

Funding

This research was financially supported by the Inner Mongolia Science and Technology Program (2019GG260), Achievement Transformation Project in Science and Technology of Inner Mongolia (2019CG041), High level talent introduction project of Inner Mongolia University (10000-22311201/016), Alfalfa breeding for high quality and industry demonstration (2022JBGS0020). The funding body had no contribution to the study design, data collection, analysis, interpretation of the data, the writing of this article, or the decision to submit for publication.

Acknowledgments

The authors are grateful for the sequencing platform and/or bioinformation analysis of Gene Denovo Biotechnology Co., Ltd (Guangzhou, China). We would like to thank MogoEdit (https://www.mogoedit.com) for its English editing during the preparation of this manuscript.

Conflict of interest

The authors declare that the research was conducted in the absence of any commercial or financial relationships that could be construed as a potential conflict of interest.

Publisher's note

Supplementary material

The Supplementary Material for this article can be found online at: https://www.frontiersin.org/articles/10.3389/fpls.2023.1100601/full#supplementary-material

References

Acharya, J. P., Lopez, Y., Gouveia, B. T., de Bem Oliverira, I., Resende, M. F. R., Munoz, P. R., et al. (2020). Breeding alfalfa (*Medicago sativa* l.) adapted to subtropical agroecosystems. *Agronomy* 10 (5), 1–13. doi: 10.3390/agronomy10050742

Agarrwal, R., Padmakumari, A. P., Bentur, J. S., and Nair, S. (2016). Metabolic and transcriptomic changes induced in host during hypersensitive response mediated resistance in rice against the Asian rice gall midge. *Rice* 9, 5. doi: 10.1186/s12284-016-0077-6

Bao, G., Tang, W., An, Q., Liu, Y., Tian, J., Zhao, N., et al. (2020). Physiological effects of the combined stresses of freezing-thawing, acid precipitation and deicing salt on alfalfa seedlings. *BMC Plant Biol.* 20 (1), 204. doi: 10.1186/s12870-020-02413-4

Bertrand, A., Bipfubusa, M., Claessens, A., Rocher, S., and Castonguay, Y. (2017). Effect of photoperiod prior to cold acclimation on freezing tolerance and carbohydrate metabolism in alfalfa (Medicago sativa l.). *Plant Sci.* 264, 122–128. doi: 10.1016/j.plantsci.2017.09.003

Bhosale, R., Giri, J., Pandey, B. K., Giehl, R. F. H., Hartmann, A., Traini, R., et al. (2018). A mechanistic framework for auxin dependent arabidopsis root hair elongation to low external phosphate. *Nat. Commun.* 9 (1), 1409. doi: 10.1038/s41467-018-03851-3

Castonguay, Y., Laberge, S., Brummer, E. C., and Volenec, J. J. (2006). Alfalfa winter hardiness: A research retrospective and integrated perspective. *Adv. Agric.* 90, 203–265. doi: 10.1016/s0065-2113(06)90006-6

Chen, W., Gong, L., Guo, Z., Wang, W., Zhang, H., Liu, X., et al. (2013). A novel integrated method for large-scale detection, identification, and quantification of widely targeted metabolites: Application in the study of rice metabolomics. *Mol. Plant* 6 (6), 1769–1780. doi: 10.1093/mp/sst080

Chen, H., Zeng, Y., Yang, Y., Huang, L., Tang, B., Zhang, H., et al. (2020). Allele-aware chromosome-level genome assembly and efficient transgene-free genome editing for the autotetraploid cultivated alfalfa. *Nat. Commun.* 11 (1), 2494. doi: 10.1038/s41467-020-16338-x

Chen, S., Zhou, Y., and Chen, Y. (2018). Fastp: An ultra-fast all-in-one FASTQ preprocessor. *Bioinformatics* 34 (17), 884–890. doi: 10.1093/bioinformatics/bty560

Cheng, G. (2008). *Effect of phosphorus on yield、quality、nutrient absorption and seedling cold tolerance of watermelon* (Wuhan: Huazhong Agricultural University).

Cho, E. K., and Choi, Y. J. (2009). A nuclear-localized HSP70 confers thermoprotective activity and drought-stress tolerance on plants. *Biotechnol. Lett.* 31 (4), 597–606. doi: 10.1007/s10529-008-9880-5

Cho, S., Kang, E., Kim, M., Yoo, S., Im, Y., Kim, Y., et al. (2010). Jasmonate-dependent expression of a alactinol synthase gene is involved in priming of systemic fungal resistance in arabidopsis thaliana. *Botany* 88, 452–461. doi: 10.1139/B10-009

Cunningham, S. M., Volenec, J. J., and Teuber, L. R. (1998). Plant survival and root and bud composition of alfalfa populations selected for contrasting fall dormancy. *Crop Sci.* 38 (4), 962–969. doi: 10.2135/cropsci1998.0011183X003800040014x

Dhont, C., Castonguay, Y., Nadeau, P., Bélanger, G., and Chalifour, F. P. (2003). Alfalfa root nitrogen reserves and regrowth potential in response to fall harvests. *Crop Sci.* 43 (1), 181–194. doi: 10.2135/cropsci2003.1810

Diatta, A. A., Min, D., and Jagadish, K. S. (2021). Drought stress responses in non-transgenic and transgenic alfalfa–current status and future research directions. *Adv. Agron.* 170, 2–66. doi: 10.1016/bs.agron.2021.06.002

Ding, N., Huertas, R., Torres-Jerez, I., Liu, W., Watson, B., Scheible, W. R., et al. (2021). Transcriptional, metabolic, physiological and developmental responses of switchgrass to phosphorus limitation. *Plant Cell Environ.* 44 (1), 186–202. doi: 10.1111/pce.13872

Dou, Y. M. (2011). Research progress on the mechanism of cold resistance of alfalfa in China. *Heilongjiang Agric. Sci.* 07, 146–148.

Du, S. (2021). *Metabolic mechanism of cold stress in rice(Oryza sativa l.) seedlings based on metabolome and transcriptome* (Nanchang: Nanchang University).

Duca,, and Maria, (2015). "Plant physiology || physiology of plant resistance to unfavorable environmental factors," in *Biological and medical physics, biomedical engineering*. Ed. B. S. Gerstman. (New York, NY: Springer), 271–308.

Edde, P. A. (2022). "Arthropod pests of alfalfa (Medicago sativa l.)," in *Field crop arthropod pests of economic importance,* ed. P. A. Edde. (Altria Client Services LLC, Richmond, VA, United States: Academic Press), 684–750.

Gaafar, Y., Richert-Pöggeler, K., Maaß, C., Vetten, H. J., and Ziebell, H. (2019). Characterisation of a novel nucleorhabdovirus infecting alfalfa (Medicago sativa). *Virol. J.* 16 (1), 55. doi: 10.1186/s12985-019-1147-3

Goplen, B. P. (1987). *Growing and managing alfalfa in Canada* (Ottawa K1A 0C7: Communications Branch, Agriculture Canada).

Gruber, B. D., Giehl, R. F., Friedel, S., and von Wiren, N. (2013). Plasticity of the arabidopsis root system under nutrient deficiencies. *Plant Physiol.* 163 (1), 161–179. doi: 10.1104/pp.113.218453

Guo, Z., Tan, J., Zhuo, C., Wang, C., Xiang, B., and Wang, Z. (2014). Abscisic acid, H2O2 and nitric oxide interactions mediated cold-induced s-adenosylmethionine synthetase in medicago sativa subsp. falcata that confers cold tolerance through up-regulating polyamine oxidation. *Plant Biotechnol. J.* 12 (5), 601–612. doi: 10.1111/pbi.12166

Guy, C. (1990). Cold acclimation and freezing stress tolerance: Role of protein metabolism. *Annu. Rev. Plant Physiol. Plant Molec. Biol.* 41, 187–224. doi: 10.1146/annurev.pp.41.060190.001155

Hans, J. B., Henry, N., and Norman, G. L. (2008). *Bioengineering and molecular biology of plant pathways* (Holland: ELsevier Publishing Group press).

Hendershot, K. L., and Volenec, J. J. (1993). Taproot nitrogen accumulation and use in overwintering alfalfa (Medicago sativa l.). *J. Plant Physiol.* 141 (1), 68–74. doi: 10.1016/s0176-1617(11)80853-9

Hong, F. Z., Wu, S. Y., Yu, K. F., Bai, Y. H., and Cheng, D. (1987). Study on introducing alfalfa with root tiller type. *Chin. pratacult. Sci.* 5, 1–4.

Hu, W., Jiang, J., Yang, H., Liu, C., and He, Y. (2012). Effect of jasmonic acid methyl ester treatment on the physiological and biochemical reactions of fresh-cut apple. *Sci. Technol. Food Ind.* 33 (16), 338–341+346. doi: 10.13386/j.issn1002-0306.2012.16.055

Hu, T., Sun, X. Y., Zhao, Z. J., Amombo, E., and Fu, J. M. (2020). High temperature damage to fatty acids and carbohydrate metabolism in tall fescue by coupling deep transcriptome and metabolome analysis. *Ecotoxicol. Environ. Saf.* 203, 110943. doi: 10.1016/j.ecoenv.2020.110943

Janz, D., Behnke, K., Schnitzler, J. P., Kanawati, B., Schmitt-Kopplin, P., and Polle, A. (2010). Pathway analysis of the transcriptome and metabolome of salt sensitive and tolerant poplar species reveals evolutionary adaption of stress tolerance mechanisms. *BMC Plant Biol.* 10, 150. doi: 10.1186/1471-2229-10-150

Jin, J., Zhang, H., Zhang, J., Liu, P., Chen, X., Li, Z., et al. (2017). Integrated transcriptomics and metabolomics analysis to characterize cold stress responses in nicotiana tabacum. *BMC Genomics* 18 (1), 496. doi: 10.1186/s12864-017-3871-7

Johnson, L. D., Marquez-Ortiz, J. J., Barnes, D. K., and Lam, J. F. S. (1996). Inheritance of root traits in alfalfa. *Crop Sci.* 36, 1482–1487. doi: 10.2135/cropsci1996.0011183X003600060011x

Johnson, L. D., Marquez-Ortiz, J. J., Lamb, J., and Barnes, D. (1998). Root morphology of alfalfa plant introductions and cultivars. *Crop Sci.* 38, 497–502. doi: 10.2135/cropsci1998.0011183X003800020037x

Kim, D., Langmead, B., and Salzberg., S. L. (2015). HISAT: A fast spliced aligner with low memory requirements. *Nat. Methods* 12 (4), 357. doi: 10.1038/nmeth.3317

Kontunen-Soppela, S., Lankila, J., Lähdesmäki, P., and Laine, K. (2002). Response of protein and carbohydrate metabolism of scots pine seedlings to low temperature. *J. Plant Physiol.* 159 (2), 175–180. doi: 10.1078/0176-1617-00538

Li, X. W., Feng, Z. G., Yang, H. M., Zhu, X. P., Liu, J., and Yuan, H. Y. (2010). A novel cold-regulated gene from camellia sinensis, CsCOR1, enhances salt- and dehydration-tolerance in tobacco. *Biochem. Biophys. Res. Commun.* 394 (2), 354–359. doi: 10.1016/j.bbrc.2010.03.011

Li, M., Shi, X., Guo, C., and Lin, S. (2016). Phosphorus deficiency inhibits cell division but not growth in the dinoflagellate amphidinium carterae. *Front. Microbiol.* 7. doi: 10.3389/fmicb.2016.00826

Li, Z., Wan, L., Li, S., Li, X., He, F., and Tong, Z. (2021). Plastic response of medicago sativa l. root system traits and cold resistance to simulated rainfall events. *PeerJ* 9, e11962. doi: 10.7717/peerj.11962

Lin, Z. H., Chen, R. B., and Guo, S. P. (2010). Research progress on physiological adaptability of plants to phosphorus deficiency. *Crops* 05), 5–9. doi: 10.16035/j.issn.1001-7283.2010.05.003

Liu, D., Li, M., Liu, Y., and Shi, L. (2020). Integration of the metabolome and transcriptome reveals the resistance mechanism to low nitrogen in wild soybean seedling roots. *Environ. Exp. Bot.* 175, 104043. doi: 10.1016/j.envexpbot.2020.104043

Liu, Z., Li, X., Wang, Z., and Sun, Q. (2015a). Contrasting strategies of alfalfa stem elongation in response to fall dormancy in early growth stage: The tradeoff between internode length and internode number. *PloS One* 10 (8), e0135934. doi: 10.1371/journal.pone.0135934

Liu, Z. Y., Xi-Liang, L. I., Feng, L. I., Tao, Y., Liu, L., Wang, Z. L., et al. (2015b). Response of alfalfa root traits to fall dormancy and its effect on winter hardiness. *Sci. Agricult. Sin.* 48 (9), 1689–1701. doi: 10.3864/j.issn.0578-1752.2015.09.03

Love, M. I., Huber, W., and Anders, S. (2014). Moderated estimation of fold change and dispersion for RNA-seq data with DESeq2. *Genome Biol.* 15 (12), 550. doi: 10.1186/s13059-014-0550-8

Lv, Y., Wu, D., Kong, C., Yang, Y., and Gong, M. (2022). Identification and interaction analysis of the Hsp70 gene family and the corresponding miRNAs and their possible roles in low temperature adaptation in jatropha curcas. *Plant Physiol. J.* 58 (7), 1–16. doi: 10.13592/j.cnki.ppj.100167

Marquez-Ortiz, J. J., Lamb, J. F. S., Johnson, L. D., Barnes, D. K., and Stucker, R. E. (1999). Heritability of crown traits in alfalfa. *Crop Sci.* 39, 38–43. doi: 10.2135/cropsci1999.0011183X003900010006x

Mo, X., Zhang, M., Liang, C., Cai, L., and Tian, J. (2019). Integration of metabolome and transcriptome analyses highlights soybean roots responding to phosphorus deficiency by modulating phosphorylated metabolite processes. *Plant Physiol. Biochem.* 139, 697–706. doi: 10.1016/j.plaphy.2019.04.033

Mohapatra, S. S., Poole, R. J., and Dhindsa, R. S. (1987). Changes in protein patterns and translatable messenger RNA populations during cold acclimation of alfalfa. *Plant Physiol. J.* 84 (4), 1172–1176. doi: 10.1104/pp.84.4.1172

Moieni-Korbekandi, Z., Karimzadeh, G., and Sharifi, M. (2013). Evaluation of total soluble protein and antioxidant activities in two spring cultivars of canola (Brassica napus l.) in response to low temperature. *Int. J. Agric. Crop Sci.* 5 (4), 401–409.

Montero-Barrientos, M., Hermosa, R., Cardoza, R. E., Gutiérrez, S., Nicolás, C., and Monte, E. (2010). Transgenic expression of the trichoderma harzianum hsp70 gene increases arabidopsis resistance to heat and other abiotic stresses. *J. Plant Physiol.* 167 (8), 659–665. doi: 10.1016/j.jplph.2009.11.012

Nasr Esfahani, M., Inoue, K., Nguyen, K. H., Chu, H. D., Watanabe, Y., Kanatani, A., et al. (2021). Phosphate or nitrate imbalance induces stronger molecular responses than combined nutrient deprivation in roots and leaves of chickpea plants. *Plant Cell Environ.* 44 (2), 574–597. doi: 10.1111/pce.13935

Nishizawa, A., Yabuta, Y., and Shigeoka, S. (2008). Galactinol and raffinose constitute a novel function to protect plants from oxidative damage. *Plant Physiol.* 147 (3), 1251–1263. doi: 10.1104/pp.108.122465

Putnam, D. H., Russelle, M. P., Orloff, S. B., Kuhn, J., Fitzhugh, L., and Godfrey, L. (2001). *Alfalfa, wildlife and the environment: The importance and benefit of alfalfa in the 21st century*. Minnesota: California Alfalfa and Forage Assiciation.

Qi, X. (2017). *The Analysis of the Differentially Expressed Genes in Alfalfa under Cold Stress at Transcriptome Level*. Doctor, Chinese Academy of Agricultural Science.

Raghothama, K., and Karthikeyan, A. (2005). "Phosphate acquisition," in *Root physiology: From gene to function*. Eds. H. Lambers and T. D. Colmer (New Y ork: Springer).

Robinson, M. D., McCarthy, D. J., and Smyth, G. K. (2010). edgeR: a bioconductor package for differential expression analysis of digital gene expression data. *Bioinformatics* 26 (1), 139–140. doi: 10.1093/bioinformatics/btp616

Rocher, S., Jean, M., Castonguay, Y., and Belzile, F. (2015). Validation of genotyping-By-Sequencing analysis in populations of tetraploid alfalfa by 454 sequencing. *PloS One* 10 (6), e0131918. doi: 10.1371/journal.pone.0131918

Roje, S. (2006). S-Adenosyl-L-methionine: Beyond the universal methyl group donor. *Phytochemistry* 67 (15), 1686–1698. doi: 10.1016/j.phytochem.2006.04.019

Sambe, M. A., He, X., Tu, Q., and Guo, Z. (2015). A cold-induced myo-inositol transporter-like gene confers tolerance to multiple abiotic stresses in transgenic tobacco plants. *Physiol. Plant* 153 (3), 355–364. doi: 10.1111/ppl.12249

Sangwan, V., Foulds, I., Singh, J., and Dhindsa, R. S. (2001). Cold-activation of brassica napus BN115 promoter is mediated by structural changes in membranes and cytoskeleton, and requires Ca2+ influx. *Plant J.* 27 (1), 1–12. doi: 10.1046/j.1365-313x.2001.01052.x

Shen, X., Zhang, Y., Wang, X., Li, Y., Guo, Y., and Yu, H. (2017). Effects of phosphorus and potassium fertilizer on the cold resistance of alfalfa roots and necks in sandy soil. *J. Inner Mongolia Univ. Natl.* 32 (2), 116–121.

Siminszky, B., Corbin, F. T., Ward, E. R., Fleischmann, T. J., and Dewey, R. E. (1999). Expression of a soybean cytochrome P450 monooxygenase cDNA in yeast and tobacco enhances the metabolism of phenylurea herbicides. *Proc. Natl. Acad. Sci. U.S.A.* 96, 1750–1755. doi: 10.1073/pnas.96.4.1750

Summers, C. G., and Putnam, D. H. (2008). *Irrigated alfalfa management for Mediterranean and desert zones* (Irvine, CA: University of California Alfalfa & Forages).

Tao, Y., Yu, Z., Sun, Q., and Zhao, S. (2009). Study on physiological adaptability of alfalfa for cold resistance. *Pratacult. Sci.* 26 (9), 151–155.

Terry, N., and Tao, I. M. (1991). *Nutrient and photosynthesis:iron and phosphorus as case studies* (University Printing House, Shaftesbury Rd, Cambridge CB2 8BS: Cambridge University Press).

Tian, Z. (2021). *Functional study on salt tolerance of PAT1 gene from betuia platyphylla* (Haerbin: Northest Forestry University).

Tian, Z. J., Li, J. P., and Yang, F. (2017). Progress in crop phosphorus utilization under abiotic stresses. *Chin. J. Ecol.* 36 (8), 2336–2342. doi: 10.13292/j.1000-4890.201708.002

Trischuk, R. G., Schilling, B. S., Low, N. H., Gray, G. R., and Gusta, L. V. (2014). Cold acclimation, de-acclimation and re-acclimation of spring canola, winter canola and winter wheat: The role of carbohydrates, cold-induced stress proteins and vernalization. *Environ. Exp. Bot.* 106, 156–163. doi: 10.1016/j.envexpbot.2014.02.013

Usman, M. G., Rafii, M. Y., Ismail, M. R., Malek, M. A., and Latif, M. A. (2015). Expression of target gene Hsp70 and membrane stability determine heat tolerance in chili pepper. *J. Am. Soc. Hortic. Sci. Am. Soc. Hortic. Sci.* 140 (2), 144–150. doi: 10.21273/JASHS.140.2.144

Usman, M. G., Rafii, M. Y., Martini, M. Y., Yusuff, O. A., and Miah, G. (2017). Molecular analysis of Hsp70 mechanisms in plants and their function in response to stress. *Biotechnol. Genet. Eng. Rev.* 33 (1), 1–14. doi: 10.1080/02648725.2017.1340546

Vance, C. P., Uhde-Stone, C., and Allan, D. L. (2003). Phosphorus acquisition and use critical adaptations by plants for securing a nonrenewable resource. *New Phytol.* 157, 423–447. doi: 10.1046/j.1469-8137.2003.00695.x

Viands, D. R. (1988). Variability and selection for characters associated with root regeneration capability in alfalfa. *Crop Sci.* 28 (2), 232–236. doi: 10.1007/BF02871603

Wang, X. (2021a). *Effect of fertilization and reseeding on the productivity, forage quality and soil properties of degraded alfalfa grassland* (Xining: Ningxia University).

Wang, X. L. (2021b). *Identification of cold tolerance and screening of cold tolerance germplasm of alfalfa* (Hohhot: Inner Mongolia Agricultural University).

Wang, R., and Xu, W. (2021). Development characteristics and trend of alfalfa industry in China. *J. Agric. Sci. Technol.* 23 (12), 7–12. doi: 10.13304/j.nykjdb.2021.0940

Wang, X., Yang, Z., Lai, Y.-c., Li, H., Zhong, P., Xu, Y.-x., et al. (2023). Effect of root traits of medicago sativa lines with fall dormancy on overwintering. *Acta Pratacult. Sin.* 32 (1), 144–153. doi: 10.11686/cyxb2022016

Wang, D., Yang, J., Rongsheng, L. I., Zou, W., and Yin, G. (2016). Physiological response of phoebe bournei seedlings with different phosphorus supply levels to natural low temperature. *J. South China Agric. Univ.* 37 (2), 101–106.

Wang, Y., Zhang, J., Yu, L., Xu, Z., and Samac, D. A. (2022). Overwintering and yield responses of two late-summer seeded alfalfa cultivars to phosphate supply. *Agronomy* 12, 327. doi: 10.3390/agronomy12020327

Wechsler, S. J., Milkove, D.U.S.D.O. AGRICULTURE (2017). *Genetically modified alfalfa production in the united states* (United States: Economic Research Service).

Wei, Z., Liu, C.-Y., Chen, H.-W., Li, L., Sun, L.-Q., Han, X.-S., et al. (2022). Analysis of ASPAT gene family based on drought-stressed transcriptome sequencing in vicia faba l. *Acta Agro. Sin.* 12, 1–12.

Wishart, D. S., Timothy, J., Chi, G. A., Michael, W., Craig, K., Liu, Y., et al. (2013). HMDB 3.0–the human metabolome database in 2013. *Nucleic Acids Res.* D1), D801.

Wu, H., Zhang, J., Shi, J., Fan, Z., Aliyan, R., and Zhang, P. (2013). Physiological responses of cotton seedlings under low temperature stress. *Acta Botanica Boreali-Occidentalia Sin.* 33 (1), 74–82.

Wu, L., Zhou, M., Shen, C., Liang, J., and Lin, J. (2012). Transgenic tobacco plants over expressing cold regulated protein CbCOR15b from capsella bursa-pastoris exhibit enhanced cold tolerance. *J. Plant Physiol.* 169 (14), 1408–1416. doi: 10.1016/j.jplph.2012.05.016

Xin, W., Zhang, L., Zhang, W., Gao, J., Yi, J., Zhen, X., et al. (2019). An integrated analysis of the rice transcriptome and metabolome reveals root growth regulation mechanisms in response to nitrogen availability. *Int. J. Mol. Sci.* 20 (23), 5893. doi: 10.3390/ijms20235893

Xu, Z., York, L. M., Seethepalli, A., Bucciarelli, B., Cheng, H., and Samac, D. A. (2022). Objective phenotyping of root system architecture using image augmentation and machine learning in alfalfa (Medicago sativa l.). *Plant Phenomics* 2022, 9879610. doi: 10.34133/2022/9879610

Yan, Z., Wang, H., Kou, X., Wu, C., Fan, G., Li, T., et al. (2022). Metabolomics analysis reveals that MeJA treatment induces postharvest blueberry resistance to botrytis cinerea. *Postharvest Biol. Technol.* 194, 112075. doi: 10.1016/j.postharvbio.2022.112075

Yang, C. L., Duan, R. J., Wu, X. X., Qi, C. Y., Ma, Y. H., and Xiong, H. Y. (2021). Genome-wide identification, sequence variation, and expression of the GPAT gene family in *Medicago truncatula*. *Pratacult. Sci.* 38 (10), 1966–1974.

Ye, C. Y., Zheng, C. P., Ying, W. W., and Weng, S. S. (2018). Up-regulation of microRNA-497 inhibits the proliferation, migration and invasion but increases the apoptosis of multiple myeloma cells through the MAPK/ERK signaling pathway by targeting raf-1. *Cell Cycle* 17 (24), 2666–2683. doi: 10.1080/15384101.2018.1542895

Yemm, E. W., and Willis, A. J. (1954). The estimation of carbohydrates in plant extracts by anthrone. *Biochem. J.* 57 (3), 508–514. doi: 10.1042/bj0570508

Yuan, Y., Fang, L., Karungo, S. K., Zhang, L., Gao, Y., Li, S., et al (2016). Overexpression of VaPAT1, a GRAS transcription factor from Vitis amurensis, confers abiotic stress tolerance in Arabidopsis. *Plant Cell Rep.* 35 (3), 655–666. doi: 10.1007/s00299-015-1910-x

Yue, Z. H., Shen, Y. H., Chen, Y. J., Liang, A. W., Chu, C. W., Chen, C., et al. (2019). Microbiological insights into the stress-alleviating property of an endophytic bacillus altitudinis WR10 in wheat under low-phosphorus and high-salinity stresses. *Microorganisms* 7 (11), 508. doi: 10.3390/microorganisms7110508

Zhang, X. (2008). *Physiological adaptability of different alfalfa varieties to low temperature conditions in autumn and winter* (Hohhot: Inner Mongolia Agriculture University).

Zhang, H. L. (2015). *Transcription analysis of summer squash in response to cold stress and the development of SSR molecular marker* (Jinzhong: Shanxi Agricultural University).

Zhang, X., Bao, Z., Gong, B., and Shi, Q. (2020). S-adenosylmethionine synthetase 1 confers drought and salt tolerance in transgenic tomato. *Environ. Exp. Bot.* 179 (17), 104226. doi: 10.1016/j.envexpbot.2020.104226

Zhang, S., Shi, Y., Cheng, N., Du, H., Fan, W., and Wang, C. (2015). *De novo* characterization of fall dormant and nondormant alfalfa (Medicago sativa l.) leaf transcriptome and identification of candidate genes related to fall dormancy. *PloS One* 10 (3), e0122170. doi: 10.1371/journal.pone.0122170

Zhang, Y., Zhao, P., Yue, S., Liu, M., Qiao, Y., Xu, S., et al. (2021). New insights into physiological effects of anoxia under darkness on the iconic seagrass zostera marina based on a combined analysis of transcriptomics and metabolomics. *Sci. Total Environ.* 768, 144717. doi: 10.1016/j.scitotenv.2020.144717

Zhao, Y., Li, M.-C., Konaté, M. M., Chen, L., Das, B., Karlovich, C., et al. (2021). TPM, FPKM, or normalized counts? a comparative study of quantification measures

for the analysis of RNA-seq data from the NCI patient-derived models repository. *J. Trans. Med.* 19 (1), 269. doi: 10.1186/s12967-021-02936-w

Zhao, Y., Wei, Y., and Zou, Y. (2015). Physiological index variation and its cultivar differences of seedling leaves and roots of early cropping rice under lower temperature stress. *J. Nucl. Agric. Sci.* 29 (4), 792–798. doi: 10.11869/j.issn.100-8551.2015.04.0792

Zhao, C., Zhang, R., Niu, K., Zhu, R., Wang, Y., Ma, X., et al. (2020). Metabonomics study of qinghai wild poa pratensis in response to low temperature stress. *Acta Agrestia Sinca* 28 (4), 904–914.

Zheng, J., Schultz, A. W., Wang, J., Johnson, C. H., Yannone, S. M., Patti, G. J., et al. (2013). Liquid chromatography quadrupole time-of-flight mass spectrometry characterization of metabolites guided by the metlin database. *Nat. Protoc.* 8 (3), 451–460. doi: 10.1038/nprot.2013.004

Zhou, L., Li, Y., Wang, W., and Zhong, S. (2017). Research progress in the metabolomics for plants response to temperature stress. *JournalofShanxi Agricult. Sci.* 45 (2), 317–320. doi: 10.3969/j.issn.1002-2481.2017.02.42

Zhu, H., Hu, H., Lu, C., and Li, X. (2007). Progresses on flavonoid metabolism in plants and it's regulation. *J. Xiamen Univ. (Natural Science)* 46 (1), 136–143.

Zhu, A., Huang, W., Han, G., Zhang, Y., Wang, X., and Wu, Q. (2021). Response of physiological and biochemical characteristics of alfalfa with different root collar diameters to low temperature stress. *Acta Agrestia Sinca* 29 (10), 2214–2220. doi: 10.11733/j.issn.1007-0435.2021.10.012

frontiers | Frontiers in Plant Science

TYPE Original Research
PUBLISHED 14 March 2023
DOI 10.3389/fpls.2023.1149880

OPEN ACCESS

EDITED BY
Jing Zhang,
Nanjing Agricultural University, China

REVIEWED BY
Mingna Li,
Chinese Academy of Agricultural Sciences (CAAS), Institute of Animal Sciences, China
Rui Dong,
Guizhou University, China

*CORRESPONDENCE
Longfa Fang
Fanglf@lzu.edu.cn
Zhipeng Liu
lzp@lzu.edu.cn

†These authors have contributed equally to this work and share first authorship

SPECIALTY SECTION
This article was submitted to Plant Abiotic Stress, a section of the journal Frontiers in Plant Science

RECEIVED 23 January 2023
ACCEPTED 23 February 2023
PUBLISHED 14 March 2023

CITATION
Qiang Y, He X, Li Z, Li S, Zhang J, Liu T, Tursunniyaz M, Wang X, Liu Z and Fang L (2023) Genome-wide identification and expression analysis of the response regulator gene family in alfalfa (*Medicago sativa* L.) reveals their multifarious roles in stress response.
Front. Plant Sci. 14:1149880.
doi: 10.3389/fpls.2023.1149880

Genome-wide identification and expression analysis of the response regulator gene family in alfalfa (*Medicago sativa* L.) reveals their multifarious roles in stress response

Yuqin Qiang[1†], Xiaojuan He[1†], Zhen Li[2], Siqi Li[1], Jia Zhang[1], Tao Liu[1], Mamateliy Tursunniyaz[1], Xinyu Wang[1], Zhipeng Liu[1*] and Longfa Fang[1*]

[1]State Key Laboratory of Herbage Improvement and Grassland Agro-ecosystems, College of Pastoral Agriculture Science and Technology, Lanzhou University, Lanzhou, China, [2]National Engineering Laboratory for Volatile Organic Compounds Pollution Control Material & Technology, University of Chinese Academy of Sciences, Beijing, China

As important components of the two-component regulatory system, response regulatory proteins (RRPs) play a crucial role in histidine phosphorylation-mediated signal transduction in response to environmental fluctuations. Accumulating evidence has revealed that RRPs play important roles in plant growth and stress response. However, the specific functions of *RR* genes (*RRs*) in cultivated alfalfa remain ambiguous. Therefore, in this study, we identified and characterized the *RR* family genes in the alfalfa genome using bioinformatics methods. Our analysis revealed 37 *RRs* in the alfalfa genome of Zhongmu No.1 that were unevenly distributed on the chromosomes. Cis-elements analysis revealed the involvement of *RRs* in responses to light, stress, and various plant hormones. Expression analysis of *RRs* in different tissues revealed their distinct tissue expression patterns. These findings provide preliminary insights into the roles of *RRs* in plant responses to abiotic stress, which can be used to improve the stress tolerance of autotetraploid-cultivated alfalfa plants *via* genetic engineering.

KEYWORDS

alfalfa, response regulators, stress response, gene family, expression analysis

Introduction

Adverse environmental conditions, such as drought, high salinity, and low temperatures (Hasanuzzaman et al., 2020; Imran et al., 2021), can greatly affect plant growth and crop production. To adapt to these challenges, plants have developed complex molecular response pathways for their survival (Razi and Muneer, 2021; Sun and Guo,

2022). The two-component system is one such response pathway that converts external stimuli into internal molecular signals in various prokaryotes, fungi, and plants (Hwang et al., 2002; Gao et al., 2008; Huo et al., 2020). The two-component system functions as a growth regulator during responses to stress factors, such as ethylene, cytokinins, light, and osmotic stress (Jain et al., 2008; Geng et al., 2022).

As important components of the two-component system, response regulators regulate the expression of downstream genes by receiving phosphate groups from receptors on conserved Asp residues in response to environmental stimuli (Kieber and Schaller, 2018; Hu et al., 2022). Various plant genome sequencing projects have improved our understanding of the functions of response regulatory (*RR*) genes in plants (Zhang et al., 2012). RRPs are encoded by a large gene family in plants (Wang et al., 2007), which can be divided into three subtypes based on their domain structure and amino acid sequence: A, B, and P. Type-A *RRs* only possess a receiver domain, and their transcripts are induced by cytokinins and nitrates (West and Stock, 2001; Hass et al., 2004). Type-B *RRs* are transcription factors that can activate their target genes, including type-A *RRs*, and act as positive regulators of the cytokinins response (Mason et al., 2005). Type-P *RRs* lack the Asp phosphorylation sites required to maintain their activity and may affect the biological clock (McClung, 2006).

To date, *RRs* have been identified on a genome-wide scale in various plant species, such as *Arabidopsis thaliana* (D'Agostino et al., 2000), *Oryza sativa* (Tsai et al., 2012), *Zea mays* (Wang et al., 2022), *Gossypium hirsutum* (Zhao et al., 2022), and *Glycine max* (Le et al., 2011). Although the number of identified *RRs* varies among plants, their functions are conserved in these different species. Many stress tolerance-related genes have been identified in different plants. For instance, *OsRR6, GmRR01*, *GmRR02*, *GmRR25*, and *GmRR32* have been reported as positive regulators of stress response, increasing the plant resistance to drought and salt stress (Le et al., 2011). In contrast, *OsRR9* and *OsRR10* negatively regulate salt tolerance (Wang et al., 2019; Bhaskar et al., 2021). *Z. mays ZmRR1* is the only gene reported to be involved in cold tolerance (Zeng et al., 2021). Some *RRs* have been found to play vital roles in developmental and environmental signals mediated by light, cytokinins, and ethylene (Doi et al., 2004; Ito and Kurata, 2006). For instance, the expression patterns of *O. sativa Ehd1* and *ZmRR3* are related to cytokinins (Pareek et al., 2006), and those of *GhRR41*, *SlPRR1*, *SlPRR2*, *SlPRR3*, *SlPRR4*, *SlPRR5*, and *SlPRR6* are mainly related to the circadian rhythm and regulation of flowering time in plants (He et al., 2016).

Alfalfa, the most widely cultivated legume forage in the world with a planting area of 32 million hectares (Ren et al., 2021), is known as the "queen of forage" because of its high nutritional value as a source of proteins, vitamins, and other nutrients for livestock. It also exhibits potential for ethanol production (Liu et al., 2021). Alfalfa is widely cultivated in the arid and semiarid areas of the Northeast, Northwest, and Central North regions of China, and its production is strongly constrained by various biotic and abiotic stresses (Dong et al., 2023). Although the stress-tolerance-related functions of *RRs* have been widely reported in other crops, only a few studies have investigated their roles in the stress response of cultivated alfalfa plants. Therefore, in this study, we systematically identified and characterized the *RRs* to understand their biological functions, physicochemical properties, gene structures, evolutionary relationships, and location on the chromosome. We also analyzed the expression patterns of *RRs* under different abiotic stresses using quantitative reverse transcription-polymerase chain reaction (qRT-PCR). Our results provide a basic understanding of the roles of *RRs* in cultivated alfalfa and lay the foundation for further breeding studies of this plant *via* genetic engineering.

Materials and methods

Plant growth, treatments, and tissue collection

Alfalfa (Zhongmu No.1) seeds from the College of Grassland Agricultural Science and Technology of Lanzhou University (humidity: 80%) were germinated in a culture dish and grown in half-concentration Murashige and Skoog nutrient solution (pH 5.8) under 16/8 h light/dark conditions at 22 °C and 80% relative humidity for 15 d. For the stress treatment, fifteen groups of alfalfa seedlings were separately treated with abscisic acid (ABA; 10 μM), NaCl (250 mM), and mannitol (400 mM) for different time points (0, 1, 3, 6, and 24 h), and each treatment group contained five plants. Whole plants from different treatments were separately stored at −80 °C in an ultra-low temperature refrigerator for subsequent analysis. Total RNA was extracted with the TRIzol Total RNA Extraction Kit (Shenggong Bioengineering Co., Ltd., Shanghai), and reverse transcribed into cDNA using the TIANScript II RT Kit (Tiangen Biochemical Technology Co., Ltd., Beijing) for gene expression verification.

Identification of *RR*s in alfalfa

Alfalfa genome coding sequence (CDS) and protein sequences were downloaded from the website (http://47.92.172.28:12088/). RR protein sequences of *A. thaliana* from the TAIR (https://www.arabidopsis.org/) were used as query sequences to identify candidate *RRs* in the alfalfa genome using the Protein Basic Local Align Search Tool (BLASTP) with an E-value cutoff of 10^{-5}. A hidden Markov model (HMM) for the response regulator receiver domain, PF00072, from the PFAM protein database (http://pfam.xfam.org/) was used to further filter the previously identified *RRs*, and the remaining protein sequences were considered to be members of *RR* gene family.

Gene characteristics, structure, conserved motif, and subcellular localization analyses

Physical parameters of putative proteins, including the lengths of amino acid sequences, molecular weights (MWs), theoretical isoelectric points (pIs), and instability index, were calculated using the online ExPASy tool (http://www.expasy.org/tools/

protparam.html), and the gene structure display server program (http://gsds.cbi.pku.edu.cn/) was used to illustrate the exon–intron structures by alignment of the CDSs of individual *RRs*. For motif structures analysis of RRPs, the online MEME program (http://meme-suite.org/tools/meme) was used with the default parameters, and the optimum motif widths were set at 6 residues. For subcellular localization analyses, the CELLO webtool (http://cello.life.nctu.edu.tw/) was used to predict the subcellular location of RRPs.

Chromosomal localization and collinearity analysis of *RRs*

To better recognize the genomic distribution of *RRs*, the R package RIdiogram was used to draft the chromosomal location map of *RRs* based on the genome annotation files of alfalfa. For gene duplication event analysis, we used the DupGen_finder pipeline (https://github.com/qiao-xin/DupGen_finder) to identify different modes of gene duplication (tandem duplication [TD], transposed duplication [TRD], whole genome duplication [WGD], proximal duplication [PD], and dispersed duplication [DSD]) using the default settings (Qiao et al., 2019). For Ka, Ks, and Ka/Ks calculations, the KaKs_Calculator 2.0 was used based on the Tamura–Nei model model (Wang et al., 2010).

Phylogenetic and cis-regulatory element analyses

To analyze the evolutionary relationships among *RRs* in alfalfa, a phylogenetic tree containing 37 alfalfa *RRs* and 32 Arabidopsis *RRs* was constructed with MEGA software (version 6.0; https://www.megasoftware.net/egasoftware.net) using the neighbor-joining method, and the bootstrap coefficient was set to 1000 times. PlantCARE database (http://bioinformatics.psb.ugent.be/webtools/plantcare/html/) was used to determine potential cis-regulatory elements within 2000 bp promoter sequences of *RRs*.

Expression analysis of *RRs*

Transcriptome data from the CADL-Gene Expression Atlas (https://www.alfalfatoolbox.org/) and National Center for Biotechnology Information Sequence Read Archive database (http://www.ncbi.nlm.nih.gov; accession numbers SRX4079528–SRX4079572) were used to explore the expression profiles of *RRs* in different tissues (leaves, flowers, pre-elongated stems, elongated stems, roots, and nodules) and with different treatments (ABA, NaCl, and mannitol). Subsequently, the expression patterns of three *RRs* under different treatments in alfalfa were explored using the 2 x SG Fast qPCR Master Mix (Sangon Biotech, Shanghai, China) on a CFX96 Real-Time PCR Detection System (Bio-Rad, Los Angeles, CA, USA). The reaction system consisted of 10 μL volume (0.2 μL of each primer, 2.6 μL of ddH_2O, and 1 μL of DAF buffer, 1 μL of cDNA, and 5 μL of 2 x SG Fast qPCR Master Mix). PCR reaction conditions were as follows: 94 °C for 30 s, followed by 20 cycles of 94 °C for 5 s and 54 °C for 30 s. The actin gene from alfalfa was selected as an internal reference, and the relative expression level of each gene was calculated using the $2^{-\Delta\Delta CT}$ method. Three biological replicates were used, and the significant differences between the treatment and control groups were determined at the same time point using a *t*-test. A histogram with error lines was drawn using R package ggplot2. All qRT-PCR validation primers used in the present study are listed in Table S1.

Results

Identification and gene characteristic analyses of the *RR* gene family in alfalfa

We identified 37 *RRs* in alfalfa based on a homology-based prediction approach using BLASTP. Further analysis of the evolutionary relationship between the structural specificity and conservation of these *RRs* led to the identification of 10 type-A, 16 type-B, and 11 type-P *RRs* (Table 1). The number of *RRs* was close to the *RR* gene family size observed in other plant species, such as *A. thaliana* (32 genes) and *O. sativa* (36 genes) (Ramírez-Carvajal et al., 2008).

In addition to the identification of *RRs* in alfalfa, we characterized the physicochemical properties of RRPs. Detailed information is provided in Table 1. The lengths of the identified RRPs ranged from 130 to 1214 amino acids (AAs), and the pIs varied from 4.54 to 8.27 (Table 1). These RRPs also displayed a wide range of MWs from 14.49 to 134.88 kDa (Table 1). Notably, most of these proteins were soluble hydrophilic proteins as the overall mean hydropathicity for all RRPs was negative (< 0) (Table 1).

Phylogenetic, gene structure, and protein domain analyses of RRPs

To confirm the evolutionary relationships among RRPs, we aligned the full-length RRPs of alfalfa and *A. thaliana* to construct a phylogenetic tree using MEGA 6.0. Based on the phylogenetic tree, 69 *RRs* (32 *RRs* in *A. thaliana* and 37 *RRs* in alfalfa) were divided into three subfamilies: 20 type-A, 32 type-B, and 17 type P-*RRs* (Figure 1B). The structural diversity of genes drives the evolution of multigene families. To better understand the structural diversity of *RRs*, we plotted exon–intron organization maps and found that all *RRs* contained more than one intron. The number of exons in the 37 genes varied from 2 to 12. Some genes, such as *MsG0880047620*, *MsG0380017187*, and *MsG0380013071*, contained more than 10 exons, and others had less than 10 introns. Notably, some type-A and type-B *RRs* contained untranslated regions (UTRs), but none of the type-P *RRs* had any UTRs (Figure 1A).

To further investigate the distribution and structural diversification of conserved motifs in alfalfa RRPs, we used the MEME software and found that most closely related members

10.3389/fpls.2023.1149880

TABLE 1 Details of the *RRs* identified in alfalfa.

Gene name	Protein length	Protein MW(Da)	PI	Protein GRAVY	instability index
MsG0780040812	139	15954.74	8.06	-0.116	37.32
MsG0180002532	183	20517.76	5.39	-0.256	55.27
MsG0180002564	369	42036.46	6.31	-0.512	29.97
MsG0780040837	130	14494.9	5.67	-0.127	40
MsG0580025893	226	24373.56	4.56	-0.137	52.87
MsG0380016661	490	54145.17	6.78	-0.502	54.59
MsG0180000565	298	34120.53	6.08	-0.702	37.39
MsG0780040418	238	26912.11	5.56	-0.763	55.33
MsG0880047619	602	67252.45	5.17	-0.555	55.22
MsG0180000563	523	59185.05	6.78	-0.615	43.42
MsG0880047620	1214	134882.9	5.04	-0.488	49.88
MsG0380016366	262	29336.13	4.54	-0.356	65.92
MsG0380012160	167	18959.93	5.96	-0.292	47.49
MsG0480022917	549	62653.28	5.8	-0.438	41.81
MsG0880047126	680	74037.8	5.75	-0.532	42.23
MsG0880046376	212	23428.01	5.84	-0.194	55.14
MsG0080047933	765	86289.36	6.24	-0.676	50.98
MsG0780041771	510	57843.29	7.16	-0.663	47.57
MsG0280008856	666	73132.27	5.93	-0.599	48.59
MsG0380017187	550	63107.1	6.05	-0.421	44.84
MsG0580027346	313	36412.24	5.78	-0.662	39.58
MsG0380013071	854	97011.48	7.17	-0.687	55.34
MsG0180002180	196	21756.03	5.53	-0.289	63.63
MsG0880042893	666	75235.66	6.14	-0.797	53.22
MsG0480019003	225	25694.76	6.5	-0.199	41.65
MsG0480020869	760	83243.94	6.09	-0.683	40.35
MsG0880045009	144	16167.73	6.3	-0.377	32.33
MsG0280007899	637	70612.32	7.3	-0.549	49.58
MsG0880043607	177	20076.19	5.55	-0.369	46.91
MsG0780041732	291	33207.86	8.27	-0.719	39
MsG0380014518	191	21446.43	5.97	-0.373	45.41
MsG0380016233	521	59588.48	5.76	-0.573	50.3
MsG0380015850	201	21795.19	6.61	-0.068	56.41
MsG0380016710	155	17090.81	6.59	-0.312	44.74
MsG0880045487	372	41397.7	6.95	-0.391	36.7
MsG0780040815	187	20432.41	5.8	-0.426	35.86
MsG0380017376	642	70348.95	6.15	-0.487	45.85

10.3389/fpls.2023.1149880

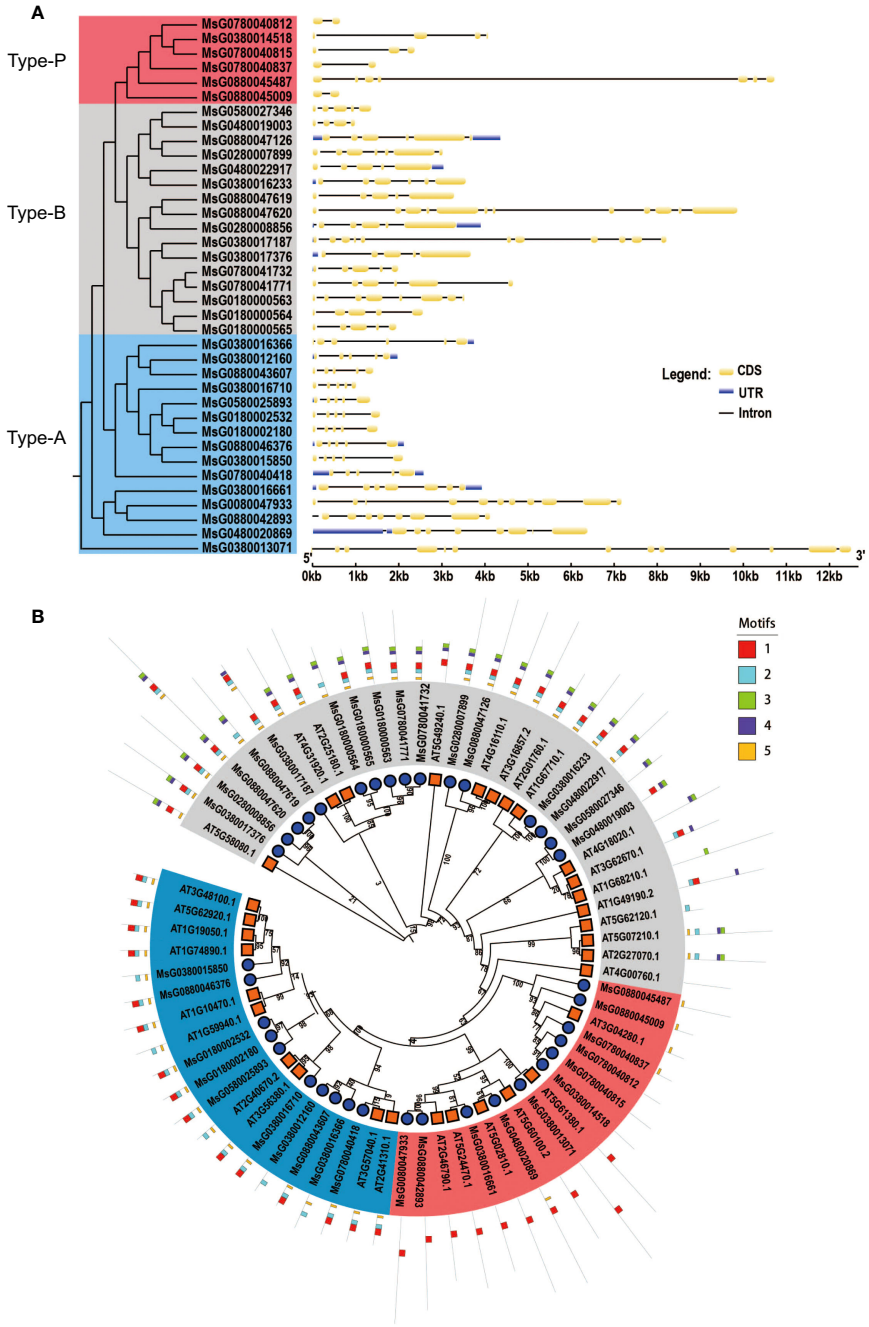

FIGURE 1
Gene structure, phylogenetic tree and meme structure analyses of *RRs*, Blue, type-A; Gray, type-B; Pink, type-P. **(A)** The rooted phylogenetic tree was constructed with 37 RR amino acid sequences of alfalfa. Exon-intron organization of corresponding of the *RRs*. The exons and introns are represented by yellow boxes and black lines, untranslated regions (UTRs) are represented by blue boxes, respectively. The length of each *RR* gene is shown as a proportion. **(B)** Phylogenetic tree and meme structure of *RRs* between alfalfa and *A. thaliana*. The phylogenetic tree was constructed using MEGA 6.0 by the neighbor-joining method with 1000 bootstrap replicates. The tree was divided into 3 subgroups. Members of different subgroups are denoted by solid circles with red, blue and gray colors, respectively. The conserved motifs in the RPPs were identified by MEME. The black lines represent no conserved sequences. Each motif is indicated by a colored box numbered at the bottom. Details are listed in Figure S1.

shared common motifs, but the conserved motifs among the subfamilies were significantly different, with some exceptions. For example, all type-A RRPs, except MsG0380016366, MsG0380012160, and MsG0380015850, contained motifs 1, 2, and 5; all type-B RRPs, except MsG0880047619, MsG0180000564, MsG0580027346, and MsG0480019003, contained motifs 1, 2, 3, 4, and 5 (Figure 1B; Figure S1).

Chromosomal distribution and subcellular localization of *RRs*

To study the orientation of *RRs* on each chromosome, we obtained accurate information about the initiation sites to construct the chromosomal location map (Figure 2A). Our results showed that the *RR* family members were distributed unevenly

10.3389/fpls.2023.1149880

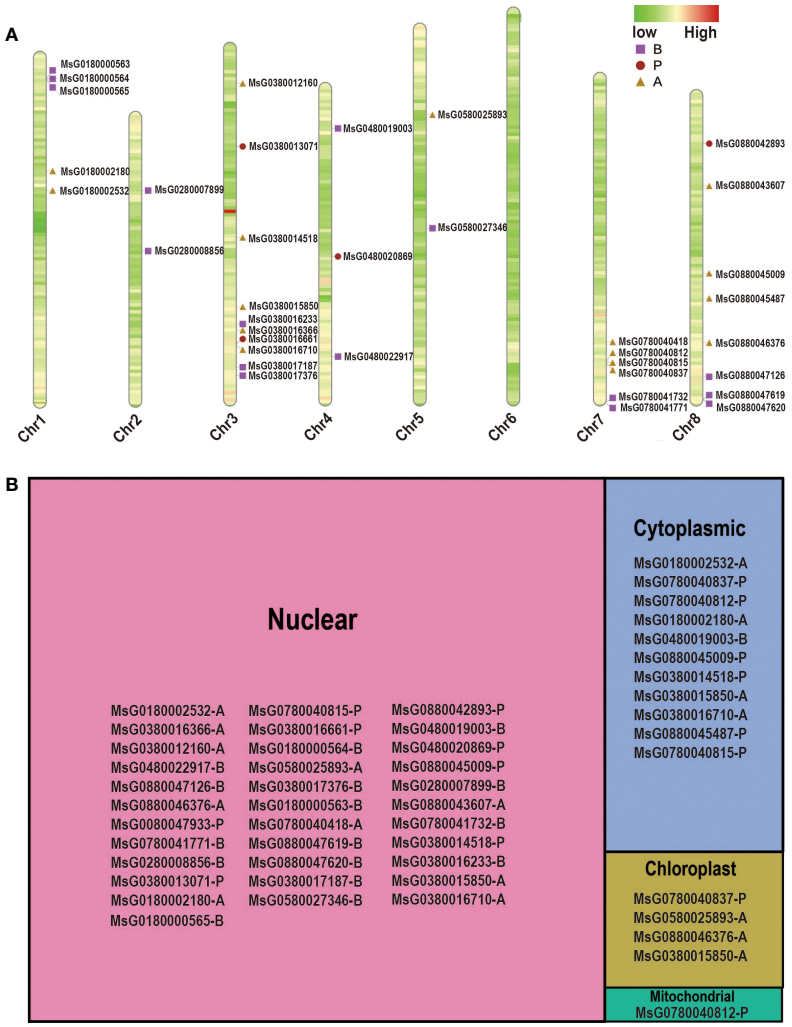

FIGURE 2
Chromosome distribution and subcellular localization of RRPs. **(A)** Chromosome distributions of different subtypes RRPs in alfalfa. The chromosome number is indicated at the bottom of each bar. **(B)** Tree map showing the subcellular localization of different subtypes RRPs in alfalfa.

across the eight chromosomes of alfalfa, with the number of *RRs* varying among the chromosomes. Almost half of the *RRs* (18 *RRs*) were present on Chr3 and Chr8 of alfalfa, but there were no *RR* genes on Chr6, and *RRs* were less distributed on Chr2, Chr4, and Chr5, with only two, three, and two genes found in these chromosomes, respectively. Interestingly, most of the *RRs* were located in the distal centromere region, indicating that these *RRs* may have experienced long-term evolution in alfalfa.

Information on subcellular localization is crucial for understanding the functions of proteins. The CELLO web server was used to determine the subcellular localization of RRPs. We found that most RRPs were mainly located in the nucleus and mitochondria (Figure 2B). This is not surprising as some RRPs can function as transcription factors. Furthermore, only a few *RR* members were predicted to be located in the chloroplast and one was found to be targeted to the mitochondria. Notably, some RRPs exhibit more than one subcellular localization. For example, MsG0780040812 is located in both the mitochondria and cytoplasm, whereas MsG0380015850 is distributed in almost all subcellular compartments, except for the mitochondria (Figure 2B). Therefore, these proteins may need to be trafficked to different subcellular organelles under different conditions to perform their functions.

Cis-acting element analysis of the *RR* promoter

Cis-acting elements located in the promoter regions are recognized by transcription factors that regulate the spatial and temporal expression patterns of their target genes. To identify these cis-regulating elements in the promoter sequence (2000 bp) of each *RR* gene, we used the PlantCARE online tool and detected many cis-elements in the promoter regions of *RRs* (Figure 3). These cis-elements included abiotic stress-related, light, and plant growth and development response elements. As shown in Figure 3, almost all *RRs* had abiotic stress-related response elements, such as the ABA-responsive element (ABRE), MeJA-responsive element (TGACG-

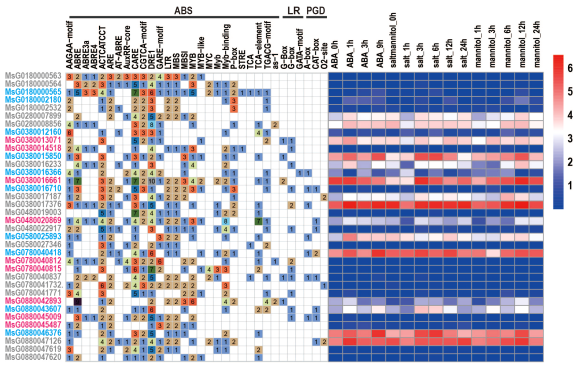

FIGURE 3
Cis-acting elements in the promoter region of *RRs* and the expression profiles of *RRs* under different stress treatments in alfalfa. ABS: abiotic stress related response elements; LR: light response elements; PGD: plant growth and development response elements. The expression levels of gene are showed in different colors; red and blue represent high and low expression level, respectively.
Figure 3. Gene duplications and collinearity analysis.

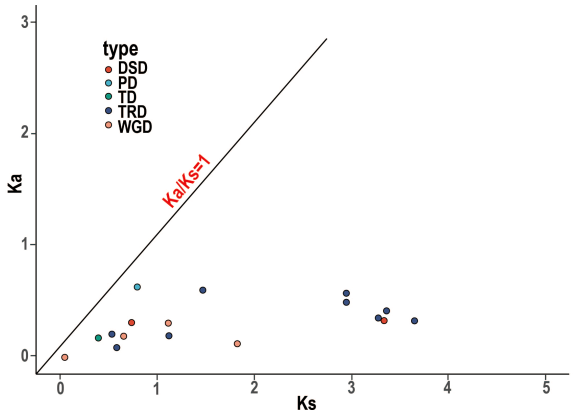

FIGURE 4
Ka/Ks ratios of duplicated *RR* gene pairs. Gene pairs from different duplication types are indicated by different scatter. The y and x axes denote the Ka and Ks values for each pair and the black line shows a Ka/Ks ratio = 1. The detail of Ka, Ks, and Ka/Ks listed in Table S2.

motif), and salicylic acid-responsive element (TCA-element), suggesting that all *RRs* have the ability to perform their functions under stress. However, not all *RRs* showed high levels of expression under stress conditions. Some genes, including *MsG0180002180*, *MsG0480022917*, *MsG0380016710*, *MsG0180000565*, *MsG0880045009*, *MsG0880045487*, *MsG0780041771*, *MsG0780041732*, *MsG0780040837*, *MsG0780040812*, *MsG0780040815*, *MsG0580027346*, *MsG0180002532*, *MsG0380012160*, *MsG0880047619*, *MsG0480019003*, *MsG0380014518*, *MsG0180000563*, *MsG0180000564*, and *MsG0880047620*, exhibit low expression or no expression under ABA, mannitol, and NaCl treatments (Figure 3). This may be caused by heterochromatin-mediated gene silence because most of *RRs* showed telomere-near-distribution. In addition, only 16 and 13 *RRs* had light response elements in plant growth and development in their promoter regions (Figure 3), respectively, indicating that some *RRs* are also associated with light response and plant growth and development.

Gene duplication and collinearity analysis of *RRs*

WGDs along with single gene duplications, such as DSDs, TRDs, PDs, and TDs, are the main driving forces for gene family evolution. In this study, we identified nine TRD events, four WGD events, two DSD events, one TD event, and one PD event (Figure 4; Table 2) in the *RR* subfamily. To further understand the evolutionary constraints acting on duplicated *RRs*, we calculated Ka (non-synonymous substitution rate), Ks (synonymous substitution rate), and the Ka/Ks ratio for each duplicated *RR* gene pair. Our results showed that all Ka/Ks ratios for the 17 segmentally duplicated gene pairs were < 1 (Table 2), indicating that the *RRs* primarily evolved under the influence of purifying selection. To further determine the origin and evolution of *RR* gene family members, four comparative synteny maps were constructed between autotetraploid alfalfa and *A. thaliana*, *Medicago truncatula*, *G. max*, and *Lotus corniculatus*. These results showed that 30 *RRs* of Zhongmu No. 1 were collinear with *G. max*, followed by *M. truncatula* (19), *L. corniculatus* (19), and *A. thaliana* (18). Among these orthologous pairs, seven *RRs* (*MsG0780040418*, *MsG0580025893*, *MsG0880046376*, *MsG0380016710*, *MsG0380016661*, *MsG0380015850*, and *MsG0180000563*) had their corresponding orthologs both in *G. max*, *L. corniculatus*, *M. truncatula*, and *A. thaliana* (Figure 5; Table 3), suggesting that these genes may play an important role in the evolution of *RRs*. The collinear relationships between the *RRs* of Chr3 and those of the other four plants were significantly greater than those of the other chromosomes.

Tissue expression patterns of *RRs* in alfalfa

Tissue expression profiles are useful in determining the potential roles of target genes and their specific properties in a particular tissue. To gain a deeper understanding of the potential function of *RRs*, we analyzed their expression profiles in six tissues (leaves, flowers, pre-elongated stems, elongated stems, roots, and nodules) using RNA-sequencing data from alfalfa and found that the expression patterns of *RRs* were distinct. Most *RRs* showed a constitutive expression pattern, but nearly half of the genes were expressed at low levels in all tissues. This may be caused by the telomere-near-distribution due to the heterochromatin-mediated epigenetic regulation of gene expression (Matzke et al., 2009; To et al., 2011). Furthermore, *MsG0380013071*, *MsG0280008856*, *MsG0880047126*, *MsG0480020869*, and *MsG0380017187* were highly expressed in all six tissues. Interestingly, we also observed tissue-specific expression patterns of some *RRs*. For example, *MsG0880043607* was expressed only in the stem, while *MsG0580025893* was highly expressed in leaves, stems, and flowers (Figure 6; Figure S2).

TABLE 2 The Ka/Ks ratios for duplicated *RRs* paralogous pairs.

Paralogous pairs	Ka	Ks	Ka/Ks	Selective type	Duplicate type
MsG0780040812- MsG0780040815	0.6292	0.7942	0.7922	Purifying	PD
MsG0180000563- MsG0380017376	0.3061	1.1144	0.2747	Purifying	WGD
MsG0180000564- MsG0180000565	0.1734	0.3929	0.4414	Purifying	TD
MsG0180002180- MsG0180002532	4.62e-05	0.0462	0.001	Purifying	WGD
MsG0280007899- MsG0880047126	0.1929	1.1210	0.1721	Purifying	TRD
MsG0280008856- MsG0380017376	0.4923	2.9517	0.1668	Purifying	TRD
MsG0380015850- MsG0880046376	0.1217	1.8265	0.0666	Purifying	WGD
MsG0380016233- MsG0480022917	0.1892	0.6540	0.2893	Purifying	WGD
MsG0380016661- MsG0880042893	0.5735	2.9514	0.1943	Purifying	TRD
MsG0380016710- MsG0380015850	0.3520	3.2814	0.1073	Purifying	TRD
MsG0380017187- MsG0380017376	0.6010	1.4707	0.4087	Purifying	TRD
MsG0580025893- MsG0180002180	0.0871	0.5824	0.1496	Purifying	TRD
MsG0780040418- MsG0880046376	0.4157	3.3662	0.1235	Purifying	TRD
MsG0780041372- MsG0180000563	0.1807	0.5805	0.3113	Purifying	TRD
MsG0780041771- MsG0180000563	0.2075	0.5327	0.3895	Purifying	TRD
MsG0880043607- MsG0880046376	0.3266	3.6549	0.0894	Purifying	TRD
MsG0880045009- MsG0880045487	0.3109	0.7354	0.4228	Purifying	DSD
MsG0380012160- MsG0380016366	0.3283	3.3412	0.0982	Purifying	DSD

Discussion

In response to abiotic stress, RRPs obtain phosphoric groups from histidine phosphate transfer proteins to stimulate the transcription of downstream functional genes. Previous studies have reported that *RRs* in various plants, such as *A. thaliana*, *O. sativa*, *Pyrus bretschneideri*, *Prunus persica*, *Fragaria vesca*, and *Brassica rapa* ssp. *Pekinensis* (Liu et al., 2014; Bhaskar et al., 2021), are crucial for the plant response to abiotic stress (Imamura et al., 1999), which can be applied in alfalfa molecular breeding for drought tolerance. It is also important to elucidate the *RR*-related genes and their functions in alfalfa and other legumes. This will expand our knowledge of *RRs* and provide a foundation for further investigation of their specific roles and functions. In this study, 37 *RRs* were identified in alfalfa, which is approximately equivalent to the *RR* family size in *A. thaliana* (32 genes) and *O. sativa* (36 genes) (Ramírez-Carvajal et al., 2008). The close relationship between *RRs* of *A. thaliana* and alfalfa, as observed in the phylogenetic tree, suggests that the functions of these *RRs* in alfalfa may be similar to those observed in *A. thaliana*. Based on evolutionary relationships and structural specificity, the 37 *RRs* can be clustered into three subfamilies: type-A, type-B, and type-P *RRs* (Figure 1B). Protein domain analysis revealed that the conserved motifs within each subfamily were similar, but those among different subfamilies were significantly different. Specifically, motifs 1 and 5 were present in the members of type-P RRPs, while motifs 1, 2, and 5 were present in the members of the type-A RRPs, and all motifs were present in most members of type-B RRPs (Figure 1B). These differences in characteristics among the different subfamilies may indicate the diverse functions of the *RR* family members in alfalfa.

Gene duplication is a fundamental source of new genes in the evolutionary process, facilitating the successful evolution of genes and contributing to the rapid expansion of gene families (Van de Peer et al., 2009; Wang et al., 2017). *RR*-related duplication events have been observed in many species, including *A. thaliana*, *Malus domestica*, and *Gossypium* species (Li et al., 2017). Our gene duplication analysis revealed that *RRs* in alfalfa also experienced different types and numbers of gene duplication events. In *Gossypium* species, no tandem duplication gene pairs were detected in the *RR* gene family, and WGD seemed to contribute more to alfalfa *RR* gene family expansion than single gene duplication events; however, our analysis documented the presence of TD events and revealed that TRD events, not WGD events, played a major role in the expansion of the *RR* gene family in alfalfa (Figure 4). These conflicting findings may be attributed to the independent evolution of genes.

RRs have been reported to be involved in stress resistance and response in various plants, such as *A. thaliana* (Nakamichi et al., 2016) and *O. sativa* (Karan et al., 2009; Rehman et al., 2022), and several *RRs* in alfalfa were also found to respond to different types of abiotic stresses (Figure 3). For example, *MsG0380016233*, *MsG0580025893*, *MsG0780040418*, *MsG0280008856*, *MsG0380013071*, *MsG0380017187*, *MsG0480020869*, and *MsG0280007899* were significantly up-regulated by ABA treatment, some of which were confirmed by qRT-PCR analysis (Figure S3). Cis-element analysis indicated that ABREs were located

10.3389/fpls.2023.1149880

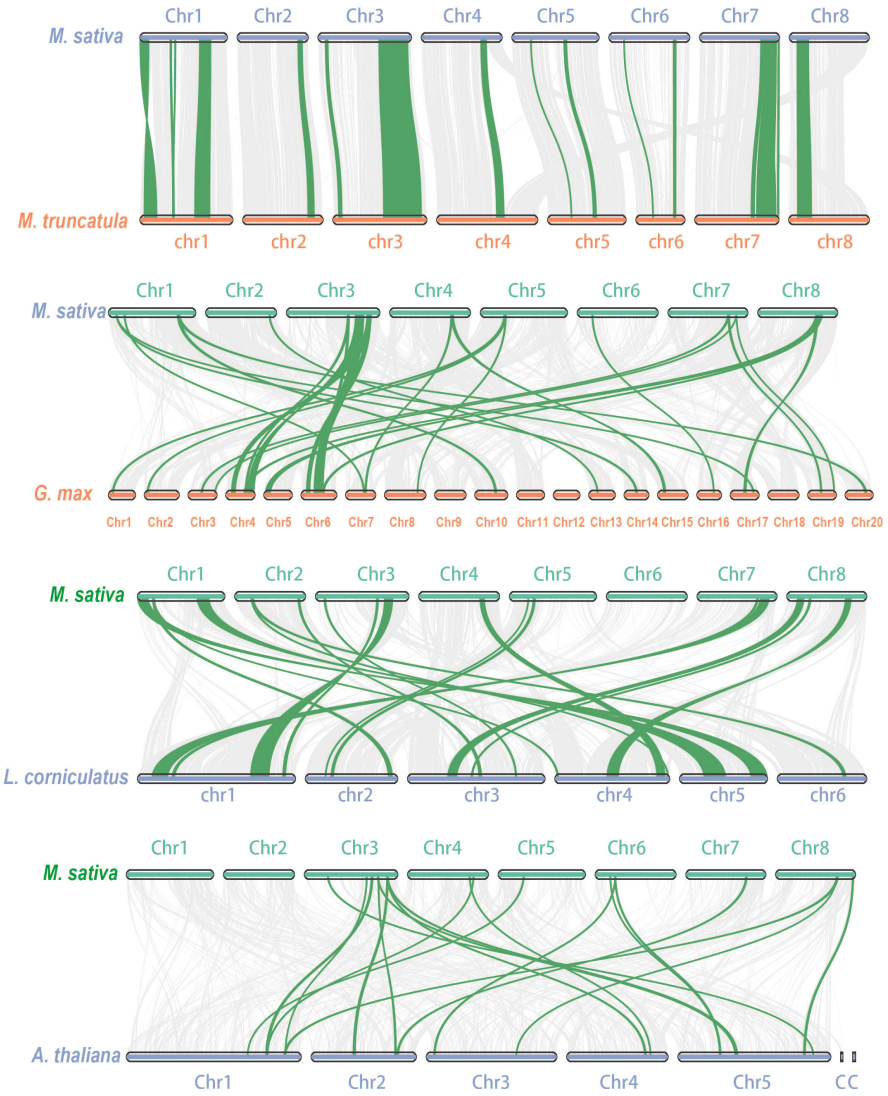

FIGURE 5
Collinearity analysis between alfalfa and *A. thaliana*/*M. truncatula*/*G. max*/*L. corniculatus*. The gray lines in the background indicate the collinear blocks between alfalfa and *A. thaliana*/*M. truncatula*/*G. max*/*L. corniculatus*, while the blue lines highlight the syntenic *RR* gene pairs.

in the promoter regions of these genes, and subcellular localization predicted analysis revealed that they were only localized in the nucleus (Figure 2B). Taken together, these results suggest that these genes may be directly regulated by ABA in response to drought stress (Figure 3) and should be transferred into the nucleus to regulate the expression of some genes in response to ABA stimuli. Interestingly, MsG0580025893 was predicted to be distributed in both the nucleus and chloroplast, and was highly expressed in

TABLE 3 The common syntenic gene pairs of *RRs* among *A. thaliana* and the five legume species.

M. sativa	*A. thaliana*	*G. max*	*L. corniculatus*	*M. truncatula*	Subfamily
MsG0880046376	*AT1G74890.1*	*Glyma.17G093900.1*	*Lj4g0019308.2*	*Medtr4g106590.1*	A
MsG0780040418	*AT3G57040.1*	*Glyma.03G130000.1*	*Lj1g0019360.1*	*Medtr7g490310.2*	A
MsG0580025893	*AT1G59940.1*	*Glyma.08G292400.1*	*Lj2g0021492.1*	*Medtr5g036480.1*	A
MsG0380016710	*AT2G40670.2*	*Glyma.04G223000.1*	*Lj1g0007309.1*	*Medtr3g093860.1*	A
MsG0380016661	*AT5G24470.1*	*Glyma.04G228300.1*	*Lj1g0026375.1*	*Medtr3g092780.1*	P
MsG0380015850	*AT3G48100.1*	*Glyma.04G177900.1*	*Lj1g0015853.1*	*Medtr3g078613.2*	A
MsG0180000563	*AT2G25180.1*	*Glyma.17G217100.1*	*Lj5g0016527.1*	*Medtr1g013180.1*	B

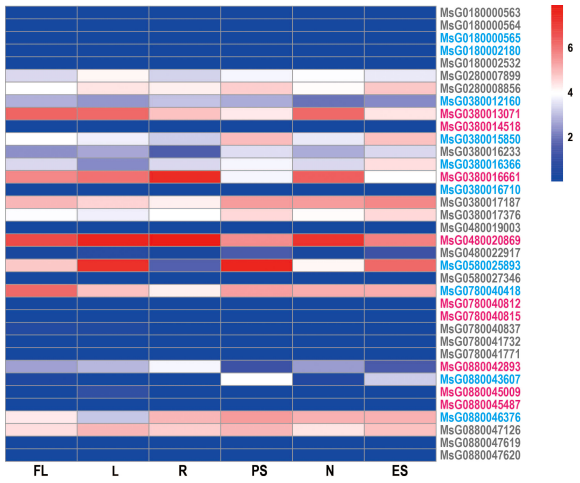

FIGURE 6
Heatmap displaying the *RRs* expression in various tissues of alfalfa. Transcriptome data from 6 tissues (FL, flower; L, leaf; R, root; PS, pre-elongated stem; N, nodule; ES, elongated stem) were used to construct the expression patterns of *RRs* in alfalfa. The bar to the right of the heat map represents the relative expression values.

leaves, stems, and flowers (Figure 2B; Figure 6), suggesting that it may function in abiotic stress by regulating both nuclear and chloroplast gene expression to enhance photosynthesis. In addition, we also identified several *RRs*, including *MsG0180002180*, *MsG0480022917*, *MsG0380016710*, *MsG0180000565*, *MsG0880045009*, *MsG0880045487*, *MsG0780041771*, *MsG0780041732*, *MsG0780040837*, *MsG0780040812*, *MsG0780040815*, *MsG0580027346*, *MsG0180002532*, *MsG0380012160*, *MsG0880047619*, *MsG0480019003*, *MsG0380014518*, *MsG0180000563*, *MsG0180000564*, and *MsG0880047620*, which were not expressed under ABA, NaCl, and mannitol treatments (Figure 3). Interestingly, ABREs were still detected in the promoter region of *MsG0180000565*. This could be partly explained by the presence of other regulatory mechanisms, such as heterochromatin-mediated gene silence, that compete with ABA induction during transcription (Peng et al., 2008). *RRs* also play important roles in plant immune response and disease resistance (Cheval et al., 2017; Bacete et al., 2020). In line with this, we found that some genes, such as *MsG0780040815* and *MsG0380016661*, have gibberellin, salicylic acid, and methyl jasmonate response elements in their promoter regions (Figure 3).

Circadian rhythms are produced by the internal clock or oscillator of many organisms and control the timing of genetic, metabolic, and physiological processes, including photosynthesis (Dodd et al., 2005; Chow and Kay, 2013), growth rate, and flowering time (Woelfle et al., 2004). Photoperiodic regulation of the flowering period is one of the most common circadian events (Yanovsky and Kay, 2003). In *A. thaliana*, the *APRR* family has been reported to be associated with the circadian clock (Murakami et al., 2004). The expression patterns of some orthologs of *AtPRRs* in *Populus* exhibit circadian waves (Liu et al., 2013), but the circadian rhythm function of alfalfa type-P *RRs* has not yet been reported. Notably, photoperiod-responsive elements, including G-box, GATA-motif, and methyl jasmonate, were also detected in the promoter region of type-P *RRs*, suggesting that members of the *RR* family may also be related to the circadian rhythm (Figure 3). Subcellular localization analysis of *A. thaliana* and *Glycyrrhiza uralensis* revealed that type-P RRPs are mainly localized in the nucleus (Fujiwara et al., 2008). However, in our predicted results, type-P RRPs were found to exist not only in the nucleus but also in the cytoplasm, mitochondria, and chloroplasts (Figure 2B). This suggests that type-P *RRs* in alfalfa have roles other than the maintenance of circadian rhythm, which require further exploration future studies.

Conclusion

In this study, we comprehensively and systematically analyzed the response regulator gene family in the autotetraploid-cultivated alfalfa genome. We identified 37 *RR* family genes unevenly distributed across eight chromosomes in the alfalfa genome and further grouped them into three subfamilies, type-A, type-B, and type-P *RRs*, based on their evolutionary relationship, structural specificity, and degree of conservation. We also analyzed the physicochemical properties, phylogenetic relationships, exon–intron structures, conserved motifs, chromosomal location, gene duplication, cis-regulatory elements, and tissue-specific expression patterns of these genes. Our findings shed light on the significant roles of alfalfa *RR* gene family in hormone induction and abiotic stress tolerance and have great scientific and practical application in alfalfa molecular breeding.

Data availability statement

The original contributions presented in the study are included in the article/Supplementary Material. Further inquiries can be directed to the corresponding authors.

Author contributions

YQ, XH and LF designed the experiments and wrote the manuscript. YQ, SL, JZ, MT, XW, TL analyzed the data. LF, ZL and ZPL edited the manuscript. All authors contributed to the article and approved the submitted version.

Funding

This research was supported by the National Natural Science Foundation of China (32201463), Major Program of Agricultural Biology Breeding (2022ZD04011) and the Fundamental Research Fund for the Central Universities (lzujbky-2021-ct21).

Conflict of interest

The authors declare that the research was conducted in the absence of any commercial or financial relationships that could be construed as a potential conflict of interest.

Publisher's note

All claims expressed in this article are solely those of the authors and do not necessarily represent those of their affiliated organizations, or those of the publisher, the editors and the reviewers. Any product that may be evaluated in this article, or claim that may be made by its manufacturer, is not guaranteed or endorsed by the publisher.

Supplementary material

The Supplementary Material for this article can be found online at: https://www.frontiersin.org/articles/10.3389/fpls.2023.1149880/full#supplementary-material

References

Bacete, L., Mélida, H., López, G., Dabos, P., Tremousaygue, D., Denancé, N., et al. (2020). *Arabidopsis* response regulator 6 (ARR6) modulates plant cell-wall composition and disease resistance. *Mol. Plant Microbe In.* 33, 767–780. doi: 10.1094/MPMI-12-19-0341-R

Bhaskar, A., Paul, L. K., Sharma, E., Jha, S., Jain, M., and Khurana, J. P. (2021). OsRR6, a type-a response regulator in rice, mediates cytokinin, light and stress responses when over-expressed in *Arabidopsis*. *Plant Physiol. Bioch.* 161, 98–112. doi: 10.1016/j.plaphy.2021.01.047

Cheval, C., Perez, M., Leba, L. J., Ranty, B., Perochon, A., Reichelt, M., et al. (2017). PRR2, a pseudo-response regulator, promotes salicylic acid and camalexin accumulation during plant immunity. *Sci. Rep.* 7, 1–13. doi: 10.1038/s41598-017-07535-8

Chow, B. Y., and Kay, S. A. (2013). Global approaches for telling time: omics and the *Arabidopsis* circadian clock. *Semin. Cell. Dev. Biol.* 24, 383–392. doi: 10.1016/j.semcdb.2013.02.005

D'Agostino, I. B., Deruere, J., and Kieber, J. J. (2000). Characterization of the response of the *Arabidopsis* response regulator gene family to cytokinin. *Plant Physiol.* 124, 1706–1717. doi: 10.1104/pp.124.4.1706

Dodd, A. N., Salathia, N., Hall, A., Kévei, E., Tóth, R., Nagy, F., et al. (2005). Plant circadian clocks increase photosynthesis, growth, survival, and competitive advantage. *Science* 309, 630–633. doi: 10.1126/science.111558

Doi, K., Izawa, T., Fuse, T., Yamanouchi, U., Kubo, T., Shimatani, Z., et al. (2004). *Ehd1*, a b-type response regulator in rice, confers short-day promotion of flowering and controls *FT-like* gene expression independently of *Hd1*. *Gene. Dev.* 18, 926–936. doi: 10.1101/gad.1189604

Dong, X. M., Han, B. C., Yin, X. Y., Mao, P., Luo, D., Zhou, Q., et al. (2023). Genome-wide identification of the GRAS transcription factor family in autotetraploid cultivated alfalfa (*Medicago sativa* l.) and expression analysis under drought stress. *Ind. Crop Prod.* 194, 116379. doi: 10.1016/j.indcrop.2023.116379

Fujiwara, S., Wang, L., Han, L. Q., Suh, S. S., Salomé, P. A., McClung, C. R., et al. (2008). Post-translational regulation of the *Arabidopsis* circadian clock through selective proteolysis and phosphorylation of pseudo-response regulator proteins. *J. Biol. Chem.* 283, 23073–23083. doi: 10.1074/jbc.M803471200

Gao, J. P., Chao, D. Y., and Lin, H. X. (2008). Toward understanding molecular mechanisms of abiotic stress responses in rice. *Rice* 1, 36–51. doi: 10.1007/s12284-008-9006-7

Geng, X. C., Zhang, C., Wei, L. N., Lin, K., and Xu, Z. F. (2022). Genome-wide identification and expression analysis of cytokinin response regulator (RR) genes in the woody plant *Jatropha curcas* and functional analysis of *JcRR12* in *Arabidopsis*. *Int. J. Mol. Sci.* 23, 11388. doi: 10.3390/ijms231911388

Hasanuzzaman, M., Bhuyan, M. B., Zulfiqar, F., Raza, A., Mohsin, S. M., Mahmud, J. A., et al. (2020). Reactive oxygen species and antioxidant defense in plants under abiotic stress: Revisiting the crucial role of a universal defense regulator. *Antioxidants* 9, 681. doi: 10.3390/antiox9080681

Hass, C., Lohrmann, J., Albrecht, V., Sweere, U., Hummel, F., Yoo, S. D., et al. (2004). The response regulator 2 mediates ethylene signalling and hormone signal integration in *Arabidopsis*. *EMBO J.* 23, 3290–3302. doi: 10.1038/sj.emboj.7600337

He, Y. J., Liu, X., Ye, L., Pan, C. T., Chen, L. T., Zou, T., et al. (2016). Genome-wide identification and expression analysis of two-component system genes in tomato. *Int. J. Mol. Sci.* 17, 1204. doi: 10.3390/ijms17081204

Hu, Y. F., Cui, H. M., Xia, P. L., Liu, G. S., Wu, X. Y., Li, Y. T., et al. (2022). Genome-wide mining of b-type cytokinin response regulators in wheat reveals the involvement of TaRR5. 1-6A in drought and salt tolerance. *Crop Pasture Sci.* 73, 997–1010. doi: 10.1071/CP21766

Huo, R. X., Liu, Z. N., Yu, X. L., and Li, Z. Y. (2020). The interaction network and signaling specificity of two-component system in *Arabidopsis*. *Int. J. Mol. Sci.* 21, 4898. doi: 10.3390/ijms21144898

Hwang, I., Chen, H. C., and Sheen, J. (2002). Two-component signal transduction pathways in *Arabidopsis*. *Plant Physiol.* 129, 500–515. doi: 10.1104/pp.005504

Imamura, A., Hanaki, N., Hussain, A., Nakamura, B. G., Suzuki, T., Taniguchi, M., et al (1999). Compilation and characterization of Arabiopsis thaliana response regulators implicated in His-Asp phosphorelay signal transduction. *Plant Cell Physiol.* 40, 733–742. doi: 10.1093/oxfordjournals.pcp.a029600

Imran, Q. M., Falak, N., Hussain, A., Mun, B. G., and Yun, B. W. (2021). Abiotic stress in plants; stress perception to molecular response and role of biotechnological tools in stress resistance. *Agronomy* 11, 1579. doi: 10.3390/agronomy11081579

Ito, Y., and Kurata, N. (2006). Identification and characterization of cytokinin-signalling gene families in rice. *Gene* 382, 57–65. doi: 10.1016/j.gene.2006.06.020

Jain, M., Tyagi, A. K., and Khurana, J. P. (2008). Differential gene expression of rice two-component signaling elements during reproductive development and regulation by abiotic stress. *Funct. Integr. Genomic.* 8, 175–180. doi: 10.1007/s10142-007-0063-6

Karan, R., Singla-Pareek, S. L., and Pareek, A. (2009). Histidine kinase and response regulator genes as they relate to salinity tolerance in rice. *Funct. Integr. Genomic.* 9, 411–417. doi: 10.1007/s10142-009-0119-x

Kieber, J. J., and Schaller, G. E. (2018). Cytokinin signaling in plant development. *Development* 145, 149344. doi: 10.1242/dev.149344

Le, D. T., Nishiyama, R., Watanabe, Y., Mochida, K., Yamaguchi-Shinozaki, K., Shinozaki, K., et al. (2011). Genome-wide expression profiling of soybean two-component system genes in soybean root and shoot tissues under dehydration stress. *DNA Res.* 18, 17–29. doi: 10.1093/dnares/dsq032

Li, Y. M., Zhang, D., Zhang, L. Z., Zuo, X. Y., Fan, S., Zhang, X., et al. (2017). Identification and expression analysis of cytokinin response-regulator genes during floral induction in apple (*Malus domestica* borkh). *Plant Growth Regul.* 83, 455–464. doi: 10.1007/s10725-017-0311-2

Liu, S. X., Qin, B., Fang, Q. X., Zhang, W. J., Zhang, Z. Y., Liu, Y. C., et al. (2021). Genome-wide identification, phylogeny and expression analysis of the *bZIP* gene family in alfalfa (*Medicago sativa*). *Biotechnol. Biotec. Eq.* 35, 905–916. doi: 10.1080/13102818.2021.1938674

Liu, W., Zhang, W., Du, M., Sha, Y., Yu, X., Ohtani, M., et al. (2013). Diurnal and circadian expression of clock-associated pseudo-response regulators in *Populus trichocarpa*. *Plant Biotechnol.* 30, 517–521. doi: 10.1007/s10725-017-0311-2

Liu, Z. N., Zhang, M., Kong, L. J., Lv, Y. X., Zou, M. H., Lu, G., et al. (2014). Genome-wide identification, phylogeny, duplication, and expression analyses of two-component system genes in Chinese cabbage (*Brassica rapa* ssp. pekinensis). *DNA Res.* 21, 379–396. doi: 10.1093/dnares/dsu004

Mason, M. G., Mathews, D. E., Argyros, D. A., Maxwell, B. B., Kieber, J. J., Alonso, J. M., et al. (2005). Multiple type-b response regulators mediate cytokinin signal transduction in *Arabidopsis*. *Plant Cell* 17, 3007–3018. doi: 10.1105/tpc.105.035451

Matzke, M., Kanno, T., Daxinger, L., Huettel, B., and Matzke, A. J. (2009). RNA-Mediated chromatin-based silencing in plants. *Curr. Opin. Cell Biol.* 21, 367–376. doi: 10.1016/j.ceb.2009.01.025

McClung, C. R. (2006). Plant circadian rhythms. *Plant Cell* 18, 792–803. doi: 10.1105/tpc.105.035451

Murakami, M., Yamashino, T., and Mizuno, T. (2004). Quintet of circadian associated APRR1/TOC1 family in *Arabidopsis thaliana*: Characterization of a transgenic line aberrantly overexpressing APRR3. *Plant Cell Physiol.* 45, S69–S69. doi: 10.1093/pcp/pch065

Nakamichi, N., Takao, S., Kudo, T., Kiba, T., Wang, Y., Kinoshita, T., et al. (2016). Improvement of *Arabidopsis* biomass and cold, drought and salinity stress tolerance by modified circadian clock-associated PSEUDO-RESPONSE REGULATORs. *Plant Cell Physiol.* 57, 1085–1097. doi: 10.1093/pcp/pcw057

Pareek, A., Singh, A., Kumar, M., Kushwaha, H. R., Lynn, A. M., and Singla-Pareek, S. L. (2006). Whole-genome analysis of *Oryza sativa* reveals similar architecture of two-component signaling machinery with *Arabidopsis*. *Plant Physiol.* 142, 380–397. doi: 10.1104/pp.106.086371

Peng, J. C., and Karpen, G. H. (2008). Epigenetic regulation of heterochromatic DNA stability. *Curr. Opin. Genet. Dev.* 18, 204–211. doi: 10.1016/j.gde.2008.01.021

Qiao, X., Li, Q. H., Yin, H., Qi, K. J., Li, L. T., Wang, R., et al. (2019). Gene duplication and evolution in recurring polyploidization-diploidization cycles in plants. *Genome Biol.* 20, 1–23. doi: 10.1186/s13059-019-1650-2

Ramírez-Carvajal, G. A., Morse, A. M., and Davis, J. M. (2008). Transcript profiles of the cytokinin response regulator gene family in populus imply diverse roles in plant development. *New Phytol.* 177, 77–89. doi: 10.1111/j.1469-8137.2007.02240.x

Razi, K., and Muneer, S. (2021). Drought stress-induced physiological mechanisms, signaling pathways and molecular response of chloroplasts in common vegetable crops. *Crit. Rev. Biotechnol.* 41, 669–691. doi: 10.1080/07388551.2021.1874280

Rehman, O. U., Uzair, M., Chao, H., Fiaz, S., Khan, M. R., and Chen, M. (2022). Role of the type-b authentic response regulator gene family in fragrant rice under alkaline-salt stress. *Physiol. Plant.* 174, e13696. doi: 10.1111/ppl.13696

Ren, L., Bennett, J. A., Coulman, B., Liu, J., and Biligetu, B. (2021). Forage yield trend of alfalfa cultivars in the Canadian prairies and its relation to environmental factors and harvest management. *Grass Forage Sci.* 76, 390–399. doi: 10.1111/gfs.12513

Sun, J., and Guo, C. (2022). Genome-wide identification and expression analysis of RR-type MYB-related transcription factors in tomato (*Solanum lycopersicum* l.). *Horticulturae* 8, 399. doi: 10.3390/horticulturae8050399

To, T. K., Kim, J. M., Matsui, A., Kurihara, Y., Morosawa, T., Ishida, J., et al. (2011). *Arabidopsis* HDA6 regulates locus-directed heterochromatin silencing in cooperation with MET1. *PloS Genet.* 7, e1002055. doi: 10.1371/journal.pgen.1002055

Tsai, Y. C., Weir, N. R., Hill, K., Zhang, W., Kim, H. J., Shiu, S. H., et al. (2012). Characterization of genes involved in cytokinin signaling and metabolism from rice. *Plant Physiol.* 158, 1666–1684. doi: 10.1104/pp.111.192765

Van de Peer, Y., Maere, S., and Meyer, A. (2009). he evolutionary significance of ancient genome duplications. *Nat. Rev. Genet.* 10, 725–32. doi: 10.1038/nrg2600

Wang, W. C., Lin, T. C., Kieber, J., and Tsai, Y. C. (2019). Response regulators 9 and 10 negatively regulate salinity tolerance in rice. *Plant Cell Physiol.* 60, 2549–2563. doi: 10.1093/pcp/pcz149

Wang, D., Pei, K., Fu, Y., Sun, Z., Li, S., Liu, H., et al. (2007). Genome-wide analysis of the auxin response factors (ARF) gene family in rice (*Oryza sativa*). *Gene* 394, 13–24. doi: 10.1016/j.gene.2007.01.006

Wang, R., Ming, M., Li, J., Shi, D., Qiao, X., Li, L., et al (2017). Genome-wide identification of the MADS-box transcription factor family in pear (Pyrus bretschneideri) reveals evolution and functional divergence. *PeerJ* 5, e3776. doi: 10.7717/peerj.3776

Wang, C., Wang, L., Liu, Q., Zhang, Y., and Dong, K. (2022). Genome-wide identification and characterization of PRR gene family and their diurnal rhythmic expression profile in maize. *Int. J. Genomics*, 6941607. doi: 10.1155/2022/6941607

Wang, D., Zhang, Y., Zhang, Z., Zhu, J., and Yu, J. (2010). KaKs_Calculator 2.0: a toolkit incorporating gamma-series methods and sliding window strategies. *Genom. Proteom. Bioinf.* 8, 77–80. doi: 10.1016/S1672-0229(10)60008-3

West, A. H., and Stock, A. M. (2001). Histidine kinases and response regulator proteins in two-component signaling systems. *Trends Biochem. Sci.* 26, 369–376. doi: 10.1016/S0968-0004(01)01852-7

Woelfle, M. A., Ouyang, Y., Phanvijhitsiri, K., and Johnson, C. H. (2004). The adaptive value of circadian clocks: An experimental assessment in cyanobacteria. *Curr. Biol.* 14, 1481–1486. doi: 10.1016/j.cub.2004.08.023

Yanovsky, M. J., and Kay, S. A. (2003). Living by the calendar: how plants know when to flower. nat. rev. mol. *Cell Biol.* 4, 265–276. doi: 10.1038/nrm1077

Zeng, R., Li, Z. Y., Shi, Y. T., Fu, D. Y., Yin, P., Cheng, J. H., et al. (2021). Natural variation in a type-a response regulator confers maize chilling tolerance. *Nat. Commun.* 12, 1–13. doi: 10.1038/s41467-021-25001-y

Zhang, Y. C., Gao, M., Singer, S. D., Fei, Z. J., Wang, H., and Wang, X. P. (2012). Genome-wide identification and analysis of the *TIFY* gene family in grape. *PloS One* 7, e44465. doi: 10.1371/journal.pone.0044465

Zhao, L. J., Guo, L. X., Lu, X. K., Malik, W. A., Zhang, Y. X., Wang, J., et al. (2022). Structure and character analysis of cotton response regulator genes family reveals that *GhRR7* responses to draught stress. *Biol. Res.* 55, 1–19. doi: 10.1186/s40659-022-00394-2

frontiers | Frontiers in Plant Science

TYPE Original Research
PUBLISHED 28 March 2023
DOI 10.3389/fpls.2023.1163195

OPEN ACCESS

EDITED BY
Maofeng Chai,
Qingdao Agricultural University, China

REVIEWED BY
Xiao Guo,
Qingdao Agricultural University, China
Rongjiang Yao,
Institute of Soil Science (CAS), China

*CORRESPONDENCE
Zhengguo Sun
sunzg@njau.edu.cn

SPECIALTY SECTION
This article was submitted to Plant Abiotic Stress, a section of the journal Frontiers in Plant Science

RECEIVED 10 February 2023
ACCEPTED 10 March 2023
PUBLISHED 28 March 2023

CITATION
Yang R, Sun Z, Liu X, Long X, Gao L and Shen Y (2023) Biomass composite with exogenous organic acid addition supports the growth of sweet sorghum (*Sorghum bicolor* '*Dochna*') by reducing salinity and increasing nutrient levels in coastal saline–alkaline soil.
Front. Plant Sci. 14:1163195.
doi: 10.3389/fpls.2023.1163195

Biomass composite with exogenous organic acid addition supports the growth of sweet sorghum (*Sorghum bicolor* '*Dochna*') by reducing salinity and increasing nutrient levels in coastal saline–alkaline soil

Ruixue Yang[1], Zhengguo Sun[1]*, Xinbao Liu[1], Xiaohua Long[2], Limin Gao[3] and Yixin Shen[1]

[1]College of Agro-grassland Science, Nanjing Agricultural University, Nanjing, China, [2]College of Resources and Environmental Sciences, Nanjing Agricultural University, Nanjing, China, [3]Ecological Research Center, Nanjing Institute of Agricultural Sciences in Jiangsu Hilly Area, Nanjing, China

Introduction: In coastal saline lands, organic matter is scarce and saline stress is high. Exploring the promotion effect of intervention with organic acid from biological materials on soil improvement and thus forage output and determining the related mechanism are beneficial to the potential cultivation and resourceful, high-value utilization of coastal mudflats as back-up arable land.

Method: Three exogenous organic acids [humic acid (H), fulvic acid (F), and citric acid (C)] were combined with four kinds of biomass materials [cottonseed hull (CH), cow manure (CM), grass charcoal (GC), and pine needle (PN)] and applied to about 0.3% of medium-salt mudflat soil. The salinity and nutrient dynamics of the soil and the growth and physiological differences of sweet sorghum at the seedling, elongation, and heading stages were observed under different treatments to screen for efficient combinations and analyze the intrinsic causes and influencing mechanisms.

Results: The soil salinity, nutrient dynamics, and forage grass biological yield during sweet sorghum cultivation in saline soils differed significantly ($p < 0.05$) depending on the type of organic acid–biomass composite applied. Citric acid–pine needle composite substantially reduced the soil salinity and increased the soil nutrient content at the seedling stage and improved the root vigor and photosynthesis of sweet sorghum by increasing its stress tolerance, allowing plant morphological restructuring for a high biological yield. The improvement effect of fulvic acid–pine needle or fulvic acid–cow manure composite was manifested at the elongation and heading stages.

Discussion: Citric acid–pine needle composite promoted the growth of saline sweet sorghum seedlings, and the effect of fulvic acid–pine needle composite lasted until the middle and late stages.

KEYWORDS

sweet sorghum, coastal saline-alkali soil, exogenous organic acid, biomass material, saline-alkali regulation, soil fertility improvement, resistant growth

Introduction

Saline–alkaline soil has many limiting factors in agricultural production due to excessive salt enrichment and high levels of exchangeable sodium (Uri, 2018) and can be classified as primary or secondary saline according to its genesis (Negacz et al., 2022). Coastal saline soils are one of the main types of primary saline soils and are formed by the siltation of incoming sediment and impregnation by highly mineralized seawater (Cui et al., 2021). These lands are extremely widely distributed in the coastal areas of China, which involve 11 provinces or municipalities with a total coastline length of 3.2×10^4 km and a total mudflat area of 1.3×10^7 ha. The total area of mudflats in Jiangsu Province alone accounts for 6.52×10^5 ha, which is about 25% of the total area of mudflats in China (Shao et al., 2019; Yang et al., 2021a; Zhang et al., 2020b). However, seed germination and crop seedling formation, establishment, and growth are greatly impaired due to the high degree of salinization, nutrient deficiency, low nutrient utilization (Wang et al., 2020b), and poor soil texture and structural stability of mudflat soils, and the seasonal salt regression and frequent salt accumulation (Odeh and Onus, 2008; Dong et al., 2020). In some cases, serious osmotic stress and ion toxicity even occur (Sun et al., 2022). Therefore, saline–alkaline soil is difficult to use directly because of the restrictive factors in agricultural production (Paul and Lade, 2014; Ranasinghe and Piyadasa, 2020). According to the current national marine economic development planning outline and other relevant documents, adopting scientific and efficient methods to manage saline–alkaline land is of great significance to maintain the red line of cultivated land, stabilize the cultivated land fertility, ensure food security, and efficiently use plant–land resources in a coastal wetland ecosystem. In addition, these techniques can be used to fully exploit the potential and orderly develop saline–alkaline land as reserve farmland and explore land management and utilization patterns in line with economic and social development in coastal areas.

The use of biological methods to improve saline soils is beneficial in the development of the virtuous cycle of the plant–soil feedback system under saline conditions (Meki et al., 2022), gradually eliminating saline components from the soil and improving soil nutrients to fully utilize them. Sweet sorghum (*Sorghum bicolor* '*Dochna*') is a saline–alkaline-tolerant C4 plant with a long history of cultivation in coastal areas of eastern China, making it more suitable than other forage grasses for bioremediation activities in mudflat soils that lack freshwater resources (Shi et al., 2022; Zhang et al., 2023). Although planting salt-tolerant forage grasses as a biological improvement measure for saline soils has received recognition and support (Wang et al., 2018), medium- to high-salinity soils still cause great stress on the seed germination and seedling establishment of salt-tolerant forage grass. For this reason, biomass materials are usually introduced to provide a favorable soil environment in the root zone for salt-tolerant forage grasses to avoid the influence of high salt; the signal information and related substances of reducing salt, regulating acidity, and increasing fertility are simultaneously sent to the soil (El Hasini et al., 2019). Biomass materials refer to environmentally friendly materials obtained by further fermentation or heat treatment using industrial by-products or waste from the production of agriculture, forestry, and livestock as raw materials (Kulikova et al., 2022). Common biomass materials include crop straw, wood chips, cottonseed hulls, cow manure, pine needles, mushroom residue, and grass charcoal. These biomass materials have a high potential for saline soil improvement due to their structural stability and adsorption properties (Wang et al., 2017). Planting salt-tolerant forage grasses grown in saline soils with low-to-medium salinity could improve the physical and hydraulic properties of saline soils through biomass material addition (Liang et al., 2021) and regulate their nutrient status and functional microbial activity (Li and Li, 2022; Yao et al., 2022a). Biomass has a unique microporous structure and some functional groups that can cut off the continuity of soil capillaries, inhibit the transport and accumulation of water and salts to the upper layers of the soil (Wu et al., 2021c), and improve soil porosity and structure by forming iron complexes to increase soil aggregates (Li et al., 2021; Chen et al., 2022). In addition, the exogenous application of biomass increases the content of energy substrates and bioactive substances in soil (Kaur et al., 2005; Wong et al., 2009), significantly increases soil microbial and enzyme activities, and regulates soil microbial community structure (Wu et al., 2021a), thus favorably affecting plant root and aboveground growth and soil ecology (Chen et al., 2021b; Li et al., 2022a). However, the differences in composition and internal mechanism among biomass materials lead to their varying effects on the growth of salt-tolerant forage grasses in saline–alkaline soil and the improvement of the soil itself (Amini et al., 2016).

With the progressive understanding of the structure and function of organic acids, composites rich in citric acid, humic acid, fulvic acid, or other organic acid components have become new products in the fields of environmental remediation and crop

growth regulation (Ma et al., 2020; Guo et al., 2022). These chemical conditioners, fertilizers, and other functional products whose main component is organic acid are referred to as organic acid products. The addition of organic acids and their products to saline soils can neutralize soil alkalinity through the acid hydrolysis of active functional groups, enhance the solubility and mobility of insoluble nutrients, and adsorb metal ions from saline–alkaline soil through complexation and chelation; as a result, the nutrient content and physical structure of the soil are further improved (Liu et al., 2020; Hu et al., 2021; Xiao et al., 2022); the rapid alkali reduction and desalting are achieved; the nutrient reservoir capacity of saline–alkaline land is increased; and the plant nutrient utilization is improved (Liu et al., 2019; Mosaad et al., 2022). It can also improve crop yield by changing the root architecture, increasing root vigor and growth, and intercepting additional nutrients from the soil by adjusting the density of primary and secondary roots and the number of branches (Liao et al., 2006; Aoki et al., 2012; Neumann et al., 2000; Zandonadi et al., 2007). It can help plants under saline stress to increase the ratio of K^+/Na^+ (Li et al., 2022b), enhance the accumulation of soluble sugar and soluble protein, increase the concentration of osmoregulatory substances and the function of the antioxidant system (Do Nascimento et al., 2006; Liu et al., 2015), alleviate lipid peroxidation, and improve the salt tolerance index of crops (Mallhi et al., 2019). Therefore, the above-mentioned biomass materials and organic acids or their products have stronger effects on salt-tolerant forage production and soil salinity reduction in saline soils. However, whether the combination of different types of organic acid with different types of biomass as a treatment for salt-tolerant forage grasses in saline soils is more effective than their individual effects at the seedling stage (when resistance is relatively weak), elongation stage (when growth is fast), and heading stage (when nutrients start to be transferred) is unknown. A comprehensive literature review revealed the lack of studies in this area. Therefore, this research proposed a technical model (Figure 1) for the exogenous application of organic acids combined with biomass for salt-tolerant forage in saline soils. The findings will broaden the perception of biomass methods for improving saline soils and serve as the basis for the application of organic acids or their products in saline soil agriculture.

For the saline–alkaline characteristics of mudflat soils and based on the physicochemical data of organic materials, three representative natural organic acids in soils, humic acid (H), fulvic acid (F), and citric acid (C), were selected with four acidic or neutral biomass materials with good structure, namely, cottonseed hull (CH), cow manure (CM), grass charcoal (GC), and pine needle (PN). Several exogenous organic acids were composited with different biomass materials and applied as a treatment for sweet sorghum growing in the coastal saline–alkaline land of eastern China to investigate their effects on plant production performance with respect to soil nutrients and salinity and to explore the mechanisms related to the interaction between different types of organic acids and biomass materials and its effect on soil improvement and alleviation of saline–alkaline stress in crops. The main objectives of this study were as follows: (i) to explore the mechanisms of the effects of different exogenous organic

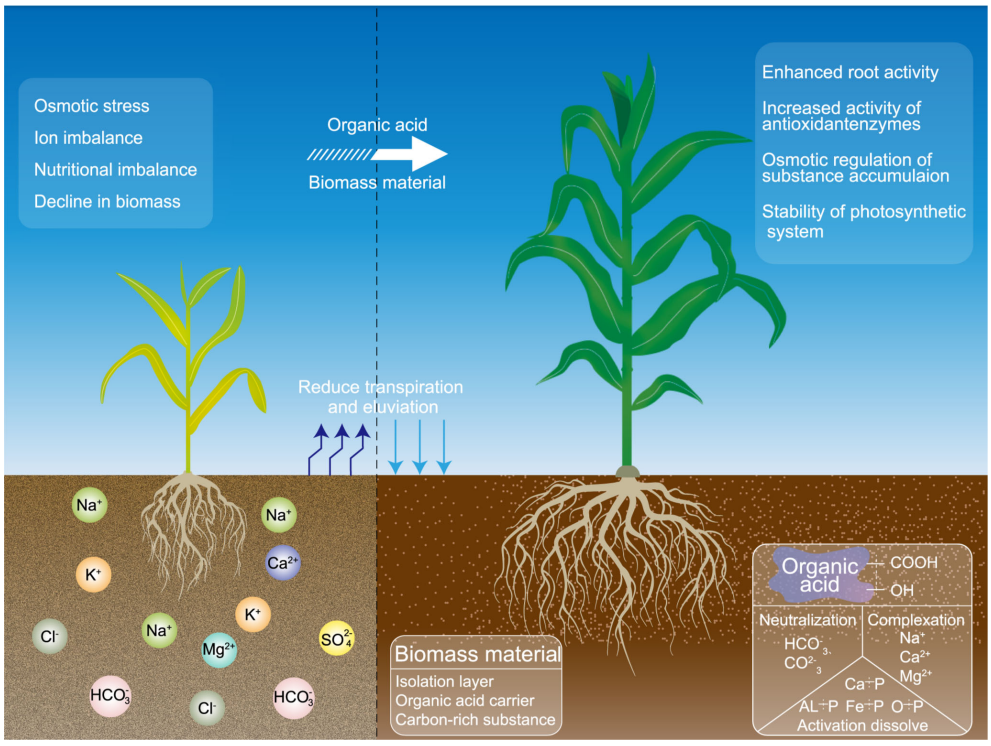

FIGURE 1
Model diagram of sweet sorghum growth improved by exogenous organic acid and biomass materials in coastal mudflat soil.

acid-biomass material composite on the salinity dynamics and nutrient accumulation in coastal mudflat soils; (ii) to determine the factor driving the relationship between different exogenous organic acid-biomass material composite with the growth, physiological changes, and accumulation of active compounds in sweet sorghum under saline stress; and (iii) to reveal the correlation between the physicochemical characteristics of mudflat soil and the growth performance of plants under treatments with different exogenous organic acid–biomass material composite. The results will help enhance the understanding of different types of exogenous organic acid–biomass composites for soil amendment or targeted improvement of plant stress tolerance and provide new ideas for organic acid utilization.

Materials and methods

Overview of the research area

The experiment was carried out in a coastal saline soil in the strip mud reclamation area of Jianggang Town, Dongtai City, Jiangsu Province, China (N 32° 83′, E 120° 96′). The soil type in this area is alluvial tidal saline soil, which belongs to silty loam and contains 20.5% sand, 8.0% clay, and 71.5% silt (0–20 cm). The specific physicochemical properties are shown in Table 1. The area has a subtropical monsoon maritime climate with an average annual temperature of 16.3°C and an average annual precipitation of 1,024 mm, which mainly occurs in summer.

Experimental design and field management

The field experiment was conducted on sweet sorghum samples under 13 treatments in June 2021 (Figure 2):(1) CK, (2) HCM, (3) HPN, (4) HCH, (5) HGC, (6) FCM, (7) FPN, (8) FCH, (9) FGC, (10) CCM, (11) CPN, (12) CCH, and (13) CGC. All treatments were replicated three times, and the application rates of organic acid and biomass were 120 and 5,000 kg ha^{-1}, respectively, in all treatments. The cultivar of sweet sorghum used was "Big Kahuna," a new forage sorghum variety that is drought and salinity tolerant and has photoperiod sensitivity and brown midrib characteristics, resulting in high biological yield and nutritional value. The sources and properties of organic acid materials are shown in Table 2. For the biomass materials, the CM was aerobically composted and fermented for about 40 days after wet and dry separation; the CH was made from the residual husk scraps of edible mushroom culture material; the GC was prepared from the accumulation of incompletely decomposed plant residues fermented in an overly wet and suspicious natural environment; and the PN were those that had accumulated on the soil surface of lacebark pine forests and collected after natural weathering and decomposition. The specific physical and chemical properties of these biomass materials are shown in Table 3. The study used a randomized block design with split plots, where organic acid was the main plot and biomass was the split plot, with a plot arrangement of 10 m^2 (4 m long and 2.5 m wide). The soil tillage layer (0–20 cm) was rototilled before the start of the experiment. In addition to the land preparation, drainage ditches (30 cm deep and 40 cm wide) were opened between the plots so that these ditches could be connected to the drainage pipes at the edges of the fields to avoid seedling damage caused by waterlogging in the fields. A double layer of mulch was placed along a vertical depth of 0–30 cm close to the edge of each plot to stop the migration of water salts, nutrients, and other substances between the plots. The base fertilizer application was 300 kg ha^{-1} of compound fertilizer (N, 15%; P, 15%; and K, 15%), which was applied during land preparation. The follow-up fertilizer was applied twice at 30 and 60 days after seedling emergence with 75 kg ha^{-1} of urea (N, 46.4%). The organic acid pellets (or powder) were mixed evenly with the biomass material and then spread into the plots and pulled back and forth with a rake to mix evenly into the topsoil. The sweet sorghum variety was Big Kahuna, which was planted in June 2021 using the strip sowing method with a row spacing of 40 cm and a sowing depth of 2 cm. The seedlings were set to a specification standard of 25 cm apart during the three-leaf period. During the growing season, timely prevention and elimination were carried out in conjunction with the occurrence of diseases, insects, and weeds in the field. Owing to the abundant rainfall during the growing season, no irrigation was carried out for moisture management and the water in the field was removed in a timely manner.

Plant and soil sampling

Samples were taken at 30 days (when the leaves reached five to seven and the plant was in the seedling stage of rapid seedling growth), 60 days (when the nodes can be touched at the base edge of the stem and the plant was in the elongation stage of rapid internode elongation), and 90 days (when the uppermost flag leaf of the plant was fully expanded and the plant was in the heading

TABLE 1 Basic physical and chemical properties of primitive soil.

Properties	Values	Properties	Values
Field water capacity (%)	23.05 ± 0.16	Organic matter content (g kg^{-1})	8.77 ± 0.02
Soil bulk density (g cm^{-3})	1.47 ± 0.04	Total nitrogen content (g kg^{-1})	0.45 ± 0.01
Soil pH	9.16 ± 0.01	Total phosphorus content (g kg^{-1})	0.52 ± 0.02
Soil electrical conductivity$_{1:5}$ (μs cm^{-1})	492.0 ± 4.73	Alkali-hydrolyzed nitrogen content (mg kg^{-1})	22.18 ± 0.13
Soil soluble salt content (g kg^{-1})	3.22 ± 0.04	Available phosphorus content (mg kg^{-1})	14.18 ± 0.02

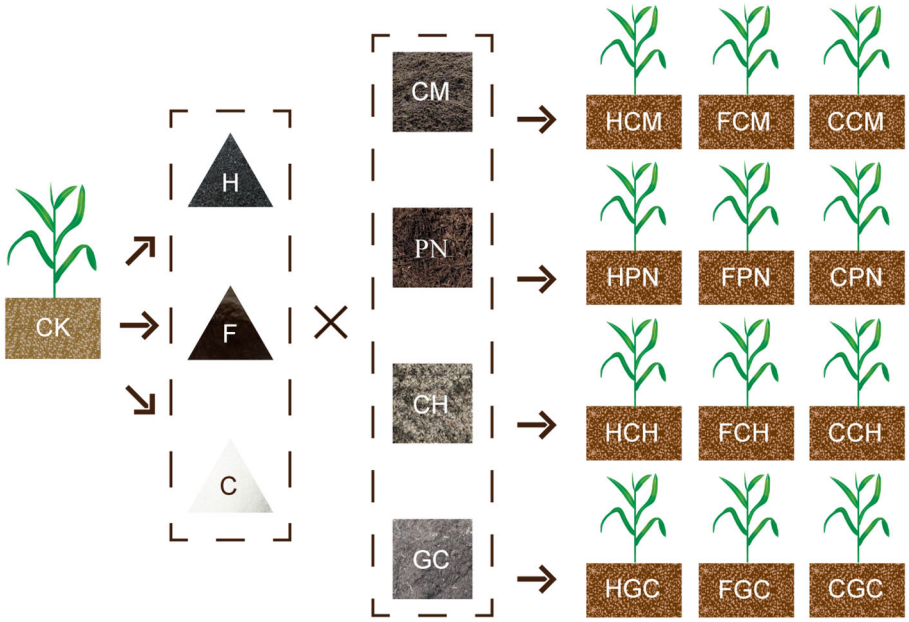

FIGURE 2
Schematic of the two-factor combination and treatment distribution. H, humic acid; F, fulvic acid; C, citric acid; CH, cottonseed hull; CM, cow manure; GC, grass charcoal; PN, pine needle; HCH, humic acid–cottonseed hull composite; HCM, humic acid–cow manure composite; HGC, humic acid–grass charcoal composite; HPN, humic acid–pine needle composite; FCH, fulvic acid–cottonseed hull composite; FCM, fulvic acid–cow manure composite; FGC, fulvic acid–grass charcoal composite; FPN, fulvic acid–pine needle composite; CCH, citric acid–cottonseed hull composite; CCM, citric acid–cow manure composite; CGC, citric acid–grass charcoal composite; CPN, citric acid–pine needle composite; CK, without the addition of organic acids and biomasses. The same as Tables 2, 3, and Figures 3–7.

stage of nutrient transfer) after emergence. Dig a 30-cm-diameter and 40-cm-deep soil column centered on sweet sorghum and remove the soil attached to the root system to obtain a complete plant. Five representative plants from each plot were collected and placed in a low-temperature preservation box and brought back to the laboratory. Soil (0–20 cm) from each plot was sampled using the five-point method ("S" distribution) using a soil auger, placed in sterile, sealed bags, and brought back to the laboratory to air-dry for testing.

Plant and soil analysis

The sweet sorghum was rinsed with water and then dried. The absolute length from the base of the plant stalk up to the absolute length of the highest point where the sword leaves were straightened was measured using a tape measure as plant height. The diameter at the middle of the first internode at the base of the plant stem was measured as stem diameter using vernier calipers. The absolute length of the plant from the base of the stem to the longest root position was measured as the root length, and the number of plant leaves was recorded. The above-ground part was then separated from the root system, heated in an oven at 105°C for 30 min, and then dried at 65°C to constant weight. The above-ground part and root system were weighed separately, and the whole plant's dry weight was labeled as single plant biomass. Root activity was determined using the triphenyltetrazolium chloride method (Lassheikki et al., 1991). The procedure and method for the determination of chlorophyll content were referred to by Ghobadi et al. (2013). Malondialdehyde content was determined using the method of Wang and Jin (2005). The procedure and calculation of proline content were referred to by Bates et al. (1973). Soluble sugar

TABLE 2 Sources and basic properties of organic acids.

Organic acid species	Solubility	Structure	Appearance	pH	C (%)	H (%)	O (%)	N (%)
H[a]	Slightly soluble in water	High molecular polymer	Black powder	6.82 ± 0.02	37.91 ± 0.24	3.46 ± 0.03	25.43 ± 0.24	0.61 ± 0.01
F[a]	Soluble in water, acid, alkali	High molecular polymer	Brown powder	5.26 ± 0.03	28.35 ± 0.18	4.23 ± 0.02	41.18 ± 0.17	3.24 ± 0.02
C[b]	Highly soluble in water	Low molecular weight	White granule	1.47 ± 0.01	36.72 ± 0.10	4.77 ± 0.03	55.30 ± 0.19	0.18 ± 0.01

[a]The H and F are provided by Xinjiang Shengda Yifang Biotechnology Co. Ltd.
[b]The C is purchased by Weifang Yingxuan Industrial Co. Ltd.

TABLE 3 Sources and basic properties of biomass materials.

Biologic material species	pH	Electrical conductivity$_{1:5}$ (μs cm$^{\pm 1}$)	Organic matter content (g kg^{-1})	Total nitrogen content (g kg^{-1})	Total phosphorus content (g kg^{-1})	Alkali-hydrolyzed nitrogen content (mg kg^{-1})	Available phosphorus content (mg kg^{-1})
CH[a]	7.3 ± 0.03	1,682 ± 15.52	297.9 ± 3.58	11.85 ± 0.63	2.95 ± 0.01	728.9 ± 8.24	776.7 ± 8.98
PN[a]	5.38 ± 0.02	1,308 ± 6.66	407.9 ± 5.54	10.2 ± 0.09	0.66 ± 0.01	1,375 ± 24.71	79.73 ± 1.87
GC[a]	5.08 ± 0.03	841.0 ± 9.07	244.1 ± 3.22	8.46 ± 0.02	0.79 ± 0.01	693.2 ± 16.13	45.82 ± 1.75
CM[b]	7.70 ± 0.03	1,416 ± 8.14	345.8 ± 4.91	9.69 ± 0.04	2.36 ± 0.02	477.6 ± 6.69	519.8 ± 8.53

[a]The CH, PN, and GC are purchased by Shijiazhuang Nongyou Biotechnology Co. Ltd.
[b]The CM is provided by Jurong Lantian Bishui Biotechnology Co. Ltd.

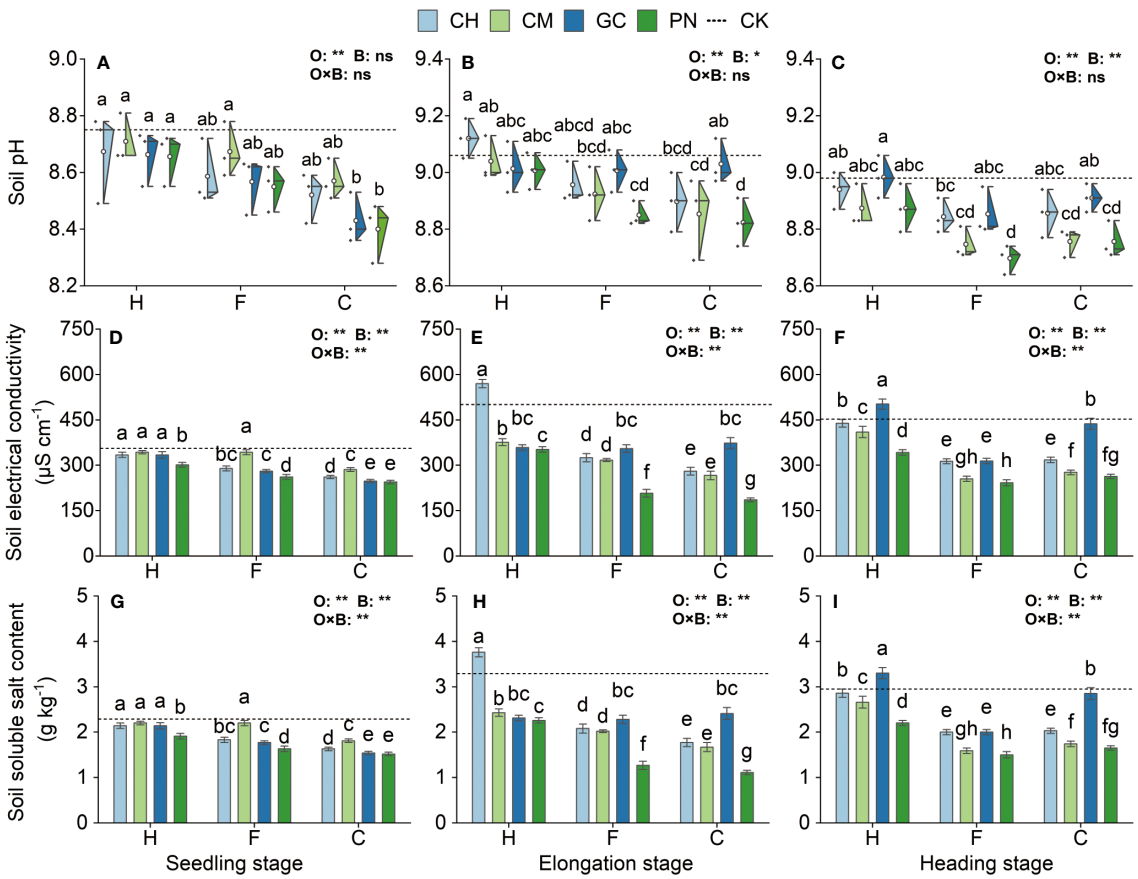

FIGURE 3
Effects of exogenous organic acids combined with biomass materials on the pH, electrical conductivity, and soluble salt content of mudflat soil. **(A, D, G)** Represent the seedling stage, **(B,E,H)** represent the elongation stage, and **(C, F, I)** indicate as the heading stage. O, organic acid treatment; B, biomass material treatment; O×B, combined treatment of organic acid and biomass material. **1% and *5%-levels of significant difference; ns, not significant at 5% level. Bars with different lowercase letters indicate a significant difference ($p < 0.05$) within one development stage. The same as Figures 4–7.

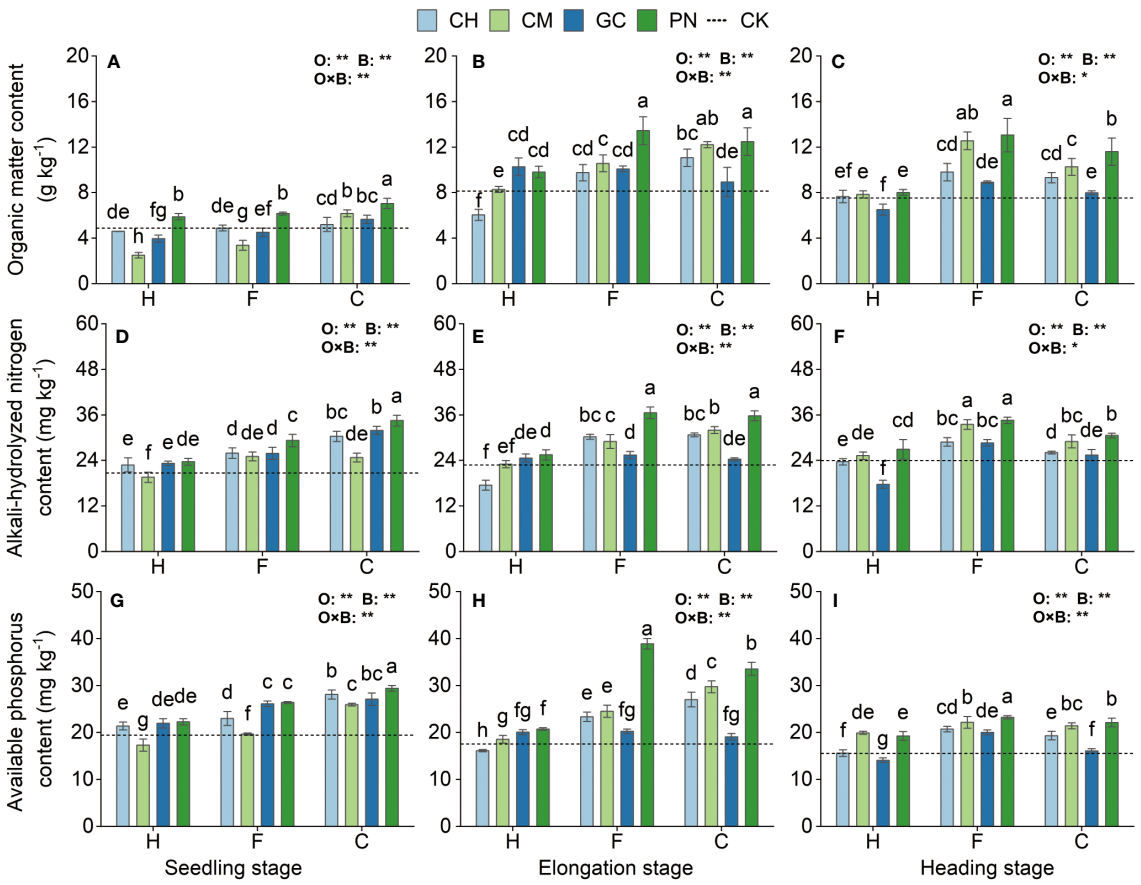

FIGURE 4
Effects of exogenous organic acids and substrates on the accumulation of organic matter, available phosphorus, and alkali-hydrolyzed nitrogen in mudflat soil at different periods. **(A, D, G)** Represent the seedling stage, **(B, E, H)** represent the elongation stage, and **(C, F, I)** indicate as the heading stage. **1% and *5%-levels of significant difference; ns, not significant at 5% level. Bars with different lowercase letters indicate a significant difference ($p < 0.05$) within one development stage.

content was determined by the modified method of Sun et al. (2015). Superoxide dismutase (SOD), peroxidase (POD), and catalase (CAT) activities were determined by the method of Raza et al. (2007). Soil organic matter content was determined by the wet digestion method using potassium dichromate reagent (Jones, 2017). Soil alkaline-hydrolyzed nitrogen content was analyzed by the diffusion absorption method, and soil available phosphorus content was determined by the colorimetric method referring to the study of Pansu and Gautheyrou (2006) for the specific analytical methods. Soil pH was determined using a pH meter (*Eutech* pH 700, USA) with a soil-to-water ratio of 1:5. Soil electrical conductivity was determined using a conductivity meter (DDS-307A, Shanghai, China) with a soil-to-water ratio of 1:5. The soil-soluble salt content was measured using the solid residue method of Makkaveev and Stunzhas (2017). After the relationship between soil soluble salt content and electrical conductivity was obtained, the soil soluble salt content of all samples was calculated according to the following formula:

$$SS = 0.0068EC - 0.1305,$$

Where SS means soil-soluble salt content ($g \cdot kg^{-1}$) and EC represents soil electrical conductivity ($\mu s \cdot cm^{-1}$)

Statistical analysis

Microsoft Excel 2010 was used for preliminary statistics, and IBM SPSS Statistics 23.0 software was employed for one- and two-way ANOVA. Duncan's test was applied for multiple comparisons of the data, and a two-way ANOVA was used to test two factors and their interactions. Origin 2022 was utilized to produce the graphs. Data were expressed as "mean ± standard error," and significant differences were expressed using the alphabetical method ($p < 0.05$). Correlation plot software in Origin 2022 was used for correlation analysis.

Results

Effects of different combinations of exogenous organic acids and biomass materials on the saline–alkaline dynamics of mudflat soil

Some differences were noted in the response values of soil pH, electrical conductivity, and soluble salt content to the application of

exogenous organic acids and biomass materials in different periods (Figure 3; Supplementary Table S1). Organic acids significantly affected soil electrical conductivity and soluble salt content at the seedling, elongation, and heading stages ($p < 0.01$), and biomass materials significantly affected soil electrical conductivity and soluble salt content at the three periods and soil pH at the elongation stage ($p < 0.01$). In addition, the interaction effect between organic acids and biomass materials highly significantly influenced soil electrical conductivity and soluble salt content in all periods ($p \leq 0.01$) but not soil pH ($p > 0.05$). Soil pH in the CPN and CGC treatments was the lowest at the seedling stage and was not significantly different ($p > 0.05$) from that in the CCH, FPN, FGC, FCH, and CCM treatments but was significantly lower ($p \leq 0.05$) than that in the remaining treatments. Soil electrical conductivity and soluble salt values were also significantly low ($p < 0.05$) in the CPN and CGC treatments. The soil pH in the CPN treatment was the lowest at the elongation stage and was not significantly different ($p > 0.05$) from that in the FPN, CCM, FCM, and FCH treatments, but it was significantly lower ($p \leq 0.05$) than that in the remaining treatments. The soil electrical conductivity and soluble salt content in the CPN treatment were also significantly lower ($p < 0.05$) than those in the other treatments. Soil pH in the FPN, CPN, FCM, and CCM treatments was the lowest at the heading stage, and the difference between these treatments was not significant ($p > 0.05$). Soil electrical conductivity and soluble salt content in the FPN treatment were the lowest and were not significantly different from those in the FCM treatment ($p > 0.05$) but were significantly lower than those in the other treatments ($p \leq 0.05$).

Effects of different combinations of exogenous organic acids and biomass materials on soil nutrient content in tidal flats

Our results show highly significant differences ($p < 0.01$) in the response values of soil organic matter, available phosphorus, and alkali-hydrolyzed nitrogen content to the application of organic acids and biomass materials in the mudflat soils from the seedling stage to the heading stage (Figure 4; Supplementary Table S1). The interaction effects of organic acids and biomass materials reached a highly significant level ($p < 0.01$) for all indicators except soil organic matter and alkali-hydrolyzed nitrogen values at the heading stage, which were only significantly affected ($p < 0.05$). At the seedling stage, the soil organic matter, available phosphorus, and alkali-hydrolyzed nitrogen contents of the CPN treatment were significantly higher ($p < 0.05$) than those of the other treatments and increased by 44.17%, 66.73%, and 51.24%, respectively, compared with those of CK. Soil organic matter and alkali-hydrolyzed nitrogen contents in the FPN and CPN treatments were the highest at the elongation stage, and all indicators were significantly higher than those in the other treatments ($p \leq 0.05$), except for soil organic matter, which was not significantly different from that in the CCM treatment ($p > 0.05$). The soil organic matter in the FPN treatment was the highest at the heading stage and was not significantly different from those in the FCM treatment ($p > 0.05$), but it was significantly higher than those in the other treatments ($p \leq 0.05$). Soil alkali-hydrolyzed nitrogen values were also significantly high ($p < 0.05$) in the FPN and FCM treatments. Soil available phosphorus in the FPN treatment was also significantly higher ($p < 0.05$) than those in the other treatments at the elongation stage and heading stage.

Effects of different combinations of exogenous organic acids and biomass materials on the morphological indexes and biomass of sweet sorghum

The morphological indicators and biomass of sweet sorghum differed in their responses to the application of exogenous organic acids and biomass materials at different growth stages (Figure 5; Supplementary Table S2). From the seedling to the heading stage, the plant height, stem diameter, leaf number, root length, and single plant biomass of sweet sorghum generally increased and showed highly significantly different changes ($p < 0.01$) in response to organic acids. Meanwhile, their responses to biomass materials also reached highly significant differences ($p < 0.01$), except for stem diameter, which only reached a significant difference level ($p < 0.05$) at the elongation stage. For the interaction effect between organic acids and biomass materials, a highly significant effect ($p < 0.01$) was observed on the plant biomass at the seedling stage, the plant height, leaf number, root length, and plant biomass at the elongation stage, and the plant height, stem diameter, and plant biomass at the heading stage; a significant effect ($p \leq 0.05$) on the plant height at the seedling stage and the root length at the heading stage; and an insignificant effect ($p > 0.05$) on the other treatments. At the seedling and elongation stages, the plant height, stem diameter, leaf number, root length, and single plant biomass were higher in the CPN treatment than in the other treatments and increased from 62.71% to 93.08%, 38.41% to 73.63%, 58.73% to 85.72%, 59.35% to 209.11%, and 297.80% to 882.72%, respectively, compared with those in the CK. At the heading stage, the plant height, leaf number, root length, and plant biomass of the FPN treatment were significantly higher than those of the other treatments ($p \leq 0.05$). The stem diameter of the FPN treatment also reached the highest but was not significantly different from that of the FCM treatment ($p > 0.05$). Each of the indexes increased by 104.23%, 318.56%, 63.00%, 78.16%, and 115.20% compared with those in the CK.

Effects of different combinations of exogenous organic acids and biomass materials on the osmotic regulators, chlorophyll, and root activity of sweet sorghum

As shown in Figure 6 and Supplementary Table S3, the response values of root activity, chlorophyll, malondialdehyde, proline, and soluble sugar of sweet sorghum to the application of exogenous organic acids and biomass materials reached highly significant

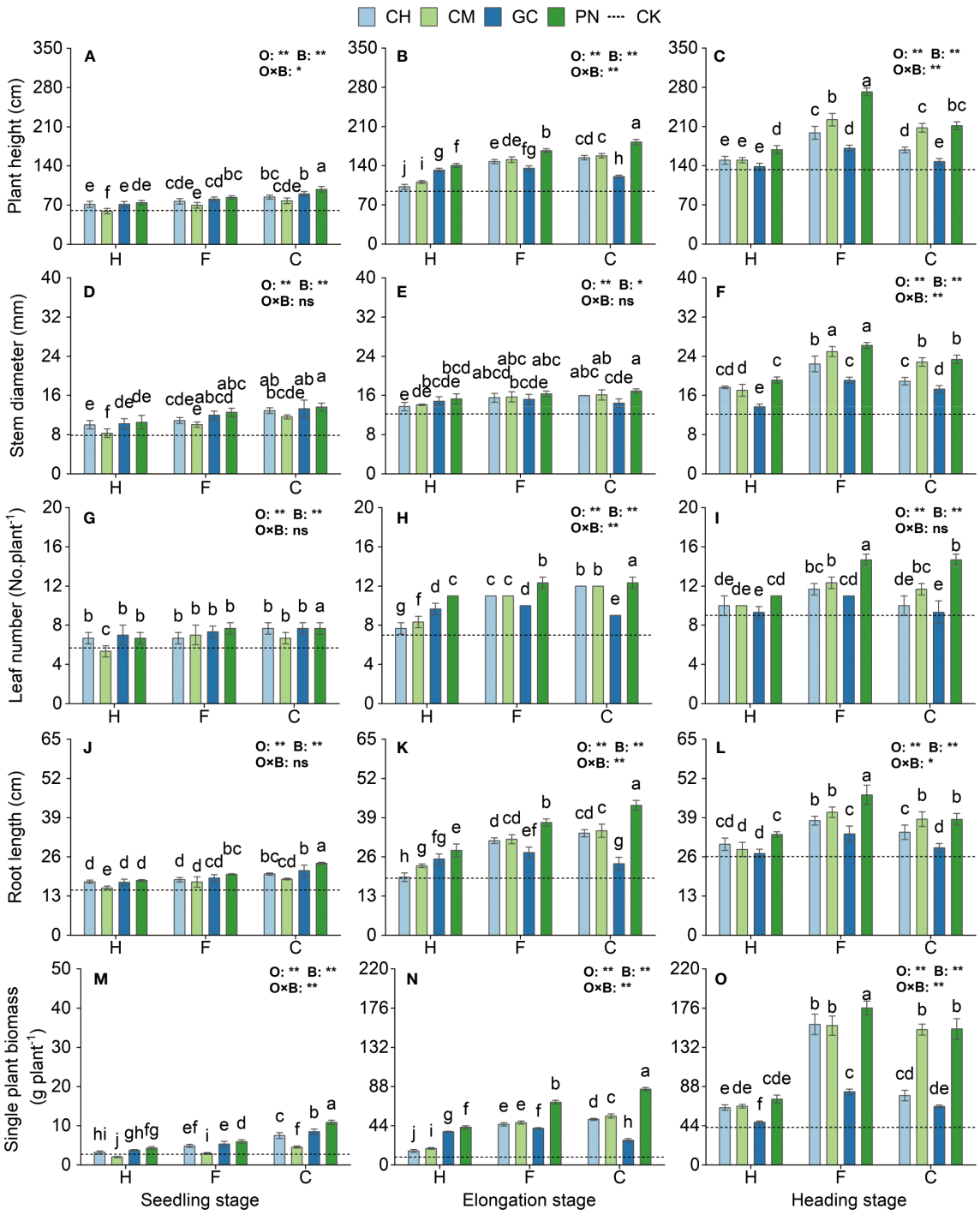

FIGURE 5
Effects of exogenous organic acids and biomass materials on the morphological indexes and biomass of sweet sorghum. **(A, D, G, J, M)** Represent the seedling stage, **(B, E, H, K, N)** represent the elongation stage, and **(C, F, I, L, O)** indicate as the heading stage. **1% and *5%-levels of significant difference; ns, not significant at 5% level. Bars with different lowercase letters indicate a significant difference (p < 0.05) within one development stage.

levels ($p < 0.01$) from the seedling to the heading stage. The interaction effect of organic acids with biomass materials had a highly significant effect ($p < 0.01$) on root activity, and chlorophyll at the seedling stage, root activity, malondialdehyde, proline, and soluble sugar at the elongation stage, and root activity, chlorophyll, and malondialdehyde values at the heading stage; a significant effect ($p \leq 0.05$) on chlorophyll at the elongation stage; and an insignificant effect ($p > 0.05$) on the other treatments. The CPN treatment had the highest chlorophyll, proline, and soluble sugar content at the seedling stage, followed by CGC; the difference between these two treatments was not significant ($p > 0.05$). Root activity in the CPN was the highest and was significantly higher than that in the other treatments ($p < 0.05$). Malondialdehyde content was significantly lower in the CPN, CGC, CCH, FPN, and

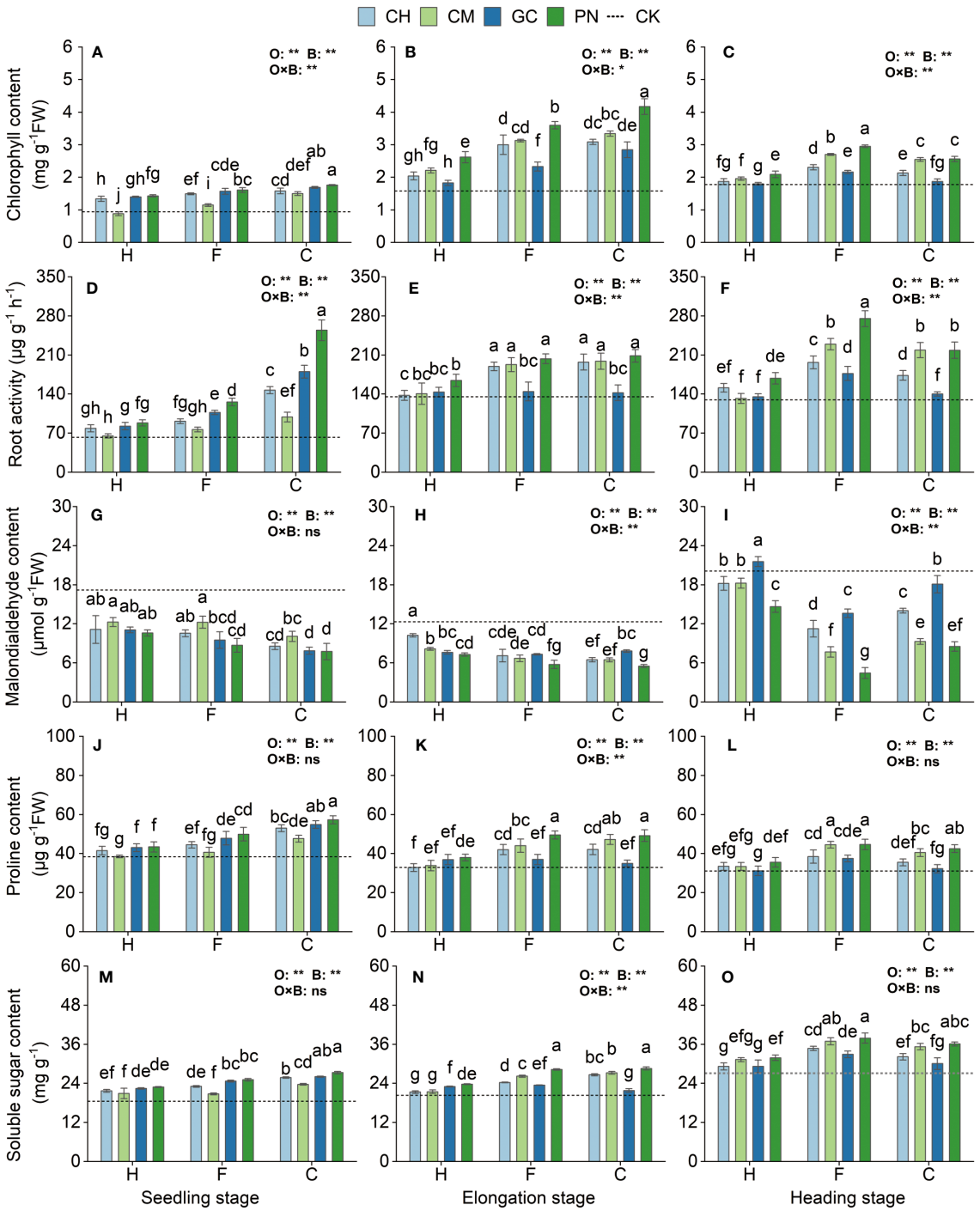

FIGURE 6
Effects of exogenous organic acids and biomass material on the osmotic regulation substances, chlorophyll, and root activity of sweet sorghum. **(A, D, G, J, M)** Represent the seedling stage, **(B, E, H, K, N)** represent the elongation stage, and **(C, F, I, L, O)** indicate as the heading stage. **1% and *5%-levels of significant difference; ns, not significant at 5% level. Bars with different lowercase letters indicate a significant difference (p < 0.05) within one development stage.

FGC treatments than in the other treatments ($p \leq 0.05$), but the differences were not significant ($p > 0.05$). Chlorophyll content was significantly higher ($p \leq 0.05$) in the CPN treatment than in the other treatments at the elongation stage. Root activity in the CPN treatment was also the highest, but it was not significantly different ($p > 0.05$) from that in the FPN, CCM, FCM, CCH, and FCH treatments. Malondialdehyde content was significantly low ($p \leq 0.05$) in the CPN and FPN treatments. Proline was the highest in the CPN treatment, but its values were not significantly different between FPN and CCM ($p > 0.05$) but were significantly different from those in the other treatments ($p < 0.05$). The soluble sugar values of the CPN and FPN treatments were significantly higher than those of the other treatments ($p < 0.05$). Chlorophyll and root activity were significantly higher ($p < 0.05$) and malondialdehyde

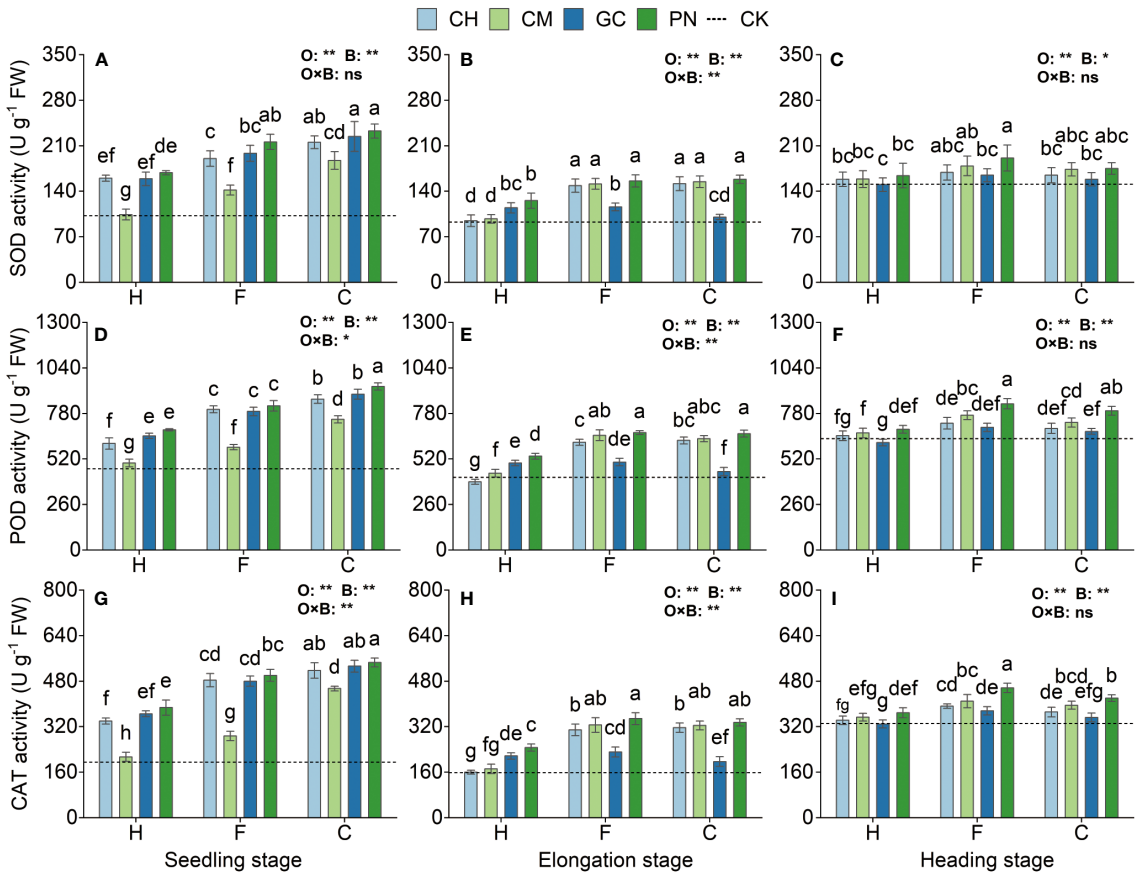

FIGURE 7
Effects of exogenous organic acids and biomass material on the antioxidant enzyme activities of sweet sorghum. **(A, D, G)** Represent the seedling stage, **(B, E, H)** represent the elongation stage, and **(C, F, I)** indicate as the heading stage. **1% and *5%-levels of significant difference; ns, not significant at 5% level. Bars with different lowercase letters indicate a significant difference (p < 0.05) within one development stage.

content was significantly lower ($p < 0.05$) in the FPN treatment than in the other treatments at the heading stage. Proline and soluble sugar were the highest ($p \leq 0.05$) in the FPN, FCM, and CPN treatments, but the differences among these three were not significant ($p > 0.05$).

Effects of different combinations of exogenous organic acids and biomass materials on the antioxidant enzyme system of sweet sorghum

The SOD, POD, and CAT activities of sweet sorghum reached their highest levels at the seedling stage and decreased, followed by a small increase as the reproductive period progressed (Figure 7; Supplementary Table S4). Highly significant differences ($p < 0.01$) in SOD, POD, and CAT were observed in response to the organic acid treatment for sweet sorghum from the seedling to the heading stage. Except for SOD at the heading stage ($p < 0.01$), the response of other indexes to biomass materials was significantly different ($p < 0.01$). For the interaction between organic acids and biomass, extremely significant effects were observed on CAT at the seedling stage and on SOD, POD, and CAT at the elongation stage ($p < 0.01$); significant effects were also found on POD at the seedling stage ($p < 0.05$). SOD activity in the CPN and CGC treatments at the seedling stage was the highest; its value was not significantly different from that in the CCH and FPN treatments ($p > 0.05$) but was significantly higher than that in the other treatments ($p \leq 0.05$). POD activity in the CPN treatment was significantly higher than that in the other treatments ($p < 0.05$). The CAT values in the CPN treatment were the highest; these values were not significantly different from those in the CGC and CCH ($p > 0.05$) but were significantly different from those in the other treatments ($p \leq 0.05$). The SOD values of CPN, FPN, CCM, CCH, FCM, and FCH treatments were not significant differently from each other ($p > 0.05$) but were significantly higher ($p \leq 0.05$) than those of the other treatments. For POD and CAT activities, both were the highest in the FPN, CPN, FCM, and CCM treatments at the elongation stage. The SOD activity of FPN, FCM, CPN, CCM, and FCH treatments at the heading stage was significantly higher than that of other treatments ($p < 0.05$). POD activity was the highest in the FPN treatment but was not significantly different from that in the CPN treatment ($p > 0.05$). CAT activity was significantly higher in the FPN treatment than in the other treatments during this period ($p \leq 0.05$).

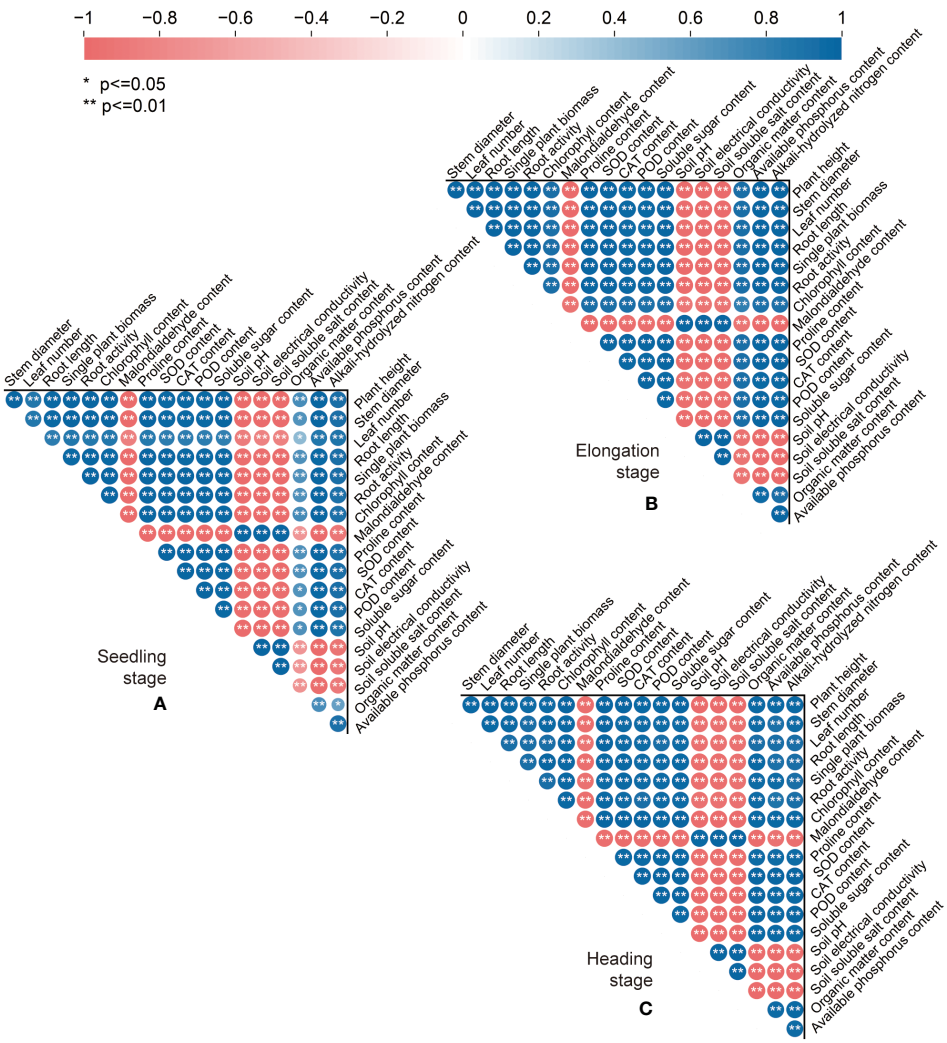

FIGURE 8
Spearman correlation analysis of the soil physical and chemical properties, physiological and biochemical characteristics, and growth indexes of sweet sorghum in different periods. **(A-C)** Represents the seedling stage, the elongation stage, and the heading stage, respectively. Blue indicates significant positive correlation, red indicates significant negative correlation, circle size indicates degree of correlation.

Correlation analysis of soil improvement and sweet sorghum growth performance upon the application of combined exogenous organic acid and biomass

Spearman correlation analysis (Figure 8) showed that after the addition of exogenous organic acid and biomass materials, the biomass and morphological indexes (the plant height, stem diameter, leaf number, root length, and single plant biomass) of sweet sorghum in the three periods were significantly positively correlated with the physiological and biochemical indexes (the chlorophyll, proline, soluble sugar, SOD, CAT, and POD) of sweet sorghum ($p \leq 0.01$), negatively correlated with the malondialdehyde content ($p \leq 0.01$), positively correlated with soil nutrient indexes (the soil organic matter, available phosphorus, and alkali-hydrolyzed nitrogen) ($p \leq 0.05$), and negatively correlated with soil saline–alkaline indexes (the soil pH, electrical conductivity, and soluble salt) ($p \leq 0.01$). Meanwhile, the soil nutrient indexes were negatively correlated with soil salinity indexes ($p \leq 0.05$), positively correlated with the physiological and biochemical indexes of sweet sorghum ($p \leq 0.05$), and significantly negatively correlated with the malondialdehyde content ($p \leq 0.05$).

Discussion

Processes and effects of treatment with exogenous organic acids and biomass materials on salinity regulation in coastal soils

The coastal mudflats in Jiangsu Province are affected by seawater groundwater and high temperatures in summer, and the phenomena of seasonal soil salting back and salt accumulation are serious. A large amount of sodium ions replace the calcium ions on

the surface of the soil colloid, and the soil aggregate structure is destroyed, further aggravating the accumulation of salt in the soil. Organic acids are always undergoing a dynamic transformation of release, adsorption, and degradation in soils, but their sources are limited in alkaline soil environments, and their average levels have been low for a long time. The exogenous addition of organic acid-based biomass materials directly regulates soil acidity and alkalinity, promotes rapid soil desalination, and inhibits the upward transport of salts by forming a surface barrier (Mindari et al., 2018; Shan et al., 2022). For the three organic acids used in the current work, the soil treated with citric acid had lower soil pH, electrical conductivity, and soluble salt than those under other treatments at the seedling and elongation stages of sweet sorghum. This phenomenon probably occurred because citric acid is a ternary acid that can dissociate a large amount of H^+ to neutralize basic ions and use anions to adsorb Na^+ in the soil, thus reducing salinity (Santos et al., 2017). However, citric acid is highly soluble and melts, so maintaining its effect until the heading stage is difficult even with the stable solubility environment provided by the biomass material. Humic acid and fulvic acid are rich in active functional groups, such as carboxyl, hydroxyl, quinone, and amide groups, which can effectively increase the amount of cation exchange and regulate soil acid–base balance (Cui et al., 2022a; Vrantsi et al., 2021). However, fulvic acid has a relatively high active carbon group aliphatic chain structure, high saturation degree, stronger solubility, lower molecular weight, and stronger ion exchange force than humic acid, so its salt reduction ability is higher than that of humic acid (Guo et al., 2019; Sun et al., 2019). This study also found that among the four biomass materials, pine needles had stronger effects during different periods compared with cottonseed hull, grass charcoal, and cow manure. The possible reason is that the pine needle structure is rough and mostly consists of acicular thick leather, making the biomass less susceptible to rainfall leaching and soil biological interference. As a result, pine needles can effectively adsorb organic acids and have a slow effect on the soil. In addition, the weak acidity of pine needles can help reduce soil alkalinity, and the decomposition products can assist organic acids to exert chelation and eliminate soil salinity (Samec et al., 2021). Owing to its powdered structure and weak acidity, grass charcoal can adsorb organic acids during the seedling stage of sweet sorghum and rapidly infiltrate the active layer of the root system to chelate with soil saline components, effectively regulating the soil pore space through its own low bulk density to improve soil structure (Wang et al., 2020a; Yang et al., 2021b). However, the large specific surface area of grass charcoal leads to a reaction between a large number of organic acids immobilized by grass charcoal and the soil solution in the early stage, making it difficult to resist the upward movement and repeated accumulation of soil salt. Cow manure is rich in humus, which can improve the water leakage and fertilizer leakage characteristics of sandy soil. Its fibrous structure can cut the capillary continuity of the soil to reduce water and salt transport and assist the efficient water storage of the soil, effectively inhibiting the upward transport of soil salt under high-temperature conditions in the middle and late periods (El Sabagh et al., 2019). Cottonseed hull has a soft and flaky texture, a small bulk density, and high porosity, all of which are conducive to improving soil water and air conditions. However, its weak water retention hinders its effects when combined with organic acids (He et al., 2016).

Regulatory effects of treatment with exogenous organic acids and biomass materials on the nutrient accumulation in coastal saline soils

Owing to their physicochemical and biological characteristics, saline–alkaline soils exhibit slow organic matter decomposition and low available nutrient stocks (Qadir and Schubert, 2002; Setia et al., 2013). As functional organic matter in the soil, high-molecular-weight humic acid and low-molecular-weight organic acids play an important role in soil morphology and fertility. Organic acids in soil are mainly derived from the decomposition of plant and animal residues, the secretion of plant roots, and the metabolism of microbes. Different types and concentrations of organic acids have varying effects on mineral dissolution and nutrient transformation in various kinds of soils. This study found that the exogenous application of citric acid, humic acid, and fulvic acid can increase soil organic matter, available phosphorus, and alkali-hydrolyzed nitrogen content. In particular, the effect of citric acid on sweet sorghum seedlings is stronger than that of fulvic acid. One reason is that the activation of difficultly soluble nutrients in the soil by organic acids relies on acid dissolution, anion complexing, and competitive adsorption; the acidity of organic acids and the number of dissociated anions determine their ability to activate nutrients (Li et al., 2014; Yang and Antonietti, 2020). Among the three organic acid treatments, citric acid has the strongest effect on phosphorus activation in alkaline soils, possibly because a large number of organic anions generated from citric acid dissociation dissolve the phosphorus that precipitated in the soil solution, aluminum, and iron; in addition, they compete for phosphorus adsorption sites in silicate minerals, effectively mobilizing the release of inorganic-bound nutrients (Wang, 2021; Wu et al., 2021b). Humic acid and fulvic acid are absorbent materials, and fulvic acid has more acidic active groups and a stronger adsorption effect on nitrogen and phosphorus than humic acid. Thus, fulvic acid effectively inhibits the transformation of activated nutrients into invalid states, continuously regulates the transformation of nutrient forms, and improves the long-term performance of nutrients, so its effect is highly significant in the middle and late stages. This finding is similar to the research results of Lv et al. (2022) and Yao et al. (2022b). The input of exogenous biomass directly increases the energy substrate of the beach soil, leading to a significant increase in the total amount of soil organic matter and nutrients. Holatko et al. (2022) and Sun et al. (2020) reported similar results. In the present study, pine needles significantly increased the contents of soil organic matter, alkali-hydrolyzed nitrogen, and available phosphorus over the whole growth period of sweet sorghum. The overall effect of cow manure was second only to that of pine needles, but the effect of cow manure at the seedling stage was not as prominent as that at the heading stage. A possible reason is that the weakly acidic pine needle material can provide a long-term suitable acid-base environment for soil nutrient activation. As leaf residues

of plants, pine needles have more soluble nutrients than the other materials; their nitrogen and phosphorus elements exhibit a trend of first enrichment, then release, and gradually increasing, allowing them to permanently assist organic acid fertilization and directly increase soil nutrient content (Gao et al., 2019; Manral et al., 2020). The colloidal properties of cow manure can enhance the bonding of organic and inorganic complexes, promote the formation of soil aggregates and the accumulation of organic matter, and effectively enhance the availability and retention of nutrients (Chen et al., 2021a). However, its own nutrient content is relatively low, and the overall effect of combining the activation function of an organic acid with cow manure is slightly lower than that compared with pine needles. In addition, the improvement of soil nutrient content in the early stage is lower than that in the later stage. In summary, the physical and chemical properties such as surface area, pore size, and nutrient content of different biomass materials are important factors to consider in their application as excellent adsorption carriers of organic acids to enhance the improvement effect of organic acids on saline–alkaline soil (Hu et al., 2022; Islam et al., 2022).

Mechanisms of the combination of exogenous organic acids and biomass materials to enhance salinity tolerance and biomass in sweet sorghum

During agricultural production, the high osmotic pressure in coastal saline soils caused by the high soluble salt content affects the kinetic and physiological–ecological processes of water and nutrient uptake by plant roots and decreases nutrient effectiveness in the soil, resulting in a long-term nutrient deficit in crops (Luo et al., 2017). Salinity stress and ion toxicity have negative effects on seed germination and root uptake, resulting in membrane lipid peroxidation, metabolic disorders, photosynthetic dysfunctions, and ultimately plant growth limitation and biomass decline (Tedeschi et al., 2011; Bhattarai et al., 2020). In this work, the addition of exogenous organic acids and biomass materials balanced the cellular osmotic potential by increasing the content of proline and soluble sugar content in plant leaves and the activity of some antioxidant enzymes used to scavenge reactive oxygen species. In addition, the accumulation of malondialdehyde was reduced to stabilize the plasma membrane, ensure the extension of the cell wall and normal cell growth, counteract the negative effects of salt ions on root activity and photosynthesis in aboveground parts, and promote biomass (Gulmezoglu and İzci, 2020; Yang et al., 2020). The added exogenous organic acids and biomass also reduced the uptake of salt ions by the root system by neutralizing and displacing saline components in the soil (Cui et al., 2022b) and stimulated the nutrient uptake and rapid growth of plants using the bioactive substances enriched in the material (Farid et al., 2017) and enhanced root vigor and aboveground photosynthesis (Chen et al., 2020; Zhang et al., 2020c), thus counteracting salinity stress by regulating root morphogenesis and cellular physiological processes (Olaetxea et al., 2016). The most significant effect of citric acid was found in sweet sorghum at the seedling and elongation stages, and the most significant effect of fulvic acid was found at the heading stage. This finding may be attributed to the different effects of exogenous organic acids on plant stems caused by their physicochemical properties (mainly acidity, interfacial activity, cation exchange capacity, complexation, adsorption, and dispersion) and type and amount of active functional groups (Shah et al., 2018). Citric acid has the highest number of carboxyl functional groups and is a low-molecular-weight organic acid that can be absorbed by plants. Its strong ligand affinity can effectively complex bond metal ions in soil or plants, quickly alleviate salt ion damage, and promote the growth of above-ground parts during the seedling stage (Tahjib-Ul-Arif et al., 2021). However, citric acid is easily leachable and has a short-duration fertilization effect, so it should be used in small amounts and at individual stages. By contrast, fulvic acid has the greatest variety of active functional groups. The number of its functional groups is higher than that of humic acid but less than that of citric acid. Fulvic acid has a strong buffering capacity, so its reaction time is slower than that of citric acid, but its effect is relatively long-lasting. It also promotes resistance enhancement and biomass accumulation in sweet sorghum (Braziene et al., 2021; Nargesi et al., 2022). When combined with the unique weak acidity and rough physical structure of pine needles, each of these two organic acids forms a salt barrier on the soil surface to reduce transpiration-induced salt transport to plant roots (Lu et al., 2012). The adsorbed organic acid functions for a long time under saline–alkaline stress by increasing plant root activity, enhancing the capacity of nutrient absorption and water retention, and reducing the osmotic stress and ion poisoning to ensure the stability of the plant photosynthetic system, maintain the physiological and biochemical reactions of sweet sorghum, and improve productivity.

Effects of the combination of exogenous organic acids and biomass materials on the feedback system of "salt-tolerant forage grass—coastal saline soil"

The essence of the plant–soil feedback system is that plants and soil interact with each other through physical, chemical, and biological reaction mechanisms at different interfaces under different spatial and temporal patterns and scale levels, resulting in intricate positive and negative feedback effects and finally a coupled system with a bidirectional regulatory function formed by long-term evolution (Kandlikar et al., 2019). When plants are under stress conditions, signal substances secreted by roots act directly on soil or induce soil microorganisms to jointly regulate the soil physical structure and nutrient environment in the root zone, thus providing good water conditions and nutrient levels for aboveground parts (Vives-Peris et al., 2020; Chai and Schachtman, 2022). At the same time, the soil transmits information to plants when water and nutrients are at critical values, prompting plants to reduce their total nutrient uptake by changing their own traits or improving nutrient availability; this process generates a win–win effect through mutual feedback and regulation (Koster et al., 2019; Gong et al., 2020). Under saline–

alkaline stress conditions, organic acids from different sources in the soil can be directly absorbed by roots and chelate salt ions in plants to convert them into binding states with relatively low activity, thus reducing the damage of salt ions to cells and strengthening the benign interaction between roots and soil (Jindo et al., 2020; Rakkammal et al., 2023). By complexing with the salts in the soil, organic acids reduce the direct contact and uptake of salts with plant roots, thus promoting root development, increasing the number of roots, and releasing a large amount of secretion to the soil in the root zone for positive feedback (Zanin et al., 2019). Among the three organic acids, citric acid had the strongest effect on soil through plants (Menezes-Blackburn et al., 2021). However, humic acid has more similarities in function and composition structure to the secreted substances from roots (Zhu et al., 2019), and their active components have similar effects on plant parts and rhizosphere soil. As plant growth regulators and soil conditioners, exogenous organic acids can directly stimulate or indirectly utilize the plant–soil feedback system to promote plant growth and physiological and biochemical reactions, regulate the soil environment, and enhance the strength of the interaction between salt-tolerant forage grass and coastal saline soil at the root surface and rhizosphere level. This treatment helps soil and plants resist salt invasion in the long term (Canellas et al., 2015). Biomass plays a role in the stable adsorption of exogenous organic acids into the soil and uses the unique water retention and nutrient metabolism characteristics given by their own physical and chemical structure; together with the function of organic acids, biomass also generates added value for the formation of the physical and chemical properties and microbial diversity of saline–alkaline soil (Abd El-Mageed et al., 2020; Abd El-Mageed et al., 2021). The effects of different organic acids and biomass materials on soil nutrient turnover and water–salt movement can lead to changes in the composition, structure, and function of soil microbial communities (Yao et al., 2021; Zhang et al., 2020a); such complex changes will be reflected back to plant productivity and the soil nutrient cycle through downward control (Lu et al., 2020; Tiwari et al., 2022). The process and role of soil microbial diversity in regulating the feedback of "salt-tolerant herbage—coastal saline–alkaline soil" will be further studied in the future.

Conclusion

Exogenous organic acids and biomass materials and their interaction effects can affect the physicochemical properties of beach soils and the growth performance of sweet sorghum. Among the three organic acids used in this work, citric acid creates a beneficial soil environment for sweet sorghum under saline stress by stimulating its physiological activity and thus promoting its growth. Meanwhile, the slow-release nature of fulvic acid provides material for the long-term improvement of soil quality. Among the four biomass materials, pine needles can steadily maintain the effectiveness of the piggyback organic acids and continuously release organic acids and their own nutrients throughout all periods. Cow manure can effectively consolidate the effect of organic acid in the middle and late stages and assist in reducing salinity to promote crop growth; however, its ability to change soil is second only to a pine needle. In summary, citric acid–pine needle composite is suitable for harvesting short-term crops in coastal mudflats, and fulvic acid–pine needle or fulvic acid–cow manure composite can be used for long-term crops to improve the soil.

Data availability statement

The raw data supporting the conclusions of this article will be made available by the authors, without undue reservation.

Author contributions

ZS and RY conceived the ideas. RY and XLi collected the data. ZS and RY analyzed the data and led the writing. RY, YS, and XLo provided more arguments in the results and conclusion. ZS, YS, and LG proved the effectivity and rationality of the method proposed in this paper. All authors contributed critically to the ideas and drafts and gave final approval for publication.

Funding

This work was supported by the Suzhou Agricultural Science and Technology Innovation Project (SNG2022049) and the Jiangsu Agricultural Science and Technology Independent Innovation Fund Project [No. CX(20)3195].

Acknowledgments

We are grateful to the chief editor and the two reviewers for their helpful comments. This original research is accessible as a preprint (doi.org/10.21203/rs.3.rs-2293797/v1).

Conflict of interest

The authors declare that the research was conducted in the absence of any commercial or financial relationships that could be construed as a potential conflict of interest.

Publisher's note

Supplementary material

The Supplementary Material for this article can be found online at: https://www.frontiersin.org/articles/10.3389/fpls.2023.1163195/full#supplementary-material

References

Abd El-Mageed, T. A., Abdurrahman, H. A., and Abd El-Mageed, S. A. (2020). Residual acidified biochar modulates growth, physiological responses, and water relations of maize (*Zea mays*) under heavy metal–contaminated irrigation water. *Environ. Sci. pollut. Res.* 27, 22956–22966. doi: 10.1007/s11356-020-08847-5

Abd El-Mageed, T. A., Belal, E. E., Rady, M. O. A., Abd El-Mageed, S. A., Mansour, E., Awad, M. F., et al. (2021). Acidified biochar as a soil amendment to drought stressed (*Vicia faba* l.) plants: influences on growth and productivity, nutrient status, and water use efficiency. *Agronomy* 11, 1290. doi: 10.3390/agronomy11071290

Amini, S., Ghadiri, H., Chen, C., and Marschner, P. (2016). Salt-affected soils, reclamation, carbon dynamics, and biochar: a review. *J. Soil. Sediment.* 16, 939–953. doi: 10.1007/s11368-015-1293-1

Aoki, M., Fujii, K., and Kitayama, K. (2012). Environmental control of root exudation of low-molecular weight organic acids in tropical rainforests. *Ecosystems* 15, 1194–1203. doi: 10.1007/s10021-012-9575-6

Bates, L. S., Waldren, R. P., and Teare, I. D. (1973). Rapid determination of free proline for water-stress studies. *Plant Soil* 39, 205–207. doi: 10.1007/BF00018060

Bhattarai, S., Biswas, D., Fu, Y. B., and Biligetu, B. (2020). Morphological, physiological, and genetic responses to salt stress in alfalfa: a review. *Agronomy* 10, 577. doi: 10.3390/agronomy10040577

Braziene, Z., Paltanavicius, V., and Avizienytė, D. (2021). The influence of fulvic acid on spring cereals and sugar beets seed germination and plant productivity. *Environ. Res.* 195, 110824. doi: 10.1016/j.envres.2021.110824

Canellas, L. P., Olivares, F. L., Aguiar, N. O., Jones, D. L., Nebbioso, A., Mazzei, P., et al. (2015). Humic and fulvic acids as biostimulants in horticulture. *Sci. hortic-amsterdam.* 196, 15–27. doi: 10.1016/j.scienta.2015.09.013

Chai, Y. N., and Schachtman, D. P. (2022). Root exudates impact plant performance under abiotic stress. *Trends Plant Sci.* 27, 80–91. doi: 10.1016/j.tplants.2021.08.003

Chen, M., Zang, S., Wu, L., Fei, C., and Ding, X. (2021a). Organic fertilization improves the availability and adsorptive capacity of phosphorus in saline-alkaline soils. *J. Soil Sci. Plant Nutt.* 21, 487–496. doi: 10.1007/s42729-020-00377-w

Chen, M., Zhang, S., Liu, L., Liu, J., and Ding, X. (2022). Organic fertilization increased soil organic carbon stability and sequestration by improving aggregate stability and iron oxide transformation in saline-alkaline soil. *Plant Soil* 474, 233–249. doi: 10.1007/s11104-022-05326-3

Chen, M., Zhang, S., Liu, L., Wu, L., and Ding, X. (2021b). Combined organic amendments and mineral fertilizer application increase rice yield by improving soil structure, p availability and root growth in saline-alkaline soil. *Soil Till. Res.* 212, 105060. doi: 10.1016/j.still.2021.105060

Chen, H. C., Zhang, S. L., Wu, K. J., Li, R., He, X. R., He, D. N., et al. (2020). The effects of exogenous organic acids on the growth, photosynthesis and cellular ultrastructure of *Salix variegata franch.* under cd stress. *Ecotoxicol. Environ. Safe.* 187, 109790. doi: 10.1016/j.ecoenv.2019.109790

Cui, L., Liu, Y., Yan, J., Hina, K., Hussain, Q., Qiu, T., et al. (2022a). Revitalizing coastal saline-alkali soil with biochar application for improved crop growth. *Ecol. Eng.* 179, 106594. doi: 10.1016/j.ecoleng.2022.106594

Cui, H., Wen, X., Wu, Z., Zhao, Y., Lu, Q., and Wei, Z. (2022b). Insight into complexation of cd (II) and Cu (II) to fulvic acid based on feature recognition of PARAFAC combined with 2DCOS. *J. Haz. Mat.* 440, 129758. doi: 10.1016/j.jhazmat.2022.129758

Cui, Q., Xia, J., Yang, H., Liu, J., and Shao, P. (2021). Biochar and effective microorganisms promote *Sesbania cannabina* growth and soil quality in the coastal saline-alkali soil of the yellow river delta, China. *Sci. Total Environ.* 756, 143801. doi: 10.1016/j.scitotenv.2020.143801

Do Nascimento, C. W. A., Amarasiriwardena, D., and Xing, B. (2006). Comparison of natural organic acids and synthetic chelates at enhancing phytoextraction of metals from a multi-metal contaminated soil. *Environ. pollut.* 140, 114–123. doi: 10.1016/j.envpol.2005.06.017

Dong, X., Li, X., Zheng, X., Jiang, T., and Li, X. (2020). Effect of saline soil cracks on satellite spectral inversion electrical conductivity. *Remote. Sens-Basel.* 12, 3392. doi: 10.3390/rs12203392

El Hasini, S., Halima, O. I., Azzouzi, M. E., Douaik, A., Azim, K., and Zouahri, A. (2019). Organic and inorganic remediation of soils affected by salinity in the sebkha of sed El mesjoune–marrakech (Morocco). *Soil Till. Res.* 193, 153–160. doi: 10.1016/j.still.2019.06.003

El Sabagh, A., Hossain, A., Barutcular, C., Gormus, O., Ahmad, Z., Hussain, S., et al. (2019). Effects of drought stress on the quality of major oilseed crops: implications and possible mitigation strategies – a review. *Appl. Ecol. Env. Res.* 17, 4019–4043. doi: 10.15666/aeer/1702_40194043

Farid, M., Ali, S., Rizwan, M., Ali, Q., Abbas, F., Bukhari, S. A. H., et al. (2017). Citric acid assisted phytoextraction of chromium by sunflower; morpho-physiological and biochemical alterations in plants. *Ecotoxicol. Environ. Safe.* 145, 90–102. doi: 10.1016/j.ecoenv.2017.07.016

Gao, J., Han, H., and Kang, F. (2019). Factors controlling decomposition rates of needle litter across a chronosequence of Chinese pine (*Pinus tabuliformis carr.*) forests. *Pol. J. Environ. Stud.* 28, 91–102. doi: 10.15244/pjoes/84770

Ghobadi, M., Taherabadi, S., Ghobadi, M. E., Mohammadi, G. R., and Jalali-Honarmand, S. (2013). Antioxidant capacity, photosynthetic characteristics and water relations of sunflower (*Helianthus annuus* l.) cultivars in response to drought stress. *Ind. Crop Prod.* 50, 29–38. doi: 10.1016/j.indcrop.2013.07.009

Gong, Z., Xiong, L., Shi, H., Yang, S., Herrera-Estrella, L. R., Xu, G., et al. (2020). Plant abiotic stress response and nutrient use efficiency. *Sci. China Life Sci.* 63, 635–674. doi: 10.1007/s11427-020-1683-x

Gulmezoglu, N., and İzci, E. (2020). Ionic responses of bean (*Phaseolus vulgaris* l.) plants under salinity stress and humic acid applications. *Not. Bot. Horti Agrobo.* 48, 1317–1331. doi: 10.15835/nbha48311950

Guo, Y., Liu, H., Gong, P., Li, P., Tian, R., Zhang, Y., et al. (2022). Preliminary studies on how to reduce the effects of salinity. *Agronomy* 12, 3006. doi: 10.3390/agronomy12123006

Guo, X., Liu, H., and Wu, S. (2019). Humic substances developed during organic waste composting: formation mechanisms, structural properties, and agronomic functions. *Sci. Total Environ.* 662, 501–510. doi: 10.1016/j.scitotenv.2019.01.137

He, Z., Uchimiya, S. M., and Guo, M. (2016). *Production and characterization of biochar from agricultural by-products: overview and use of cotton biomass residues* (Madison, Wis: SSSA).

Holatko, J., Hammerschmiedt, T., Mustafa, A., Kintl, A., Radziemska, M., Baltazar, T., et al. (2022). Carbon-enriched organic amendments differently affect the soil chemical, biological properties and plant biomass in a cultivation time-dependent manner. *Chem. Biol. Technol. Ag.* 9, 52. doi: 10.1186/s40538-022-00319-x

Hu, Y. W., Li, Q. K., Song, C. J., and Jin, X. H. (2021). Effect of humic acid combined with fertilizer on the improvement of saline-alkali land and cotton growth. *Appl. Ecol. Env. Res.* 19, 1279–1294. doi: 10.15666/aeer/1902_12791294

Hu, M., Wu, W., Lin, D., and Yang, K. (2022). Adsorption of fulvic acid on mesopore-rich activated carbon with high surface area. *Sci. Total Environ.* 838, 155918. doi: 10.1016/j.scitotenv.2022.155918

Islam, M. S., Gao, R. L., Gao, J. Y., Song, Z. T., Ali, U., and Hu, H. Q. (2022). Cadmium, lead, and zinc immobilization in soil using rice husk biochar in the presence of citric acid. *Int. J. Environ. Sci. Te.* 19, 567–580. doi: 10.1007/s13762-021-03185-6

Jindo, K., Olivares, F. L., Malcher, D. J. D. P., Sánchez-Monedero, M. A., Kempenaar, C., and Canellas, L. P. (2020). From lab to field: role of humic substances under open-field and greenhouse conditions as biostimulant and biocontrol agent. *Front. Plant Sci.* 11. doi: 10.3389/fpls.2020.00426

Jones, J. (2017). Laboratory guide for conducting soil tests and plant analysis. Boca Raton, FL: CRC Press.

Kandlikar, G. S., Johnson, C. A., Yan, X., Kraft, N. J. B., and Levine, J. M. (2019). Winning and losing with microbes: how microbially mediated fitness differences influence plant diversity. *Ecol. Lett.* 22, 1178–1191. doi: 10.1111/ele.13280

Kaur, K., Kapoor, K. K., and Gupta, A. P. (2005). Impact of organic manures with and without mineral fertilizers on soil chemical and biological properties under tropical conditions. *J. Plant Nutr. Soil Sc.* 168, 117–122. doi: 10.1002/jpln.200421442

Koster, P., Wallrad, L., Edel, K. H., Faisal, M., Alatar, A. A., and Kudla, J. (2019). The battle of two ions: Ca^{2+} signalling against na^{+} stress. *Plant Biol. J.* 21, 39–48. doi: 10.1111/plb.12704

Kulikova, M. V., Krylova, A. Y., Zhagfarov, F. G., Krysanova, K. O., and Lapidus, A. L. (2022). Plant biomass as a raw material for producing basic organic sysnthesis products. *Chem. Technol. Fuels. Oils.* 58, 320–326. doi: 10.1007/s10553-022-01387-3

Lassheikki, M., Puttonen, P., and Räsänen, P. K. (1991). Planting performance potential of *Pinus sylvestris* seedlings as evaluated by root growth capacity and triphenyl tetrazolium chloride reduction methods. *Scand. J. For. Res.* 6, 91–104. doi: 10.1080/02827589109382652

Li, Y., and Li, G. (2022). Mechanisms of straw biochar's improvement of phosphorus bioavailability in soda saline-alkali soil. *Environ. Sci. pollut. R.* 29, 47867–47872. doi: 10.1007/s11356-022-20489-3

Li, H., Liu, Y., Zeng, G., Zhou, L., Wang, X., Wang, Y., et al. (2014). Enhanced efficiency of cadmium removal by *Boehmeria nivea* (L.) gaud. in the presence of exogenous citric and oxalic acids. *J. Environ. Sci-China.* 26, 2508–2516. doi: 10.1016/j.jes.2014.05.031

Li, S., Wang, B., Wang, Y., Ma, X., Su, L., Wang, Y., et al. (2022a). Soluble organic nutrients induce *ClaPhys* expression to enhance phytase activity of watermelon roots. *Ann. Appl. Biol.* 181, 80–92. doi: 10.1111/aab.12756

Li, X., Yao, T., Huang, X., Li, X., Li, P., Du, S., et al. (2022b). Biochar increases rice yield by improving root morphological and root physiological functions in heavily saline-sodic paddy soil of northeast China. *Bioresources* 17, 1241–1256. doi: 10.15376/biores.17.1.1241-1256

Li, R., Zhang, S., Zhang, M., Fei, C., and Ding, X. (2021). Phosphorus fractions and adsorption–desorption in aggregates in coastal saline-alkaline paddy soil with organic fertilizer application. *J. Soil Sediment.* 21, 3084–3097. doi: 10.1007/s11368-021-02999-8

Liang, J., Li, Y., Si, B., Wang, Y., Chen, X., Wang, X., et al. (2021). Optimizing biochar application to improve soil physical and hydraulic properties in saline-alkali soils. *Sci. Total Environ.* 771, 144802. doi: 10.1016/j.scitotenv.2020.144802

Liao, H., Wan, H., Shaff, J., Wang, X., Yan, X., and Kochian, L. V. (2006). Phosphorus and aluminum interactions in soybean in relation to aluminum tolerance. exudation of specific organic acids from different regions of the intact root system. *Plant Physiol.* 141, 674–684. doi: 10.1104/pp.105.076497

Liu, H., Liu, Y., Zeng, G., Xie, J., Zheng, B., Tan, X., et al. (2015). Mitigation mechanism of cd-contaminated soils by different levels of exogenous low-molecular-weight organic acids and *Phytolacca americana*. *RSC Adv.* 5, 4552–4559. doi: 10.1039/C5RA05700K

Liu, M., Wang, C., Liu, X., Lu, Y., and Wang, Y. (2020). Saline-alkali soil applied with vermicompost and humic acid fertilizer improved macroaggregate microstructure to enhance salt leaching and inhibit nitrogen losses. *Appl. Soil Ecol.* 156, 103705. doi: 10.1016/j.apsoil.2020.103705

Liu, M., Wang, C., Wang, F., and Xie, Y. (2019). Maize (*Zea mays*) growth and nutrient uptake following integrated improvement of vermicompost and humic acid fertilizer on coastal saline soil. *Appl. Soil Ecol.* 142, 147–154. doi: 10.1016/j.apsoil.2019.04.024

Lu, S., Chen, C., Zhou, X., Xu, Z., Bacon, G., Rui, Y., et al. (2012). Responses of soil dissolved organic matter to long-term plantations of three coniferous tree species. *Geoderma* 170, 136–143. doi: 10.1016/j.geoderma.2011.11.023

Lu, P., Yang, T., Li, L., Zhao, B., and Liu, J. (2020). Response of oat morphologies, root exudates, and rhizosphere fungal communities to amendments in a saline-alkaline environment. *PloS One* 15, e243301. doi: 10.1371/journal.pone.0243301

Luo, X., Liu, G., Xia, Y., Chen, L., Jiang, Z., Zheng, H., et al. (2017). Use of biochar-compost to improve properties and productivity of the degraded coastal soil in the yellow river delta, China. *J. Soil. Sediment.* 17, 780–789. doi: 10.1007/s11368-016-1361-1

Lv, D., Sun, H., Zhang, M., and Li, C. (2022). Fulvic acid fertilizer improves garlic yield and soil nutrient status. *Gesunde Pflanz.* 74, 685–693. doi: 10.1007/s10343-022-00644-z

Ma, H., Li, X., Wei, M., Zeng, G., Hou, S., Li, D., et al. (2020). Elucidation of the mechanisms into effects of organic acids on soil fertility, cadmium speciation and ecotoxicity in contaminated soil. *Chemosphere* 239, 124706. doi: 10.1016/j.chemosphere.2019.124706

Makkaveev, P. N., and Stunzhas, P. A. (2017). Salinity measurements in hyperhaline brines: a case study of the present aral sea. *Oceanology* 57, 892–898. doi: 10.1134/S0001437017060091

Mallhi, Z. I., Rizwan, M., Mansha, A., Ali, Q., Asim, S., Ali, S., et al. (2019). Citric acid enhances plant growth, photosynthesis, and phytoextraction of lead by alleviating the oxidative stress in castor beans. *Plants* 8, 525. doi: 10.3390/plants8110525

Manral, V., Bargali, K., Bargali, S. S., and Shahi, C. (2020). Changes in soil biochemical properties following replacement of banj oak forest with chir pine in central himalaya. *India. Ecol. Process.* 9, 30. doi: 10.1186/s13717-020-00235-8

Meki, K., Liu, Q., Wu, S., and Yuan, Y. (2022). Plant- and microbe-assisted biochar amendment technology for petroleum hydrocarbon remediation in saline-sodic soils: a review. *Pedosphere* 32, 211–221. doi: 10.1016/S1002-0160(21)60041-3

Menezes-Blackburn, D., Bol, R., Klumpp, E., Missong, A., Nischwitz, V., and Haygarth, P. M. (2021). Citric acid effect on the abundance, size and composition of water-dispersible soil colloids and its relationship to soil phosphorus desorption: a case study. *J. Soil Sci. Plant Nutt.* 21, 2436–2446. doi: 10.1007/s42729-021-00534-9

Mindari, W., Sasongko, P. E., Kusuma, Z., Syekhfani,, and Aini, N. (2018). Efficiency of various sources and doses of humic acid on physical and chemical properties of saline soil and growth and yield of rice. *Aip Conf. Proc.* 2019, 030001. doi: 10.1063/1.5061854

Mosaad, I. S. M., Serag, A. H. I., and Sheta, M. H. (2022). Promote sugar beet cultivation in saline soil by applying humic substances in-soil and mineral nitrogen fertilization. *J. Plant Nutr.* 45, 2447–2464. doi: 10.1080/01904167.2022.2046063

Nargesi, M. M., Sedaghathoor, S., and Hashemabadi, D. (2022). Effect of foliar application of amino acid, humic acid and fulvic acid on the oil content and quality of olive. *Saudi J. Biol. Sci.* 29, 3473–3481. doi: 10.1016/j.sjbs.2022.02.034

Negacz, K., Malek, Ž., Vos, A. D., and Vellinga, P. (2022). Saline soils worldwide: Identifying the most promising areas for saline agriculture. *J. Arid Environ.* 203, 104775. doi: 10.1016/j.jaridenv.2022.104775

Neumann, G., Massonneau, A., Langlade, N., Dinkelaker, B., Hengeler, C., Römheld, V., et al. (2000). Physiological aspects of cluster root function and development in phosphorus-deficient white lupin (*Lupinus albus* l.). *Ann. Bot.* 85, 909–919. doi: 10.1006/anbo.2000.1135

Odeh, I. O. A., and Onus, A. (2008). Spatial analysis of soil salinity and soil structural stability in a semiarid region of new south Wales, Australia. *Environ. Manage.* 42, 265–278. doi: 10.1007/s00267-008-9100-z

Pansu, M., and Gautheyrou, J.. (2006). Handbook of soil analysis: mineralogical, organic and inorganic methods. (Heidelberg, Berlin: Springer)

Olaetxea, M., Mora, V., Garcia, A. C., Santos, L. A., Baigorri, R., Fuentes, M., et al. (2016). Root-shoot signaling crosstalk involved in the shoot growth promoting action of rhizospheric humic acids. *Plant Signal. Behav.* 11, e1161878. doi: 10.1080/15592324.2016.1161878

Paul, D., and Lade, H. (2014). Plant-growth-promoting rhizobacteria to improve crop growth in saline soils: a review. *Agron. Sustain. Dev.* 34, 737–752. doi: 10.1007/s13593-014-0233-6

Qadir, M., and Schubert, S. (2002). Degradation processes and nutrient constraints in sodic soils. *Land Degrad. Dev.* 13, 275–294. doi: 10.1002/ldr.504

Rakkammal, K., Maharajan, T., Ceasar, S. A., and Ramesh, M. (2023). Biostimulants and their role in improving plant growth under drought and salinity. *Cereal Res. Commun* 51, 61–74. doi: 10.1007/s42976-022-00299-6

Ranasinghe, T. K. G. P., and Piyadasa, R. U. K. (2020). Optimising usage of salinized lands in the lower part of the river basin for the coastal community in bentota, Sri Lanka. *J. Natl. Sci. Found. Sri.* 48, 379–396. doi: 10.4038/jnsfsr.v48i4.8814

Raza, S. H., Athar, H. R., Ashraf, M., and Hameed, A. (2007). Glycinebetaine-induced modulation of antioxidant enzymes activities and ion accumulation in two wheat cultivars differing in salt tolerance. *Environ. Exp. Bot.* 60, 368–376. doi: 10.1016/j.envexpbot.2006.12.009

Samec, P., Volánek, J., and Bajer, A. (2021). Indication of natural boreo-continental pine sites through discrimination analysis of the soil biochemical and water-holding properties. *Ekol.* 40, 25–36. doi: 10.2478/eko-2021-0004

Santos, S. R., Silva, E. D. B., Alleoni, L. R. F., and Grazziotti, P. H. (2017). Citric acid influence on soil phosphorus availability. *J. Plant Nutr.* 40, 2138–2145. doi: 10.1080/01904167.2016.1270312

Setia, R., Gottschalk, P., Smith, P., Marschner, P., Baldock, J., Setia, D., et al. (2013). Soil salinity decreases global soil organic carbon stocks. *Sci. Total Environ.* 465, 267–272. doi: 10.1016/j.scitotenv.2012.08.028

Shah, Z. H., Rehman, H. M., Akhtar, T., Alsamadany, H., Hamooh, B. T., Mujtaba, T., et al. (2018). Humic substances: determining potential molecular regulatory processes in plants. *Front. Plant Sci.* 9. doi: 10.3389/fpls.2018.00263

Shan, Y. Y., Li, G., Bai, Y. G., Liu, H. B., Zhang, J. H., Wei, K., et al. (2022). Effects of gypsum combined with different amounts of biochemical humic acid on soil improvement and cotton (*Gossypium hirsutum* l.) yield on saline-alkali land. *Appl. Ecol. Env. Res.* 20, 841–854. doi: 10.15666/aeer/2001_841854

Shao, T., Gu, X., Zhu, T., Pan, X., Zhu, Y., Long, X., et al. (2019). Industrial crop *Jerusalem artichoke* restored coastal saline soil quality by reducing salt and increasing diversity of bacterial community. *Appl. Soil Ecol.* 138, 195–206. doi: 10.1016/j.apsoil.2019.03.003

Shi, X., Xiong, J., Yang, X., Siddique, K. H. M., and Du, T. (2022). Carbon footprint analysis of sweet sorghum-based bioethanol production in the potential saline-alkali land of northwest China. *J. Clean. Pr.* 349, 131476. doi: 10.1016/j.jclepro.2022.131476

Sun, C., Li, X., Hu, Y., Zhao, P., Xu, T., Sun, J., et al. (2015). Proline, sugars, and antioxidant enzymes respond to drought stress in the leaves of strawberry plants. *Hortic. Sci. Techno.* 33, 625–632. doi: 10.7235/hort.2015.15054

Sun, R., Wang, X., Tian, Y., Guo, K., Feng, X., Sun, H., et al. (2022). Long-term amelioration practices reshape the soil microbiome in a coastal saline soil and alter the richness and vertical distribution differently among bacterial, archaeal, and fungal communities. *Front. Microbiol.* 12. doi: 10.3389/fmicb.2021.768203

Sun, Y., Yang, J., Yao, R., and Chen, X. (2019). Biochar and fulvic acid to activate soil fertility for achieving agro-ecology benefits in a newly reclaimed coastal wetland of China. *Emir. J. Food Agr.* 36, 459–469. doi: 10.9755/ejfa.2019.v31.i6.1967

Sun, Y., Yang, J., Yao, R., Chen, X., and Wang, X. (2020). Biochar and fulvic acid amendments mitigate negative effects of coastal saline soil and improve crop yields in a three year field trial. *Sci. Rep.* 10, 8946. doi: 10.1038/s41598-020-65730-6

Tahjib-Ul-Arif, M., Zahan, M. I., Karim, M. M., Imran, S., Hunter, C. T., Islam, M. S., et al. (2021). Citric acid-mediated abiotic stress tolerance in plants. *Int. J. Mol. Sci.* 22, 7235. doi: 10.3390/ijms22137235

Tedeschi, A., Lavini, A., Riccardi, M., Pulvento, C., and d'Andria, R. (2011). Melon crops (*Cucumis melo* l., cv. tendral) grown in a mediterranean environment under saline-sodic conditions: Part i. yield and quality. *Agric. Water Manage.* 98, 1329–1338. doi: 10.1016/j.agwat.2011.04.007

Tiwari, S., Sharma, B., Bisht, N., and Tewari, L. (2022). Role of beneficial microbial gene pool in mitigating salt/nutrient stress of plants in saline soil through underground phytostimulating signalling molecules: a review. *Pedosphere.* 33, 153–171 . doi: 10.1016/j.pedsph.2022.06.029

Uri, N. (2018). Cropland soil salinization and associated hydrology: trends, processes and examples. *Water* 10, 1030. doi: 10.3390/w10081030

Vives-Peris, V., de Ollas, C., Gómez-Cadenas, A., and Pérez-Clemente, R. M. (2020). Root exudates: from plant to rhizosphere and beyond. *Plant Cell Rep.* 39, 3–17. doi: 10.1007/s00299-019-02447-5

Vrantsi, E., Lakka, A., Bozinou, E., Athanasiadis, V., Papadaki, E. S., Dourtoglou, V. G., et al. (2021). Humic and fulvic acids as specific sorbents of herbicides in water. *Clean-Soil Air Water* 49, 2000467. doi: 10.1002/clen.202000467

Wang, Y. (2021). Mobilization of recalcitrant phosphorus from soil using citric acid wastewater. *Environ. Earth Sci.* 80, 134. doi: 10.1007/s12665-021-09447-3

Wang, H., and Jin, J. Y. (2005). Photosynthetic rate, chlorophyll fluorescence parameters, and lipid peroxidation of maize leaves as affected by zinc deficiency. *Photosynthetica* 43, 591–596. doi: 10.1007/s11099-005-0092-0

Wang, J., Qian, W., He, Y., Xiong, Y., Song, P., and Wang, R. M. (2017). Reutilization of discarded biomass for preparing functional polymer materials. *Waste Manage.* 65, 11–21. doi: 10.1016/j.wasman.2017.04.025

Wang, J., Wu, J., Lu, J., and Yuan, G. (2020a). Effects of leonardite on the coastal saline soil improvement. *Chem. Ecol.* 36, 750–765. doi: 10.1080/02757540.2020.1787997

Wang, J., Yuan, G., Lu, J., Wu, J., and Wei, J. (2020b). Effects of biochar and peat on salt-affected soil extract solution and wheat seedling germination in the yellow river delta. *Arid Land Res. Manage.* 34, 287–305. doi: 10.1080/15324982.2019.1696423

Wang, Z., Zhuang, J., Zhao, A., and Li, X. (2018). Types, harms and improvement of saline soil in songnen plain. *IOP Conf. Ser.: Mater. Sci. Eng.* 322, 52059. doi: 10.1088/1757-899X/322/5/052059

Wong, V. N. L., Dalal, R. C., and Greene, R. S. B. (2009). Carbon dynamics of sodic and saline soils following gypsum and organic material additions: a laboratory incubation. *Appl. Soil Ecol.* 41, 29–40. doi: 10.1016/j.apsoil.2008.08.006

Wu, L., Wang, Y., Zhang, S., Wei, W., Kuzyakov, Y., and Ding, X. (2021a). Fertilization effects on microbial community composition and aggregate formation in saline-alkaline soil. *Plant Soil* 463, 523–535. doi: 10.1007/s11104-021-04909-w

Wu, L., Zhang, S., Chen, M., Liu, J., and Ding, X. (2021b). A sustainable option: Biochar addition can improve soil phosphorus retention and rice yield in a saline-alkaline soil. *Environ. Technol. Inno.* 24, 102070. doi: 10.1016/j.eti.2021.102070

Wu, L., Zheng, H., and Wang, X. (2021c). Effects of soil amendments on fractions and stability of soil organic matter in saline-alkaline paddy. *J. Environ. Manage.* 294, 112993. doi: 10.1016/j.jenvman.2021.112993

Xiao, F., Zhou, B., Wang, H., Duan, M., and Feng, L. (2022). Effects of different soil amendments on physicochemical property of soda saline-alkali soil and crop yield in northeast China. *Int. J. Agric. Biol. Eng.* 15 (1), 192–198. doi: 10.25165/j.ijabe.20221501.6252

Yang, F., and Antonietti, M. (2020). Artificial humic acids: sustainable materials against climate change. *Adv. Sci.* 7, 1902992. doi: 10.1002/advs.201902992

Yang, Z., Li, J. L., Liu, L. N., Xie, Q., and Sui, N. (2020). Photosynthetic regulation under salt stress and salt-tolerance mechanism of sweet sorghum. *Front. Plant Sci.* 10. doi: 10.3389/fpls.2019.01722

Yang, H., Xia, J., Cui, Q., Liu, J., Wei, S., Feng, L., et al. (2021a). Effects of different *Tamarix chinensis*-grass patterns on the soil quality of coastal saline soil in the yellow river delta, China. *Sci. Total Environ.* 772, 145501. doi: 10.1016/j.scitotenv.2021.145501

Yang, M., Yang, R., Li, Y., Pan, Y., Sun, J., and Zhang, Z. (2021b). Effects of different biomass materials as a salt-isolation layer on water and salt migration in coastal saline soil. *PeerJ* 9, e11766. doi: 10.7717/peerj.11766

Yao, R. J., Li, H. Q., Yang, J. S., Wang, X. P., Xie, W. P., and Zhang, X. (2022a). Biochar addition inhibits nitrification by shifting community structure of ammonia-oxidizing microorganisms in salt-affected irrigation-silting soil. *Microorganisms* 10, 436. doi: 10.3390/microorganisms10020436

Yao, R., Li, H., Zhu, W., Yang, J., Wang, X., Yin, C., et al. (2022b). Biochar and potassium humate shift the migration, transformation and redistribution of urea-n in salt-affected soil under drip fertigation: soil column and incubation experiments. *Irrigation Sci.* 40, 267–282. doi: 10.1007/s00271-021-00763-x

Yao, R., Yang, J., Zhu, W., Li, H., Yin, C., Jing, Y., et al. (2021). Impact of crop cultivation, nitrogen and fulvic acid on soil fungal community structure in salt-affected alluvial fluvo-aquic soil. *Plant Soil* 464, 539–558. doi: 10.1007/s11104-021-04979-w

Zandonadi, D. B., Canellas, L. P., and Façanha, A. R. (2007). Indolacetic and humic acids induce lateral root development through a concerted plasmalemma and tonoplast h^+ pumps activation. *Planta* 225, 1583–1595. doi: 10.1007/s00425-006-0454-2

Zanin, L., Tomasi, N., Cesco, S., Varanini, Z., and Pinton, R. (2019). Humic substances contribute to plant iron nutrition acting as chelators and biostimulants. *Front. Plant Sci.* 10. doi: 10.3389/fpls.2019.00675

Zhang, M., Liu, Y., Liu, Y., Zhao, Y., Yuan, F., and Chen, M. (2023). Rotation of triticale and sweet sorghum improves saline-alkali soil and increases productivity in a saline soil. *Commun. Soil Sci. Plan.* 54, 910–925. doi: 10.1080/00103624.2022.2137181

Zhang, N., Song, F., Su, M., and Duan, F. (2020a). Organic material combined with beneficial bacteria improves soil fertility and corn seedling growth in coastal saline soils. *Rev. Bras. Cienc. Solo.* 44, e0190179. doi: 10.36783/18069657rbcs20190179

Zhang, L., Wang, Y., Soda, S., He, X., Hao, S., You, Y., et al. (2020b). Effect of fulvic acid on bioreactor performance and on microbial populations within the anammox process. *Bioresource Technol.* 318, 124094. doi: 10.1016/j.biortech.2020.124094

Zhang, P., Yang, F., Zhang, H., Liu, L., Liu, X., Chen, J., et al. (2020c). Beneficial effects of biochar-based organic fertilizer on nitrogen assimilation, antioxidant capacities, and photosynthesis of sugar beet (*Beta vulgaris* l.) under saline-alkaline stress. *Agronomy* 10, 1562. doi: 10.3390/agronomy10101562

Zhu, C. Q., Ghoto, K., Gao, G. F., Chen, J., Hu, W. J., Qiao, F., et al. (2019). Trace metals complexation behavior with root exudates induced by salinity from a mangrove plant *Avicennia marina* (Forsk.) vierh. *Bioremediat. J.* 23, 82–93. doi: 10.1080/10889868.2019.1602108

frontiers | Frontiers in Plant Science

TYPE Original Research
PUBLISHED 28 March 2023
DOI 10.3389/fpls.2023.1112002

OPEN ACCESS

EDITED BY
Jing Zhang,
Nanjing Agricultural University, China

REVIEWED BY
Mingjiu Wang,
Inner Mongolia Agricultural University, China
Mingna Li,
Chinese Academy of Agricultural Sciences (CAAS), China
Wuwu Wen,
Shanghai Jiao Tong University, China

*CORRESPONDENCE
Guowen Cui
cuigw603@126.com
Xiujie Yin
yinxiujie@126.com

SPECIALTY SECTION
This article was submitted to Plant Abiotic Stress, a section of the journal Frontiers in Plant Science

RECEIVED 30 November 2022
ACCEPTED 02 February 2023
PUBLISHED 28 March 2023

CITATION
Meng L, Wu Y, Mu M, Wang Z, Chen Z, Wang L, Ma Z, Cui G and Yin X (2023) Effects of different concentrations of biochar amendments and Pb toxicity on rhizosphere soil characteristics and bacterial community of red clover (*Trifolium pretense L.*). *Front. Plant Sci.* 14:1112002. doi: 10.3389/fpls.2023.1112002

Effects of different concentrations of biochar amendments and Pb toxicity on rhizosphere soil characteristics and bacterial community of red clover (*Trifolium pretense L.*)

Lingdong Meng, Yuchen Wu, Meiqi Mu, Zicheng Wang, Zirui Chen, Lina Wang, Zewang Ma, Guowen Cui* and Xiujie Yin*

College of Animal Science and Technology, Northeast Agricultural University, Harbin, China

Amending soil with biochar can reduce the toxic effects of heavy metals (HM) on plants and the soil. However, the effects of different concentrations of biochar on the properties and microbial activities in lead (Pb)-contaminated soils are unclear. In this study, two Pb concentrations were set (low, 1000 mg/kg; high, 5000 mg/kg), and five corn straw biochar (CSB) concentrations (0, 2.5, 5, 10 and 15%) were used to determine the response of the growth and rhizosphere of red clover (*Trifolium pretense* L.) (in terms of soil properties and bacteria) to CSB and Pb application. The results showed that 5% CSB better alleviated the toxicity of Pb on the shoot length of red clover, the biomass increased by 74.55 and 197.76% respectively and reduced the enrichment factor (BCF) and transport factor (TF) of red clover. Pb toxicity reduced soil nutrients, catalase (CAT), acid phosphatase (ACP) and urease activity, while the addition of CSB increased soil pH, soil organic matter (SOM) content and soil enzyme activity. 16S rDNA amplicon sequencing analysis showed that Pb toxicity reduced the diversity of rhizosphere bacteria in red clover and reduced the relative abundance of plant growth-promoting rhizobacteria such as *Gemmatimonas*, *Devosia* and *Bryobacter*. Spearman correlation analysis showed that the addition of alkaline CSB restored the relative abundance of rhizobacteria positively correlated with pH, such as *Chitinophaga*, *Sphingomonas*, *Devosia* and *Pseudomonas*, and thus restored the rhizosphere soil environment. This study demonstrates that 5% CSB can better alleviate the toxicity of Pb to red clover and soil. We also provide a theoretical basis for the subsequent use of beneficial bacteria to regulate the repair efficiency of red clover.

KEYWORDS

lead stress, corn straw biochar, 16S rDNA amplicon sequencing, bacterial, red clover, soil enzyme activity

1 Introduction

Soil accumulation of heavy metals (HM) from natural and human sources has become a major problem in terrestrial ecosystems (Mourad et al., 2021). The main human sources of these HM are metal mining activities, industrial activities, automobile exhaust emissions and wastewater irrigation. HM not only poison soils and water resources but also hinder plant productivity. HM can also accumulate in the food chain, ultimately threatening human health (Azadi and Raiesi, 2021). Lead (Pb) is one of the most common HM pollutants in the environment. The Pb concentration is approximately 50 mg/kg in the soil in nature (Bamagoos et al., 2022). However, due to the use of paint, Pb-containing gasoline and other Pb-containing products and the lack of effective treatment methods, the Pb concentration in the environment is much higher than the recommended safe concentration (Salam et al., 2016). In addition, Pb is nonbiodegradable and can persist in the soil environment for a long time (Kumar et al., 2020). Studies have shown that children have a stronger absorption capacity for Pb than adults, and Pb exposure can cause cognitive, hearing and cardiovascular problems (Fewtrell et al., 2004). Physical and chemical remediation methods for removing Pb from contaminated soils can reduce Pb toxicity and mitigate the risk of Pb exposure (Xinde et al., 2011). However, widespread application of these soil remediation techniques is limited due to high costs and the destruction of the soil structure (Muthusaravanan et al., 2018). Therefore, identifying economic, efficient and environmentally friendly sustainable soil remediation techniques is urgently needed.

Biochar is a carbon-rich porous material produced *via* pyrolysis of biomass under anaerobic conditions (Uchimiya et al., 2010). As a soil conditioner, biochar can cause changes in soil physical and chemical properties and has been widely used in the remediation of HM-contaminated soil (Omidi et al., 2019; Yang et al., 2022). Studies have shown that, owing to its porous structure, biochar can adsorb and fix pollutants in the soil, reduce the bioavailability of HM (Zhao et al., 2021), and reduce both the migration of HM in the soil and the incorporation of HM from the soil into plants, thereby preventing HM from threatening human health *via* the food chain. It has been reported that biochar application has remediation effects on chromium, arsenic, Pb and cadmium. In addition, biochar can improve soil properties and increase both the soil pH and soil organic matter content (Qiu et al., 2021), thereby mitigating damage caused by HM and promoting plant growth; this has been shown for foxtail millet (Kang et al., 2022) and wheat (Yanru et al., 2022). There are many studies on the effects of the pyrolysis temperature of biochar on its ability to improve Pb-contaminated soils (Chi et al., 2017; Yang et al., 2021); however, the application amount of biochar may be the most important factor affecting its ability to remediate Pb. Jing et al. reported that wheat straw-derived biochar reduced the migration of Pb (Jing et al., 2020), and Cheng et al. showed that adding 5% tobacco straw-derived biochar reduced the available Pb concentration better than a low dose (Jianzhong et al., 2018). In China, the annual yield of corn straw is high, but the utilization rate is low. The imbalance between yield and utilization leads to a large amount of corn straw being discarded or burned, which wastes resources and pollutes the environment (Yang et al., 2019). Therefore, corn straw biochar (CSB) was used as a soil amendment to reduce Pb pollution.

Red clover (*Trifolium pretense* L.) is a legume perennial herb with high protein content, good palatability and low demand for nitrogen fertilizer (Chao et al., 2018). Previous studies have found that red clover has a strong tolerance to heavy metals and shows the ability to accumulate heavy metals (Jin et al., 2013). Therefore, it has received extensive attention in the remediation and detoxification of contaminated field (Cruz et al., 2021). Mo found that the photosynthetic capacity and antioxidant enzyme activity of red clover could maintain a certain level under heavy metal environment. In addition, the migration ability of roots to heavy metals was low (Mo et al., 2021). This means that it may have good potential for resistance to heavy metal toxicity.

Soil microorganisms may be the most sensitive soil organisms to subtle changes in the soil environment. Therefore, the toxic effect of Pb in the soil can reduce soil microbial biomass (Nahid and Fayez, 2021), inhibit microbial metabolism (Xu et al., 2021) and alter microbial community composition (Jianhua et al., 2021). Kamaruzzaman et al. found that Pb exposure enhanced the Pb resistance of microorganisms; for example, *Bacillus* and *Enterobacter* were found to have high tolerance to Pb stress (Kamaruzzaman et al., 2020). The application of biochar to cadmium (Cd)-contaminated soil increased the abundance of *Pseudomonas*, thereby reducing the absorption of Cd by plants. The porous structure and large surface area of biochar provide shelter for microorganisms (Chuchu et al., 2022). Soil pH plays an important role in the degradation of contaminants by influencing the activity of cells, the positive or negative surface charge of substances, HM solubility and the ionization state of functional groups. Microbes are vulnerable to the environmental pH balance. Under normal conditions, the optimum pH value for the reproduction and vivacity of most microorganisms is between 6.0 and 8.0 (Youyuan et al., 2021). At suitable pH values, *Bacillus* has a stronger ability to remove pollutants (Zhang et al., 2020). In addition, pH also affects the mobility of HM and biochar surface charges, thereby affecting the interaction between pollutants and biochar (Chuchu et al., 2022). Overall, the addition of biochar increased the relative abundance of C and N cycling-related microorganisms in the soil. However, the correlation between red clover growth, physiological changes and soil physical and chemical properties and the changes in rhizosphere soil bacteria under Pb toxicity are still unclear.

In this study, soil physicochemical properties and 16S rDNA amplicon sequencing were combined to elucidate the response mechanism of red clover rhizosphere soil to different concentrations of Pb and different application rates of CSB. The purposes of this study were (a) to investigate the effects of Pb toxicity and biochar amendments on soil physicochemical properties and the soil bacterial community; (b) to analyze the interactions between soil characteristics and the bacterial community; and (c) to determine the optimal biochar concentration for mitigating Pb toxicity red clover. Our results should provide new insights into the interactions between soil physicochemical properties and the soil bacterial community in response to different doses of biochar.

2 Materials and methods

2.1 Plant, soil, and corn straw biochar

In this study, the soil was collected from the experimental field of Northeast Agricultural University in Harbin, China (E 126°14′; N 45°05′), then quickly transported back to the laboratory, dried at 25°C, and keep

the soil moisture at 60%. The surfaces of the selected red clover seeds were disinfected (Liu et al., 2021), washed three times with distilled water, and germinated in a dark environment at 25°C. Biochar was produced by pyrolysis of corn straw at 500°C using furnace equipment (LZ-LS-600*800-420, China). The initial soil pH, SOM, available phosphorus (AP) and available potassium (AK) were 6.13, 29.37 g/kg, 139.34 mg/kg and 59.06 mg/kg respectively. In addition, the CSB had a pH of 9.4 and Pb concentration of 8.12 mg/kg.

2.2 Experimental design

The Pb-containing soil was set to 1000 mg/kg (low lead) and 5000 mg/kg (high lead) with $Pb(NO_3)_2$, and 1 kg of soil was preserved in each pot. After two weeks of passivation, CSB was mixed with Pb-containing soil at five ratios, i.e., 0, 2.5, 5, 10 and 15%. Then, the plants were selected with consistent growth and planted 10 plants in a pot (planting environment: 16 h/8 h light/dark cycle, 25 ± 1°C) (Wang et al., 2022), 70% relative humidity (Zhang et al., 2021). In addition, impervious plates were placed under pots to absorb the leachate from the pots and return it to the soil every two days. The treatments were set as CK (0 mg/kg Pb + 0% CSB), LB0 (1000 mg/kg Pb + 0% CSB), LB2.5 (1000 mg/kg Pb + 2.5% CSB), LB5 (1000 mg/kg Pb + 5% CSB), LB10 (1000 mg/kg Pb + 10% CSB), LB15 (1000 mg/kg Pb + 15% CSB), HB0 (5000 mg/kg Pb + 0% CSB), HB2.5 (5000 mg/kg Pb + 2.5% CSB), and HB5 (5000 mg/kg Pb + 5% CSB). HB10 (5000 mg/kg Pb + 10% CSB) and HB15 (5000 mg/kg Pb + 15% CSB), with total of 11 treatments, and each treatment had 3 replicates. Red clover plants and soil samples were collected 45 days later. The loose soil was divided into bulk soil and collected the soil around the roots as rhizosphere soil for subsequent 16S rDNA amplicon sequencing.

2.3 Plant growth index and Pb content

After exposure to Pb stress for 45 days, the stem length of red clover was measured using a ruler with a precision of 1 mm. In the determination of Pb concentration, plant stems and roots were dried (105°C and 12h), and the soil was ground to a diameter of less than 0.02 mm. Then, 0.5 g of the sample was added to 37% HCl and 63% HNO_3 (150°C) for digestion, diluted with HNO_3, and finally analyzed by inductively coupled plasma–mass spectrometry (Agilent, 7800 ICP–MS, USA) (Helaoui et al., 2020).

2.4 The bioconcentration factor and translocation factor of Pb

Using the method reported by Meng (Meng et al., 2022), we calculated the bioaccumulation factor (BCF =Pb concentration in plant/Pb concentration in soil) and transport factor (TF =Pb concentration in shoot/Pb concentration in root).

2.5 Soil properties

According to the method of Liu et al., the pH and electrical conductance (EC) of the soil suspension (1:5, w/v) were measured by a pH meter and conductivity meter, respectively. SOM was determined by the dry combustion method (Liu et al., 2020). Available phosphorus (AP), available potassium (AK), ammonia nitrogen and nitrate nitrogen were measured by Lu et al. (Lu et al., 2000). Catalase, acid phosphatase, urease and sucrose (SC) levels in the rhizosphere soil of red clover were measured by using a kit purchased from Shanghai Enzyme-linked Biotechnology Co., Ltd. (www.mlbio.cn), and then measured the absorbance at 450 nm using a microplate reader (k6600-a, Beijing Kaiao Technology Development Co., Ltd).

2.6 Rhizosphere bacterial community analysis

Genomic DNA was extracted from rhizosphere soil by the CTAB/SDS method. Amplicons were amplified according to the manufacturer's instructions as follows: initial denaturation at 98°C for 1 min, followed by denaturation at 98°C for 10 s (30 cycles), followed by annealing and extension at 50°C and 72°C for 30 s, respectively, and centrifugation at 72°C for 5 min. An equal volume of 1X loading buffer containing SYB green was mixed with PCR products and purified using a Qiagen Gel Extraction Kit (Qiagen, Germany). The TruSeq ® DNA PCR-Free Sample Programming Kit (Illumina, USA) was used to generate sequencing libraries and add index codes as recommended by the manufacturer. Library quality assessment was performed on a Qubit @ 2.0 fluorometer (Thermo Scientific) and an Agilent Bioanalyzer 2100 system. Finally, the library was sequenced on the Illumina Nova Seq platform, resulting in 250 bp double-ended reads.

The raw tags were filtered with reference to the QIIME (V 1.9.1) tag quality control process (Caporaso et al., 2010). Compare the above tags with the SILVA database and use the UCHIME Algorithm (Brian et al., 2011) to detect the chimera sequence and remove it. Finally, obtain effective tags. The sequences were clustered into operational taxonomic units (OTUs) with 97% identity, and the OTU sequences were annotated. The species annotation analysis was performed using the Mothur method and SILVA138 (http://www.arb-silva.de/) SSUrRNA database (the threshold was set to 0.8–1) (Wang et al., 2007; Edgar, 2013).

2.7 Statistical analysis

Statistical calculations were carried out by Microsoft Office Excel 2016, Origin 2018, IBM SPSS version 26.0 software and R package. In addition to one-way ANOVA, the Wilcox test was used for analyzing bacterial richness and diversity (Bauer, 1972). The images were merged using Adobe Photoshop 2020. The correlation between the physicochemical properties of rhizosphere soil and rhizosphere bacterial community structure was analyzed by Spearman correlation analysis. SIMPER ranked OTUs according to the contribution rate of each treatment group to the difference score. The Silva database was used to identify 25 OTUs identified by SIMPER analysis of CK *vs.* HB0 and HB0 *vs.* HB5.

3 Results

3.1 Plant growth and accumulation and transport of Pb

In this study, compared with CK, the stem length of red clover was significantly reduced by 32.78% and 64.48% at LB0 and HB0,

10.3389/fpls.2023.1112002

respectively ($P < 0.05$). The application of CSB alleviated the toxic effect of Pb on the stem growth of red clover, and the effects were dependent on CSB concentration. Compared with LB0 and HB0, LB5, LB2.5, HB5 and HB2.5 significantly increased by 44.69, 27.61, 73.88 and 40.23%, respectively. However, the mitigation effects of 10% and 15% CSB on Pb toxicity decreased (Figures 1A, B). And the biomass change trend of red clover is similar to stem length, compared with LB0 and HB0, the biomass of LB5 and HB5 increased by 74.55 and 197.75%, respectively. (Figure 1C). Combining the data on Pb concentration in the soil and in red clover, we calculated the Pb enrichment factor (BCF) and transport coefficient (TF) of red clover (Table S1). High concentration of Pb caused a significant increase in the BCF of red clover plants, and the addition of CSB to the Pb-contaminated soil caused a downward trend in the BCF and TF. These results showed that Pb toxicity inhibited the growth of red clover, and the addition of CSB resulted in more fixing of Pb in the soil, alleviated Pb toxicity, reduced the Pb enrichment and transport capacity, and stimulated plant growth. Moreover, the remediation effect of 5% CSB was better than that of the other treatment groups.

3.2 Effects of Pb and CSB on soil physicochemical properties

At the same Pb concentration, the soil pH significantly increased with increasing CSB concentration ($P < 0.05$), and the highest soil pH values were recorded in LB15 (pH = 7.505) and HB15 (pH = 7.129) (Figure 1D). At the same CSB level, the pH of the low-Pb treatment was higher than that of the high-Pb treatment. When the Pb concentration in the soil was 1000 and 5000 mg/kg, the electrical conductivity (EC) was in the order of CK < LB0 < HB0. Compared with the levels of their respective control treatments, all CSB levels increased the soil EC regardless of Pb concentration, and the EC was highest in the two Pb concentration treatments when 10% CSB was added (Figure 1E).

Compared with the no-Pb stress treatment, the 1000 and 5000 mg/kg Pb concentration treatments had no significant effect on the SOM content. At the 1000 mg/kg Pb level, CSB application significantly increased the SOM content, and the highest SOM content was recorded in LB15 (53.12 g/kg). For the high Pb concentration treatments, the SOM contents of HB2.5, HB5, HB10 and HB15 were 10.86, 24.83, 54.67 and 66.72% higher than that of HB0, respectively (Figure 1F).

Pb treatment significantly reduced the soil AP content ($P < 0.05$) compared with that of the CK. Except for LB5, with the increase in CSB concentration, the AP content increased in the two Pb treatments; the AP content increased by 74.58 and 37.34% in LB15 and HB15, respectively, compared with LB0 and HB0, respectively (Figure 2A). The AK content under low Pb stress was significantly lower than that under the CK treatment, but no significant effect was found under high Pb stress. With the increase in CSB concentration, both Pb levels were in the following order: 0% < 0.5% < 5% < 10% < 15% (Figure 2B).

Under low Pb stress (1000 mg/kg), the soil ammonium-nitrogen content in the CSB-treated samples was higher than that under high Pb stress (5000 mg/kg). Compared with the CK treatment, low Pb stress promoted the soil ammonium-nitrogen content, but high Pb stress inhibited it, indicating that a high Pb concentration has a negative impact on the soil ammonium-nitrogen content; CSB application could alleviate this inhibition (Figure 2C). Adding CSB increased the soil nitrate-nitrogen content. When 5% CSB was applied, the soil nitrate-nitrogen content peaked, and the LB5 and HB5 nitrate-nitrogen contents were 29.53 and 23.33 mg/kg, respectively. An increasing CSB concentration decreased the nitrate-nitrogen content, indicating that the application of CSB can improve the soil nitrate-nitrogen level, but there was a limit, as excessive CSB concentrations result in too much nitrate-nitrogen inhibition (Figure 2D).

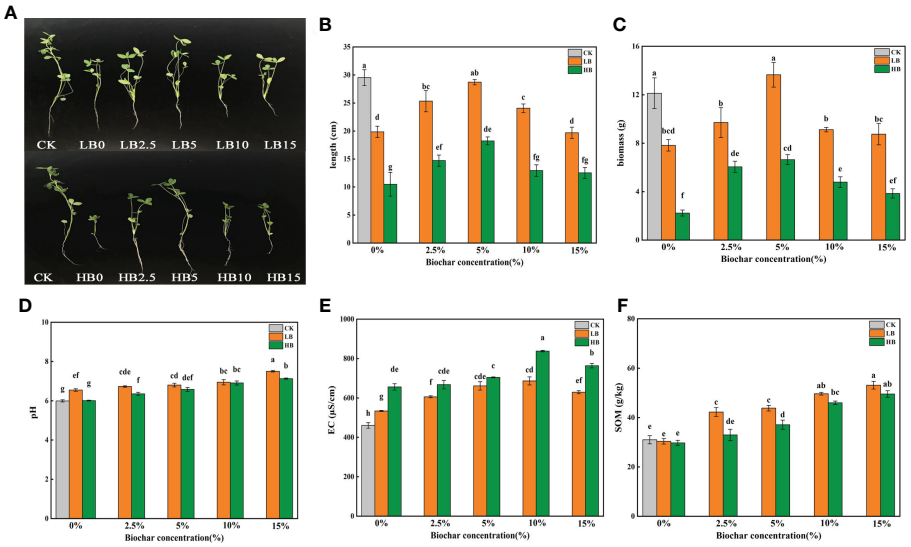

FIGURE 1
Effects of CSB at different concentrations on **(A, B)** shoot length of red clover, **(C)** biomass of red clover, **(D)** rhizosphere soil pH, **(E)** EC and **(F)** SOM under Pb toxicity. Different small letters indicate significant differences under different Pb concentration treatments and different biochar doses ($P<0.05$).

10.3389/fpls.2023.1112002

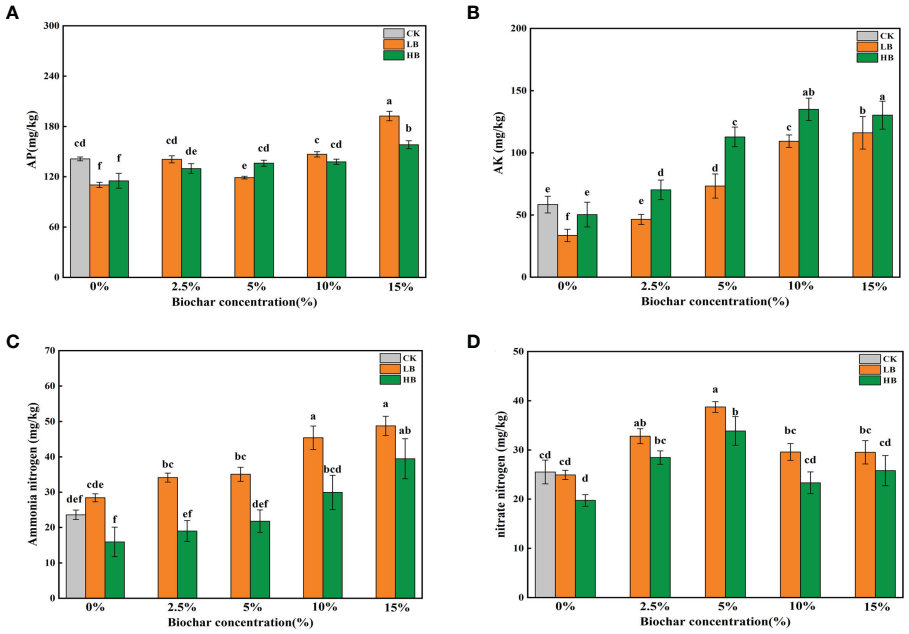

FIGURE 2
Effects of CSB at different concentrations on **(A)** available phosphorus, **(B)** available potassium, **(C)** ammonium nitrogen and **(D)** nitrate nitrogen under Pb toxicity. Different small letters indicate significant differences under different Pb concentration treatments and different biochar doses (*P*<0.05).

3.3 Effects of Pb and CSB on soil enzyme activity

Figure 3 shows the effects of different concentrations of Pb and CSB on soil enzyme activity after 45 days. Compared with that of CK, the catalase (CAT) activity of LB0 and HB0 decreased by 37.63 and 57.31%, respectively (Figure 3A). The addition of CSB could alleviate the effect of Pb stress on CAT activity to a certain extent but with a limit; moreover, the recovery effect was best when 5% CSB was added. Similarly, under the two Pb stresses, the addition of 5% CSB had the

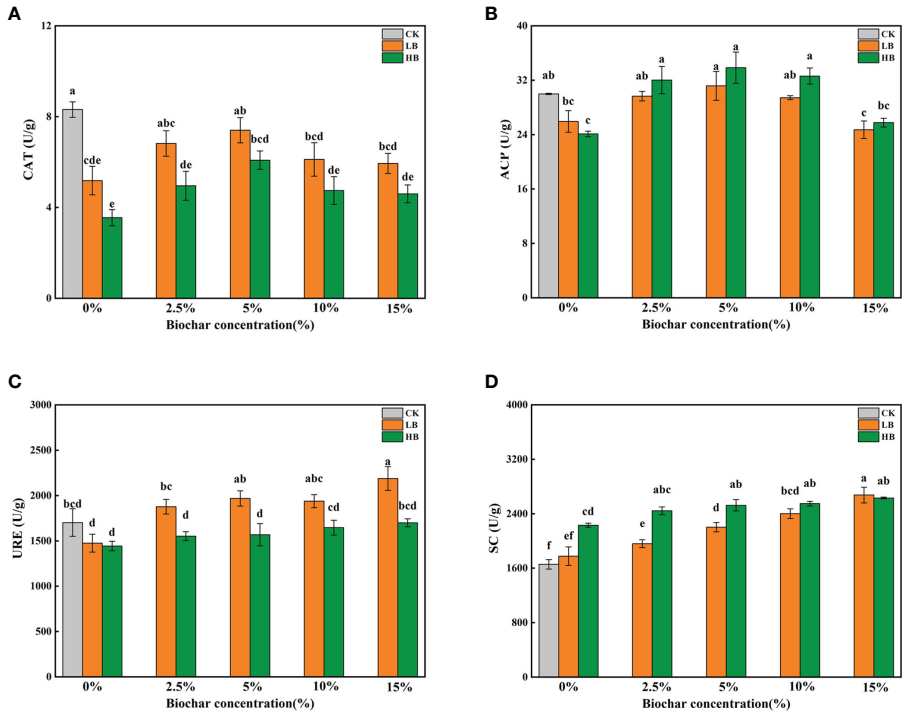

FIGURE 3
Effects of different concentrations of CSB on enzyme activities in Pb-contaminated rhizosphere soil. **(A)** CAT, **(B)** ACP, **(C)** URE and **(D)** SC. Different small letters indicate significant differences under different Pb concentration treatments and different biochar doses (P<0.05).

best improvement effect on ACP activity (Figure 3B). The soil ACP activities of LB5 and HB5 were 31.17 U/g and 33.85 U/g, respectively. A continued increase in CSB concentration negatively affected the soil ACP activity. With increasing Pb concentration, the URE activity gradually decreased (Figure 3C). After adding CSB, the URE activity (2188.06 U/g) of LB15 was significantly higher than that of LB0, and the URE activity of LB15 was the highest in all treatment groups. Under high Pb concentrations, with increasing CSB concentration, the URE activity slightly increased. In contrast to the activity of the above three enzymes, the soil SC activity increased with increasing Pb concentration, especially in HB0, and the SC activity increased by 34.80% compared with that of the CK (Figure 3D). At the same CSB level, except for 15% CSB, the SC activity of the 5000 mg/kg Pb treatment group was higher than that of the 1000 mg/kg Pb treatment group. Taken together, these results showed that Pb stress alone could alter soil enzyme activity and that adding CSB to soil on the basis of Pb stress can improve soil enzyme activity. According to the activity of the different types of enzymes, the best CSB concentration is also not always the same. For CAT and ACP, more than 10% CSB inhibited their activity.

3.4 16S rDNA amplicon sequencing data

Bacterial 16S rDNA amplicon sequencing generated 2,355,232 original reads. After filtering low-quality sequences, short-read sequences and chimeric sequences, the clean bacterial reads (1,781,336) were clustered into 11495 bacterial operational taxonomic units (OTUs) at a 97% similarity level (Table S2). The dilution curves of the 11 treatment groups ranged from 2344 to 3350, indicating that the 16S rDNA amplicon sequencing data were reasonable (Figure S1A). The species uniformity and homogeneity of each treatment were relatively high (Figure S1B).

The number of specific OTUs in LB0 and HB0 was lower than that in CK, indicating that Pb stress may inhibit the growth of some bacterial groups in contaminated soils (Figures S1C, D). The number of OTUs in the LB2.5 and HB5 groups was higher than that in the LB0 and HB0 groups, respectively, indicating that the CSB concentration promoted the growth of certain bacterial species, and the most suitable concentration for CSB to mitigate Pb contamination varied according to the degree of Pb contamination in the soil.

3.5 Variation in rhizosphere bacterial communities

3.5.1 Bacterial community diversity

The bacterial species richness (ACE and Chao1) and species diversity (Shannon and Simpson) were compared (Table 1). Compared with those of the CK, the ACE richness index and Chao1 richness index of the low-Pb treatment group were not significantly affected, while the high-Pb treatment significantly reduced the soil bacterial richness ($P < 0.05$). Compared with those of the low-Pb treatment group, the Shannon diversity index and Simpson diversity index of the HB5, HB10 and HB15 groups significantly decreased ($P < 0.05$). These results indicate that among all the treatment groups, LB15 had the highest richness and diversity. The results of the above analysis showed that soil community diversity was more sensitive to changes in Pb concentration than to changes in CSB concentration; this was especially true under high Pb conditions, which caused a significant decrease in soil bacterial diversity. The Wilcoxon test analysis shows this result more clearly (Figure S2).

Principal coordinate analysis (PCoA) was performed at the OTU level (Figure S3). PCoA by weighted UniFrac revealed a significant difference between the high-Pb treatment and the low-Pb treatment. PC1 and PC2 explained 37.92 and 12.31% of the total variance in the soil bacterial community, respectively. When the unweighted UniFrac distance was used, the two axes explained more than 20% of the difference (Figure S4).

3.5.2 Bacterial community composition and structure

The phylum distribution of all the samples showed significant changes in rhizosphere microbial composition in response to Pb and CSB. A total of 83 phyla were detected in the rhizosphere soil samples

TABLE 1 Analysis of Alpha diversity index of soil bacteria between groups.

Treatment	shannon	simpson	chao1	ACE
CK	9.87 ± 0.11a	0.997 ± 0.001a	3553.81 ± 325.04abc	3635.08 ± 341.39abc
LB0	9.71 ± 0.18ab	0.996 ± 0.001a	3642.80 ± 423.22ab	3627.27 ± 396.82abc
LB2.5	9.67 ± 0.14ab	0.996 ± 0.000a	3515.80 ± 338.84abc	3586.01 ± 304.18abc
LB5	9.64 ± 0.46ab	0.994 ± 0.004a	3508.93 ± 317.14abc	3614.55 ± 285.71abc
LB10	9.88 ± 0.18a	0.997 ± 0.001a	3677.98 ± 133.98ab	3795.05 ± 179.31ab
LB15	9.92 ± 0.11a	0.997 ± 0.000a	3917.51 ± 209.94a	3973.20 ± 188.98a
HB0	9.15 ± 0.17abc	0.992 ± 0.002a	3239.23 ± 179.19bcd	3399.14 ± 231.68abc
HB2.5	8.97 ± 0.32bcd	0.991 ± 0.002a	3017.79 ± 286.91bcd	3131.05 ± 291.06cd
HB5	8.24 ± 0.87d	0.976 ± 0.019b	2947.09 ± 412.04cd	3025.69 ± 345.84cd
HB10	8.72 ± 0.47cd	0.985 ± 0.010ab	3114.64 ± 9.37bcd	3198.04 ± 14.01cd
HB15	8.45 ± 0.32cd	0.984 ± 0.005ab	2645.43 ± 193.00d	2757.54 ± 196.67d

(Table S3), and the top ten were Proteobacteria (37.80%), Actinobacteriota (7.77%), Bacteroidota (7.24%), Acidobacteriota (5.47%), Firmicutes (3.78%), Chloroflexi (3.67%), Myxococcota (2.36%), Gemmatimonadetes (1.76%), Verrucomicrobia (1.23%) and unknown bacterial phyla (20.44%) (Figure 4A). Pb stress alone significantly altered the rhizosphere bacterial community structure. Within these communities, the abundance of Acidobacteriota, Myxococcota and Gemmatimonadetes decreased significantly with increasing Pb concentration, while the abundance of Proteobacteria, Bacteroidota and Firmicutes increased in response to Pb pollution. In addition, the abundance of Actinobacteriota and Chloroflexi increased only in response to high concentrations of Pb. Notably, compared with that in LB0, the relative abundance of Actinobacteriota in LB2.5 and LB5 increased by 118.56 and 147.25%, respectively. In addition, compared with that in HB0, the relative abundance of Bacteroidota and Myxococcota in HB5 increased by 280.76 and 138.54%, respectively. The relative abundance of Acidobacteriota and Gemmatimonadetes also increased slightly.

In addition, *Chitinophagales* and *Chitinophagaceae* had higher relative abundances at the order level and family levels, respectively, especially under 5000 mg/kg Pb stress. This indicated that the addition of high concentrations of Pb and 5% CSB could promote an increased abundance of *Chitinophaga*. Moreover, at the family level, the relative abundance of *Sphingomonadaceae* in the LB5 treatment group was 69.46% higher than that in the LB0 treatment group and was the highest among the values in all the treatment groups (Figure S5).

To further explore the effects of Pb and CSB addition on rhizosphere bacterial community structure, the community composition of red clover rhizosphere bacteria was analyzed at the genus level. High concentrations of Pb significantly reduced the relative abundance of *Gemmatimonas* and *MND1*. Correspondingly, the relative abundance of *Chitinophaga*, *Rhodanobacter* and *Sphingomonas* was positively correlated with the Pb concentration. After adding biochar, the relative abundance of *Sphingomonas* in LB5 was 95.01% higher than that in LB0 and that the relative abundance of *Chitinophaga*, *Rhodanobacter* and *Nannocystis* in HB5 peaked; in particular, the relative abundance of *Chitinophaga* (belonging to Bacteroidota) was 113.9 times higher than that in HB0 (Figure 4B). Notably, the relative abundance of *Chitinophaga* increased in HB5, and the relative abundance of Myxococcota recovered compared with HB0. However, LB5 did not obtain a similar conclusion. In addition, the relative abundance of *Gemmatimonas* and *MND1* was also restored in response to the addition of CSB.

3.5.3 SIMPER analysis

SIMPER analysis, combined with hierarchical clustering heatmap displays, was used to show the OTUs that contributed most to Bray–Curtis dissimilarities between treatments. The top 25 OTUs in the CK *vs*. HB0 comparison accounted for 22.02% of the total contribution between treatments (Table S4), while the top 25 OTUs in the HB0 *vs*. HB5 comparison accounted for 26.08% (Table S5). Figure 5 shows their contribution to the relative abundance of samples. For the CK and HB0 comparison groups, 25 taxa clustered between samples were divided into three large groups (Figure 5A), with top clusters likely to be Pb-sensitive and lower clusters considered to be Pb-resistant or Pb-tolerant. Some of these OTUs identified at the genus level among the resistant Pb toxicity samples were OTU_1 *Rhodanobacter*, OTU_6514 *Sphingomonas*, OTU_6 *Lysobacter*, and OTU_23 *Nitrolancea*.

Proportions of the 25 taxa across treatments that contributed most to Bray–Curtis dissimilarity based on the HB0 *vs*. HB5 SIMPER analysis (Figure 5B). According to the rate of CSB, the dendrogram divides co-occurrences of taxa over samples into four main groups. One subcluster at the bottom of the heatmap had five taxa, they were less sensitive to CSB and could survive in a Pb-contaminated niche. In addition, OTU_3 *Chitinophaga*, OTU_8 *Rhodanobacter*, OTU_19 *Cytophaga*, OTU_25 *Nannocystis* and OTU_20 *Lactobacillus* were highly sensitive to 5% CSB treatment. Thus, as visualized in the heatmap, Pb and CSB may exert synergistic effects on the development of the rhizosphere bacterial community, including perhaps an alleviating effect of CSB on Pb toxicity.

Dendrograms illustrate the clustering of taxa among samples.

3.6 Regulatory mechanism through which CSB promotes red clover growth and Pb toxicity resistance

To determine the bacterial biomarkers in the Red clover rhizosphere under the combined action of different levels of Pb pollution alone and Pb pollution together with different CSB concentrations, LDA effect size (LEfSe) analysis (linear discriminant analysis (LDA) score > 4.0, $P < 0.05$) was used to examine the changes in microbial community structure. In the 11 treatments studied here, after different concentrations of Pb and CSB were added, the abundances of several OTUs were significantly different, especially in the high concentration of Pb pollution and CSB treatment. Under Pb pollution alone, three kinds of bacteria were closely related to high Pb stress: *Actinomycetes* (class), *Flavomonas* (from one order to one

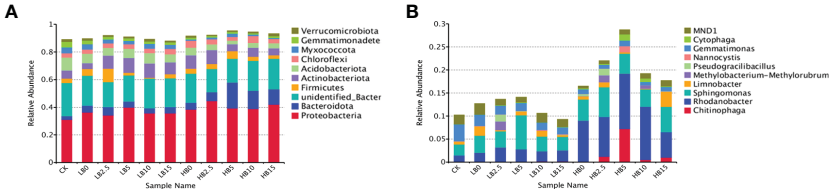

FIGURE 4
Relative abundance of bacterial community structure in different treatments. **(A)** Phylum level and **(B)** genus level.

10.3389/fpls.2023.1112002

family) and *Bacteroides* (class) (Figure 6A). Four types of bacteria were closely related to CSB, namely, *Actinomycetes* (one class), *Chitinophaga* (one class to one family), fibrophagocytizing bacteria (one class to one genus) and Proteus (one class to one family) (Figure 6C). For low Pb stress, the addition of only 5% CSB resulted in significant differences from CK (Figure 6B).

Redundancy analysis and Spearman correlation analysis were used to determine correlations between soil physicochemical properties and rhizosphere microbial structure. The RDA results showed that soil physical properties (pH and EC), AK and SC were mainly affected by high Pb levels, and they were more closely related to Proteobacteria and Bacteroidota. Acidobacteriota and Myxococcota are more closely related to ammonium nitrogen, CAT and URE (Figure 7A). Plant growth-promoting rhizosphere bacteria identified in this study, such as *Rhodanobacter*, *Sphingomonas*, *Devosia* and *Lysobacter*, were positively correlated with EC, AK content and SOM content. In addition, *MND1*, *Gemmatimonas* and *Nannocystis* were positively correlated with CAT, ACP and URE activity (Figure 7B). Notably, CSB was alkaline, and CSB increased the soil pH. The abundance of *Chitinophaga*, *Sphingomonas*, *Devosia* and

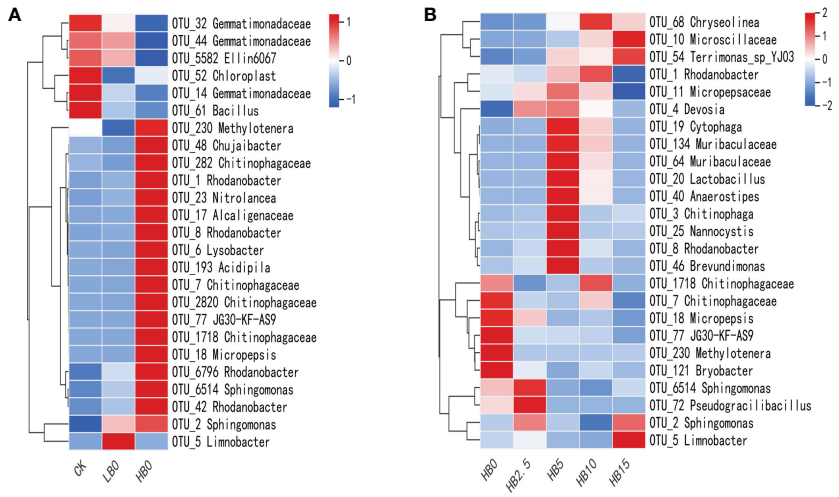

FIGURE 5
Effects of Pb and CSB on bacterial communities among treatments. **(A)** Most abundant 25 taxa within the treatment identified from CK *vs*. HB0 SIMPER analysis. **(B)** Most abundant 25 taxa within treatments of combined HB0 *vs*. HB5 SIMPER analyses.

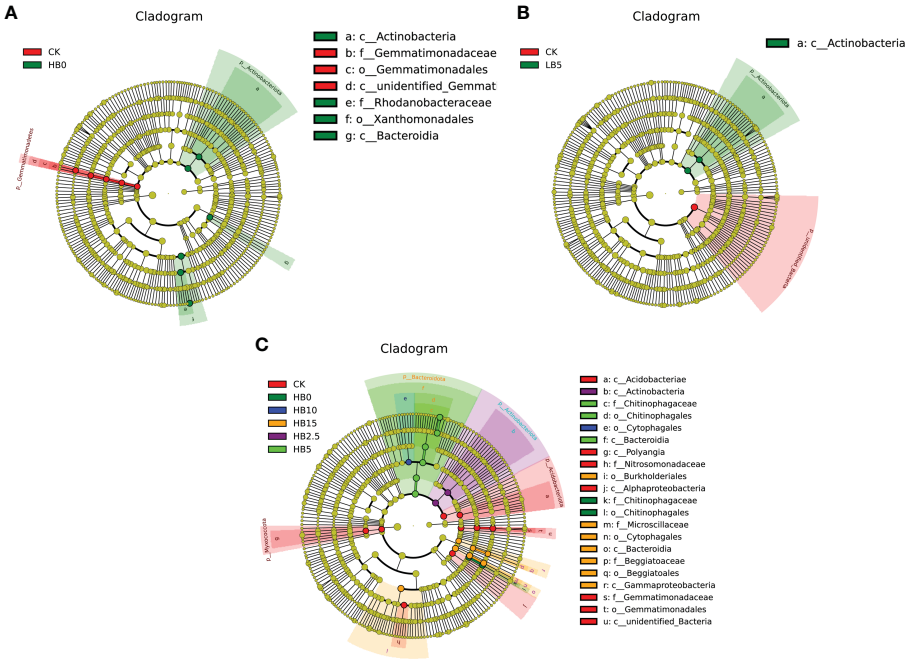

FIGURE 6
LefSE analysis results of bacterial community members. **(A)** Pb application alone, **(B)** CSB effect under low Pb toxicity and **(C)** CSB effect under high Pb toxicity.

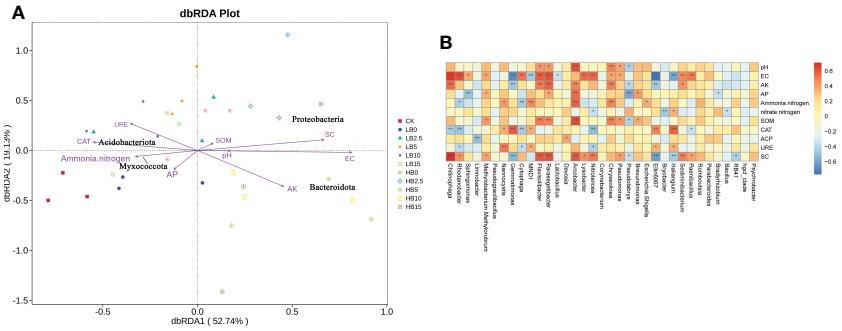

FIGURE 7
(A) Redundancy analysis (RDA) ordination of Pb-contaminated soil bacteria (phylum level) and soil physicochemical properties after CSB amendment. **(B)** Spearman correlation analysis between the soil bacterial community (genus level) and soil physicochemical properties.

Pseudomonas increased with increasing pH, which led to increases in AK content, nitrate-nitrogen content, SOM content and soil enzyme activity. In addition, Figure S6 shows the correlations between rhizosphere microorganisms at the phylum level and soil properties.

4 Discussion

Pb is classified as a nonessential HM and is highly toxic to plants (Gul et al., 2021). Pb-contaminated soils can affect plants in many complex ways. In most cases, the effects of pollutants on plant growth depend on the concentration of the pollutants. Our previous studies have shown that Pb can inhibit the biosynthesis of photosynthetic pigments in red clover, resulting in a significant decrease in biomass (Meng et al., 2022). High Pb pollution causes a decrease in chlorophyll content and damages chloroplast structure, thereby hindering plant photosynthesis (Šimonová et al., 2007), which is essential for plant growth (Zhang et al., 2022). However, the addition of CSB to contaminated soils alleviated the toxicity of Pb to plant growth (Figure 1A). Appropriate doses of biochar have been shown to increase bud growth and root biomass in plants grown in copper tailings (Munir et al., 2021), and similar results have been found in the study of alfalfa (Zhang et al., 2019). This phenomenon may be due to the strong affinity of biochar surface functional groups, which can bind with metals to form metal-ligand complexes and then fix more Pb in the soil (Ho et al., 2017). In addition, the improvement of soil fertility by biochar may be a good explanation for the improvement of plant growth (Figure 2). The BCF is an indication of the ability of plants to accumulate HM (Shahbaz et al., 2018). The addition of biochar affects the accumulation and transport of Pb in plants (Huang et al., 2020). Compared with the addition of Pb alone, the addition of CSB reduced the migration of Pb from the soil to plants (Table S1). Interestingly, the length of red clover stems was not linearly related to the amount of CSB added. This study showed that adding 5% CSB had the most significant effect on the length of red clover stems, but 10% and 15% CSB inhibited any increase in the length of red clover stems (Figure 1A), which means that high concentrations of CSB had a negative impact on crop growth and yield. For example, Liu et al. found that excessive biochar could lead to a decline in crop productivity (Xiaoyu et al., 2013), and similar findings have been obtained in rice (Asai et al., 2009) and maize (Uzoma et al., 2011). Asai et al. found that excessive biochar reduced nitrogen uptake by plants and was related to the fixation of nitrogen by toxic or harmful substances, thereby reducing nutrient uptake (Asai et al., 2009). Many studies have shown that soil nutrient contents are closely related to plant growth (Ahmad et al., 2022; Vaish et al., 2022). Generally, high soil nutrient contents drive plant photosynthesis, stomatal conductance and transpiration, ultimately promoting plant growth (Qi et al., 2021). Biochar is a highly porous carbon structure that is rich in C, N and P nutrients and can be used as a soil amendment (Rahi et al., 2022). Adding CSB can improve the soil pH and soil physical and chemical properties (Figure 1D). Biochar can not only desorb nutrients that are present in high abundance and is easily absorbed by plants but also has high nutritional value, which may be the reason why adding raw CSB improves soil physical and chemical properties. (Biederman and Harpole, 2013). Similarly, pot experiments confirmed that an increase in the abundance of several microbes promoted soil fertility after 45 days of incubation in the greenhouse. The increase in available nitrogen, phosphorus and potassium is beneficial to plant growth, especially under HM stress, because the lack of plant-available nutrients hinders plant growth and development.

Soil enzyme activity is closely related to soil nutrients and is a key indicator for maintaining soil fertility-related nutrients (Lin et al., 2021). CAT can detoxify HM, and hydrolases (URE, ACP and SC) are closely related to N, C and P cycling in the soil (Zhu et al., 2022). The activities of URE and CAT in the soil are considered sensitive biomarkers of HM and are widely used to determine the effects of amendments on the mobility and bioavailability of HM in the soil. The increase in CAT activity after biochar addition may be due to the decrease in HM toxicity or bioavailability and may be related to the increase in soil enzyme activity because of the porous structure of biochar particles (Irshad et al., 2022). In addition, studies have shown that the increase in CAT and URE activity is conducive to soil carbon and nitrogen cycling (Li et al., 2021). In our experiment, the CAT activity peaked in LB5 and HB5 (Figure 3A), and increasing CSB dose led to decreasing CAT activity, which may be because biochar can absorb a variety of organic and inorganic molecules and may both block the reaction point and inhibit the activity of certain soil enzymes or their substrates (Bailey et al., 2011; Leiyi et al., 2019). The contents of URE and SC were positively correlated with the CSB dose (Figures 3C, D), which may be because the sensitivity of CAT

was higher than that of hydrolases (Yang et al., 2016). Notably, URE is involved in the soil nitrogen cycle, which involves the hydrolysis of urea into carbonic acid and ammonia, thereby transforming unused nitrogen into a bioavailable form (Liu et al., 2022), which may play an important role in the growth of red clover under high doses of CSB treatment. Sucrose can be hydrolyzed into glucose and fructose by SC, which disrupts glycosidic bonds and affects the transformation of soil organic carbon (Yang et al., 2020). Unlike for the other three enzymes, the application of Pb alone can promote the activity of SC, which may be due to the stimulation of microbial enzyme production by low Pb concentrations or the improvement in the unit respiratory metabolic quotient under HM stress (Belyaeva et al., 2005).

Bacteria are the most abundant and widely distributed microorganisms in the soil; bacteria play an important role in soil formation, material cycling and fertility, and bacterial abundance is restricted by subtle factors in the ecological environment (Jing et al., 2022). Our results were compared with those of Wan et al. under 400 and 1200 mg/kg Pb stress. Wan et al. showed that Pb toxicity had a negative effect on bacterial diversity (Wan et al., 2022). Interestingly, the bacterial diversity under the 400 mg/kg Pb treatment was higher than that under the 1200 mg/kg Pb treatment. This means that lower Pb concentrations can increase bacterial diversity to some extent, but there is a limit. In our study, the effects of CSB on rhizosphere microorganisms depended on the soil Pb concentration and CSB concentration used, and the Pb concentration and CSB concentration determined the degree to which biochar could improve various soil properties. A study by Li et al. showed that high applications of biochar can destroy the environment for microbial growth and thus reduce microbial diversity (Li et al., 2020), which is consistent with our findings in high-Pb soils. However, the high application of biochar in low-Pb soils did not have the same effect. The possible reason is that although a large amount of biochar application destroys the environment for microbial growth to a certain extent, more importantly, it improves soil properties. Under low Pb stress, high-dose biochar had better improvement effects on SOM, AP and ammonia nitrogen, which may create an environment conducive to the growth of more bacteria. Therefore, there was no significant decrease in diversity in low Pb soil. In addition, under the stress of high Pb concentration, the combined action of Pb and biochar may accelerate the activity intensity and metabolic activity of some resistant dominant bacteria, which increases the individual size or quantity difference of this part of dominant bacterial community, reduces the community evenness, and leads to the decrease of diversity.

At the phylum level, Pb toxicity significantly reduced the relative abundance of Acidobacteriota, Myxococcota and Gemmatimonadetes (Figure 4A). Studies have shown that acidic environments contribute to stronger phylogenetic aggregation of Acidobacteriota (Conradie and Jacobs, 2021). In addition, acidophilic bacteria have unique physiological characteristics, such as photonutrition, and Pb stress can lead to an increase in soil pH (Figure 1D), thus damaging the environment of acidophilic bacteria. Our previous study showed that high concentrations of Pb stress reduce the photosynthetic capacity of red clover (Meng et al., 2022), which may be the cause of the decrease in the relative abundance of acidophilic bacteria under Pb stress. Because of the groups of HM tolerance genes found in Firmicutes and Proteobacteria, these bacteria have been identified as dominant in mining soils. Their ability to live together in contaminated soil was considered to be the reason for the self-healing of HM-contaminated soil in mining areas (Zhao et al., 2019). Actinobacteriota can decompose a variety of organic compounds and can use different carbohydrates as energy sources (Liu et al., 2022). Therefore, the increase in the relative content of Actinobacteriota in Pb-contaminated soil may lead to a large amount of carbohydrate consumption and a reduction in plant available energy reserves, which led to the change in the growth strategy of red clover and the reduction in plant height to maintain life activities. This idea is also supported by a positive correlation between SC activity and Actinobacteriota relative abundance (Figure S6). Chloroflexi is an anaerobic bacterium that has been found to play an important role in regulating soil bacterial community composition and forming stable bacterial communities (Kikuchi et al., 2007). Combined with SIMPER analysis, OTU_23 and OTU_77 were found to belong to Chloroflexi, which could stabilize the rhizosphere bacterial community and resist Pb toxicity (Figure 5A). In general, low levels of Pb toxicity can create a soil environment conducive to the development of Pb resistance strategies by microbes, while high concentrations of Pb mainly induce physiological adaptations (Renella et al., 2003).

Plant resistance to HM stress depends largely on beneficial interactions between the soil environment and rhizosphere microorganisms. The application of biochar altered the microbial community structure in Pb-containing rhizosphere soils. Along with the effect of 5% CSB on the growth of red clover, the effect of 5% CSB on rhizosphere microorganisms was also studied. *Gemmatimonas* can fix atmospheric nitrogen, increase the availability of nutrients in the soil, improve soil structure, prevent diseases and insect pests, promote plant growth, and increase phosphorus and potassium availability (Liu, 2021). Under the two levels of Pb toxicity, the relative abundance of *Gemmatimonas* decreased but recovered at HB5, which indicates that it may play a role in alleviating Pb toxicity at 5% CSB. Members of the genus *Chitinophaga*, which belongs to the Bacteroidetes, are predominant in soils under high Pb toxicity and have an excellent ability to degrade cellulose and chitin, which can improve the immunity of plants and promote the growth of crops (Kishi et al., 2017). In addition, a study showed that Myxococcota had a predation relationship with *Chitinophaga*. Myxococcota could prey on bacteria through multiple predation mechanisms, which are generally considered to be the key bacteria that regulate the structure and function of the soil microbial community (Dai, 2020). However, HB5 treatment caused a significant increase in the relative abundance of *Chitinophaga* (Figure 4B), so the abundance of HB5 Myxococcota recovered, while LB5 did not. This may be the specific detoxification mechanism of CSB under high Pb toxicity. In addition, the potential of *Chitinophaga* yields plant-polysaccharide-degrading enzymes (Funnicelli et al., 2021), which is consistent with the Spearman correlation analysis in this study, indicating that *Chitinophaga* is significantly positively correlated with SC (Figure 7B). In summary, Pb toxicity altered the community structure of rhizosphere microorganisms, and the addition of an appropriate amount of CSB could alleviate the effect of Pb and changed the bacterial diversity, which may be due to the addition of biochar to improve the characteristics of lead-containing soil, such as pH, SOM, AP, AK and ammonia nitrogen. In addition, the pore structure and rich functional groups of biochar can also provide more niches for

microorganisms. In addition, studies by Zhang showed that biochar may cause soil bulk density to decrease and water retention capacity to increase (Zhang et al., 2020). These changes are conducive to microbial survival and thus change bacterial diversity. Under the combined action of CSB and Pb, the soil microbial community structure composition differed according to the different CSB and Pb concentrations. This may partly explain why the application of appropriate concentrations of CSB can promote the growth of red clover and improve its resistance to Pb toxicity.

5 Conclusion

This study showed that Pb at concentrations of 1000 mg/kg and 5000 mg/kg was toxic to red clover, and 5000 mg/kg was more toxic than 1000 mg/kg. Pb toxicity reduced the effective nutrient content of the rhizosphere soil, inhibited the enzyme activity, altered the rhizosphere microbial community structure, and ultimately affected the biomass of red clover. Adding appropriate doses of biochar successfully alleviated the effects of 1000 mg/kg and 5000 mg/kg Pb on the stem length and biomass of red clover, significantly reducing the accumulation of Pb in red clover and promoting increased stem length. In addition, CSB increased the soil pH and EC; increased the soil AP, AK, ammonium-nitrogen, nitrate-nitrogen and SOM contents; and increased the enzyme activity and relative abundance of beneficial rhizosphere microorganisms. CSB (5%) had the best effect on alleviating Pb toxicity in red clover. Under this CSB dose, the addition of biochar increased the pH of the rhizosphere soil; stimulated the relative abundance of *Chitinophaga*, *Sphingomonas*, *Devosia* and *Pseudomonas*; and positively affected the soil available potassium, nitrate-nitrogen and organic matter contents and enzyme activity to maintain plant growth and alleviate Pb toxicity. Future experiments should focus on the molecular response of red clover to Pb and CSB.

Data availability statement

The data presented in the study are deposited in the online repository, accession number PRJNA907524. Further inquiries can be directed to the corresponding authors.

Author contributions

LM: investigation, writing – original draft, data curation, and software. YW: data curation and software. MM: software. ZC: software. ZW: investigation. LW: investigation. GC: conceptualization and methodology. XY: conceptualization, methodology, supervision, and funding acquisition. All authors contributed to the article and approved the submitted version.

Funding

This work was supported by research and the Natural Science Foundation of Heilongjiang Province of China [grant numbers LH2021C040]; the National Natural Science Foundation of China [grant number 31802120]; and Academic Backbone Fund Project of Northeast Agricultural University.

Conflict of interest

The authors declare that the research was conducted in the absence of any commercial or financial relationships that could be construed as a potential conflict of interest.

Publisher's note

Supplementary material

The Supplementary Material for this article can be found online at: https://www.frontiersin.org/articles/10.3389/fpls.2023.1112002/full#supplementary-material

References

Ahmad, A., Chowdhary, P., Khan, N., Chaurasia, D., Varjani, S., Pandey, A., et al. (2022). Effect of sewage sludge biochar on the soil nutrient, microbial abundance, and plant biomass: A sustainable approach towards mitigation of solid waste. *Chemosphere* 287 (Pt 1), 132112. doi: 10.1016/j.chemosphere.2021.132112

Asai, H., Samson, B. K., Stephan, H. M., Songyikhangsuthor, K., Homma, K., Kiyono, Y., et al. (2009). Biochar amendment techniques for upland rice production in northern Laos. *Field Crops Res.* 111 (1-2), 81–84. doi: 10.1016/j.fcr.2008.10.008

Azadi, N., and Raiesi, F. (2021). Salinity-induced changes in cadmium availability affect soil microbial and biochemical functions: Mitigating role of biochar. *Chemosphere* 274, 129924. doi: 10.1016/j.chemosphere.2021.129924

Bailey, V. L., Fansler, S. J., Smith, J. L., and Bolton, H. (2011). Reconciling apparent variability in effects of biochar amendment on soil enzyme activities by assay optimization. *Soil Biol. Biochem.* 43 (2), 296–301. doi: 10.1016/j.soilbio.2010.10.014

Bamagoos, A. A., Alharby, H. F., and Abbas, G. (2022). Differential uptake and translocation of cadmium and lead by quinoa: A multivariate comparison of physiological and oxidative stress responses. *Toxics* 10 (2), 68. doi: 10.3390/toxics10020068

Bauer, D. F. (1972). Constructing confidence sets using rank statistics. *J. Am. Stat. Assoc.* 67 (339), 687–690. doi: 10.1080/01621459.1972.10481279

Belyaeva, O. N., Haynes, R. J., and Birukova, O. A. (2005). Barley yield and soil microbial and enzyme activities as affected by contamination of two soils with lead, zinc or copper. *Biol. Fertil. Soils* 41 (2), 85–94. doi: 10.1007/s00374-004-0820-9

Biederman, L. A., and Harpole, W. S. (2013). Biochar and its effects on plant productivity and nutrient cycling: A meta-analysis. *GCB Bioenergy* 5 (2), 202–214. doi: 10.1111/gcbb.12037

Brian, O., Nicholas, B., and Adam, P. (2011). Interactive metagenomic visualization in a web browser. *BMC Bioinf.* 12, 385. doi: 10.1186/1471-2105-12-385

Caporaso, G., Kuczynski, J., Stombaugh, J., Bittinger, K., Bushman, F., Costello, E., et al. (2010). QIIME allows analysis of highthroughput community sequencing data. *Nat. Methods* 7 (5), 335–336. doi: 10.1038/nmeth.f.303

Chao, Y., Yuan, J., Li, S., Jia, S., Han, ,L., and Xu, L. (2018). Analysis of transcripts and splice isoforms in red clover (Trifolium pratense L.) by single-molecule long-read sequencing. *BMC Plant Biol.* 18 (1), 300. doi: 10.1186/s12870-018-1534-8

Chi, T., Zuo, J., and Liu, F. (2017). Performance and mechanism for cadmium and lead adsorption from water and soil by corn straw biochar. *Front. Environ. Sci. Eng.* 11 (2). doi: 10.1007/s11783-017-0921-y

Chuchu, W., Dan, Z., Bin, Y., Yuzhou, Z., Yuan, Y., and Yaoyu, Z. (2022). Immobilization of microbes on biochar for water and soil remediation. *A review. Environ. Res.* 212 (PB), 113226. doi: 10.1016/J.ENVRES.2022.113226

Conradie, T. A., and Jacobs, K. (2021). Distribution patterns of acidobacteriota in different fynbos soils. *PloS One* 16 (3), e0248913. doi: 10.1371/journal.pone.0248913

Cruz, Y., Villar, S., Gutierrez, K., Montoya-Ruiz, C., Gallego, J.L., Delgado, M.D.P., and Saldarriaga, J.F.. (2021). Gene expression and morphological responses of Lolium perenne L. exposed to cadmium (Cd(2+)) and mercury (Hg(2+)). *Sci. Rep.* 11 (1), 11257. doi: 10.1038/S41598-021-90826-Y

Dai, W. (2020). *Regulation mechanism of myxobacteria on soil microecology* (Henan University of Science and Technology).

Edgar, R. C. (2013). UPARSE: highly accurate OTU sequences from microbial amplicon reads. *Nat. Methods* 10 (10), 996–998. doi: 10.1038/nmeth.2604

Fewtrell, L. J., Prüss-Üstün, A., Landrigan, P., and Ayuso-Mateos, J. L. (2004). Estimating the global burden of disease of mild mental retardation and cardiovascular diseases from environmental lead exposure. *Environ. Res.* 94 (2), 120–133. doi: 10.1016/S0013-9351(03)00132-4

Funnicelli, M. I. G., Pinheiro, D. G., Gomes-Pepe, E. S., de Carvalho, L. A. L., Campanharo, J. C., Fernandes, C. C., et al. (2021). Metagenome-assembled genome of a chitinophaga sp. and its potential in plant biomass degradation, as well of affiliated pandoraea and labrys species. *World J. Microbiol. Biotechnol.* 37 (9), 162. doi: 10.1007/s11274-021-03128-w

Gul, I., Manzoor, M., Hashim, N., Shah, G. M., Waani, S. P. T., Shahid, M., et al. (2021). Challenges in microbially and chelate-assisted phytoextraction of cadmium and lead - a review. *Environ. pollut.* 287, 117667. doi: 10.1016/j.envpol.2021.117667

Helaoui, S., Boughattas, I., Hattab, S., Mkhinini, M., Alphonse, V., Livet, A., et al. (2020). Physiological, biochemical and transcriptomic responses of medicago sativa to nickel exposure. *Chemosphere* 249, 126121. doi: 10.1016/j.chemosphere.2020.126121

Ho, S. H., Zhu, S., and Chang, J. S. (2017). Recent advances in nanoscale-metal assisted biochar derived from waste biomass used for heavy metals removal. *Bioresour. Technol.* 246, 123–134. doi: 10.1016/j.biortech.2017.08.061

Huang, F., Zhou, H., Gu, J., Liu, C., Yang, W., Liao, B., et al. (2020). Differences in absorption of cadmium and lead among fourteen sweet potato cultivars and health risk assessment. *Ecotoxicol. Environ. Saf.* 203, 111012. doi: 10.1016/j.ecoenv.2020.111012

Irshad, M. K., Ibrahim, M., Noman, A., Shang, J., Mahmood, A., Mubashir, M., et al. (2022). Elucidating the impact of goethite-modified biochar on arsenic mobility, bioaccumulation in paddy rice (Oryza sativa l.) along with soil enzyme activities. *Process Saf. Environ. Prot.* 160, 958–967. doi: 10.1016/j.psep.2022.02.069

Jianhua, Q., Yihang, Y., Xinmiao, Z., Lei, W., Yue, T., Zhao, J., et al. (2021). Stabilization of lead and cadmium in soil by sulfur-iron functionalized biochar: Performance, mechanisms and microbial community evolution. *J. hazard. mater.* 425, 127876. doi: 10.1016/J.JHAZMAT.2021.127876.

Jianzhong, C., Yunlong, L., Weichang, G., Yi, C., Wenjie, P., Xinqing, L., et al. (2018). Effects of biochar on cd and Pb mobility and microbial community composition in a calcareous soil planted with tobacco. *Biol. Fertil. Soils* 54 (3), 373–383. doi: 10.1007/s00374-018-1267-8.

Jin, Z., Sha, W., Zhang, Y., Liu, L., and Zhao, J. (2013). Effects of EDDS on lead and cadmium contaminated fescue and red clover. *J. Northeast For. Univ.* 41 (3), 3.

Jing, F., Chen, X., Wen, X., Liu, W., Hu, S., Yang, Z., et al. (2020). Biochar effects on soil chemical properties and mobilization of cadmium (Cd) and lead (Pb) in paddy soil. *Soil Use Manage.* 36 (2), 320–327. doi: 10.1111/sum.12557

Jing, H., Chunquan, Z., Yali, K., Xiaochuang, C., Lianfeng, Z., Yongchun, Z., et al. (2022). Biochar application alleviated rice salt stress *via* modifying soil properties and regulating soil bacterial abundance and community structure. *Agronomy* 12 (2), 409. doi: 10.3390/AGRONOMY12020409

Kamaruzzaman, M. A., Abdullah, S. R. S., Hasan, H. A., Hassan, M., Othman, A. R., and Idris, M. (2020). Characterisation of Pb-resistant plant growth-promoting rhizobacteria (PGPR) from scirpus grossus. *Biocatal. Agric. Biotechnol.* 23 (C), 101456. doi: 10.1016/j.bcab.2019.101456

Kang, X., Geng, N., Li, X., Yu, J., Wang, H., Pan, H., et al. (2022). Biochar alleviates phytotoxicity by minimizing bioavailability and oxidative stress in foxtail millet (Setaria italica l.) cultivated in cd- and zn-contaminated soil. *Front. Plant Sci.* 13. doi: 10.3389/fpls.2022.782963

Kikuchi, H., Watanabe, T., Jia, Z., Kimura, M., and Asakawa, S. (2007). Molecular analyses reveal stability of bacterial communities in bulk soil of a Japanese paddy field: Estimation by denaturing gradient gel electrophoresis of 16S rRNA genes amplified from DNA accompanied with RNA. *Soil Sci. Plant Nutr.* 53 (4), 448–458. doi: 10.1111/j.1747-0765.2007.00177.x

Kishi, L. T., Lopes, E. M., Fernandes, C. C., Fernandes, G. C., Sacco, L. P., Carareto Alves, L. M., et al. (2017). Draft genome sequence of a chitinophaga strain isolated from a lignocellulose biomass-degrading consortium. *Genome Announc.* 5 (3), e01056–16. doi: 10.1128/genomeA.01056-16

Kumar, A., Kumar, A., Cabral-Pinto, M. M. S., Chaturvedi, A. K., Shabnam, A. A., Subrahmanyam, G., et al. (2020). Lead toxicity: Health hazards, influence on food chain, and sustainable remediation approaches. *Int. J. Environ. Res. Public Health* 17 (7), 2179. doi: 10.3390/ijerph17072179

Leiyi, Z., Yangzhou, X., Yiming, J., and Renduo, Z. (2019). Biochar amendment effects on the activities of soil carbon, nitrogen, and phosphorus hydrolytic enzymes: A meta-analysis. *Environ. Sci. pollut. Res. Int.* 26 (22), 22990–23001. doi: 10.1007/s11356-019-05604-1

Li, S., Li, Z., Feng, X., Zhou, F., Wang, J., and Li, Y. (2021). Effects of biochar additions on the soil chemical properties, bacterial community structure and rape growth in an acid purple soil. *Plant Soil Environ. 67(No.* 3), 121–129. doi: 10.17221/390/2020-pse

Li, X., Wang, T., Chang, S. X., Jiang, X., and Song, Y. (2020). Biochar increases soil microbial biomass but has variable effects on microbial diversity: A meta-analysis. *Sci. Total Environ.* 749, 141593. doi: 10.1016/j.scitotenv.2020.141593

Lin, H., Liu, C., Li, B., and Dong, Y. (2021). Trifolium repens l. regulated phytoremediation of heavy metal contaminated soil by promoting soil enzyme activities and beneficial rhizosphere associated microorganisms. *J. Hazard Mater.* 402, 123829. doi: 10.1016/j.jhazmat.2020.123829

Liu, (2021). Study on Soil Bacterial Diversity in Mining Area and Isolation, Identification and Application of Dominant Strains. Changchun University of Technology.

Liu, X., Guo, D., Ren, C., Li, R., Du, J., Guan, W., et al. (2020). Performance of streptomyces pactum-assisted phytoextraction of cd and Pb: in view of soil properties, element bioavailability, and phytoextraction indices. *Environ. Sci. pollut. Res. Int.* 27 (35), 43514–43525. doi: 10.1007/s11356-020-09842-6

Liu, C., Li, B., Dong, Y., and Lin, H. (2022). Endophyte colonization enhanced cadmium phytoremediation by improving endosphere and rhizosphere microecology characteristics. *J. Hazard Mater.* 434, 128829. doi: 10.1016/j.jhazmat.2022.128829

Liu, C., Lin, H., Li, B., Dong, Y., and Menzembere, E. (2021). Endophyte pseudomonas putida enhanced trifolium repens l. growth and heavy metal uptake: A promising in-situ non-soil cover phytoremediation method of nonferrous metallic tailing. *Chemosphere* 272, 129816. doi: 10.1016/J.CHEMOSPHERE.2021.129816

Lu, R., et al. (2000). *Soil agricultural chemical analysis method*. China Agricultural Science and Technology Press, first ed. Beijing.

Meng, L., Yang, Y., Ma, Z., Jiang, J., Zhang, X., Chen, Z., et al. (2022). Integrated physiological, transcriptomic and metabolomic analysis of the response of trifolium pratense l. @ to Pb toxicity. *J. Hazard Mater.* 436, 129128. doi: 10.1016/j.jhazmat.2022.129128

Mo, F., Wang, M., Li, H., Li, Y., Li, Z., Deng, N., Chai, R., and Wang, H. (2021). Biological effects of silver ions to Trifolium pratense L. revealed by analysis of biochemical indexes, morphological alteration and genetic damage possibility with special reference to hormesis. *Environ. Exp. Bot.* 186. doi: 10.1016/J.ENVEXPBOT.2021.104458

Mourad, A. M. I., Amin, A.E.-E.A.Z., and Dawood, M. F. A. (2021). Genetic variation in kernel traits under lead and tin stresses in spring wheat diverse collection. *Environ. Exp. Bot.* 192. doi: 10.1016/j.envexpbot.2021.104646

Munir, M. A. M., Irshad, S., Yousaf, B., Ali, M. U., Dan, C., Abbas, Q., et al. (2021). Interactive assessment of lignite and bamboo-biochar for geochemical speciation, modulation and uptake of Cu and other heavy metals in the copper mine tailing. *Sci. Total Environ.* 779, 146536. doi: 10.1016/j.scitotenv.2021.146536

Muthusaravanan, S., Sivarajasekar, N., Vivek, J., Paramasivan, T., Naushad, M., Prakashmaran, J., et al. (2018). Phytoremediation of heavy metals: Mechanisms, methods and enhancements. *Environ. Chem. Lett.* 16 (4), 1339–1359. doi: 10.1007/s10311-018-0762-3

Nahid, A., and Fayez, R. (2021). Biochar alleviates metal toxicity and improves microbial community functions in a soil co-contaminated with cadmium and lead. *Biochar* 3 (4), 485–498. doi: 10.1007/S42773-021-00123-0.

Omidi, A. H., Cheraghi, M., Lorestani, B., Sobhanardakani, S., and Jafari, A. (2019). Biochar obtained from cinnamon and cannabis as effective adsorbents for removal of lead ions from water. *Environ. Sci. pollut. Res. Int.* 26 (27), 27905–27914. doi: 10.1007/s11356-019-05997-z

Qi, C., Zhaoming, Q., Zeli, L., Zixin, Z., Guohua, M., Zhiguang, L., et al. (2021). Coated diammonium phosphate combined with humic acid improves soil phosphorus availability and photosynthesis and the yield of Maize&13. *Front. Plant Sci.* 12. doi: 10.3389/FPLS.2021.759929

Qiu, B., Tao, X., Wang, H., Li, W., Ding, X., and Chu, H. (2021). Biochar as a low-cost adsorbent for aqueous heavy metal removal: A review. *J. Anal. Appl. Pyrolysis* 155, 105081. doi: 10.1016/j.jaap.2021.105081

Rahi, A. A., Younis, U., Ahmed, N., Ali, M. A., Fahad, S., Sultan, H., et al. (2022). Toxicity of cadmium and nickel in the context of applied activated carbon biochar for improvement in soil fertility. *Saudi J. Biol. Sci.* 29 (2), 743–750. doi: 10.1016/j.sjbs.2021.09.035

Renella, G., Ortigoza, A. L. R., Landi, L., and Nannipieri, P. (2003). Additive effects of copper and zinc on cadmium toxicity on phosphatase activities and ATP content of soil as estimated by the ecological dose (ED 50). *Soil Biol. Biochem.* 35 (9), 1203–1210. doi: 10.1016/S0038-0717(03)00181-0

Salam, M. M. A., Kaipiainen, E., Mohsin, M., Villa, A., Kuittinen, S., Pulkkinen, P., et al. (2016). Effects of contaminated soil on the growth performance of young salix (salix schwerinii e. l. wolf) and the potential for phytoremediation of heavy metals. *J. Environ. Manage.* 183 (Pt 3), 467–477. doi: 10.1016/j.jenvman.2016.08.082.

Shahbaz, A. K., Iqbal, M., Jabbar, A., Hussain, S., and Ibrahim, M. (2018). Assessment of nickel bioavailability through chemical extractants and red clover (Trifolium pratense l.) in an amended soil: Related changes in various parameters of red clover. *Ecotoxicol. Environ. Saf.* 149, 116–127. doi: 10.1016/j.ecoenv.2017.11.022

Šimonová, E., Henselová, M., Masarovičová, E., and Kohanová, J. (2007). Comparison of tolerance of brassica juncea and vigna radiata to cadmium. *Biol. PLANTARUM* 51 (3), 488–492. doi: 10.1007/s10535-007-0103-z

Uchimiya, M., Lima, I. M., Klasson, K. T., and Wartelle, L. H. (2010). Contaminant immobilization and nutrient release by biochar soil amendment: Roles of natural organic matter. *Chemosphere* 80 (8), 935–940. doi: 10.1016/j.chemosphere.2010.05.020

Uzoma, K. C., Inoue, M., Andry, H., Fujimaki, H., Zahoor, A., and Nishihara, E. (2011). Effect of cow manure biochar on maize productivity under sandy soil condition. *Soil Use Manage.* 27 (2), 205–212. doi: 10.1111/j.1475-2743.2011.00340.x

Vaish, B., Srivastava, V., Singh, U. K., Gupta, S. K., Chauhan, P. S., Kothari, R., et al. (2022). Explicating the fertilizer potential of anaerobic digestate: Effect on soil nutrient profile and growth of solanum melongena l. *Environ. Technol. Innovation* 27, 102471. doi: 10.1016/j.eti.2022.102471

Wan, Y., Devereux, R., George, S. E., Chen, J., Gao, B., Noerpel, M., et al. (2022). Interactive effects of biochar amendment and lead toxicity on soil microbial community. *J. Hazard Mater.* 425, 127921. doi: 10.1016/j.jhazmat.2021.127921

Wang, J., Chen, X., Chu, S., You, Y., Chi, Y., Wang, R., et al. (2022). Comparative cytology combined with transcriptomic and metabolomic analyses of solanum nigrum l. @ in response to cd toxicity. *J. Hazard Mater.* 423 (Pt B), 127168. doi: 10.1016/j.jhazmat.2021.127168

Wang, Q., Garrity, G. M., Tiedje, J. M., and Cole, J. R. (2007). Naive Bayesian classifier for rapid assignment of rRNA sequences into the new bacterial taxonomy. *Appl. Environ. Microbiol.* 73 (16), 5261–5267. doi: 10.1128/AEM.00062-07

Xiaoyu, L., Afeng, Z., Chunying, J., Stephen, J., Rongjun, B., Lianqing, L., et al. (2013). Biochar's effect on crop productivity and the dependence on experimental conditions–a meta-analysis of literature dsata. *Plant Soil* 373 (1/2), 583–594. doi: 10.1007/s11104-013-1806-x

Xinde, C., Lena, M., Yuan, L., Bin, G., and Willie, H. (2011). Simultaneous immobilization of lead and atrazine in contaminated soils using dairy-manure biochar. *Environ. Sci. Technol.* 45 (11), 4884–9. doi: 10.1021/es103752u

Xu, M., Cui, Y., Beiyuan, J., Wang, X., Duan, C., and Fang, L. (2021). Heavy metal pollution increases soil microbial carbon limitation: Evidence from ecological enzyme stoichiometry. *Soil Ecol. Lett.* 3 (3), 230–241. doi: 10.1007/s42832-021-0094-2

Yang, F. L., Li, W. Z., Li, Q., Li, P. F., Wang, Z. J., and Luo, L. N. (2019). Unravelling the influence of sulfate loading on enhancing anaerobic co-digestion of corn stover and bio-kerosene production wastewater. *J. Biosci. Bioeng.* 127 (1), 99–106. doi: 10.1016/j.jbiosc.2018.07.010

Yang, C., Liu, J., and Lu, S. (2021). Pyrolysis temperature affects pore characteristics of rice straw and canola stalk biochars and biochar-amended soils. *Geoderma* 397. doi: 10.1016/j.geoderma.2021.115097

Yang, K., Wang, X., Cheng, H., and Tao, S. (2022). Enhanced immobilization of cadmium and lead adsorbed on crop straw biochars by simulated aging processes. *Environ. pollut.* 302, 119064. doi: 10.1016/j.envpol.2022.119064

Yang, R., Xia, X., Wang, J., Zhu, L., Wang, J., Ahmad, Z., et al. (2020). Dose and time-dependent response of single and combined artificial contamination of sulfamethazine and copper on soil enzymatic activities. *Chemosphere* 250, 126161. doi: 10.1016/j.chemosphere.2020.126161

Yang, J., Yang, F., Yang, Y., Xing, G., Deng, C., Shen, Y., et al. (2016). A proposal of "core enzyme" bioindicator in long-term Pb-zn ore pollution areas based on topsoil property analysis. *Environ. pollut.* 213, 760–769. doi: 10.1016/j.envpol.2016.03.030

Yanru, W., Xinxin, M., Muhammad, S., Yong, Y., and Qingming, Z. (2022). Effects of corn stalk biochar and pyrolysis temperature on wheat seedlings growth and soil properties stressed by herbicide sulfentrazone. *Environ. Technol. Innovation* 25. doi: 10.1016/J.ETI.2021.102208

Youyuan, C., Haixia, W., Ping, S., Jiaxin, L., Shixuan, Q., Dakuan, Z., et al. (2021). Remediation of chromium-contaminated soil based on bacillus cereus WHX-1 immobilized on biochar: Cr(VI) transformation and functional microbial Enrichment&13. *Front. Microbiol.* 12. doi: 10.3389/FMICB.2021.641913

Zhang, J., Li, H., Huang, X., Xing, J., Yao, J., Yin, T., et al. (2022). STAYGREEN-mediated chlorophyll a catabolism is critical for photosystem stability during heat-induced leaf senescence in perennial ryegrass. *Plant Cell Environ.* 45 (5), 1412–1427. doi: 10.1111/pce.14296

Zhang, C., Li, J., Wu, X., Long, Y., An, H., Pan, X., et al. (2020). Rapid degradation of dimethomorph in polluted water and soil by bacillus cereus WL08 immobilized on bamboo charcoal-sodium alginate. *J. Hazard Mater.* 398, 122806. doi: 10.1016/j.jhazmat.2020.122806

Zhang, F., Liu, M., Li, Y., Che, Y., and Xiao, Y. (2019). Effects of arbuscular mycorrhizal fungi, biochar and cadmium on the yield and element uptake of medicago sativa. *Sci. Total Environ.* 655, 1150–1158. doi: 10.1016/j.scitotenv.2018.11.317

Zhang, J., Zhang, Q., Xing, J., Li, H., Miao, J., and Xu, B. (2021). Acetic acid mitigated salt stress by alleviating ionic and oxidative damages and regulating hormone metabolism in perennial ryegrass (Lolium perenne l.). *Grass Res.* 1 (1), 1–10. doi: 10.48130/gr-2021-0003

Zhao, W., Cui, Y., Sun, X., Wang, H., and Teng, X. (2021). Corn stover biochar increased edible safety of spinach by reducing the migration of mercury from soil to spinach. *Sci. Total Environ.* 758, 143883. doi: 10.1016/j.scitotenv.2020.143883

Zhao, X., Huang, J., Lu, J., and Sun, Y. (2019). Study on the influence of soil microbial community on the long-term heavy metal pollution of different land use types and depth layers in mine. *Ecotoxicol. Environ. Saf.* 170, 218–226. doi: 10.1016/j.ecoenv.2018.11.136

Zhu, X., Li, X., Shen, B., Zhang, Z., Wang, J., and Shang, X. (2022). Bioremediation of lead-contaminated soil by inorganic phosphate-solubilizing bacteria immobilized on biochar. *Ecotoxicol. Environ. Saf.* 237, 113524. doi: 10.1016/j.ecoenv.2022.113524

frontiers | Frontiers in Plant Science

TYPE Original Research
PUBLISHED 25 April 2023
DOI 10.3389/fpls.2023.1165567

OPEN ACCESS

EDITED BY
Jin-Lin Zhang,
Lanzhou University, China

REVIEWED BY
Amany H. A. Abeed,
Assiut University, Egypt
Lei Wang,
Xinjiang Institute of Ecology and Geography (CAS), China
Yan Xie,
Wuhan Botanical Garden (CAS), China

*CORRESPONDENCE
Jinmin Fu
turfcn@qq.com

SPECIALTY SECTION
This article was submitted to Plant Abiotic Stress, a section of the journal Frontiers in Plant Science

RECEIVED 14 February 2023
ACCEPTED 31 March 2023
PUBLISHED 25 April 2023

CITATION
Li X, Zhang T, Xue Y, Xu X, Cui X and Fu J (2023) *Aspergillus aculeatus* enhances nutrient uptake and forage quality in bermudagrass by increasing phosphorus and potassium availability. *Front. Plant Sci.* 14:1165567. doi: 10.3389/fpls.2023.1165567

Aspergillus aculeatus enhances nutrient uptake and forage quality in bermudagrass by increasing phosphorus and potassium availability

Xiaoning Li, Ting Zhang, Ying Xue, Xiao Xu, Xinyu Cui and Jinmin Fu*

Coastal Salinity Tolerant Grass Engineering and Technology Research Center, Ludong University, Yantai, China

Introduction: Potassium and phosphorus are essential macronutrients for plant growth and development. However, most P and K exist in insoluble forms, which are difficult for plants to directly absorb and utilize, thereby resulting in growth retardation of plants under P or K deficiency stress. The *Aspergillus aculeatus* fungus has growth-promoting characteristics and the ability to dissolve P and K.

Methods: Here, to investigate the physiological effects of *A. aculeatus* on bermudagrass under P or K deficiency, *A. aculeatus* and bermudagrass were used as experimental materials.

Results and discussion: The results showed that *A. aculeatus* could promote tolerance to P or K deficiency stress in bermudagrass, decrease the rate of leaf death, and increase the contents of crude fat as well as crude protein. In addition, *A. aculeatus* significantly enhanced the chlorophyll a+b and carotenoid contents. Moreover, under P or K deficiency stress, bermudagrass inoculated with *A. aculeatus* showed higher N, P, and K contents than non-inoculated plants. Furthermore, exogenous *A. aculeatus* markedly decreased the H_2O_2 level and CAT and POD activities. Based on our results, *A. aculeatus* could effectively improve the forage quality of bermudagrass and alleviate the negative effects of P or K deficiency stress, thereby playing a positive economic role in the forage industry.

KEYWORDS

***Aspergillus aculeatus*, bermudagrass, potassium, phosphorus, P or K deficiency stress**

Abbreviations: APX, ascorbate peroxidase; CAT, catalase; DLB, dead leaf biomass; DLR, dead leaf rate; GB, growth biomass; GPX, glutathione peroxidase; H_2O_2, hydrogen peroxide; K, potassium; K_0A_0, no K-feldspar and *A. aculeatus* treatment; K_0A_1, only *A. aculeatus*; K_1A_0, only K-feldspar; K_1A_1, K-feldspar and *A. aculeatus* treatment; LB, leaf biomass; P, phosphorus; P_0A_0, no tricalcium phosphate and *A. aculeatus* treatment; P_0A_1, only *A. aculeatus*; P_1A_0, only tricalcium phosphate; P_1A_1, tricalcium phosphate and *A. aculeatus* treatment; POD, peroxidase; ROS, reactive oxygen species; SOD, superoxide dismutase.

1 Introduction

Phosphorus (P) and potassium (K) are the major macronutrients for plant growth and development (Wang et al., 2021). P and K play dominant roles in maintaining a variety of physiological metabolic processes in plants, including nucleic acid synthesis, energy metabolites, membrane lipids, photosynthesis, membrane polarization, and protein biosynthesis (Clarkson and Hanson, 1980; Poirier and Bucher, 2002). However, P and K in soil exist in the form of insoluble K, which cannot be directly absorbed and used by plants (Illmer and Schinner, 1995; Meena et al., 2016). Therefore, it is of great interest to investigate management strategies that can improve the availability of phosphorus and potassium.

As fundamental mineral nutrients, P and K have been documented to be involved in plant photosynthesis processes (Wang et al., 2012; Krishnaraj and Dahale, 2014). Previous investigators proposed that P deficiency triggered reddish leaf and necrosis on the tips of old leaves and could result in a decrease in the maximum PSII efficiency and electron transport rate (Guo et al., 2002; Luiz et al., 2018). Chlorosis along the leaf margins is an obvious symptom of K deficiency. In severe cases, the leaf will turn yellow and fall off (Meena et al., 2016). Previous research has reported that K deficiency disrupts leaf photosynthetic performance and causes a lower net photosynthetic rate and stomatal conductance, which directly affects the yield of plants (Zhao et al., 2016).

A deficiency of mineral nutrition in plants could cause oxidative stress due to the disequilibrium between the scavenging and production of excess reactive oxygen species (ROS) (Cakmak, 2005; Shin et al., 2005). An excess of ROS triggers protein denaturation, cell membrane lipid peroxidation, and nucleic acid degradation, which restrains normal cellular physiological processes (Mittova et al., 2002). Fortunately, ROS can be scavenged through synergistic and interactive enzymatic and non-enzymatic antioxidant defense systems. The enzymatic systems mainly include peroxidase (POD), superoxide dismutase (SOD), catalase (CAT), ascorbate peroxidase (APX), and glutathione peroxidase (GPX) (Apel and Hirt, 2004).

Whenever the soil cannot adequately supply the P and K required for plant growth, people must supplement soil reserves with chemical P and K fertilizers. However, not all fertilizers that have been applied to the soil are fully taken up and utilized by plants. A portion of the applied fertilizers are left behind, thereby causing environmental contamination, such as eutrophication, and soil fertility depletion (Sharma et al., 2013; Meena et al., 2016; Kumar et al., 2021). Therefore, the emergence of phosphorus and potassium fertilizers has not given the ultimate solution. Such environmental concerns have triggered the exploration of sustainable P and K nutrition in plants. Given this circumstance, phosphate-solubilizing microorganisms have been considered an eco-friendly and cost-effective approach for the supply of P nutrition to plants (Sharma et al., 2013; Meena et al., 2016; Garcia et al., 2017). Mounting evidence suggests that P-solubilizing microorganisms (such as *Azotobacter*, *Bradyrhizobium*, *Penicillium*, and *Aspergillus*) can convert insoluble P into the bioavailable form through various mechanisms of solubilization and mineralization (Bargaz et al., 2018). Similarly, diverse groups of K-solubilizing microorganisms (*Bacillus mucilaginosus*, *Aspergillus terreus*, and *Aspergillus niger*) were proven to be involved in solubilizing the insoluble forms of K into available forms that are directly absorbed and utilized by plants (Prajapati and Modi, 2012; Gundala et al., 2013; Zarjani et al., 2013). Therefore, improvement of P and K utilization efficiency provides a potential strategy to overcome the adverse effects of P and K deficiencies. Investigation of the characteristics of fungi in dissolving P and K is an important prerequisite to improve plant nutrient utilization efficiency.

Aspergillus aculeatus is isolated from the rhizosphere of bermudagrass in heavy metal-contaminated areas (Xie et al., 2014). Our previous study proved that *A. aculeatus* can facilitate plant growth by producing indole-3-acetic acid, ACC deaminase, and siderophores (Xie et al., 2017). In addition, we have demonstrated that the fungus possessed P- and K-solubilizing characteristics, which accelerated the uptake and utilization of P and K nutrient elements, thereby promoting the growth and development of plants (Li et al., 2019; Li et al., 2021). However, the critical function of *A. aculeatus* in increasing the performance of bermudagrass exposed to P and K deficiency is still ambiguous. Bermudagrass [*Cynodon dactylon* (L.) Pers] is a typical warm season turfgrass and forage and is widely used in urban greening, sports fields, slope protection, and animal husbandry due to its high reproduction rate, short-term turf establishment, and strong mechanical stress resistance (Fan et al., 2014; Shi et al., 2014).

The objective of this experiment was to explore *A. aculeatus*-mediated protective responses to P or K deficiency stress in bermudagrass. We measured important physiological indicators of P or K deficiency stress, such as biomass, dead leaf rate, chlorophyll, carotenoids, forage quality, ion content, and antioxidant enzyme activities.

2 Materials and methods

2.1 Culture of bermudagrass and *Aspergillus aculeatus*

The experimental materials were obtained from the artificially bred bermudagrass 'Wrangler' in the coastal grass germplasm resources and breeding base located in Ludong University, Yantai City, Shandong Province. The fourth to sixth stem segments (three stem segments) of the biological upper end of the bermudagrass were selected, and stems with the same length and thickness were inserted into the pots (10 cm in diameter and 15 cm in height) on 25 July 2021. All the materials were placed in a plant growth incubator at 30°C/25°C (day/night), with a 14-h photoperiod, 400 μmol photons m^{-2} s^{-1} of light intensity, and 60% relative humidity for 7 weeks to establish the roots and leaves. The grass was irrigated with 0.5× Hoagland nutrient solution every 2 days and cut based on a one-third principle. *Aspergillus aculeatus* was cultured and massively propagated in a Martin liquid medium according to our previous study (Xie et al., 2017).

2.2 Experimental treatment

A mixture of sand and sawdust (v:v = 3:1) was used as the growth substance for this experiment. Subsequently, on 10 September 2021, all the substances were sterilized at 127°C for 1 h in an autoclave and then dispensed into 24 pots (10 cm in diameter and 18 cm in height) with 550 g of the mixed matrix. On 12 September 2021, all the roots and shoots of the materials were washed and trimmed, and the length or height was maintained at 8 and 10 cm, respectively. The initial weight was recorded as W_0, the trimmed plants were transferred into the above pots, and the 0.5× Hoagland nutrient solution (not present at the source of phosphorus or potassium, i.e., P or K deficiency treatment), was used to irrigate the plants every 2 days (100 ml pot^{-1}). For the P deficiency experiment, tricalcium phosphate was evenly mixed into the growth substance at a concentration of 5 g per pot before the plants were transplanted. Four groups and three replicates were designed, including P_0A_0 (no tricalcium phosphate and *A. aculeatus* treatment), P_0A_1 (only *A. aculeatus*), P_1A_0 (only tricalcium phosphate), and P_1A_1 (tricalcium phosphate and *A. aculeatus* treatment). In the same way, for the K deficiency experiment, K-feldspar was evenly mixed into the growth substance at a concentration of 5 g per pot before the plants were transplanted. The four groups and three replicates were designed, including K_0A_0 (no K-feldspar and *A. aculeatus* treatment), K_0A_1 (only *A. aculeatus*), K_1A_0 (only K-feldspar), and K_1A_1 (K-feldspar and *A. aculeatus* treatment). For the inoculated *A. aculeatus* treatment groups, 100 ml of fungal spore suspension was inoculated into the growth substances. The treatment lasted for 4 weeks, and then the plants were harvested for further analysis on 10 October 2021.

2.3 Determination of growth parameters and forage quality

For growth biomass (GB) determination, the whole bermudagrass (including aboveground and underground) were washed and weighed (W_1) at the end of the experiment. GB (kg day^{-1}) = (W_1 – W_0)/D. W_0 is the fresh weight before treatment, W_1 is the fresh weight at the end of treatment, and D is the treatment days. To calculate the dead leaf rate (DLR), the leaf biomass (LB) and dead leaf biomass (DLB) of bermudagrass were weighed and recorded. DLR = DLB/LB × 100%.

For crude protein content measurement, the dried samples (0.20 g) were digested with 10 ml of H_2SO_4 using a graphite digestion apparatus (SH220N; Jinan Hanon, Shandong, China). The crude protein content was measured by an automatic Kjeldahl apparatus (Hanon K9860). Crude protein content (%) = N content × 6.25 × 100%.

To assess the crude fat content, the dried sample powder was weighed and measured with the Soxhlet extraction method. The samples were mixed with 50 ml of petroleum ether and dried in an oven at 120°C for 3 h with a Soxhlet apparatus (SOX406; Jinan Hanon, Shandong, China), and the residue was weighed and recorded.

2.4 Determination of ion content

To measure the N, P, and K contents, dried samples of the leaves (0.20 g) were digested with 10 ml of 99% sulfuric acid (H_2SO_4) in a graphite digestion apparatus. The contents of P and N were determined by a fully automatic intermittent chemical analyzer (SmartChem 200; AMS Alliance, Guidonia, Rome, Italy) (Zhang et al., 2020). The K content was assessed with flame photometry (Jackson, 1973).

2.5 Determination of chlorophyll and carotenoid content

Chlorophyll and carotenoids were extracted with dimethyl sulfoxide from all leaf segments (200 mg) and were determined using ultraviolet spectrophotometry (UV1700; Meixi, Shanghai, China) according to the method of Wellburn (1994).

2.6 Determination of antioxidant enzyme activity

Antioxidant enzymes were extracted at 4°C using 200 mg of tissue from the fresh samples of bermudagrass leaves. Plant samples were homogenized with 8 ml of phosphate buffer (pH = 7.8) and were centrifuged at 12,000 rpm for 20 min, and then the supernatants were collected for the determination of the activities of antioxidant enzymes. POD activity was assayed by measuring the increase in absorbance at 470 nm with guaiacol as the substrate. CAT activity was determined by calculating the substrate consumption of H_2O_2 in absorbance at 240 nm (Hu et al., 2011). The content of H_2O_2 was determined according to the method of the hydrogen peroxide kit (Nanjing Jiancheng Bioengineering Institute, A064, Nanjing, China), and the absorbance value at 405 nm was measured with a spectrophotometer to calculate the content of H_2O_2.

2.7 Statistical analysis

The raw data of the whole experiment were statistically analyzed with one-way ANOVA using SPSS software (Statistical Product and Service Solutions, version 20; IBM, Chicago, United States). The overall significance of the treatment was tested by the SNK test at the p <0.05 level. Correlation analysis was performed using the Pearson method.

3 Results

3.1 Phenotypic characteristics

Phosphorus and potassium play an important role in the growth and development of plants. As shown in Figure 1A, the growth

10.3389/fpls.2023.1165567

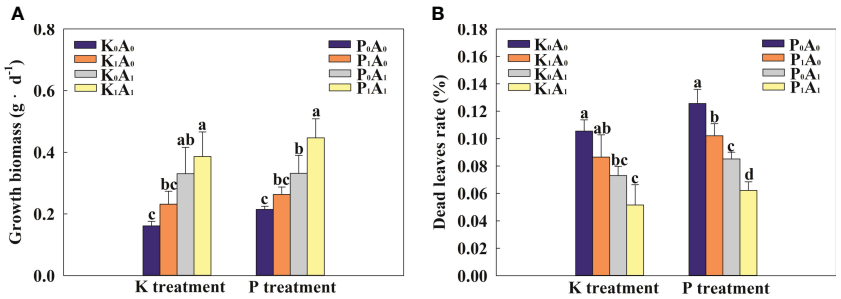

FIGURE 1
Effects of *Aspergillus aculeatus* on growth biomass **(A)** and death leaf rate **(B)** of bermudagrass under K or P deficiency stress. K_0A_0 represents no potassium feldspar and *A. aculeatus* treatment; K_1A_0 represents only potassium feldspar treatment; K_0A_1 represents only *A. aculeatus* treatment; K_1A_1 represents potassium feldspar + *A. aculeatus* treatment; P_0A_0 represents no tricalcium phosphate and *A. aculeatus* treatment; P_1A_0 represents only tricalcium phosphate treatment; P_0A_1 represents only *A. aculeatus* treatment; P_1A_1 represents tricalcium phosphate + *A. aculeatus* treatment. Columns marked with the same small letter indicate insignificant differences between the four treatment groups ($p < 0.05$).

biomass of bermudagrass was significantly increased by 105.4% in the K_0A_1 group compared with the K_0A_0 treatment. In addition, the K_1A_1 treatment significantly enhanced the growth of bermudagrass by 66.7% compared with the K_1A_0 treatment. At the same time, bermudagrass biomass had an obvious increase (by 69.7%) in the P_1A_1 group compared with the P_1A_0 regime. In the K treatment group, compared with the K_0A_0 group, the dead leaf rate of bermudagrass was significantly reduced by 44.3% in the K_0A_1 group (Figure 1B). K_1A_1 treatment significantly improved the growth of bermudagrass under the K_1A_0 stress, which showed a significant decrease of 40.4% in the dead leaf rate. Similarly, P_1A_1 treatment showed a significant decrease of 39.0% in the rate of dead leaf compared with the P_1A_0 group. Taken together, *A. aculeatus* could enhance the growth situation of bermudagrass by improving biomass and decreasing the dead leaf rate under P- or K-deficient conditions.

3.2 Chlorophyll and carotenoid contents of bermudagrass

Under K-deficient conditions, the chlorophyll a+b and carotenoid contents were not obviously different in the K_0A_0, K_1A_0, and K_0A_1 groups (Figure 2). Nevertheless, the K_1A_1 treatment significantly increased the chlorophyll a+b and carotenoid contents of bermudagrass by 48.5% and 45.4%, respectively, compared with the K_1A_0 treatment. Similarly, under P-deficient conditions, the chlorophyll a+b and carotenoid contents were increased by 30.1% and 23.6% in inoculated plants (P_0A_1 treatment) compared with the P_0A_0 treatment. Compared with the P_1A_0 treatment, the chlorophyll a+b and carotenoid contents in the P_1A_1 group increased remarkably (16.7% and 26.9%, respectively) (Figure 2). These results implied that *A. aculeatus* promoted the biosynthesis of chlorophyll a+b and carotenoid contents through its P- or K-releasing characteristics.

3.3 Forage quality

The *A. aculeatus* treatment obviously increased the crude fat content of bermudagrass by 38.6% compared with the K_0A_0 treatment and had no effect on crude protein content under K deficiency stress (Figure 3). However, *A. aculeatus* inoculations combined with K-feldspar (K_1A_1 regime) remarkably elevated the crude protein and crude fat content by 14.9% and 65.7%,

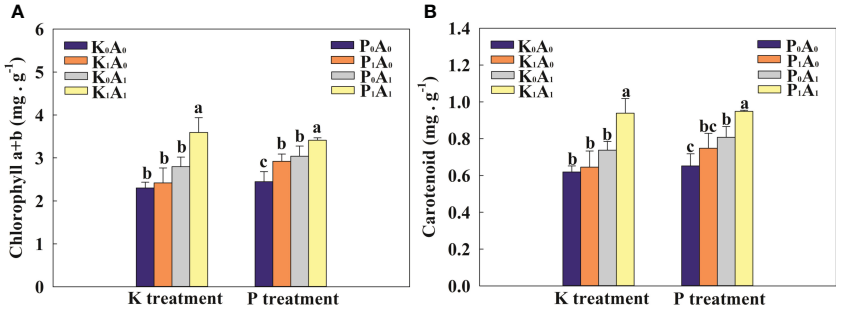

FIGURE 2
Effects of *Aspergillus aculeatus* on chlorophyll **(A)** and carotenoid **(B)** contents of bermudagrass under K or P deficiency stress. K_0A_0 represents no potassium feldspar and *A. aculeatus* treatment; K_1A_0 represents only potassium feldspar treatment; K_0A_1 represents only *A. aculeatus* treatment; K_1A_1 represents potassium feldspar + *A. aculeatus* treatment; P_0A_0 represents no tricalcium phosphate and *A. aculeatus* treatment; P_1A_0 represents only tricalcium phosphate treatment; P_0A_1 represents only *A. aculeatus* treatment; P_1A_1 represents tricalcium phosphate + *A. aculeatus* treatment. Columns marked with the same small letter indicate insignificant differences between the four treatment groups ($p < 0.05$).

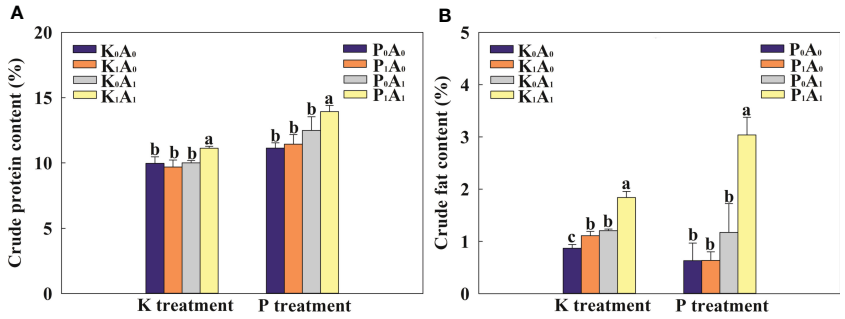

FIGURE 3
Effects of *Aspergillus aculeatus* on crude protein **(A)** and crude fat **(B)** contents of bermudagrass under K or P deficiency stress. K_0A_0 represents no potassium feldspar and *A. aculeatus* treatment; K_1A_0 represents only potassium feldspar treatment; K_0A_1 represents only *A. aculeatus* treatment; K_1A_1 represents potassium feldspar + *A. aculeatus* treatment; P_0A_0 represents no tricalcium phosphate and *A. aculeatus* treatment; P_1A_0 represents only tricalcium phosphate treatment; P_0A_1 represents only *A. aculeatus* treatment; P_1A_1 represents tricalcium phosphate + *A. aculeatus* treatment. Columns marked with the same small letter indicate insignificant differences between the four treatment groups ($p < 0.05$).

respectively, in bermudagrass, compared with the K-feldspar treatment (K_1A_0 group). Similarly, under P-deficient conditions, the P_1A_1 treatment significantly increased the crude protein and crude fat contents by 21.8% and 377.7%, respectively, compared with the P_1A_0 treatment. In the environment of K or P deficiency, exogenous *A. aculeatus* effectively increased the contents of crude protein and crude fat and then improved the forage quality of bermudagrass.

3.4 Ion homeostasis

Compared with K_0A_0, the K_1A_0 and K_0A_1 treatments had no obvious effect on the contents of N, P, and K in the leaves (Figure 4). The K_1A_1 treatment markedly enhanced the contents of N, P, and K in the leaves of bermudagrass by 14.9%, 13.2%, and 16.1%, respectively, compared with the K_1A_0 treatment. Under P-deficient conditions, the P_1A_1 treatment significantly increased the contents of N, P, and K in the leaves of bermudagrass by 21.8%, 14.4%, and 16.3%, respectively, compared with the P_1A_0 group (Figure 4). These results suggest that *A. aculeatus* can dissolve insoluble K and P into soluble K and P, thereby promoting the uptake of K and P and enhancing the contents of N, P, and K in the leaves of bermudagrass.

3.5 Antioxidant system

Adverse environments can trigger the excessive accumulation of ROS and aggravate lipid peroxidation in plants. Compared with K_0A_0, the POD, CAT, and H_2O_2 of bermudagrass in the K_1A_0 treatment group were significantly reduced by 55.8%, 30.4%, and 37.8%, while in the K_0A_1 treatment group, the POD, CAT, and H_2O_2 activities of bermudagrass were significantly reduced by 62.6%, 25.8%, and 184.2%, respectively (Figure 5). Compared with the K_1A_0 treatment, the POD activity and H_2O_2 level were significantly decreased by 49.5% and 51.5%, respectively, in the K_1A_1 treatment. Simultaneously, under P deficiency stress, the P_1A_1 treatment significantly decreased the POD activity and H_2O_2 content (by 61.6% and 59.0%, respectively), compared with the P_1A_0 treatment. These results indicate that under the P- or K-deficient conditions, *A. aculeatus* might decrease the activity of the antioxidant enzymes CAT and POD and alleviate membrane lipid peroxidation.

3.6 Correlation analysis

Two correlation plots were depicted for each K or P deficiency stress treatment and are presented in Figures 6A, B, respectively. These correlation plots provide an observation to visually compare the correlation of measured traits. Under K or P deficiency stress, the growth biomass was significantly positively correlated with chlorophyll a+b, carotenoid, and P contents and negatively correlated with the dead leaf rate (Figure 6). There was a significant positive correlation between forage quality (crude protein and crude fat) and chlorophyll a+b, carotenoids, P content, K content, and N content in the leaves of bermudagrass. However, the phenotypic indicators (growth biomass, chlorophyll a+b, carotenoid, crude protein, crude fat, N content, P content, and K content) showed a significant negative correlation with H_2O_2 content.

4 Discussion

Nitrogen, phosphorus, and potassium play a fundamental role in the growth and development of plants, and they are important mineral nutrients involved in photosynthesis (Wang et al., 2012; Ding et al., 2021). Under the conditions of P or K deficiency, the accumulation of N, P, and K in plants decreases, thereby inhibiting the absorption and utilization of nutrients and impeding the photosynthesis of plants. Photosynthetic pigments are one of the key factors affecting photosynthesis, and their content can directly affect the photosynthesis of plants,

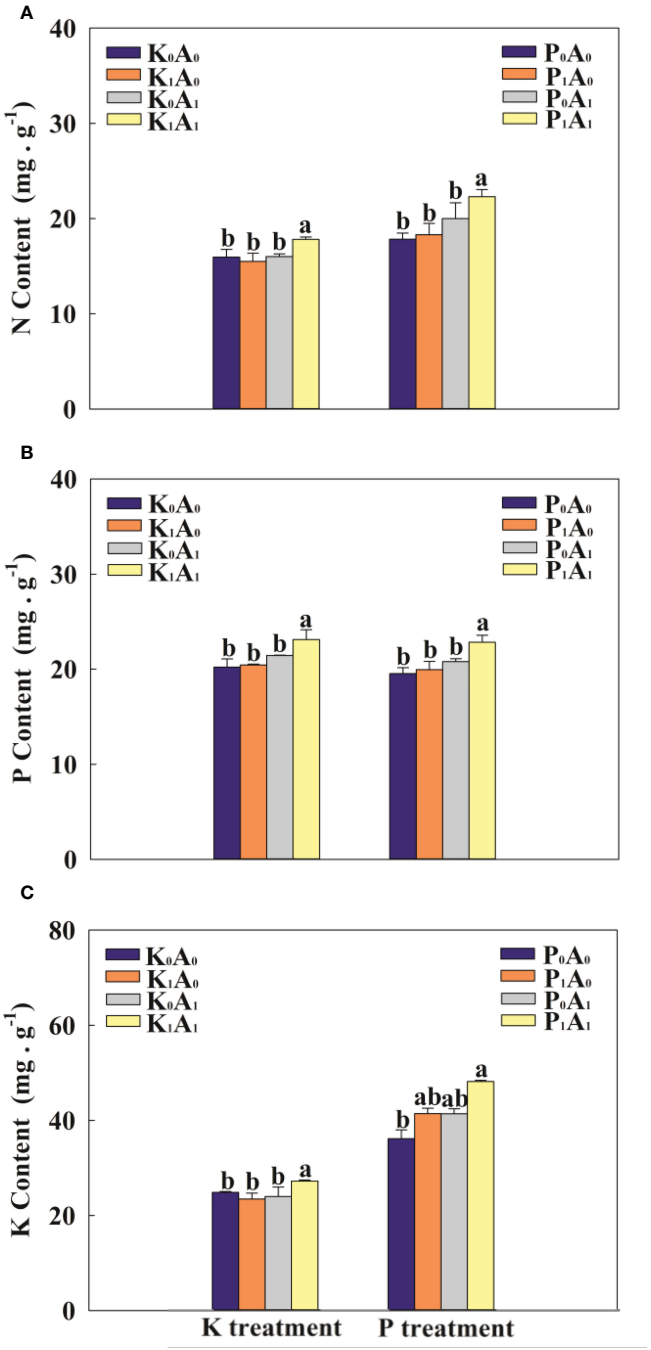

FIGURE 4
Effects of *Aspergillus aculeatus* on N content **(A)**, P content **(B)** and K content **(C)** of bermudagrass under K or P deficiency stress. K_0A_0 represents no potassium feldspar and *A. aculeatus* treatment; K_1A_0 represents only potassium feldspar treatment; K_0A_1 represents only *A. aculeatus* treatment; K_1A_1 represents potassium feldspar + *A. aculeatus* treatment; P_0A_0 represents no tricalcium phosphate and *A. aculeatus* treatment; P_1A_0 represents only tricalcium phosphate treatment; P_0A_1 represents only *A. aculeatus* treatment; P_1A_1 represents tricalcium phosphate + *A. aculeatus* treatment. Columns marked with the same small letter indicate insignificant differences between the four treatment groups ($p < 0.05$).

particularly chlorophyll and carotenoid contents (Bode et al., 2009). Our results showed that under P or K deficiency stress, the contents of N, P, and K in the leaves increased significantly when *A. aculeatus* was inoculated. Previous studies have confirmed the P- and K-solubilizing activities of *A. aculeatus* (Li et al., 2019; Li et al., 2021). In addition, the chemical characteristics of soils with poor fertility have also been measured. We found that the content of available P, K, total N, and total K in the soil was significantly increased after inoculating *A. aculeatus* into the soil with poor fertility (unpublished data). The beneficial effect of *A. aculeatus* amendment on bermudagrass under P or K deficiency supports earlier studies. The research reported that co-inoculation of P- and K-solubilizing microorganisms in conjunction with the direct application of

10.3389/fpls.2023.1165567

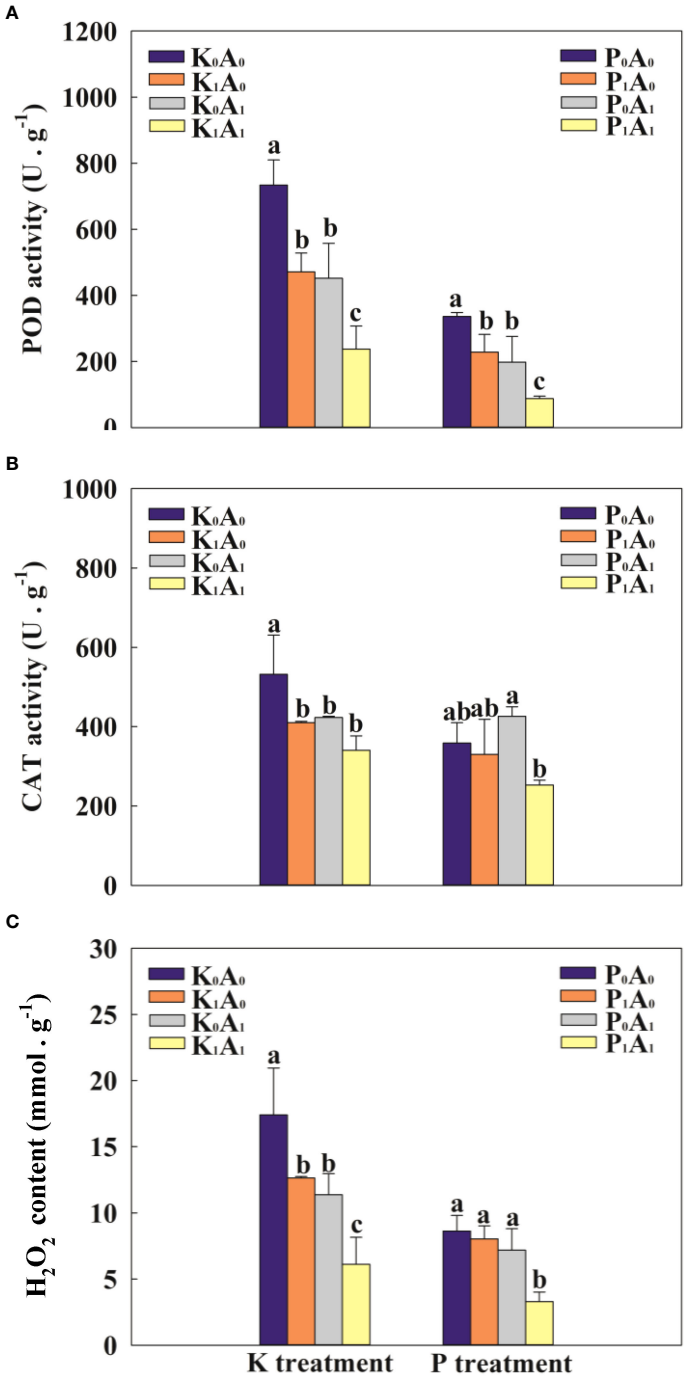

FIGURE 5
Effects of *Aspergillus aculeatus* on POD activity **(A)**, CAT activity **(B)** and H_2O_2 content **(C)** of bermudagrass under K or P deficiency stress. K_0A_0 represents no potassium feldspar and *A. aculeatus* treatment; K_1A_0 represents only potassium feldspar treatment; K_0A_1 represents only *A. aculeatus* treatment; K_1A_1 represents potassium feldspar + *A. aculeatus* treatment; P_0A_0 represents no tricalcium phosphate and *A. aculeatus* treatment; P_1A_0 represents only tricalcium phosphate treatment; P_0A_1 represents only *A. aculeatus* treatment; P_1A_1 represents tricalcium phosphate + *A. aculeatus* treatment. Columns marked with the same small letter indicate insignificant differences between the four treatment groups ($P < 0.05$).

insoluble P and K into the soil enhanced N, P, and K uptake of plants grown on P- and K-limited soils (Meena et al., 2016). As we observed, the contents of chlorophyll a+b and carotenoids were distinctly increased in *A. aculeatus*-inoculated bermudagrass (P_1A_1 and K_1A_1 groups) compared with the other groups and were significantly positively correlated with N, P, and K, as well as significantly negatively correlated with the dead leaf rates. The correlation between these functional traits could provide a relatively comprehensive evaluation of plant adaptability to P or K deficiency stress. This is fully aligned with a previous study, which documented that inoculation with a P-solubilizing strain stimulates an increase in chlorophyll (chl a and b) content and nutrient uptake (N, P, and K) in plants (Marathe et al., 2017). Overall, we suggested that *A. aculeatus* could contribute to better

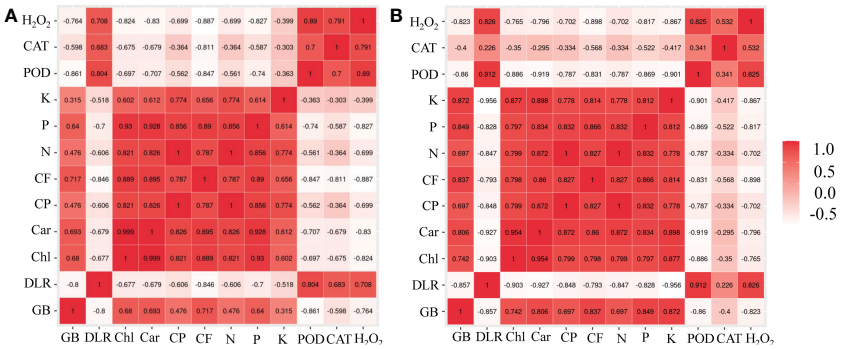

FIGURE 6
Correlation plot designed by the R software for all measured traits in bermudagrass under K deficiency **(A)** and P deficiency stress **(B)**. In the plots, red, pink, and white represent positive, zero, and negative correlations, respectively, and the darker the color (either red or white), the stronger the correlation. GB, growth biomass; DLR, dead leaf rate; Chl, chlorophyll a+b; Car, carotenoid; CP, crude protein; CF, crude fat; N, N content; P, P content; K, K content; POD, peroxidase; CAT, catalase; H_2O_2, hydrogen peroxide.

photosynthetic activity (increased chlorophyll a and b content) and growth characteristics when plants are exposed to P or K deficiency stress.

Forage quality is one of the indicators for evaluating the value of forage utilization. A higher feed value was accompanied by a higher crude protein and crude fat content in pasture (Li et al., 2018). Studies have demonstrated that N, P, and K effectively enhanced the content of crude protein and crude fat in plants (Osuagwu and Edeoga, 2013; Ogunyemi et al., 2018). Compared with P- or K-deficient treatments, the contents of crude protein and crude fat were markedly enhanced in the leaves of bermudagrass inoculated with *A. aculeatus* and were significantly positively correlated with the N and P contents. Nitrogen is an important component of chlorophyll and protein in plants, and a sufficient nitrogen supply can increase the content of chlorophyll and soluble protein (Amy et al., 2006; Fredeen et al., 2010), which is consistent with our results. In addition, P is a component of a series of important biochemical substances, such as nucleic acids, coenzymes, phosphoproteins, and phospholipids, and its deficiency affects nitrogen metabolism. According to Baier and Kristan (1986), the application of P could increase the uptake of N by plants, thereby enhancing the content of crude protein and forage quality (Baier and Kristan, 1986). In the same way, K deficiency could reduce the energy conversion rate and, thus, decrease the crude protein content of herbage, leading to the degradation of forage quality. Combining the above results, we concluded that the inoculation of *A. aculeatus* enhanced plant forage quality by improving P and K solubilizers. Enhancement of plant forage quality by improving P and K solubilizers is another beneficial effect of microorganisms with P- and K-solubilizing potential characteristics.

In this study, important indicators such as POD, CAT, and H_2O_2 were assessed to investigate the role of *A. aculeatus* for P or K deficiency stress tolerance in bermudagrass. When plants are exposed to abiotic stresses, increased cellular damage is associated with the production of ROS (Fadzilla et al., 1997). In our results, we found that inoculated bermudagrass showed remarkably lower H_2O_2 levels than uninoculated bermudagrass under P- or K-deficient conditions, indicating that *A. aculeatus* could significantly attenuate stress-induced oxidative damage. Although plants cannot escape from deleterious environments, they have already developed and established a mathematical regulatory mechanism to cope with stress damage (Abeed et al., 2022). Usually, stress-induced ROS accumulation is scavenged by diverse enzymatic scavengers, such as POD, CAT, SOD, or other antioxidants (Apel and Hirt, 2004). H_2O_2 is an important ROS produced in the catalytic process of SOD, resulting in oxidative damage (Mittler, 2002). CAT and POD are the major antioxidant enzymes in plants, and CAT could degrade H_2O_2 into water and oxygen to scavenge H_2O_2. Our results indicated that inoculation with *A. aculeatus* significantly decreased the CAT and POD activities and the concentration of H_2O_2 in the P_1A_1 and K_1A_1 groups compared with the P_1A_0 and K_1A_0 groups. These studies reveal that *A. aculeatus* can alleviate the antioxidant damage caused by low phosphorus or potassium stress by decreasing ROS accumulation and altering the activity of antioxidant enzymes.

Therefore, our results demonstrated the regulatory mechanism of *A. aculeatus* on K or P deficiency stresses in bermudagrass. First, *A. aculeatus* increases the contents of N, P, and K in the leaves of bermudagrass and enhances the accumulation of chlorophyll and carotenoids, thereby promoting plant photosynthesis. Second, *A. aculeatus* increases the content of crude protein and crude fat accompanied by the growing N and P contents in the leaves of bermudagrass. Finally, *A. aculeatus* could mitigate membrane lipid peroxidation and decrease the activities of the antioxidant enzymes CAT and POD. Therefore, *A. aculeatus* has great promotion value and economic benefit in K- or P-deficient soil as a microbial agent.

Data availability statement

The original contributions presented in the study are included in the article/supplementary material. Further inquiries can be directed to the corresponding author.

Author contributions

XL conceived the experiments and wrote the manuscript. TZ performed the experiments. XL and XX analyzed the data. YX and XC cultivated the experimental materials. JF guided this experiment. All authors contributed to the article and approved the submitted version.

Funding

This work was supported by the Natural Science Foundation of Shandong Province (grant no. ZR2020QC051).

Conflict of interest

The authors declare that the research was conducted in the absence of any commercial or financial relationships that could be construed as a potential conflict of interest.

Publisher's note

References

Abeed, A. H. A., Mahdy, R. E., Alshehri, D., Hammami, I., Eissa, M. A., Latef, A. A. H., et al. (2022). Induction of resilience strategies against biochemical deteriorations prompted by severe cadmium stress in sunflower plant when *Trichoderma* and bacterial inoculation were used as biofertilizers. *Front. Plant Sci.* 13, 1004173. doi: 10.3389/fpls.2022.1004173

Amy, K., Veronica, C., Neal, B., Lena, H., and Tala, A. (2006). Ecophysiological responses of *Schizachyrium scoparium* to water and nitrogen manipulations. *Great Plains Res.* 16, 29–36.

Apel, K., and Hirt, H. (2004). Reactive oxygen species: metabolism, oxidative stress, and signal transduction. *Annu. Rev. Plant Biol.* 55, 373–399. doi: 10.1146/annurev.arplant.55.031903.141701

Baier, J., and Kristan, V. (1986). Effect of phosphorus fertilizer application on increasing nutrient uptake. *Agrochemica.* 26, 343–345.

Bargaz, A., Lyamlouli, K., Chtouki, M., Zeroual, Y., and Dhiba, D. (2018). Soil microbial resources for improving fertilizers efficiency in an integrated plant nutrient management system. *Front. Microbiol.* 9, 1606. doi: 10.3389/fmicb.2018.01606

Bode, S., Quentmeier, C. C., Liao, P. N., Mafi, N., Barros, T., Wilk, L., et al. (2009). On the regulation of photosynthesis by excitonic interactions between carotenoids and chlorophylls. *P. Natl. A. Sci.* 106 (30), 12311–12316. doi: 10.1073/pnas.0903536106

Cakmak, I. (2005). The role of potassium in alleviating detrimental effects of abiotic stresses in plants. *J. Plant Nutr. Soil Sci.* 168, 521–530. doi: 10.1002/jpln.200420485

Clarkson, D. T., and Hanson, J. B. (1980). The mineral nutrition of higher plants. *Annu. Rev. Plant Physiol.* 31, 239–298. doi: 10.1146/annurev.pp.31.060180.001323

Ding, Z., Ali, E. F., Almaroai, Y. A., Mamdouh, A. E., and Amany, H. A. A. (2021). Effect of potassium solubilizing bacteria and humic acid on faba bean (*Vicia faba* l.) plants grown on sandy loam soils. *J. Soil Sci. Plant Nutr.* 21, 791–800. doi: 10.1007/s42729-020-00401-z

Fadzilla, N. A. M., Finch, R. P., and Burdon, R. H. (1997). Salinity, oxidative stress and antioxidant responses in shoot cultures of rice. *J. Exp. Bot.* 48, 325–331. doi: 10.1093/jxb/48.2.325

Fan, J., Ren, J., Zhu, W., Amombo, E., Fu, J., and Chen, L. (2014). Antioxidant responses and gene expression in s under cold stress. *J. Am. Soc Hortic. Sci.* 139, 699–705. doi: 10.21273/JASHS.139.6.699

Fredeen, A. L., Gamon, J. A., and Field, C. B. (2010). Responses of photosynthesis and carbohydrate-partitioning to limitations in nitrogen and water availability in field-grown sunflower. *Plant Cell Environ.* 14 (9), 963–970.

Garcia, K., Chasman, D., Roy, S., and Ané, J. M. (2017). Physiological responses and gene co-expression network of mycorrhizal roots under k(+) deprivation. *Plant Physiol.* 173 (3), 1811–1823. doi: 10.1104/pp.16.01959

Gundala, P. B., Chinthala, P., and Sreenivasulu, B. (2013). A new facultative alkaliphilic, potassium solubilizing, bacillus spp. SVUNM9 isolated from mica cores of nellore district, andhra pradesh, India. *J. Microbiol. Biotechnol.* 2 (1), 1–7.

Guo, Y. P., Chen, P. Z., Zhang, L. C., and Zhang, S. L. (2002). Effects of different phosphorus nutrition levels on photosynthesis in satsuma mandarin (*Citrus unshiu marc.*) leaves. *Plant Nutr. Fertil. Sci.* 8, 186–191.

Hu, T., Li, H. Y., Zhang, X. Z., Luo, H. J., and Fu, J. M. (2011). Toxic effect of NaCl on ion metabolism, antioxidative enzymes and gene expression of perennial ryegrass. *Ecotox. Environ. Safe.* 74, 2050–2056. doi: 10.1016/j.ecoenv.2011.07.013

Illmer, P. A., and Schinner, F. (1995). Solubilization of inorganic calcium phosphates solubilization mechanisms. *Soil. Biol. Biochem.* 27, 257–263. doi: 10.1016/0038-0717(94)00190-C

Jackson, M. L. (1973). *Soil chemical analysis* (New Delhi, India: Prentice Hall Private Ltd).

Krishnaraj, P. U., and Dahale, S. (2014). Mineral phosphate solubilization: concepts and prospects in sustainable agriculture. *Proc. Ind. Natl. Sci. Acad.* 80, 389–405. doi: 10.16943/ptinsa/2014/v80i2/55116

Kumar, S., Diksha,, Sindhu, S. S., and Kumar, R. (2021). Biofertilizers: An ecofriendly technology for nutrient recycling and environmental sustainability. *Curr. Res. Microb. Sci.* 3, 100094. 10.1016/j.crmicr.2021.100094

Li, C., Peng, F., Xue, X., You, Q., Lai, C., Zhang, W., et al. (2018). Productivity and quality of alpine grassland vary with soil water availability under experimental warming. *Front. Plant Sci.* 9, 1790. doi: 10.3389/fpls.2018.01790

Li, X., Sun, X., Wang, G., Amombo, E., Zhou, X., Du, Z., et al. (2019). Inoculation with *Aspergillus aculeatus* alters the performance of perennial ryegrass under phosphorus deficiency. *J. Am. Soc Hortic. Sci.* 144, 182–192. doi: 10.21273/JASHS04581-18

Li, X., Yin, Y., Fan, S., Xu, X., Amombo, E., Xie, Y., et al. (2021). *Aspergillus aculeatus* enhances potassium uptake and photosynthetic characteristics in perennial ryegrass by increasing potassium availability. *J. Appl. Microbiol.* 00, 1–12.

Luiz, J., Young, M., Kanashiro, S., Jocys, T., and Reis, A. (2018). Scientia horticulturae silver vase bromeliad: Plant growth and mineral nutrition under macronutrients omission. *Scientia Hortic.* 234, 318–322. doi: 10.1016/j.scienta.2018.02.002

Marathe, R., Phatake, Y., Shaikh, A., Shinde, B., and Gajbhiye, M. (2017). Effect of IAA produced by pseudomonas aeruginosa 6a (bc4) on seed germination and plant growth of glycin max. *J. Exp. Biol. Agric. Sci.* 5, 351–358. doi: 10.18006/2017.5(3).351.358

Meena, V. S., Maurya, B. R., Verma, J. P., and Meena, R. S. (2016). *Potassium solubilizing microorganisms for sustainable agriculture* (New Delhi: Springer).

Mittler, R. (2002). Oxidative stress, antioxidants and stress tolerance. *Trends. Plant Sci.* 7, 405–410. doi: 10.1016/S1360-1385(02)02312-9

Mittova, V., Tal, M., Volokita, M., and Guy, M. (2002). Salt stress induces up-regulation of an efficient chloroplast antioxidant system in the salt-tolerant wild tomato species lycopersicon pennellii but not in the cultivated species. *Physiol. Plant* 115 (3), 393–400. doi: 10.1034/j.1399-3054.2002.1150309.x

Ogunyemi, A. M., Otegbayo, B. O., and Fagbenro, J. A. (2018). Effects of NPK and biochar fertilized soil on the proximate composition and mineral evaluation of maize flour. *Food Sci. Nutr.* 6 (8), 2308–2313. doi: 10.1002/fsn3.808

Osuagwu, G. G. E., and Edeoga, H. O. (2013). Influence of npk inorganic fertilizer treatment on the proximate composition of the leaves of *Ocimum gratissimum* (L.) and gongronema latifolium (Benth). *Pakistan J. Biol. Sci.* 16, 372–378. doi: 10.3923/pjbs.2013.372.378

Poirier, Y., and Bucher, M. (2002). Phosphate transport and homeostasis in arabidopsis. *Arabidopsis Book* 1, e0024. doi: 10.1199/tab.0024

Prajapati, K., and Modi, H. (2012). Isolation and characterization of potassium solubilizing bacteria from ceramic industry soil. *CIB Technol. J. Microbiol.* 1 (2-3), 8–14.

Sharma, S. B., Sayyed, R. Z., Trivedi, M. H., and Gobi, T. A. (2013). Phosphate solubilizing microbes: sustainable approach for managing phosphorus deficiency in agricultural soils. *SpringerPlus.* 2, 587. doi: 10.1186/2193-1801-2-587

Shi, H., Ye, T., Zhong, B., Liu, X., and Chan, Z. (2014). Comparative proteomic and metabolomic analyses reveal mechanisms of improved cold stress tolerance in bermudagrass (*Cynodon dactylon* (L.) pers.) by exogenous calcium. *J. Integr. Plant Biol.* 56, 1064–1079. doi: 10.1111/jipb.12167

Shin, R., Berg, R., and Schachtman, D. (2005). Reactive oxygen species and root hairs in arabidopsis root response to nitrogen, phosphorus and potassium deficiency. *Plant Cell Physiol.* 46, 1350–1357. doi: 10.1093/pcp/pci145

Wang, Y., Chen, Y. F., and Wu, W. H. (2021). Potassium and phosphorus transport and signaling in plants. *J. Integr. Plant Biol.* 63 (1), 34–52. doi: 10.1111/jipb.13053

Wang, N., Hua, H., Eneji, A. E., Li, Z., Duan, L., and Tian, X. (2012). Genotypic variations in photosynthetic and physiological adjustment to potassium deficiency in cotton (*Gossypium hirsutum*). *J. Photochem. Photobiol.* 110, 1–8. doi: 10.1016/j.jphotobiol.2012.02.002

Wellburn, A. R. (1994). The spectral determination of chlorophylls a and b, as well as total carotenoids, using various solvents with spectrophotometers of different resolution. *J. Plant Physiol.* 144, 307–313. doi: 10.1016/S0176-1617(11)81192-2

Xie, Y., Han, S., Li, X., Amombo, E., and Fu, J. M. (2017). Amelioration of salt stress on bermudagrass by the fungus *Aspergillus aculeatus*. *Mol. Plant-Microbe Interact.* 30, 245–254. doi: 10.1094/MPMI-12-16-0263-R

Xie, Y., Luo, H., Du, Z., Hu, L., and Fu, J. M. (2014). Identification of cadmium-resistant fungi related to cd transportation in bermudagrass [*Cynodon dactylon* (L.) pers.]. *Chemosphere.* 117, 786–792. doi: 10.1016/j.chemosphere.2014.10.037

Zarjani, J. K., Aliasgharzad, N., Oustan, S., Emadi, M., and Ahmadi, A. (2013). Isolation and characterization of potassiumsolubilizing bacteria in some Iranian soils. *Arch. Agron. Soil Sci.* 59, 1713–1723. doi: 10.1080/03650340.2012.756977

Zhang, Y. K., Yin, Y. L., Amombo, E., Li, X., and Fu, J. M. (2020). Different mowing frequencies affect nutritive value and recovery potential of forage bermudagrass. *Crop Pasture Sci.* 71, 610–619. doi: 10.1071/CP19369

Zhao, X., Du, Q., Zhao, Y., Wang, H., Li, Y., Wang, X., et al. (2016). Effects of different potassium stress on leaf photosynthesis and chlorophyll fluorescence in maize (*Zea mays* l.) at seedling stage. *Agr. Sci.* 07 (1), 44–53.

Frontiers in
Plant Science

Cultivates the science of plant biology and its applications

The most cited plant science journal, which advances our understanding of plant biology for sustainable food security, functional ecosystems and human health.

Discover the latest Research Topics

See more →

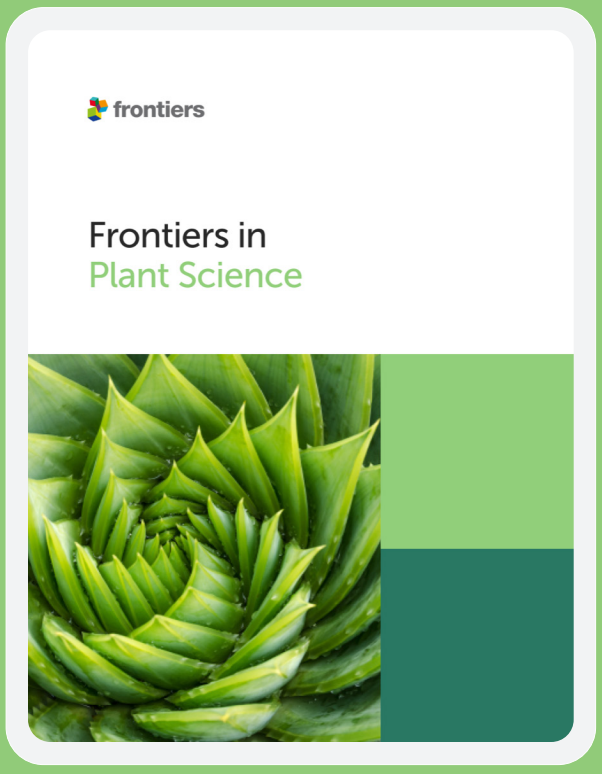

Frontiers

Avenue du Tribunal-Fédéral 34
1005 Lausanne, Switzerland
frontiersin.org

Contact us

+41 (0)21 510 17 00
frontiersin.org/about/contact